https://dspace.org/

Geology and mineralisation of the Sheba's Ridge area, Eastern Bushveld Complex, South Africa

Stevens, Fiona Jean

2008-07-09T11:33:49Z
http://hdl.handle.net/10539/5013

Downloaded from a DSpace repository. https://dspace.org/

Geology and Mineralisation of the Sheba's Ridge area, Eastern Bushveld Complex, South Africa

By
Fiona Jean Stevens

A dissertation submitted to the Faculty of Science, University of the Witwatersrand in fulfillment of the requirements for the degree of Master of Science

Johannesburg 2007

Declaration

I declare that this dissertation is my own, unaided work. It is being submitted for the Degree of Master in Science in the University of the Witwatersrand, Johannesburg. It has not been submitted before for any degree or examination in any other University.

_____

Signature of Candidate

_____ **Day of** _____ **2007.**

Abstract

Sheba's Ridge forms an area of approximately 20 km^2 in the far western extension of the eastern limb of the Bushveld Complex. It is peripheral to the main Complex and lies within a structurally complex setting to the south-west of the Mineral Range area. The ultramafic-mafic rocks strike approximately east-west and lie to the southeast of the Dennilton Dome and to the west of the Rietfontein Dome. In the northwestern sector of the area, igneous rocks onlap onto an irregular floor rock topography of Transvaal Supergroup metasediments. The ultramafic-mafic sequence dips to the south, in contrast to the normal dip of the main Bushveld Complex, which dips inwards towards the centre of the intrusion. The basal pyroxenite at Sheba's Ridge is host to a contact style Ni, Cu, PGE deposit. Succeeding intrusive pulses interfingered with earlier layers and incorporated disorientated xenoliths of country rock and earlier mafics. These norites and pyroxenites have similar mineralogical and geochemical signatures to Critical Zone lithologies of the eastern and western limbs of the Bushveld Complex. The final intrusion appears to have been gabbronorites which have been equated with the Main Zone of the Bushveld Complex.

The complex stratigraphy of Sheba's Ridge has been subdivided on the basis of Mg#, An# and element ratios Sr/Al_2O_3, Cr/MgO, Sr/Ba, Cu/Zr, Cr/V, and SiO_2/Al_2O_3. Two distinct geochemical groupings are recorded and infer that the sequence at Sheba's Ridge comprises an interfingering of these two distinct packages. From a comparison with the main eastern and western lobes of the Bushveld Complex, these two packages have been correlated to the upper Critical Zone and Main Zone of the Bushveld Complex. Furthermore, element ratios show that peaks in mineralisation occur where these two packages have interacted. This mineralised unit shows considerable similarities to the Platreef in the northern limb of the Bushveld Complex. Both have a hanging wall of norite with inverted pigeonite, both have varying Pt:Pd ratios throughout the mineralised package unlike that of the Merensky Reef.

However the Platreef is directly overlain by the Main Zone and does not possess any upper mineralised layers.

A model for the emplacement of the igneous rocks at Sheba's Ridge envisages an early 'Marginal Zone' magma intruded into cold Transvaal Supergroup sediments. This was followed by the successive intrusion of pyroxenitic layers which incorporated both country rock xenoliths and earlier 'Marginal Zone' intrusives. The next phase of magma influx was the noritic package, which disrupted the pyroxenite package and formed discontinuous interfingering sills. The final magma influx was the gabbronorite package which now forms Sheba's Ridge. This phase may have dislodged and incorporated earlier mafic lithologies. This atypical sequence at Sheba's Ridge may have formed from a separate feeder to the main limbs of the Bushveld Complex. Alternatively, the peripheral location of the basin and dome topography may have locally controlled and isolated the magma from the main Bushveld intrusion, such that the stratigraphic succession that crystallised not only differs somewhat from the Bushveld as a whole but also occurs as an interfingered package rather than a typical layered sequence.

Acknowledgements

I would like to gratefully acknowledge Ridge Mining for providing funding for this research project and providing geochemical data for borehole LPR12/9. I thank Dr Martin Sharpe for providing the opportunity and Dr Chris Lee for guidance throughout. I thank Peter Chadwick, Mark Cronje, Mike Haslett and Janette Pieterson for their friendship, assistance and support whilst in the field and Eric Roodt for his assistance and positive support whilst gathering data for this dissertation.

I am indebted to my supervisor, Prof. Judith Kinnaird. Judith you have provided me with academic and personal guidance and support throughout. My gratitude is boundless.

I would also like to thank Prof. R. Grant Cawthorn for many academic discussions on geochemistry. For technical support I would like to thank Prof. Johan Kruger for assistance with Sr isotope work, Sharon Turner and Bheki Makhatini for laboratory assistance on XRF work and Alex Mathebula who made my thin sections.

I would like to thank Dr Iain McDonald for showing me how wonderful a science geology can be and for providing the opportunity to come to South Africa to study for a post-graduate degree.

I have met many academics along the way, both form the geological field and from other faculties and thank them for their friendship and understanding during the constriction of this dissertation. In particular I would like to thank Dr Jock Harmer, Dr Paul Nex, Dr Dave Hutchinson, Dr Katie Mooney, Prof. Tony Naldrett, Prof. Phil Bonner, Dr Roger Wedlake, Dr Danie Pienaar, Dr Andrew Dinsmore, Dr Dave Holwell, Dr Charlie Seabrook and Dr John Hancox.

From the geological industry I thank Trevor Richardson, Dr John Hancox, Stephan van As and Ian McCuthcheon from Caracle Creek International for support and friendship whilst in the field. I thank Cecelia and Josh Hattingh from Rock and Stock Investments. I thank Pete Chadwick, Gordon Chunnett Dr Chris Lee, Dr Jock Harmer and Richard Hornsey for their encouragement.

Last but not least I would like to acknowledge the many friends I have made since my arrival in South Africa. My office mate Louise Coney, a true inspiration what more can I say..thanks bird! The terrible trio Geraldine Titchener, Katie Mooney and myself. David McKenzie, Andy Dinsmore, Danie Pienaar, Madeleine Greber, Dave Huthchinson, Libby Sharman-Harris, Martin Tuscherer, Charlie Seabrook, Dave Holwell, Gavin Gordon, Mabel, and many many more. Thanks and see you soon!

I thank my family who I miss terribly and hope to see very soon. My sister Mandy, my brothers Allan and Jamie, Mavis and my Mum for being there over many late night long distance phone calls.

Finally I thank my husband Neil Scholes for his patience and assistance in the final stages of this dissertation and for setting my mind free. I look forward…

Contents

Declaration ii

Abstract iii

Acknowledgements v

List of Figures xi

List of Tables xviii

List of Appendices xix

Chapter 1 Introduction

1.1 Magmatic Sulphide Deposits 1

1.2 Contact-type Ni, Cu, PGE mineralisation in ultramafic-mafic intrusions 2

1.3 The Bushveld Complex 3

1.4 Aims of this study and specific areas of investigation 11

Chapter 2 Regional Geology and Stratigraphy of Sheba's Ridge

2.1 Regional Geology of Sheba's Ridge 13

2.2 Exploration History 16

2.3 General geology of Sheba's Ridge 17

2.4 Basal Mineralisation at Sheba's Ridge 19

2.5 Other Mineralised Intervals at Sheba's Ridge 21

2.6 Sampling procedure 21

2.7 Borehole LSD34 22

2.8 Borehole LSD22 27

2.9 Borehole LPR6/12 29

2.10 Borehole LPR8/15 32

2.11 Borehole LPR12/9 34

2.12 Summary 34

Chapter 3 Petrography

3.1 Introduction 37

3.2 Floor rocks and Country rock Xenoliths (Unit 1) 44

3.3 Quartz-bearing micro-norites, micro-gabbronorites (Unit 1) 44

3.4 Basal Mineralised Pyroxenites (Unit 2) 45

3.5 Hanging wall Norites 48

3.6 Pyroxenite/Norite Interlayers (Unit 3) 50

3.7 Gabbronorites (Unit 4) 52

3.8 Discussion 54

3.8.1 Inverted Pigeonite in the Hanging wall 55

3.8.2 Stratigraphic Correlations 56

3.9 Summary 60

Chapter 4 Whole Rock Geochemistry

4.1 Introduction 62

4.2 Sample Preparation and Analysis by Whole Rock X-ray Fluorescence Spectrometry 63

4.3 Whole Rock Geochemistry – Major Element Oxides 63

4.4 Whole rock Mg# 73

4.5 Whole rock An# 79

4.6 Whole Rock Geochemistry - Trace Elements 81

4.7 Element Ratios 94

4.8 Discussion 97

4.8.1 Whole Rock Mg# 99

4.8.2 Whole Rock An# 101

4.8.3 Major and Trace Element Ratios 101

4.8.4 Comparison with the Bushveld Complex 102

4.9 Summary 104

Chapter 5 Mineral Chemistry

5.1 Introduction 105

5.2 Mineral Separate analytical techniques 106

5.3 Pyroxenes 110

5.4 Plagioclase 112

5.5 LPR8/15 ‘disorientated’ block 115

5.6 Strontium Isotope analyses of plagioclase separates 116

5.7 Discussion 119

Chapter 6 Basal Mineralisation

6.1 Introduction 121

6.2 Basal Mineralisation 125

6.3 Sulphides in the Basal Mineralisation, Unit (2) 128

6.4 PGE’s 129

6.5 Geochemistry of the basal mineralisation. 131

6.6 Discussion 134

Chapter 7 Discussions and Conclusions

7.1 Introduction 138

7.2 Stratigraphic Correlations at Sheba’s Ridge 138

7.3 Geochemical Correlations at Sheba’s Ridge 141

7.4 Comparison of Mineralised Layers at Sheba’s Ridge with the eastern and western limbs, Bushveld Complex 143

7.5 Model for the Formation of the Succession at Sheba's Ridge 145

7.6 A Comparison with the Bushveld Complex and other Ni-Cu-PGE deposits 148

7.7 Current Progress in Exploration at Sheba's Ridge 149

7.8 Conclusions 150

7.9 Suggestions for Further Work in the Loskop Area 151

References 152

List of Figures

Figure 1.1 Geographical setting of the world's Ni-Cu, PGE, Pt placer and Os-Ir placer deposit. **2**

Figure 1.2 A) Schematic geological location map of the Bushveld Complex, South Africa. B) Schematic map of the regional geology surrounding Sheba's Ridge. **5**

Figure 1.3 Stratigraphic succession of the BC, showing mineralised intervals, geochemical variation with height and Zones of the BC. Modified from Eales & Cawthorn (1996). **6**

Figure 1.4 Regional geology of the project area. **12**

Figure 2.1 A) Schematic geological location map of the Bushveld Complex, South Africa. B) Schematic map of the regional geology surrounding Sheba's Ridge. **14**

Figure 2.2 'Disorientated' noritic block on the western sector of Loskop South 53 JS. **15**

Figure 2.3 A stratigraphic column through the lower Transvaal Supergroup modified from Department of Mines Geological Series 2828 Pretoria. **16**

Figure 2.4 Generalised stratigraphy showing mineralisation within the stratigraphic sequence on the farm Loskop South 53 JS. **19**

Figure 2.5 Positions of boreholes on the farm Loskop South 53 JS. **20**

Figure 2.6 Borehole log for LSD34. **25**

Figure 2.7 Detailed borehole log through the 'Mineralised cyclic Unit' (MCU) of LSD34. **26**

Figure 2.8 Borehole log of LSD22. **28**

Figure 2.9 Borehole log of LPR6/12. **31**

Figure 2.10 Borehole log of LPR8/15. **33**

Figure 2.11 Borehole log of LPR12/9. **36**

Figure 3.1 Generalised stratigraphy on Loskop South 53 JS. **39**

Figure 3.2 Summarised stratigraphic borehole log showing sample number and depth in borehole for A) LSD34 and B) LSD22. **40**

Figure 3.3 Summarised stratigraphic borehole log showing sample number and depth for A) borehole LPR6/12 and B) through the basal mineralisation in borehole LPR6/12. **41**

Figure 3.4 Summarised stratigraphic borehole log with sample number and depth for borehole LPR8/15. **42**

Figure 3.5 Summarised stratigraphic borehole log with sample number and depth for A) borehole LPR12/9, samples taken in this study and B) samples taken by Ridge Mining through the basal mineralisation. **43**

Figure 3.6 Photomicrographs of hornfels and micronorites from Unit 1 and mineralised olivine-bearing pyroxenite from unit 2. A) LPR8/15-457.00 m. B) LPR8/15 422.00. C) LPR8/15 432.00. D) LPR6/12-47. **46**

Figure 3.7 Photomicrographs of mineralised pyroxenites from unit 2 and norites in Unit 3. A) LPR6/12-26. B) LPR6/12-26 C) LSD 34 489.00. D) LSD34 447.00. **48**

Figure 3.8 Photomicrographs of the hanging wall norite marking the base of Unit 3 from sample LSD34 618.50 m. **49**

Figure 3.9 Photomicrographs of norites from the 'disorientated' noritic block and below from borehole LPR8/15. A) LPR8/15 27.00, B) LPR8/15 82.50, C) LPR8/15 82.50. D) LPR8/15 141.00. **51**

Figure 3.10 Photomicrographs of gabbronorite from Unit 4. A) LSD22/1. B) LSD22/1. C) LSD22/2. D) LSD22/2. **53**

Figure 3.11 Stratigraphy of the Pretoria Group of the Transvaal Super Group. **57**

Figure 3.12 General stratigraphy from: A) the farm on the west of Loskop South, Rietfontein 73 JS (Crous, 1995), B) this study, Loskop South 53 JS, Sheba's Ridge (modified from Roodt, 2004) and C) general stratigraphy of the Bushveld Complex (Eales & Cawthorn, 1996). **58**

Figure 3.13 Schematic cross section through the farm directly to the west of Loskop South 53 JS, Rietfontein 73 JS, modified from Crous (1995). **59**

Figure 4.1 Harker plots of whole rock Al_2O_3 plotted against MgO + Fe_2O_3 (representing total Fe) for A) borehole LSD34 and B) LPR8/15. **65**

Figure 4.2 Harker plots of whole rock Al_2O_3 plotted against MgO + Fe_2O_3 (representing total Fe) for A) borehole LPR6/12 and B) LPR12/9. **66**

Figure 4.3 Bivariate plots of wt% major element oxides against wt% MgO from boreholes LSD34 and LSD22. **68**

Figure 4.4 Bivariate plots of wt% major element oxides against wt% MgO from borehole LPR6/12. **70**

Figure 4.5 Bivariate plots of wt% major element oxides against wt% MgO from borehole LPR8/15. **71**

Figure 4.6 Bivariate plots of wt% major element oxides against wt% MgO from borehole LPR12/9. **72**

Figure 4.7 Selected whole rock major and trace element ratios plotted against depth in borehole LSD34. **74**

Figure 4.8 Selected whole rock major and trace element ratios plotted against depth in borehole LPR6/12. **75**

Figure 4.9 Selected whole rock major and trace element ratios plotted against depth in borehole LPR8/15. **77**

Figure 4.10 Selected whole rock major and trace element ratios plotted against depth in borehole LPR12/9. **78**

Figure 4.11 Whole Rock XRF trace element data plotted against depth for borehole LSD34. **83**

Figure 4.12 Whole rock trace element data plotted against depth for borehole LSD34. **84**

Figure 4.13 Whole Rock XRF trace element data plotted against depth for borehole LPR6/12. **87**

Figure 4.14 Whole rock trace element data plotted against depth for borehole LPR6/12. **88**

Figure 4.15 Whole rock XRF trace element data plotted against depth for borehole LPR8/15. **90**

Figure 4.16 Whole rock trace element data plotted against depth for borehole LPR8/15. **91**

Figure 4.17 Whole rock XRF trace element data plotted against depth for borehole LPR12/9. **92**

Figure 4.18 Whole rock trace element data plotted against depth for borehole LPR12/9. **93**

Figure 4.19 Showing A) Sr/Al_2O_3 ratio from whole rock XRF data B) corrected Sr/Al_2O_3* ratio corrected for the small amount of Al occurring in pyroxene using equation 5.1. Mineral separate data is taken from microprobe analysis. **95**

Figure 4.20 Plots of whole rock Mg# versus wt% MgO from borehole A) LSD34, B) LPR6/12, C) LPR8/15 and D) LPR12/9. **100**

Figure 4.21 Stratigraphic succession of the Bushveld Complex, showing mineralised intervals, geochemical variation with height and Zones of the Complex. Modified from Eales & Cawthorn (1996). **103**

Figure 5.1 Microprobe data plotted on a ternary diagram of average pyroxene compositions for this study, the Critical and Main Zones, and the Platreef, BC. Interstitial clinopyroxenes and augite lamellae from inverted pigeonite are also plotted. **111**

Figure 5.2 Microprobe data for orthopyroxene grains in samples from borehole LSD34 showing element ratios A) Cr/MgO and B) Mg#. **112**

Figure 5.3 Ternary diagrams of major element oxides in plagioclase from microprobe data: A) borehole LSD34, B) LSD22 and C) LPR6/12 and D) XRF plagioclase mineral separate data from boreholes LSD34 and LPR8/15 **113**

Figure 5.4 An# from whole rock and plagioclase mineral separate data plotted against depth from boreholes: A) LSD34, D) LPR6/12 and G) LSD22 and Sr ppm values from plagioclase mineral separate data from boreholes: C) LSD34, E) LPR6/12 and H) LSD22. Note the different scale for Sr ppm on 5.3F due to contamination in sample LSD22-5 causing low Sr concentrations. An# from microprobe data are plotted against depth from boreholes: B) LSD34 and F) LPR8/15. **114**

Figure 5.5 Microprobe data for orthopyroxene grains in borehole LSD8/15 from the 'disorientated' block and the norites below showing: A) Mg# in orthopyroxene with depth, B) Cr/MgO in orthopyroxene with depth and C) An# in plagioclase with depth. **116**

Figure 5.6 Average $^{87}Sr/^{86}Sr$ ratios for the zones of the Bushveld Complex (Kruger, 2003). **117**

Figure 5.7 Initial Sr isotopic ratios plotted against depth in boreholes: A) LSD22, B) LPR6/12 and C) LSD34. **118**

Figure 6.1 Generalised stratigraphy showing mineralisation within the stratigraphic sequence on the farm Loskop South 53 JS. **122**

Figure 6.2 Regional geology of the project area (Roodt, 2004). **123**

Figure 6.3 Positions of boreholes on the farm Loskop South 53 JS. **124**

Figure 6.4 A schematic cross section of the basal mineralisation (Unit 2)-'Platreef' on Sheba's Ridge, modified from Roodt (2004). Data is compiled from borehole core on the farm Loskop South 53 JS. **126**

Figure 6.5 Photographs of typical mineralised cores: A) Hanging wall norite to the basal mineralisation at Sheba's Ridge, B) & C) the boundary between heterogeneous taxitic gabbronorite and feldspathic pyroxenite above at 654.7 m in borehole LSD34, disseminated sulphides are circled in red. D) Olivine-bearing feldspathic pyroxenite with interstitial blebby and net-textured sulphides and magnetite as an alteration mineral in borehole LPR12/9. **127**

Figure 6.6 Photomicrographs of the basal mineralised pyroxenite from sample LPR6/12-19. **128**

Figure 6.7 Backscatter electron photomicrographs: A) cumulate sulphides, chalcopyrite and pentlandite with a discrete palladium telluride in association with a chalcopyrite grain, B) Multiphase sulphide pyrrhotite and chalcopyrite with nickel arsenide and argentopentlandite occurring in association with the sulphides, C) & D) multiphase sulphides pentlandite and pyrrhotite with a discrete grain of palladium tellurium bismuthide in association with pentlandite. All images taken from sample number LPR6/12-19. **130**

Figure 6.8 Plots of geochemical data with depth in borehole LPR12/09. **133**

Figure 6.9 Bivariate plots of whole rock XRF data from borehole LPR12/9: A) Ni + Cu vs Pt + Pd and B) Ni + Cu vs S. **134**

Figure 7.1 Suggested sequence of events for the emplacement of the mafic rocks at Sheba's Ridge. **146**

List of Tables

Table 3.1 Suggested correlations of Sheba's Ridge with that of the Bushveld Complex and with the farm Rietfontein 73 JS from Crous (1995). **61**

Table 4.1 Variation in wt% MgO + Fe2O3 and wt% Al2O3 for different rock types found at Sheba's Ridge. **64**

Table 4.2 Geochemical characteristics of two geochemically distinct magmas at Sheba's Ridge. **98**

Table 5.1 Results of Isotope Dilution Mass Spectrometry of plagioclase separates for 10 selected samples. **109**

Table 6.1 A comparison of Sheba's Ridge basal mineralised Unit 2 and the Platreef. **137**

Table 7.1 Key characteristics of the subdivisions of the mafic successions at Sheba's Ridge. **139**

Table 7.2 Suggested correlations of Sheba's Ridge with that of the Bushveld Complex. **141**

Table 7.3 Geochemical characteristics of two geochemically distinct packages at Sheba's Ridge. **142**

Appendices

Appendix 1

Appendix 1A	LSD34 Borehole Log	**167**
Appendix 1B	LSD22 Borehole Log	**175**
Appendix 1C	LPR6/12 Borehole Log	**177**
Appendix 1D	LPR8/15 Borehole Log	**180**
Appendix 1E	LPR12/9 Borehole Log	**188**

Appendix 2

Appendix 2	Triangular diagrams for the classification and nomenclature of gabbroic rocks	**190**

Appendix 3

Appendix 3	XRF Standards	**191**

Appendix 4

Appendix 4A	LSD22 XRF Whole Rock Analyses	**196**
Appendix 4B	LSD34 XRF Whole Rock Analyses	**197**
Appendix 4C	LPR6/12 XRF Whole Rock Analyses	**201**
Appendix 4D	LPR8/15 XRF Whole Rock Analyses	**205**
Appendix 4E	LPR12/9 XRF Whole Rock Analyses (University of the Witwatersrand)	**207**
Appendix 4F	LPR12/9 XRF Whole Rock Analyses (provided by Ridge Mining)	**209**
Appendix 4G	Fire Assay Analyses (provided by Ridge Mining)	**212**

Appendix 5	Operating Conditions for Electron Microprobe Analyses	**214**

Appendix 5A LSD34 Microprobe Analyses – Orthopyroxene Compositions **215**
Appendix 5B LSD34 Microprobe Analyses – Plagioclase Compositions **217**
Appendix 5C LPR8/15 Microprobe Analyses – Orthopyroxene Compositions **219**
Appendix 5D LPR8/15 Microprobe Analyses – Plagioclase Compositions **220**
Appendix 5E LSD34 & LPR8/15 Microprobe Analyses – Clinopyroxene Compositions **221**
Appendix 5F Orthopyroxene Compositions from Literature **222**

Appendix 6

Appendix 6A LSD34 XRF Major and Trace Element data – Plagioclase Separates **224**
Appendix 6B LPR6/12 XRF Major and Trace Element data – Plagioclase Separates **225**
Appendix 6C LSD22 XRF Major and Trace Element data – Plagioclase Separates **226**

CHAPTER 1

Introduction

Introduction to Sheba's Ridge

The Ni-Cu-PGE mineralisation at Sheba's Ridge in the Groblersdal area of Mpumalanga Province in South Africa, occurs in an atypical Bushveld Complex (BC) stratigraphy. The mineralisation has similarities both with the Platreef of the northern limb and the satellite Uitkomst Complex to the southeast. The detailed work undertaken in this dissertation aims to set the deposit in context both with the BC and other magmatic sulphide deposits.

1.1 Magmatic Sulphide Deposits

Magmatic Nickel-Copper-Platinum-group element (PGE) sulphide deposits form as the result of the segregation and concentration of droplets of liquid sulphides from mafic or ultramafic magma, and the partitioning of chalcophile elements into these from the silicate magma (Naldrett, 2004). There are many deposits world-wide which can be sub-divided into those which are sulphide rich and relatively poor in PGE's and vice versa (Figure 1.1). Naldrett (2004) further sub-divides these deposits on the basis of tectonic and 'petro-tectonic setting', which is ultimately responsible for magma type of deposits of this nature. From this it can be seen that the world's largest PGE deposits occur as intrusions e.g. the BC, Stillwater Complex and the Great Dyke of Zimbabwe (Naldrett, 2004). These are characterised by a high proportion of an early magma with a distinctive Al_2O_3-poor and MgO-, Cr- and SiO_2-rich (U-type) composition (Sharpe, 1981; Davies & Tredoux, 1985; Naldrett, 2004). This U-type magma is typically followed by a more tholeiitic magma. Many of the mineralised horizons in these intrusions occur at levels where these two magmas have mixed or 'mingled'

(e.g. Kruger, 2005; Kinnaird, 2005; Seabrook, 2005). The key aspects of the formation of magmatic sulphides deposits to economic levels are as Naldrett (1999; 2004) states:

- That a magma develops which contains sufficient concentrations of Ni, Cu and PGE so that, if immiscible sulphides develop within it, these sulphides will become enriched in these metals.
- That this magma becomes saturated in sulphides and segregates immiscible sulphide.
- That these sulphides react with a sufficient amount of magma to concentrate chalcophile elements to an economic level.
- That sulphides are themselves concentrated in a restricted locality where their abundance is sufficient to constitute ore.

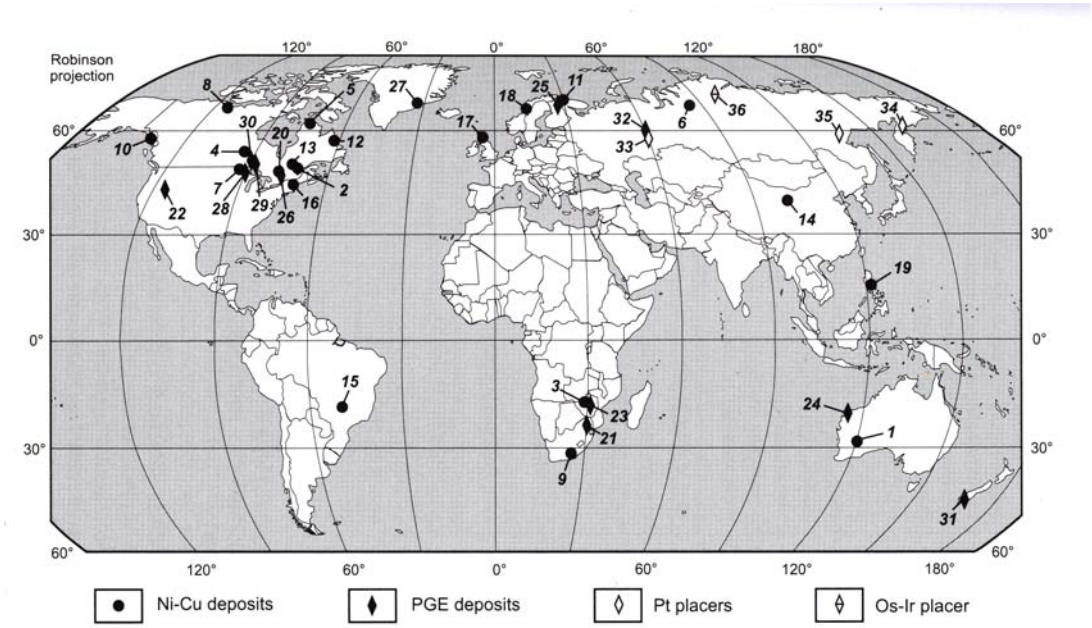

Figure 1.1 Geographical setting of the world's Ni-Cu, PGE, Pt placer and Os-Ir placer deposits. Figure from Naldrett (2004), numbered deposits are identified in his text.

1.2 Contact-type Ni, Cu, PGE mineralisation in ultramafic-mafic intrusions

'Contact-type' mineralisation here refers to the occurrence of ore-hosting ultramafic-mafic units that are in contact with the floor rocks in their respective areas. This also encompasses

the term basal mineralisation. Thus, this excludes stratiform intervals within a layered sequence such as the UG2 chromitite and Merensky Reef of the BC or the J-M Reef of the Stillwater Complex. The world's most important deposits of Ni-Cu sulphides (as opposed to those of interest primarily because of their PGE content) occur almost exclusively at the base of their associated igneous bodies (Naldrett, 1999). Furthermore, it is becoming increasingly recognised that peripheral areas of ultramafic-mafic igneous intrusions can host concentrations of Ni, Cu, PGE mineralisation of economic potential.

1.3 The Bushveld Complex

The BC is a 2.05 Ga old (Walraven *et al.,* 1990) layered suite intruded into the sedimentary and volcanic rocks of the Transvaal Supergroup and is the largest layered igneous intrusion known on Earth. The Complex covers an area of ~65 000 km^2 and has a thickness of 7-9 km. Rock types within the layered mafic rocks range between dunite and pyroxenite to anorthosite and pure oxide layers (Eales & Cawthorn, 1996). The complex outcrops in four regions namely the western, far western, eastern and northern limbs with the fifth Bethal limb being identified from gravity data (Figure 1.2A). The Complex consists of a suite of ultra-mafic to mafic sills, which underlie the layered sequence and intrude the country rock sediments, the layered ultramafic-mafic Rustenburg Layered Suite and an overlying granophyre suite. The Rustenburg Layered Suite is subdivided into the Marginal, Lower (LZ), Critical (CZ), Main (MZ) and Upper (UZ) Zones (Figure 1.3).

It is considered that the BC was emplaced as a large lopolith type sill between the felsic Rooiberg Group and the underlying Pretoria Group (Cawthorn & Webb, 2000). As well as similarities in the age of the rocks and stratigraphic correlation between eastern and western limbs, gravity data of Cawthorn & Webb (2000) indicates that there is connectivity between

the eastern and western limbs at depth. The eastern Bushveld is divided into a central sector with a complete stratigraphy through Lower, Critical, Main to Upper Zone and a southern sector, south of the Steelpoort Lineament where the LZ is absent, the CZ and MZ are present and the UZ is considerably thinner than in the central sector (Scoon & Teigler, 1995). Scoon and Teigler (1994) also divided the western limb into six different compartments each of which is structurally controlled and has a unique lithostratigraphy (Kinnaird *et al.*, 2002).

The Marginal Zone forms the basal contact of the Complex with sequences of up to 880 m of heterogeneous noritic rocks and related sills. Two areas are known not to contain Marginal norite: north of Potgietersrus in the northern limb contact rocks are extremely coarse-grained melanorites and pyroxenites constituting the Ni-Cu- PGE bearing Platreef and near Burgersfort in the eastern limb coarse harzburgite is in contact with metasediments (Eales & Cawthorn, 1996).

The LZ is an olivine and orthopyroxene-rich sequence with accessory chromite and intercumulus plagioclase, biotite and clinopyroxene (Eales & Cawthorn, 1996). The thickest sections of dunites, harzburgites and bronzitites are developed in the central sector of the eastern limb, in the far western limb, near the Union Section in the western limb and south of Mokopane in the northern limb (Kinnaird *et al.*, 2002).

The CZ is divided into a lower subzone (C_LZ) which comprises a thick succession of ultramafic orthopyroxenitic cumulates overlying harzburgite of the Lower Zone and an upper subzone (C_UZ). The C_uZ comprises packages of chromitite, pyroxenite, through norite to anorothosite. There are nine cycles recognised in the C_LZ and 8 cycles in the C_UZ (Eales & Reynolds, 1986).

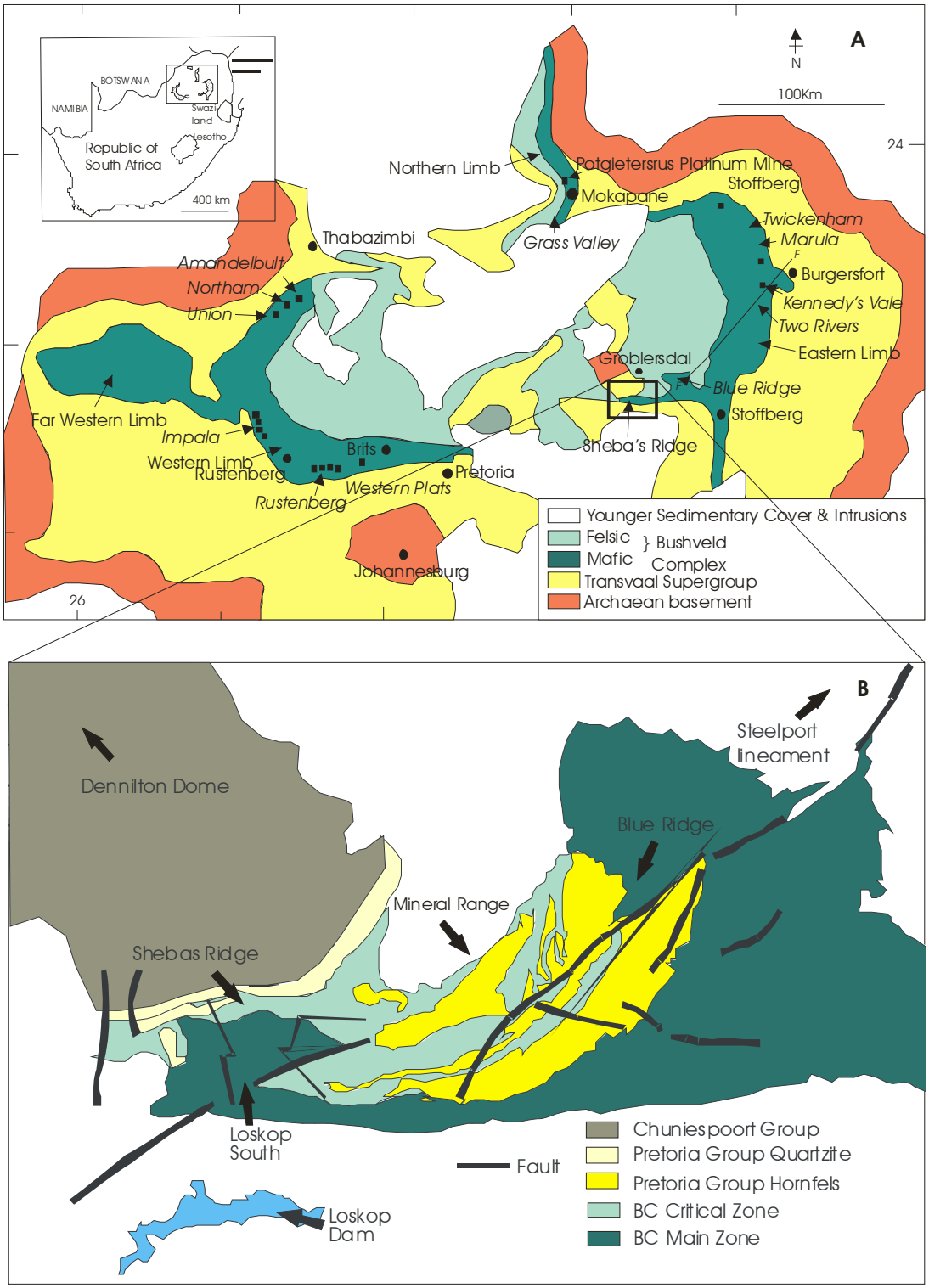

Figure 1.2 Schematic geological location map of the Bushveld Complex, South Africa. The current sites of mining and exploration are indicated and Sheba's Ridge is shown at the far southwestern extension of the eastern limb. B) Schematic map of the regional geology surrounding Sheba's Ridge.

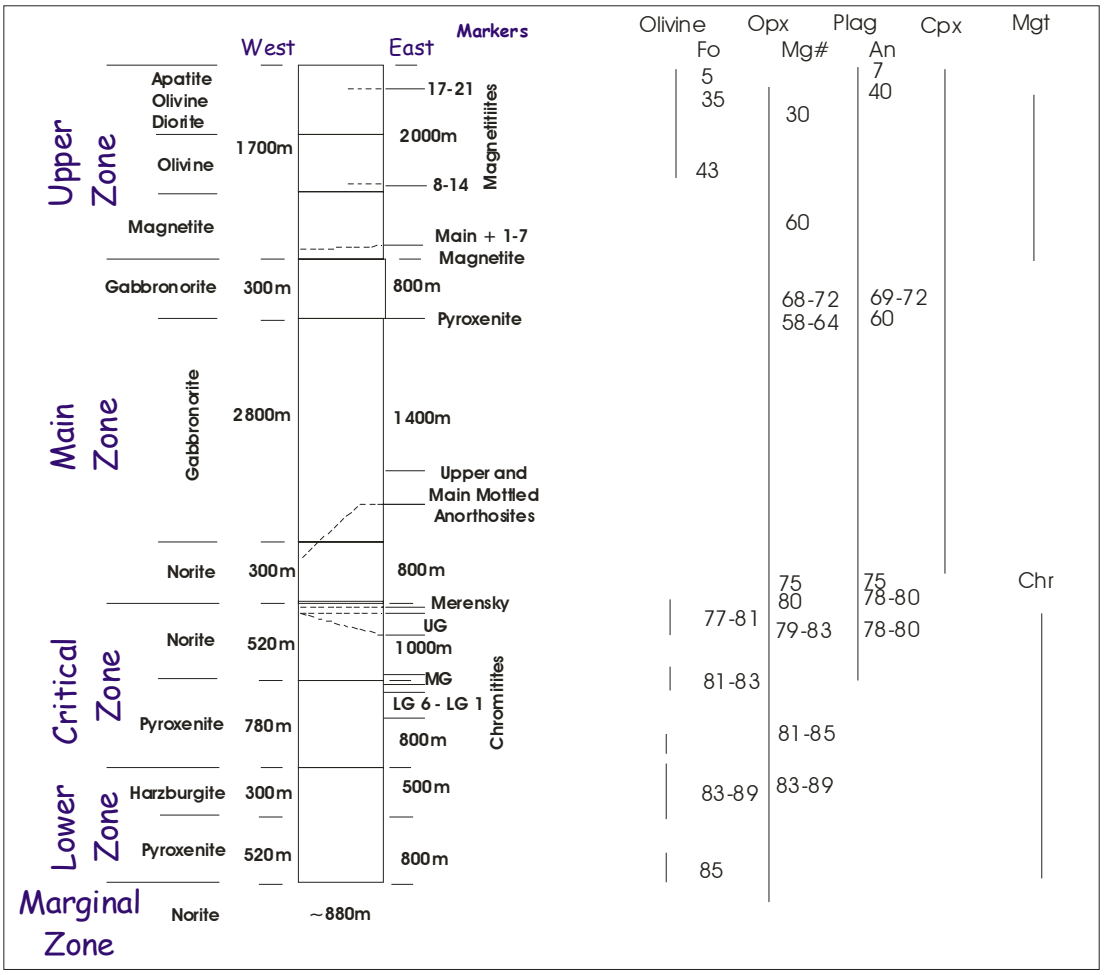

Figure 1.3 Stratigraphic succession of the BC, showing mineralised intervals, geochemical variation with height and Zones of the BC. Modified from Eales & Cawthorn (1996).

The appearance of cumulus plagioclase in the lowermost anorthositic layer between Middle Group chromitite 2 (MG2) and Middle Group chromitite 3 (MG3) marks the base of the C_UZ (Eales & Cawthorn, 1996; Hatton & Von Gruenewaldt, 1987). The C_uZ hosts the PGE bearing Upper Group chromitite 2 (UG2). The CZ-MZ boundary marker horizon has been traditionally placed at the top of the Giant Mottled Anorthosite capping the Bastard unit, stratigraphically above the Merensky Reef, although geochemical evidence suggests the true boundary is situated at the base of the Merensky cyclic unit (e.g. Kruger, 1994, Seabrook, 2005).

The MZ is the thickest zone of the layered suite comprising a ~3500 m succession of gabbronorites in which olivine and chromite are absent and anorthosites are rare (Von Gruenewaldt, 1973, Molyneux, 1974, Mitchell, 1990, Eales & Cawthorn, 1996).

The UZ is ~2000 m thick and is characterised by 25 magnetitite layers in four groups of lithologies of anorthosite, troctolite and ferrogabbro. The basal contact is defined by the first appearance of cumulus magnetite, although a sudden break in Sr-isotope ratios occurs at a prominent Pyroxenite Marker some several hundred metres below the first appearance of cumulus magnetite (Kruger, 1994, Eales & Cawthorn, 1996). These subdivisions encompass the general stratigraphy of the layered sequence on a broad scale.

Geochemical variation occurs within the layered sequence and may also be used to further constrain subdivisions (Figure 1.3). There is an overall decrease in Fo#, Mg# and An# with increasing stratigraphic height. In general the LZ has a high Mg# in orthopyroxene (83-89), a high Fo# (83-89) in olivine, the C_lZ has Mg# in orthopyroxene of 81-85, Fo# of 81-83 in olivine and plagioclase occurring as an interstitial phase (Eales & Cawthorn, 1996). The C_uZ zone, which is marked by the first appearance of cumulus plagioclase, has an An# of 78-80, Mg# in orthopyroxene of 79-83 and a Fo# of 77-81 in olivine. Olivine is only found to occur in the Western Limb of the C_uZ (Eales & Cawthorn, 1996). The boundary between the C_uZ and MZ is complex. There are variations in geochemical signatures and Sr isotopic ratios which have been attributed to either magma mixing or mingling such that there appears to be a transitional unit between C_uZ and lower MZ (Kruger 1990, 1994; Cawthorn 1999; Seabrook *et al.*, 2005). The MZ above this 'transitional' unit is predominantly homogenous up to the Pyroxenite Marker and has an Mg# in orthopyroxene of 58-64 and an An# of 60 below the marker and an Mg# in orthopyroxene of 68-72 and an An# of 69-72 above the marker. The

UZ, as defined by SACS, which is marked by the first appearance of cumulus magnetite, has low Fo#, Mg# and An# of 5-43, ~30, 7-40 respectively.

Significant breaks in Sr isotope ratios also coincide with major and minor subdivisions and have been used to demarcate stratigraphic boundaries (Kruger, 1994). These breaks in isotopic composition indicate either a different source for the magma or contamination from isotopically different materials (Faure, 1986; Seabrook, 2005). In general, the $^{87}Sr/^{86}Sr$ ratios from whole rock and plagioclase separates show cryptic variation. Kruger (1994) shows that there is an increase from 0.705 to 0.707 in the LZ with a decrease to 0.705 in the C_LZ and C_UZ. The upper MZ and UZ have steady signatures with stratigraphic height from the Pyroxenite Marker at 0.7085 and 0.7073 respectively (Sharpe, 1985; Kruger, 1994). Whereas, the C_UZ has a complex $^{87}Sr/^{86}Sr$ ratio profile through the sequence. Kinnaird *et al.*, (2002) following Schoenberg *et al.*, (1999) showed that, from 91 samples taken from lithologies below the Lower Group chromitite 5 (LG5) to those above the UG2 layer, abnormally high isotopic ratios occurred only in chromitites, implying that the influx of a new primitive or evolved magma was contaminated by roof rocks for each chromitite layer. The C_UZ/lower MZ boundary also shows a more complex profile with stratigraphic height (Kruger & Marsh, 1982; Sharpe, 1985; Lee & Butcher, 1990; Kruger, 1994; Kinnaird *et al.*, 2002; Seabrook, 2005). Seabrook (2005) showed that isotopic ratios in orthopyroxene and plagioclase separates, sampled from the Merensky Pegmatoid in the eastern limb, differ significantly and suggest a magma 'mingling' process, demarcating a Transitional Zone between the C_UZ and lower MZ at the position of the PGE bearing Merensky and Bastard Reefs.

Mineralised intervals within the BC include the strata-bound Merensky Reef and UG2 in the western and eastern limbs, the basal contact-type Platreef of the northern limb and the basal mineralised Uitkomst Complex, an outlier to the BC (e.g. Hornsey, 1999). As mineralised units in the Sheba's Ridge study area are thought to have analogues to both stratabound and contact-type reef it is necessary to summary each to enable a comparison to be made between the occurrence within the eastern, western and northern limbs with that of Sheba's Ridge.

The Merensky Reef occurs in both the western and eastern limbs. It is stratabound within the Merensky Cyclic Unit at the C_UZ/Lower MZ boundary. The cyclic unit is composed of a basal chromitite, and a pyroxenite ± olivine which grades into norite and anorthosite. Facies variations include a basal pegmatoidal feldspathic pyroxenite with an upper chromitite. In the western lobe the cyclic unit thins from ~20 m in the north to ~9 m in the south and reaches thicknesses of ~ 42 m in the eastern lobe (Eales & Cawthorn, 1996). The economic horizon contains ~3% base metal sulphides with associated platinum-group minerals (PGM) and mineralisation can occur in the hanging wall and footwall rocks, particularly in the thinner reef facies (Kinloch, 1982, Viljoen & Schürmann, 1998). The base of the Merensky pyroxenite represents an unconformity characterised by potholes, where the pyroxenite transgresses its footwall and forms a basin shaped depression. This can occur on a regional scale of hundreds of metres across, to small circular areas of less than 10 m in diameter (Lomberg *et al.*, 1999). The reef carries grades of up to 10 g/t 3PGE + Au (Cawthorn, 1999) and has an average Pt:Pd ratio of 2:1 (Barker, 2004).

All chromitite layers of the BC contain concentrations of PGE but it is the UG2 that contains the highest concentrations, with grades of up to 10 g/t. The UG2 is a stratabound chromitite layer which varies in relative height below the Merensky Reef from 20 – ~400 m with

reported thicknesses varying from ~ 0.7 – 1.3 m in the western limb (Viljoen & Schürmann, 1998; Kinnaird *et al.*, 2002). As with the Merensky Reef, the chromitite seam is often disrupted when potholes and rolling reef occurs. The Pt:Pd ratio in the UG2 chromitite is also variable along strike and ranges from ~2:1 in the eastern limb south of the Steelpoort Fault to ~1:1 north of the Steelpoort Fault and is 2:1 in the western limb.

The Platreef is a 50 - 250 m thick mineralised interval in the mafic rocks of the northern limb of the BC. The northern limb outcrops for ~100 km striking approximately N-S and transgresses successively younger floor rocks northward of Transvaal quartzites, banded iron formations, dolomites and Archaean granites in the north. Abundant metasedimentary xenoliths are present. Studies show that sulphur isotopes from bulk samples indicate a crustal contribution of sulphur to the Platreef (Buchanan *et al.*, 1981) and recent sulphur isotope studies from sulphide separates indicate a significant input of sulphur from pyritic black shales and anhydrite-bearing dolomite (Sharman-Harris & Kinnaird, 2004). This process of contamination is also supported by Harris & Chaumba (2001) who suggest post-magmatic fluid interaction and Armitage *et al.*, (2000) who note the similarities in PGE signatures found in the footwall rocks to those of the Platreef itself. It is necessary to compare the mineralised Platreef of the northern limb with that of this study as both are 'basal' or 'contact' Ni-Cu-PGE-bearing reefs which may have originated from a similar source magma.

The link between the Sheba's Ridge geology and that of the main BC has not yet been established unequivocally. The mafic succession at Sheba's Ridge dips to the south whereas the eastern limb dips to the north towards the centre of the Complex. The basal Ni-Cu-PGE mineralisation occurs in a 50-250m thick interval along approximately 7 km of strike in

the pyroxenites of the lower part of the intrusive succession (Figure 1.6). It may be analogous to the southern part of Platreef in the northern limb. Succeeding mineralised layers are potentially equivalent to the Lower, Middle and Upper Group chromitites of the BC and to the Merensky Reef. These are in ascending order the intermediate chromite layer (ICL), possibly equivalent to the lower or middle group chromitites of the BC; the Platchro (PCH), possibly analogous to the middle group chromitite of the BC; the hanging wall mineralised norite (HMN) and the upper mineralised pyroxenite (UMP) possibly analogous to the Merensky Reef (Sharpe *et al.*, 2002).

1.4 Aims of this study and specific areas of investigation

This MSc research project was sponsored by Ridge Mining in order to gain a greater understanding of the mineralogy and geochemistry of the Sheba's Ridge deposit. The field-based exploration team already had a good database on the regional geology and were characterising the basal mineralisation using mapping, borehole logging, fire-assay analysis and ore body modelling. In order to add to this existing database, this research concentrated on rock types below, within and above the basal 'sulphide-bearing' mineralisation.

As this 'contact' style of mineralisation in the BC is only known to occur in the Platreef proper of the northern limb this study aimed to log and then correlate the stratigraphic sequence at Sheba's Ridge with that of the major limbs of the BC.

In addition, this thesis aims:

- To document the unusual stratigraphic sequence that occurs at Sheba's Ridge compared to that of the BC as a whole.
- To collect data through the basal sulphide zone to document its characteristics and enable comparisons with the Platreef and other contact-style ore bodies of this nature.

- To make a comparison with mineralisation of the Platreef proper and other Ni-Cu-PGE deposits of this nature.

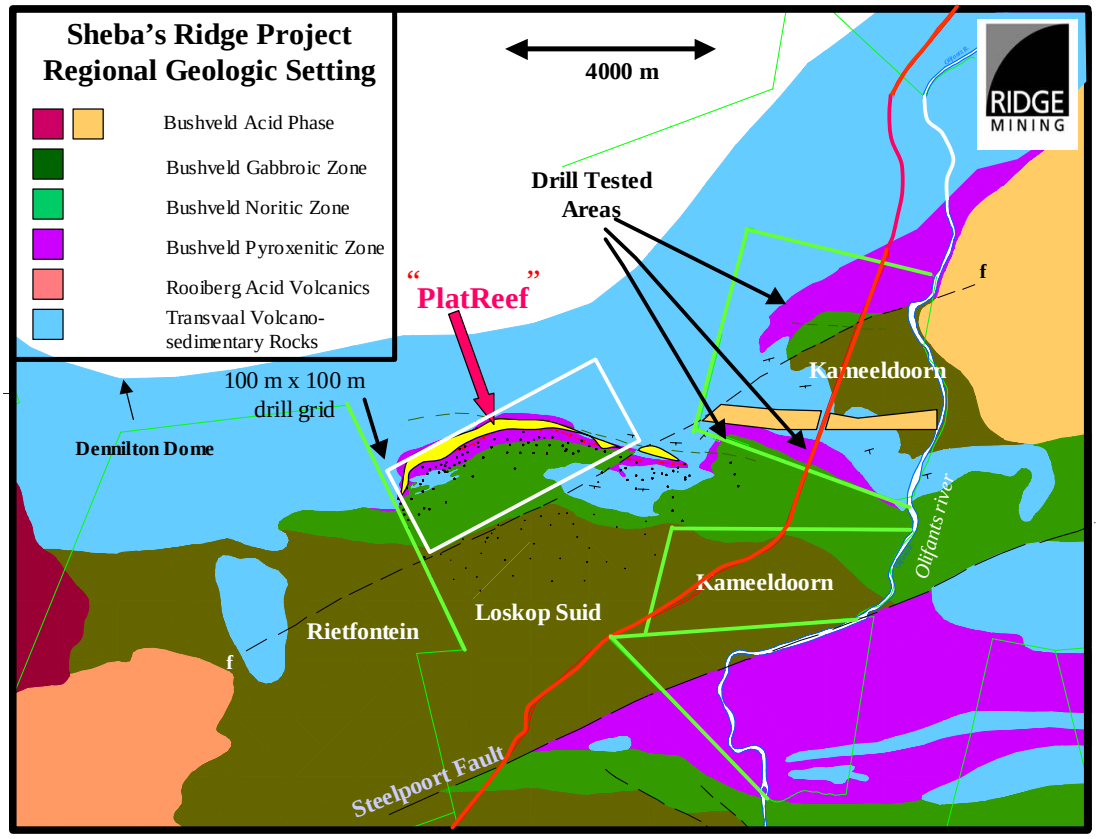

Figure 1.4 Regional geology of the project area. The Ni-Cu-PGE basal mineralisation is shown in yellow striking approximately E-W and outcropping in an arcuate nature. The term 'Platreef' was assigned by Ridge Mining during exploration. North of outcrop, steeply dipping quartzites form a ridge in the north and gabbros form Sheba's Ridge to the south. Domal features in the area include the Dennilton Dome to the northeast and the Rietfontein Dome to the west. (Map courtesy of Roodt, 2004).

The methods chosen include whole rock and mineral separate XRF major and trace element analysis, strontium isotope analysis of plagioclase separates and microprobe analysis of plagioclase and orthopyroxene crystals in polished thin section. These were chosen as previous studies have similar data sets that are widely available on the Bushveld Complex and other igneous intrusions, to enable comparisons to be made.

CHAPTER 2

Regional geology and stratigraphy of Sheba's Ridge

2.1 Regional Geology of Sheba's Ridge

The basal Ni-Cu-PGE mineralisation at Sheba's Ridge, on the farm Loskop South 53 JS, Mpumalanga Province, South Africa forms the focus for this MSc project. The project area is situated on the periphery of the far-western extension of the eastern limb of the Bushveld Complex on the farm Loskop South 53 JS (Figure 2.1). The mafic rocks of the prospect are in a basin to the east of the Rietfontein Dome and to the southeast of the Dennilton Dome. Thus, they lie in a 'basin and dome' setting, peripheral to the layered sequence of the BC. The contact between the basic intrusives and the floor rocks is undulatory, causing a thinning of the intrusive units where floor rock highs occur. The magmatic rocks unconformably onlap on to the floor rocks of the basin in the west. Regional strike of the mafics is approximately E-W with a dip at ~20° S. Within the basic rock succession (Figure 2.2), 'disorientated' blocks of norite, anorthosite and chromitite were recorded by the field team. The floor rocks include quartzite, hornfels and calcsilicate of the Transvaal Supergroup (Figure 2.3). The quartzite forms a prominent ridge in the north, striking approximately E-W and dipping at ~70°S. The hornfels and calcsilicates occur as lenses and xenoliths in the layered ultramafic-mafic rocks that have intruded into the Transvaal sediments. The Rooiberg Group forms the roof to the south of the project area. The Rashoop Granophyre, Lebowa Granite suite and granitic dykes intrude the ultramafic-mafic layered suite. This section outlines the regional geological setting and describes in detail the boreholes chosen for this study. The location of sample positions, together with detailed hand specimens and thin section descriptions are given in chapter 3.

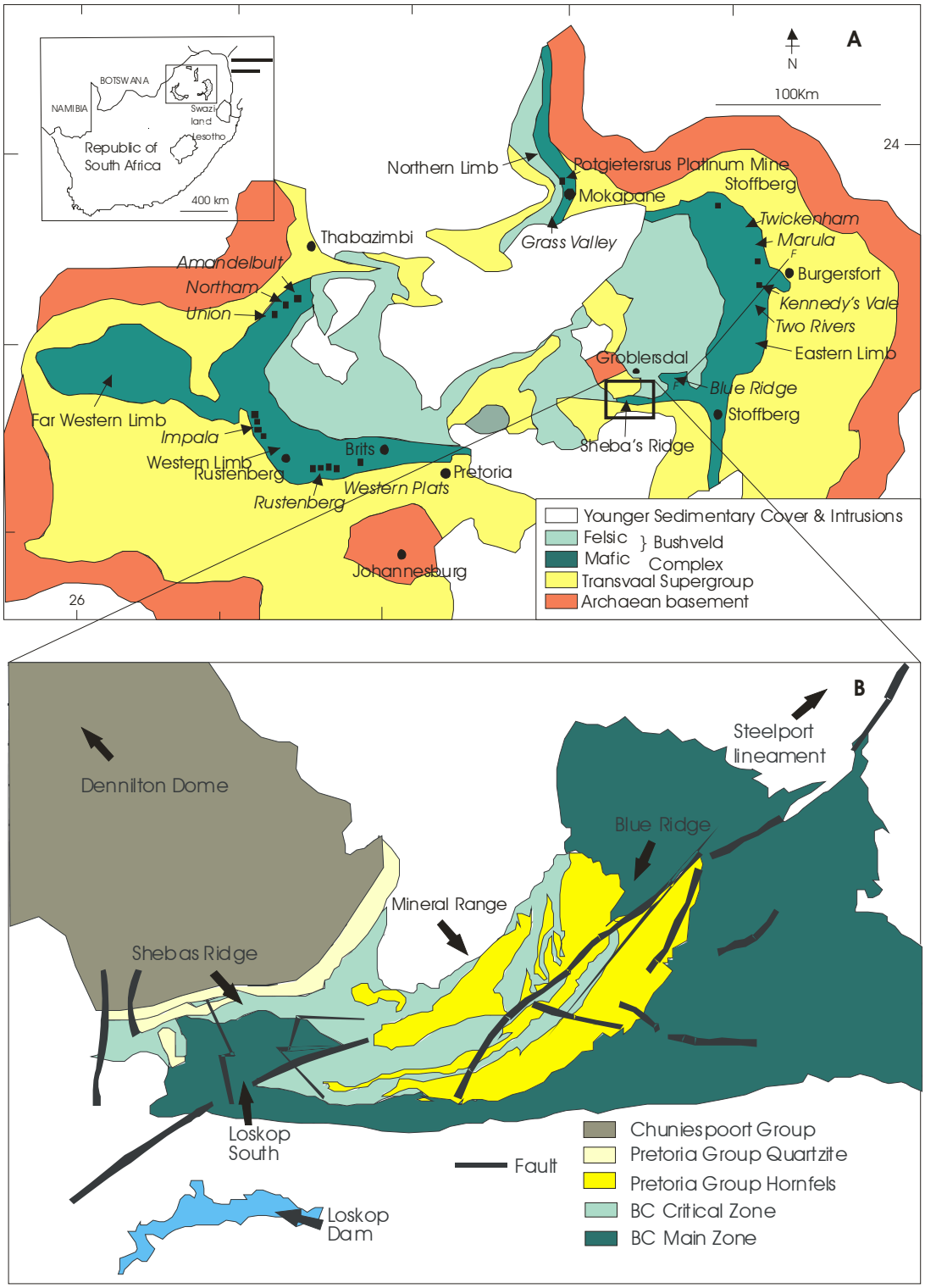

Figure 2.1 A) Schematic geological location map of the Bushveld Complex, South Africa. The current sites of mining and exploration are indicated in italics and Sheba's Ridge is shown in the far south western extension of the eastern limb. B) Schematic map of the regional geology surrounding Sheba's Ridge. The Pretoria Group quartzites form a ridge to the north of the farm Loskop South 53 JS.

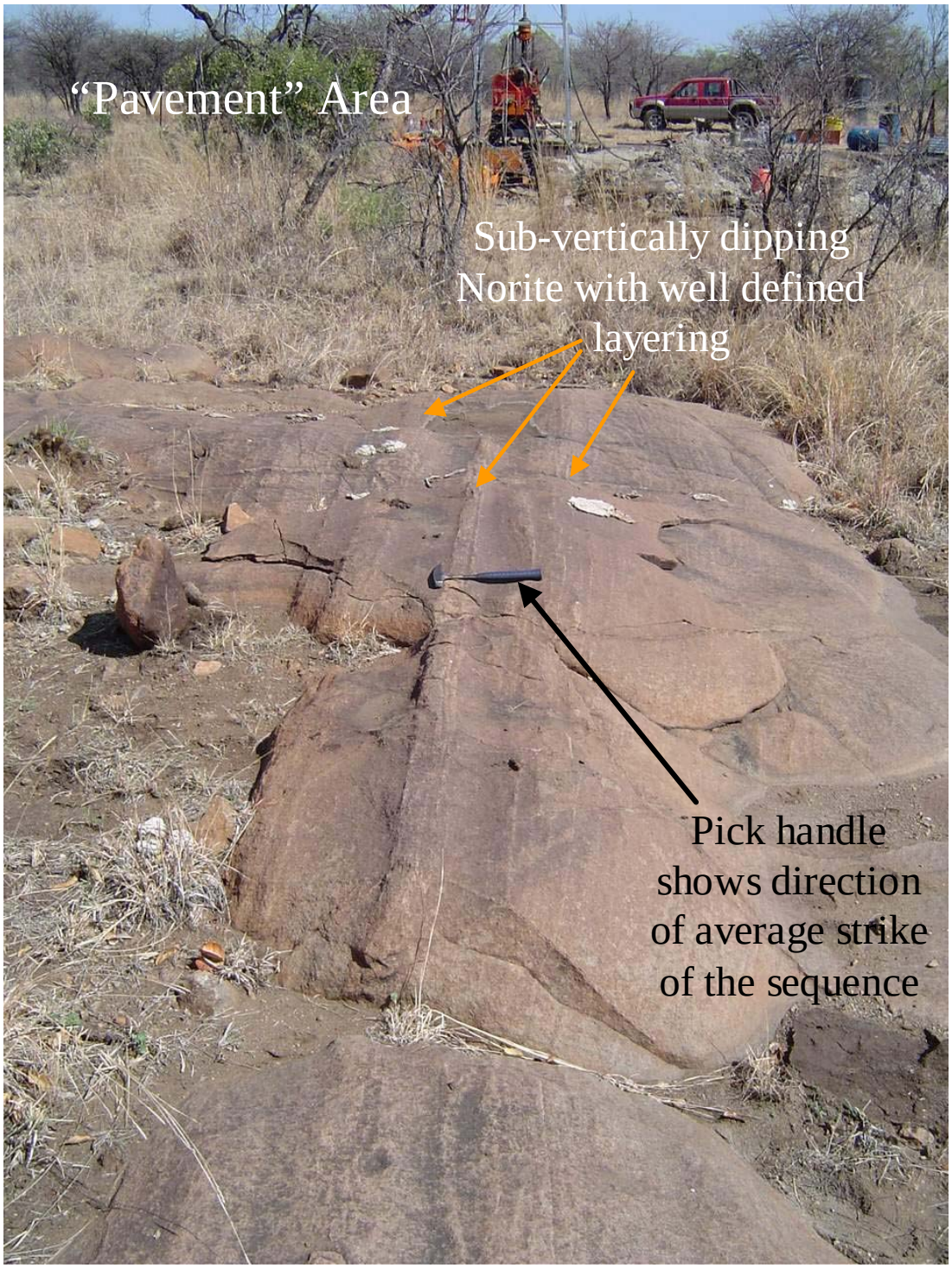

Figure 2.2 'Disorientated' noritic block on the western sector of Loskop South 53 JS. Well-defined layering strikes approximately perpendicular to the regional strike (Roodt, 2004).

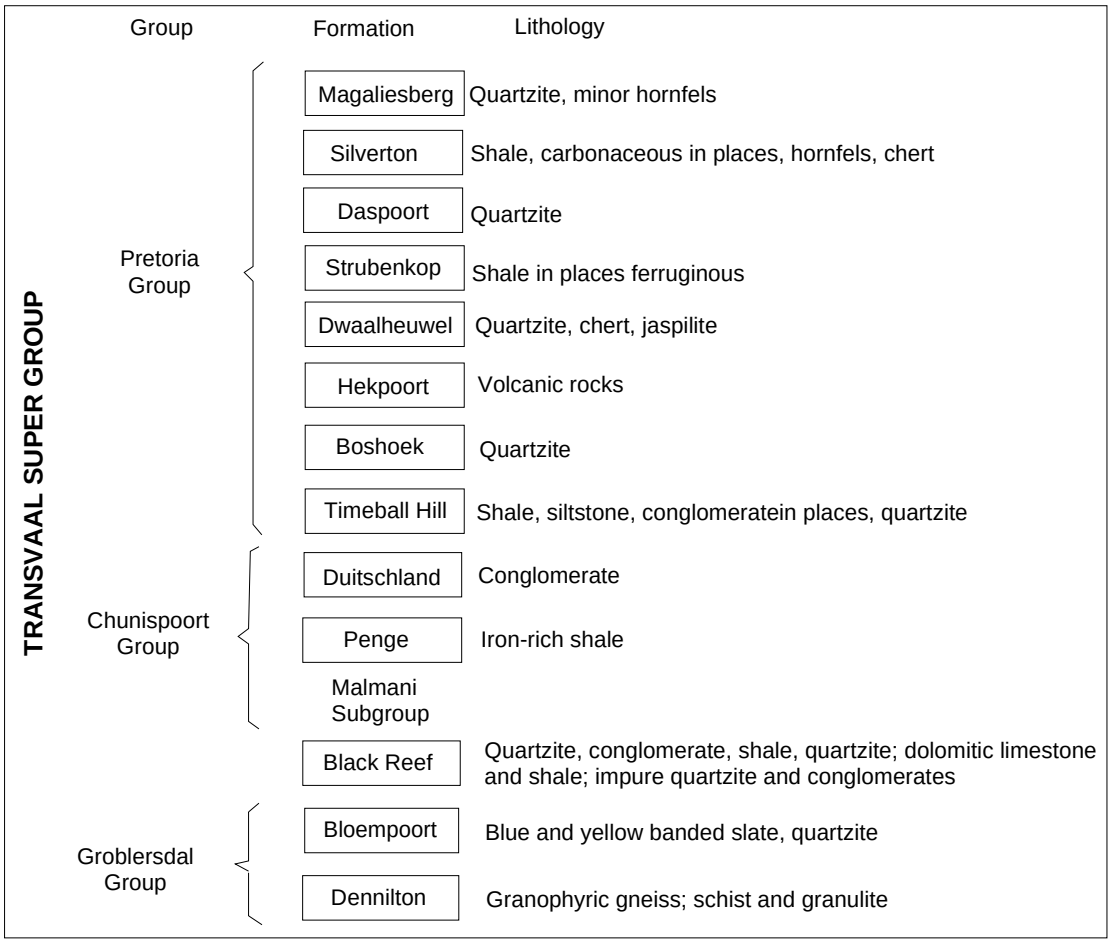

Figure 2.3 A stratigraphic column through the lower Transvaal Supergroup modified from Department of Mines Geological Series 2828 Pretoria.

2.2 Exploration History

The following summary of the exploration history for Sheba's Ridge was taken from Roodt (2004).

> "Initially copper-enriched shear-hosted veins were the focus of the base metal mineralisation at Sheba's Ridge. A relict shaft and adits are evidence for past exploration at unknown times in the past. JCI then began exploration in the early 1980's on the farms Rietfontein 70JS, Loskop Suid 63JS and Kameeldoorn 71JS. Initial work using soil geochemical surveys for Cu, Ni and Cr delineated

discontinuous E-W trending anomalies on the northern side of Sheba's Ridge. Ground geophysics delineated a continuous E-W striking sulphide zone only when a dipole-dipole IP survey was conducted due to the depth of burial. The discovery of this sulphide zone refocused the target for exploration from base metals to platinum-group metals (PGM) and the project was taken over by Rustenburg Platinum Holdings (then part of the JCI group). A one-metre thick chromite layer thought to be analogous to the UG2 was intersected but this was found to be discontinuous along strike. Drilling also delineated a mineralised feldspathic pyroxenite on the eastern side of Loskop Suid 53 JS. However, at this stage exploration at Sheba's Ridge was discontinued as PGE values and Pt:Pd ratios were more favourable on the Platreef in the northern limb (BC) at Potgietersrus. Buchanan demarcated a geologically continuous Lower Mineralised Zone with cryptic variation in orthopyroxene composition towards the lower contact with the floor. Davenport indicated a continuous zone of low-grade mineralisation 13.4 m thick along 4 km of strike whilst Nowak estimated a 7.7 to 39 m thick 'Platreef', which became the target of exploration by Ridge Mining (formally Cluff Mining) in early 2001."

2.3 General geology of Sheba's Ridge

The generalised stratigraphic sequence on the farm Loskop South 53 JS is shown in Figure 2.4. A summary of the sequence follows and has been taken from information from all 5 boreholes and observations made in the field. A detailed description of each borehole is given later in this chapter.

Unit 1 at the base comprises fine-grained norites interfingered with hornfels and metaquartzite floor rocks.

Unit 2 is unconformable on the basal Unit 1. It is the main mineralised unit in the stratigraphic succession. It is comprised of orthopyroxenites with varying proportions of accessory olivine, plagioclase, clinopyroxene, magnetite and phlogopite. It is a sulphide-bearing unit where the occurrence of sulphides is variable and maybe disseminated, net-textured (usually associated with altered olivine-bearing horizons), interstitial and blebby or with a combination of textures. Fine-grained quartz-bearing norites and gabbronorites are localised and occur as sills at the base of Unit 2 and into the floor rocks of Unit 1.

Unit 3 comprises norite-pyroxenite interlayers with 'enclaves' of disoriented blocks of norite, chromitite and anorthosite.

Unit 4 is marked by a distinctive mottled anorthosite at the base, with thick gabbronorites above.

The basal mineralisation (within Unit 2) was intersected in all of the 5 boreholes studied. The upper mineralised intervals in Unit 3 are only present in boreholes LSD34, LSD22, LPR8/15 and LPR6/12. However, not all of the upper mineralised units identified throughout the property are present in all of these boreholes. It is unclear as to whether these zones of mineralisation are strike continuous on the farm Loskop South 53 JS from this data alone. As the exploration program by Ridge Mining was concentrated on the basal mineralisation this study is predominantly concerned with this mineralised interval.

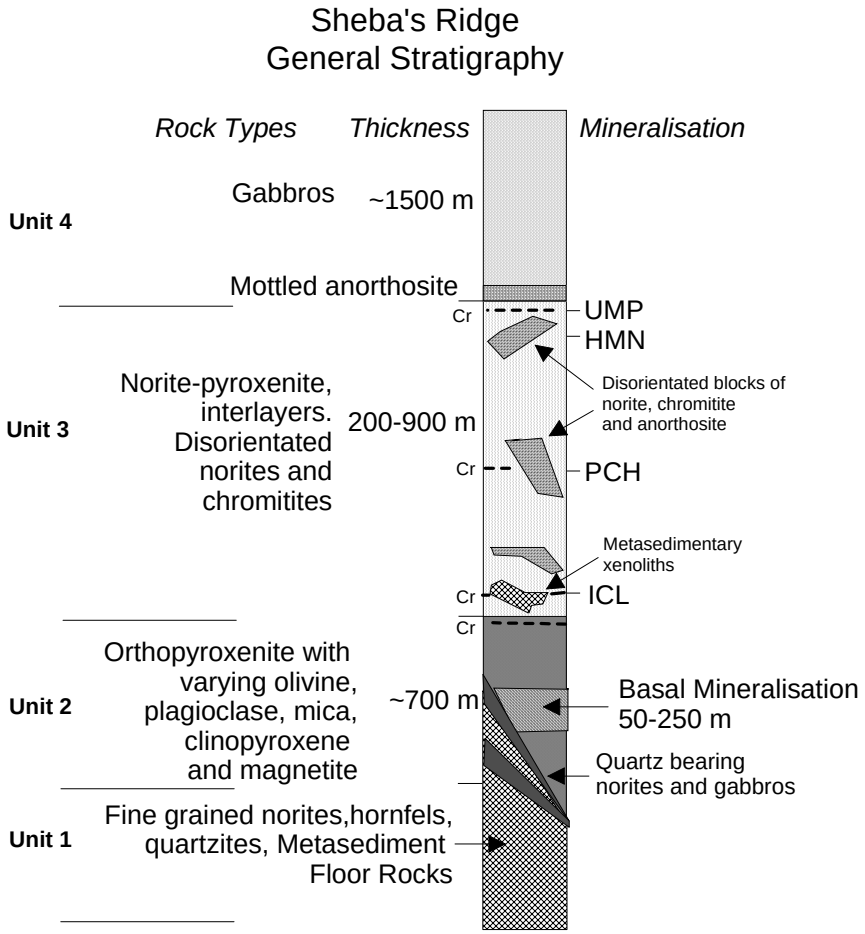

Figure 2.4 Generalised stratigraphy showing mineralisation within the stratigraphic sequence on the farm Loskop South 53 JS. The focus of this study, the basal mineralisation (Unit 2), onlaps floor rocks in the west and is variable in composition and texture up dip and along strike. The hanging wall norite and varying footwall lithologies are often sulphide-bearing. Chromitite layers in Unit 2 are often discontinuous and were found in outcrop to be orientated perpendicular to the regional strike. The mineralised cyclic units towards the top of Unit 2 are bimodal rather than complete cycles and it is unclear if layers within the unit correlate along strike. Modified from Roodt (2004).

2.4 Basal Mineralisation at Sheba's Ridge

The basal mineralisation at Sheba's Ridge is a ~50 - 250m thick strike-continuous Ni-Cu-PGE deposit. Host rocks are comprised of predominantly orthopyroxenite with varying olivine, plagioclase, mica, clinopyroxene and magnetite. Outcrop is arcuate and occurs across

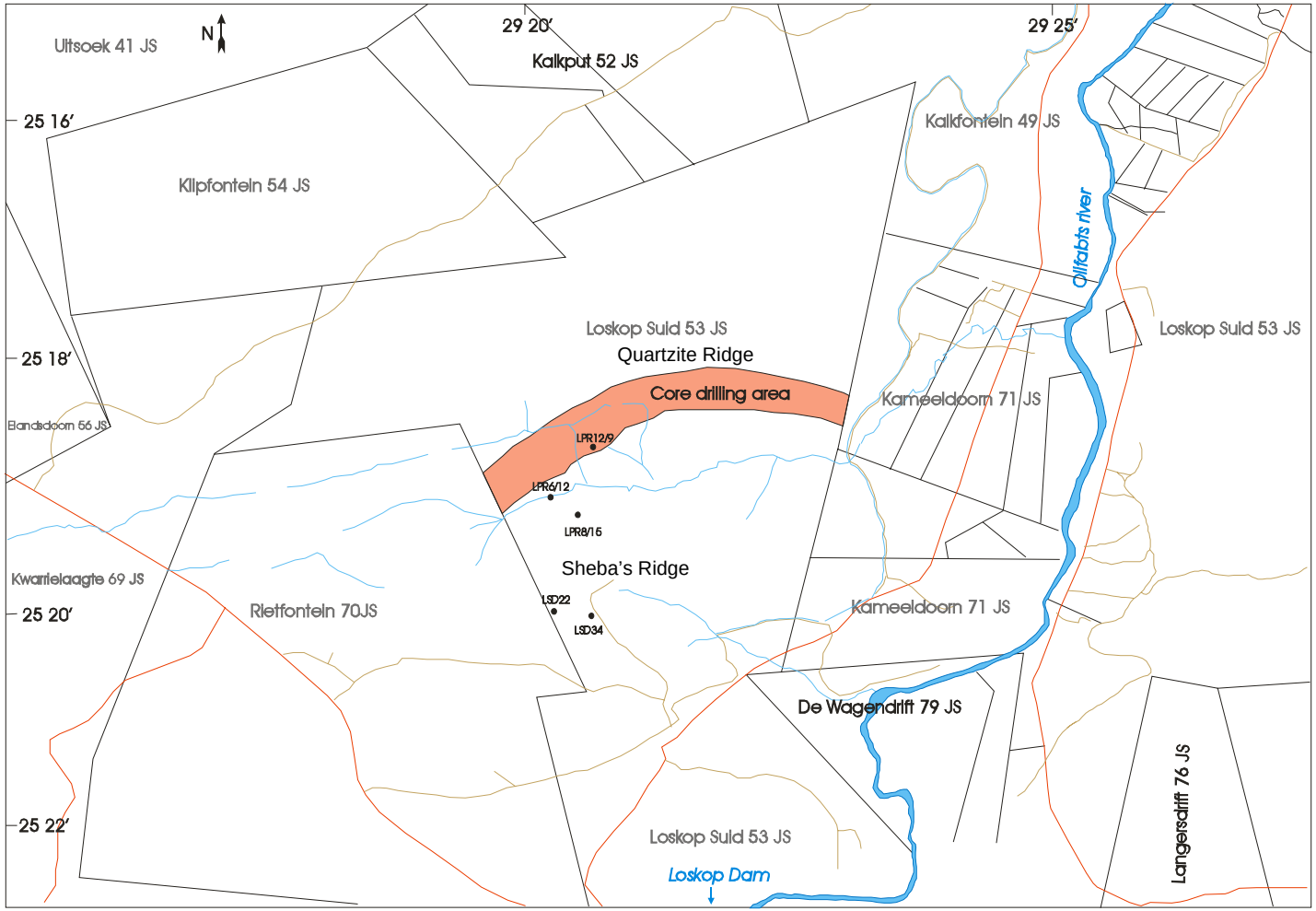

Figure 2.5 Positions of boreholes on the farm Loskop South 53 JS. LSD34 and LSD22 are located on the southern side of Sheba's Ridge. LPR6/12, LPR8/15 and LPR12/9 are located updip through the ultramafic-mafic layered rocks. The perennial Olifants river has ephemeral eastwardly-flowing tributaries through the field area. The main access road to the farm Loskop South 53 JS is the N11 running NE-SW to the east of the farm.

the centre of the farm Loskop South, south of the quartzite ridge (Figure 2.5). The contact with the floor rocks is undulatory and the mafic intrusives accumulated in a basin on the periphery of the Dennilton and Rietfontein domes. Fire assay analyses from extensive drilling demarcated a three peaked profile of the mineralisation termed the 'lower sulphide zone', the 'sulphide zone' and the 'upper sulphide zone'. These terms were introduced as the nature of the deposit has not been documented in the BC. In summary, the mineralisation is not a stratiform ore body. It is a sulphide-bearing zone, peripheral to the eastern limb. where sulphides are hosted in a 50 – 250 m thick package of ultramafic-mafic rocks. These rocks are in contact with floor rocks and include sedimentary xenoliths.

2.5 Other Mineralised Intervals at Sheba's Ridge

A number of mineralised units occur above the basal mineralisation (Figure 2.4). These are in ascending order: the intermediate chromite layer (ICL), possibly equivalent to the lower or middle group chromitites of the BC; the Platchro (PCH), possibly analogous to the middle group chromitite of the BC; the hanging wall mineralised norite (HMN) and the upper mineralised pyroxenite (UMP) possibly analogous to the Merensky Reef (Sharpe *et al.*, 2002).

2.6 Sampling procedure

Samples were taken from 5 boreholes on the farm Loskop South 53 JS (Figure 2.5). Detailed descriptions of the boreholes logged in this study are given in Appendix 1. Boreholes LSD34 and LSD22 were logged to display a comprehensive stratigraphic representation of the area. They are both situated on the southwestern section of the farm Loskop South 53 JS on the southern side of Sheba's Ridge. The prefix LSD is from the initial phase of drilling on Loskop South and refers to Loskop South Drilling (LSD). Borehole LPR8/15 was chosen to

enable analysis of the 'disorientated' noritic block found in outcrop. Boreholes LPR12/9 and LPR6/12 were chosen to facilitate representative sampling of the basal mineralisation. LPR12/9 was drilled directly into outcrop of the mineralised reef and LPR6/12 was collared into hanging wall norites and is considered to sit on a floor rock high. The prefix LPR refers to the second phase of exploration drilling that concentrated on the basal mineralisation which was informally referred to as the Loskop Plat Reef (LPR). As there are major variations up dip and along strike it is necessary to consider each borehole individually before any correlation can be attempted.

2.7 Borehole LSD34

Borehole LSD34 is situated on the southern flanks of Sheba's Ridge and was collared into the homogeneous gabbronorites that form the ridge (Figure 2.5 & 2.6). Vertical diamond drilling intersected floor rocks at 675 m and the borehole was drilled to a depth of 760 m. In Unit 1 at the base, heavily altered calcsilicate metasediments are inter-layered with fine-grained quartz –bearing gabbronorites/norites. Contacts between these units are sharp. Above this at 696 m depth, a 8 m thick fine-grained equigranular norite occurs that contains minor disseminated base metal sulphides (BMS). This is considered to be the footwall to the basal mineralisation in this borehole. These rocks are categorised into Unit 1 and comprise the floor rocks and footwall to the mineralisation.

In this borehole the basal mineralisation (Unit 2) lies between 629 m and 671 m. This comprises a sulphidic zone hosted in a variably textured feldspathic pyroxenite and taxitic gabbronorite. Nomenclature is based on the BGS Rock Classification Scheme (Gillespie & Styles, 1999) as shown in Appendix 2. The term taxitic refers to a combination of strikingly different fabrics in one rock. This is due to the presence of intergrown clusters of pegmatitic

to intermediate-grained plagioclase laths and pyroxene (Schissel *et al*, 2002; Sharkov *et al*, 1995). The occurrence of sulphides is not restricted to this zone and they are often found sparsely disseminated in the hanging wall and footwall norites. This unit is categorised as Unit 2 and is defined by the occurrence of Ni, Cu, PGE + Au (SSZ in Figure 2.6). At the base of the mineralisation in Unit 2, mafics are gradually inter-fingered with floor rocks and are altered to varying degrees.

From the hanging wall of the basal sulphide zone to the appearance of the homogeneous gabbronorite forming Sheba's Ridge (stratigraphically above the 'cyclic' units) between 629 m and 193 m is categorised as Unit 3. At the base of Unit 3 between 627 m – 629 m the hanging wall to the mineralisation is a norite and above this there is a complex interaction of feldspathic pyroxenites, taxitic gabbronorites, norites and meta-sedimentary xenoliths. Pyroxenites and taxitic gabbronorites often host magnetite stringers in varying proportions. Sporadic chromitite blebs occur in the pyroxenites. Contacts of norites are generally sharp and often at a high angle. Unit 3 is host to, where present, the upper mineralised zones on the farm Loskop South 53 JS. The upper mineralised zones comprise, in ascending order, the Intermediate Chromitite Layer (ICL), the Lower Mineralised Pyroxenite (LMP), the Platchro (PCH), the Hanging wall Mineralised Norite (HMN) and the Upper Mineralised Pyroxenite (UMP), as defined by Sharpe *et al* (2002). In this borehole the UMP was identified as a mineralised zone of pyroxenite-norite-anorthosite 'cyclic' units hosting BMS that occurs towards the top of Unit 3 between 233 m and 293 m (Figure 2.6). An attempt was made to identify the number of 'cyclic' units that occur in this zone (Figure 2.7). However, the units are often incomplete i.e. they do not contain a full chromite-pyroxenite-norite-anorthosite cycle. Instead a bimodal trend is recorded e.g. pyroxenite-norite-pyroxenite. It is also

unclear as to whether each layer correlates from borehole to borehole on Loskop South 53 JS. The top of this unit is at a depth of 193 m.

Unit 4 comprises a thick package of homogeneous gabbronorite with giant mottling and extends from 193 m to the top of the borehole.

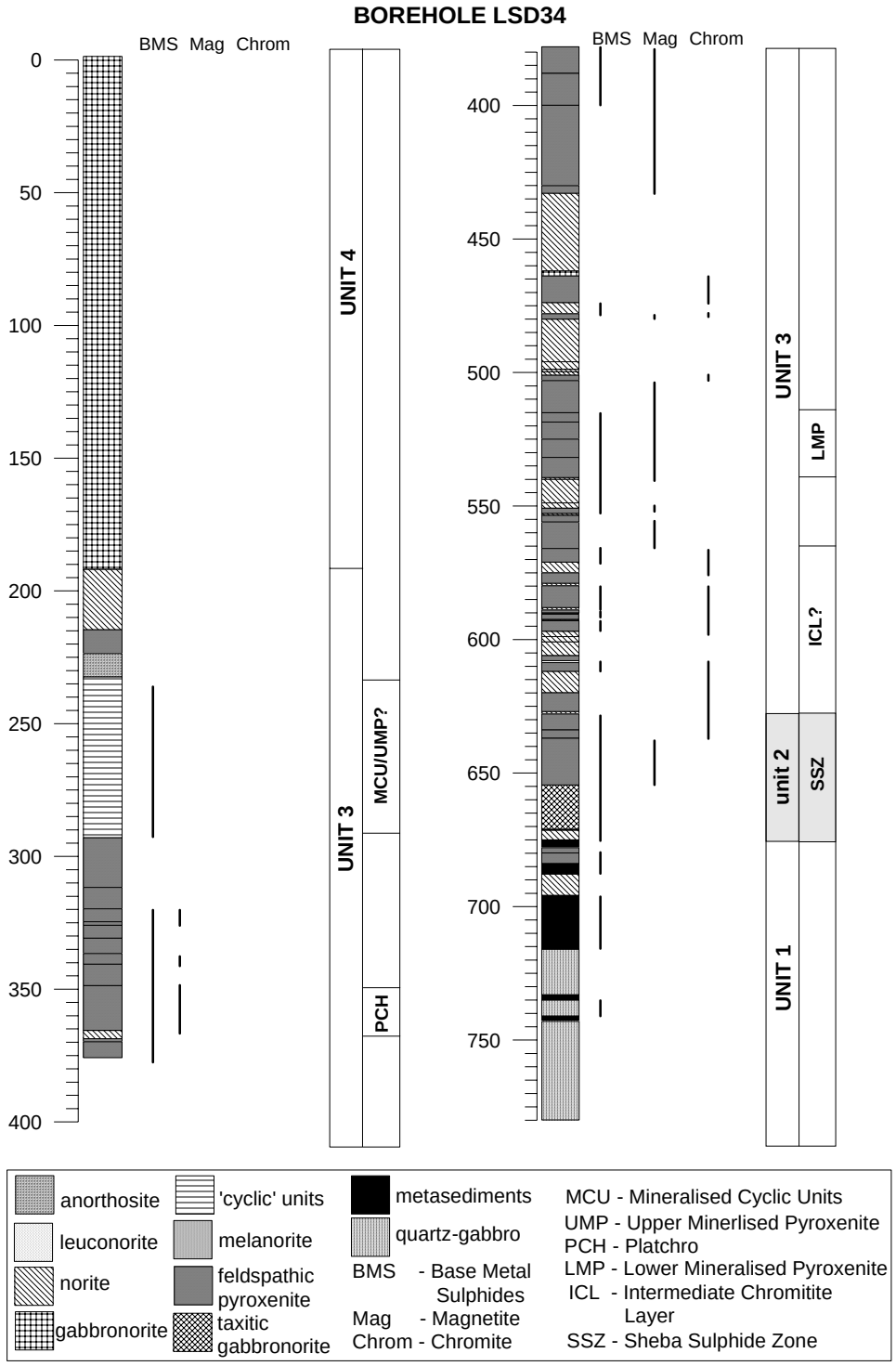

Figure 2.6 Borehole log for LSD34 showing base metal sulphide, chromite and magnetite occurrences through the sequence. Sub-divisional units and nomenclature for the mineralised units demarcated by Ridge mining are indicated. Detailed core descriptions are presented in Appendix 1A.

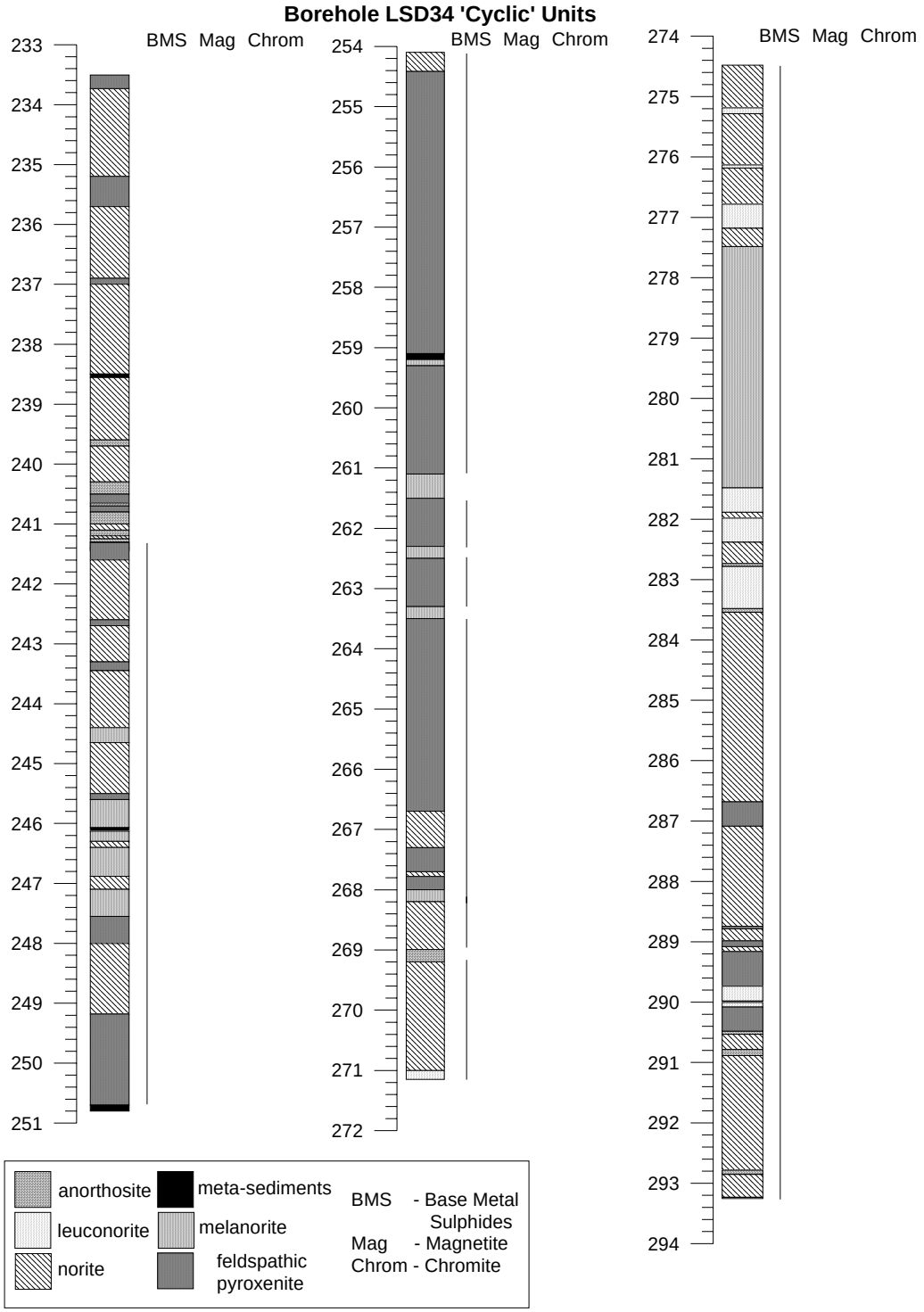

Figure 2.7 Detailed borehole log through the 'Mineralised Cyclic Unit' (MCU) of LSD34, showing the occurrence of base metal sulphides, magnetite and chromite in the sequence. The 'cyclic' units are not complete and show a bimodal trend (pyroxenite-norite-pyroxenite) rather than full cyclicity, e.g. chromite-pyroxenite-norite-anorthosite.

2.8 Borehole LSD22

Borehole LSD22 was collared into the homogeneous gabbronorites forming Sheba's Ridge and is situated on the southern side of the ridge (Figure 2.5). Vertical diamond drilling intersected floor rocks at 618 m and was stopped at a depth of 680 m (Figure 2.8). Hornfels floor rocks at the base are interlayered with fine-grained quartz-bearing norites and gabbronorites that are altered to varying degrees. The alternating sequence of floor rock and fine-grained 'marginal' rocks extends to a depth of 618 m. At the top of these interlayered rocks a 4 m thick layer of graphite occurs and is the footwall to the basal mineralisation. These meta-sedimentary floor rocks and 'marginal' rocks together comprise Unit 1.

Unit 2 hosts the basal mineralisation (SSZ) and occurs between 545 to 606 m. The host rock predominantly comprises a medium-grained feldspathic pyroxenite. However, grain size is variable and an acicular texture of pyroxenes is often developed. Zones of taxitic gabbronorite occur where plagioclase content increases significantly and textures are highly variable. Hornfels xenoliths are common through the basal mineralisation. Base metal sulphides occur throughout and in general decrease in abundance at the margins of xenoliths. Chromite blebs occur sporadically in feldspathic pyroxenites. Minor layers of fine-grained norite occur and always have sharp contacts. Magnetite stringers are present towards the top of the sulphide-bearing zone. Mica occurs to varying proportions throughout this unit. Through the 73 m thick sulphide-bearing basal mineralisation there is varying degrees of alteration and a wide variability of mineralogy and texture in the host mafics.

The hanging wall to the mineralisation is a 16 m thick mottled and spotted norite between 529 m and 545 m. The contact at the base is sharp and there are no BMS. This hanging wall norite is the base of Unit 3, which comprises a complex interaction of pyroxenites, norites,

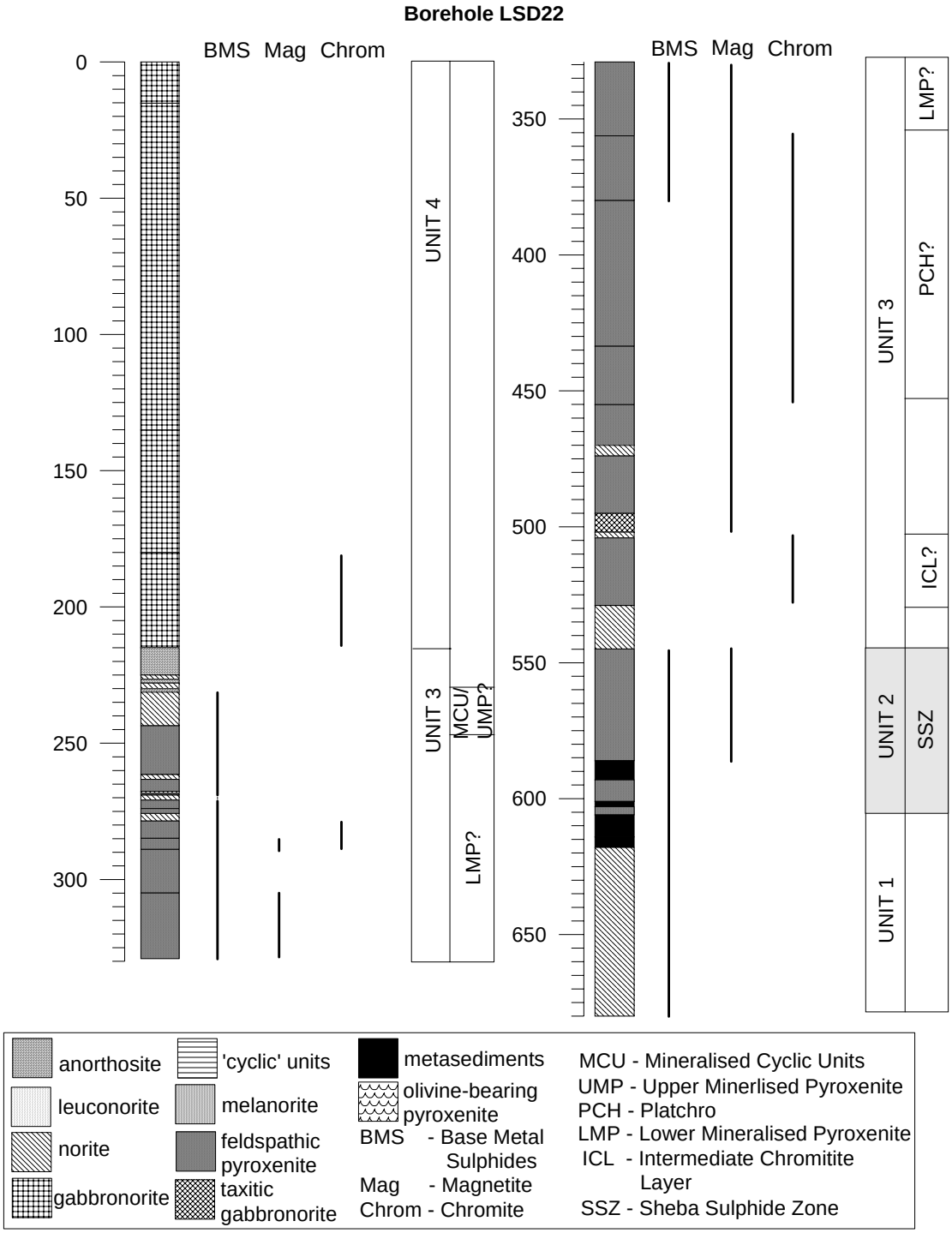

Figure 2.8 Borehole log of LSD22 showing the occurrence of base metal sulphides, magnetite and chromite in the sequence. Allocated sub-divisional units and suggested nomenclature of mineralised units are indicated. 'Cyclic' units towards the top of Unit 3 occur on a metre scale and are more clearly described in Appendix 1B.

and country rock xenoliths. In this borehole the ICL was not identified. There is however, a feldspathic pyroxenite with a taxitic texture between 502 m to a depth of 529 m that is host to sporadic chromite blebs which could be potentially correlated to the ICL. The PCH is defined by the occurrence of chromite as blebs and 4 chromitite layers in a feldspathic pyroxenite which occurs at a depth of 358.17 m to 365.43 m. Base metal sulphides are disseminated and increase in concentration in this unit. Magnetite stringers occur in the pyroxenites. A second PCH was postulated to occur at a depth of 267.96 m to 314.42 m. Here chromite blebs occur sporadically through a feldspathic pyroxenite. Grain size is variable and magnetite stringers and BMS occur throughout. A 4 m thick magnetitite layer occurs from 285 m to 289 m. The top of the PCH is marked by a hanging wall norite with an overlying anorthosite at a depth of 267.96 m. Base metal sulphides are sparsely disseminated throughout the PCH. Above this the UMP occurs to a depth of 243.15 m. The UMP is in general, an homogenous sulphide-bearing medium-grained feldspathic pyroxenite. The top of the UMP has a sharp contact and is overlain by cyclic units of norite-anorthosite on a scale of ~ 2 -3 m. The top of Unit 3 is marked by the appearance of an homogeneous mottled gabbronorite at 135 m which extends to the top of the borehole and represents sub-divisional Unit 1.

2.9 Borehole LPR6/12

Borehole LPR6/12 was collared into gabbronorite/norites of Unit 4 on the central-western sector of the farm Loskop South 53 JS (Figure 2.5). Vertical diamond drilling intersected floor rock at 220 m and was drilled to a relatively shallow depth of 254 m (Figure 2.9). This is because of the occurrence of a floor rock high which was interpreted from the relatively shallow depth of the floor rocks at 220 m. At the base of Unit 1 a 30 m thick hornfels lies

beneath a mixed zone of calcsilicate metasediments and interlayered pyroxenites. The pyroxenites are heavily altered and original textures are unrecognisable.

The basal sulphide-bearing Unit 2 is between 178 m and 220 m and is characterised by the appearance of disseminated, chalcopyrite, pyrrhotite, pentlandite and pyrite. It is predominantly composed of a medium-grained, locally olivine-bearing equigranular orthopyroxene-dominant feldspathic pyroxenite. Orthopyroxene is equigranular and forms a sugary texture. Olivines are subhedral and contain magnetite within internal fractures. Where clinopyroxene is present a porphyritic texture is developed. Biotite is present and often constitutes a modal proportion of up to ~ 20 % of the rock. In this borehole the basal mineralisation is a 42 m thick sulphidic zone in which sulphides are blebby and disseminated throughout. Magnetite stringers are present below 190 m. Compared to the basal mineralised unit in the other logged boreholes this unit has little alteration.

At the base of Unit 3 the hanging wall norite is 10 m thick at a depth of 168 m to 178 m and has a mottled texture. The basal contact with the underlying mineralised pyroxenites is gradual. There is a gradual decrease of plagioclase with depth where a melanorite is developed. No BMS were recorded in this melanorite. Above this norite in Unit 3 there are pyroxenite/norite interlayers until a depth of 33.5 m. The pyroxenites are variable in texture and magnetite stringers are common. Chromite blebs occur sporadically. Base metal sulphides are present in the lower pyroxenite/norite layers between 165 m and 168 m and towards the top of the unit between 35.2 m and 46 m. These could be the upper mineralised ICL, Platchro and UMP as indicated in Figure 2.9. Norite occurs to the top of the borehole and this is categorised into Unit 3.

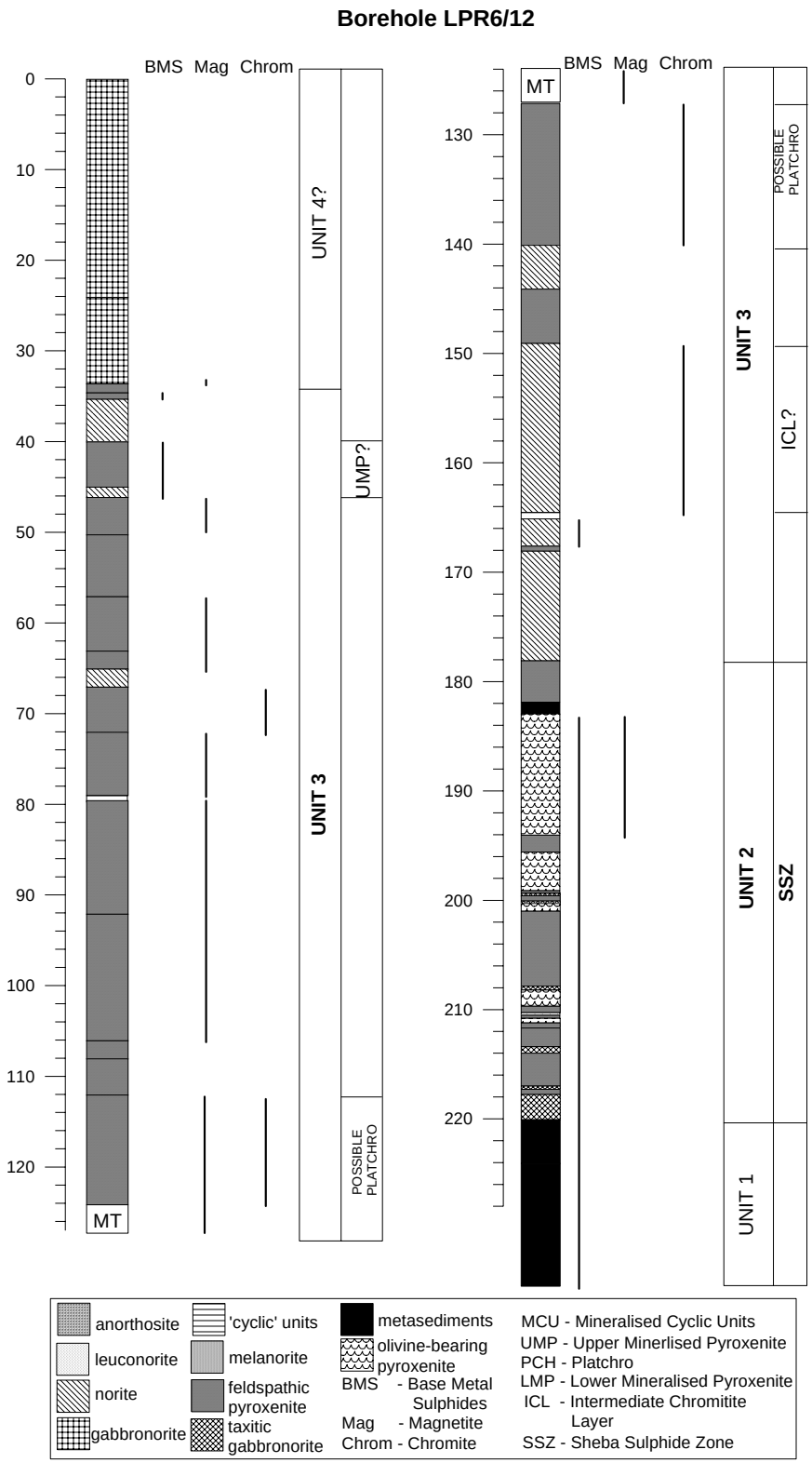

Figure 2.9 Borehole log of LPR6/12 showing the occurrence of base metal sulphides, magnetite and chromite in the sequence. Nomenclature for mineralised zones and allocated sub-divisional units are indicated.

2.10 Borehole LPR8/15

Borehole LPR8/15 is situated on the central-western sector of the farm Loskop South 53 JS and was collared into the 'disorientated' noritic pavement identified in the field (Figure 2.5). Vertical diamond drilling intersected floor rocks at a depth of 390.77 m and was drilled to a depth of 500 m (Figure 2.10). In Unit 1, floor rocks comprise a fine-grained cordierite-hornfels from the base of the borehole to a depth of 465.32 m. Above this a fine-grained quartz-bearing norite is interlayered with irregular layers of calcsilicate and hornfels. The hornfels often contains finely disseminated BMS. Calcsilicate is footwall to the basal mineralisation in this borehole. The basal sulphide-bearing zone (Unit 2) here is ~ 70 m thick and occurs between 320.5 m to 390.77 m. It comprises a heterogeneous feldspathic pyroxenite with interlayers of taxitic gabbronorite and olivine-bearing feldspathic pyroxenite. The term olivine-bearing feldspathic pyroxenite was developed in the field to describe a feldspathic pyroxenite that has varying proportions of olivine. Alteration to serpentine is common. Chromite blebs occur sporadically through the pyroxenites. Base metal sulphides are present throughout this unit with up to 5 modal percent at the base decreasing to ~0.1 % towards the top of the unit.

The base of Unit 3 is a mottled norite which is hanging wall to the mineralisation. Above this in sub-divisional Unit 3 there is a complex interaction of pyroxenite/norite/chromitite layers. Pyroxenites are heterogeneous and taxitic gabbronorite is often developed. Magnetite stringers occur in the pyroxenites and olivine-bearing pyroxenites. Six chromitite layers were recorded at depths, in ascending order, of 294.51 - 294.05 m, 293.52 - 292.33 m, 182.69 - 182.63 m, 170.96 - 170.90 m, 169.66 - 169.53 m and 117.03 - 116.61 m.

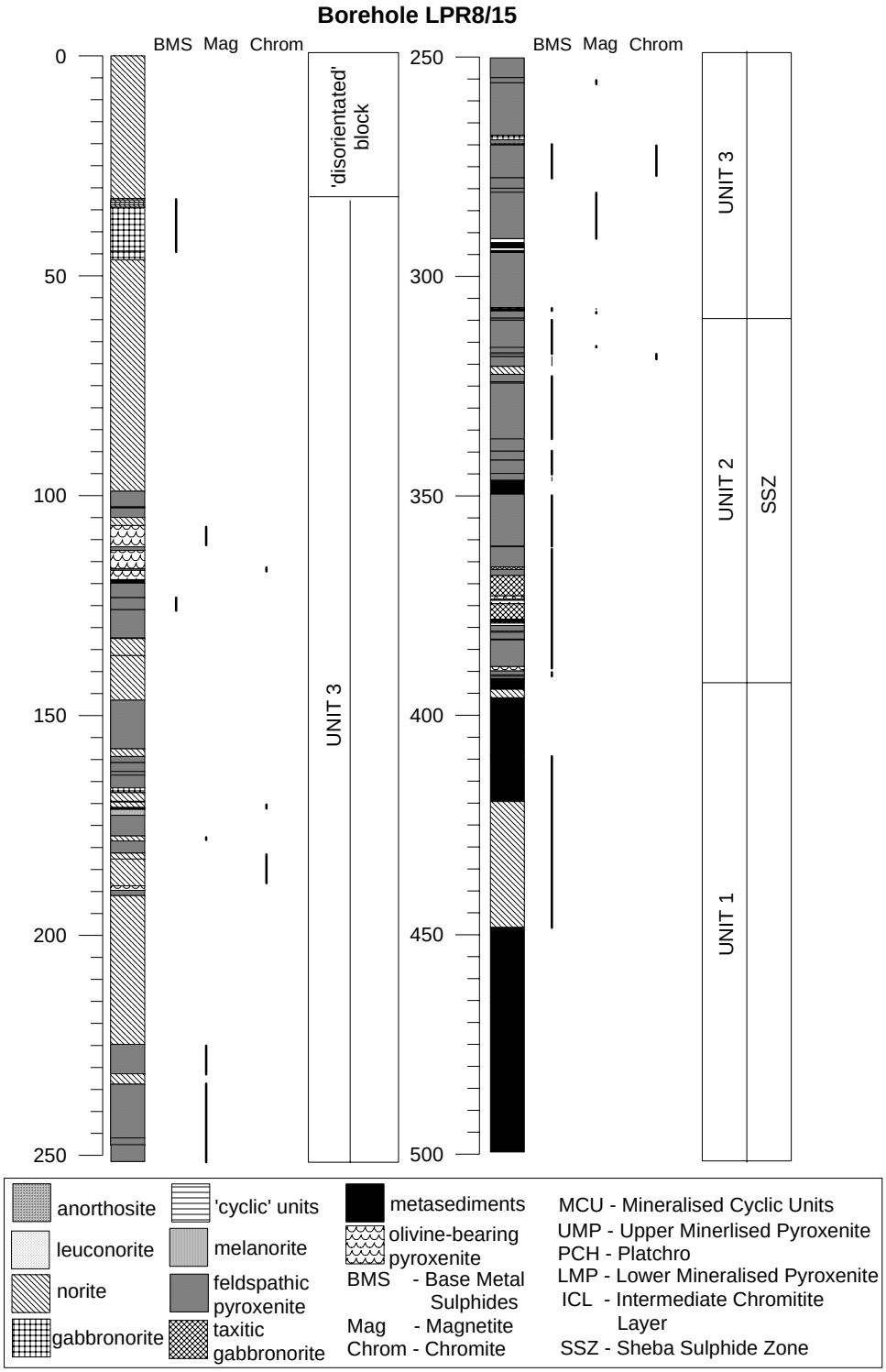

Figure 2.10 Borehole log of LPR8/15. The 'disorientated' block, at the top of the core the occurrence of base metal sulphides, magnetite and chromite, the allocated sub-divisional units and nomenclature for mineralised units are all indicated.

Sulphide bearing zones occur between 307.67 to 317.27 m, 270.05 to 277.19 m and 123.22 to 125.96 m. This borehole was collared into the 'disorientated' noritic pavement which extends to a depth of 35.52 m. The 'disorientated' block was identified by the field team when a well layered norite was found in outcrop and exposed an approximately 200 x 400 m pavement. The well defined layering had a strike perpendicular to the regional strike.

2.11 Borehole LPR12/9

Borehole LPR12/9 is situated in the northern sector of the farm Loskop 53 JS and was collared into the mineralised Unit 2 (Figures 2.5). Vertical diamond drilling intersected floor rocks at 293 m and was drilled to a depth of 350 m (Figure 2.11). Floor rock is a hornfels and is 50 m thick at the base of the core. A 3 m thick fine-grained quartz-bearing norite occurs towards the top of the hornfels. These represent Unit 1 in this borehole.

Unit 2, which extends to a depth of 293 m, is predominantly a heterogeneous olivine-bearing pyroxenite with sulphides present throughout. Magnetite layers and stringers occur throughout this basal mineralisation.

2.12 Summary

The subdivisions of Units 1-4 were developed by the field team at Sheba's Ridge. From the boreholes studied it is clear that the sequence at Sheba's Ridge can be subdivided on a macro scale into these sub-divisional units. However, correlation between individual layers within these units becomes difficult. The basal mineralisation was intersected in all of the 5 boreholes studied. The upper mineralised intervals are only present in boreholes LSD34, LSD22, LPR8/15 and LPR6/12. However, not all of the upper mineralised intervals identified throughout the property in general are present in all of these boreholes. It is

unclear as to whether these zones of mineralisation are strike continuous on the farm Loskop South 53 JS from this data alone.

Unit 1 includes an interfingering of fine-grained quartz-bearing norites and gabbronorites with floor rock metasediments. The top of Unit 1 is marked by the appearance of the sulphide-bearing pyroxenites of Unit 2.

In Unit 2 the composition of the host rocks varies from olivine-bearing feldspathic pyroxenite to orthopyroxene dominant pyroxenite to taxitic gabbronorite. There is a hanging wall norite to the basal mineralised unit in all of the boreholes.

Unit 3 comprises norite-pyroxenite interlayers with 'enclaves' of disoriented blocks of norite, chromitite and anorthosite. The thickness of Unit 3 is variable and it is host to a number of mineralised intervals that do not appear to be continuous along strike. Unit 4 is marked by a distinctive mottled anorthosite at the base, with thick gabbronorites above that form Sheba's Ridge in the south of the farm Loskop South 53 JS. The depths at which the upper mineralised intervals occur have been suggested for each borehole. However, not all of the intervals identified throughout the property in general are present in all of the boreholes. Furthermore, discontinuity of the upper mineralised units was suggested in the field due to the occurrence of discordant chromitite layers that strike perpendicular to the regional strike. In the 5 boreholes studied the basal mineralised unit is present and varies in thickness from 42 m to 293 m. As the exploration program by Ridge Mining was concentrated on the basal mineralisation this study is predominantly concerned with this mineralised horizon. A more detailed description of the rock types found in hand specimen and thin section is given through each stratigraphic interval in chapter 3.

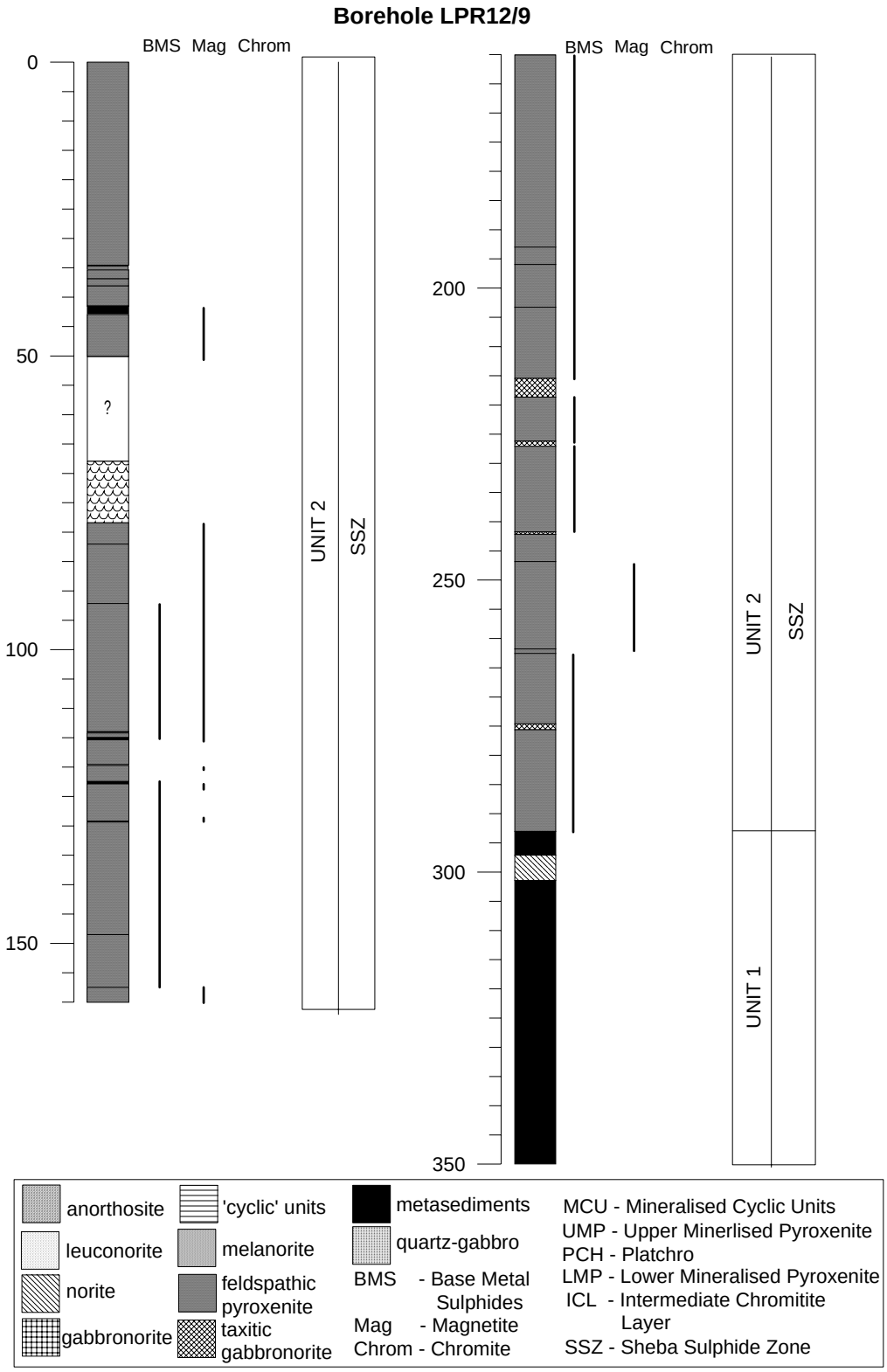

Figure 2.11 Borehole log of LPR12/9. The occurrence of base metal sulphides and magnetite in the sequence are indicated. No chromite occurs in this borehole. This borehole was collared into outcrop of the basal mineralisation zone on Loskop South and therefore there are no rocks representative of Units 3 and 4.

CHAPTER 3

Petrography

3.1 Introduction

The stratigraphic sequence at Sheba's Ridge has been subdivided into 4 units as outlined in Chapter 2 (Figure 3.1). Descriptions of these units in this chapter are based on 135 core samples and 70 thin sections which were selected to be representative of the 'typical' rock types found in the 5 boreholes studied (Figures 3.2, 3.3, 3.4 & 3.5). In summary, the stratigraphic sequence on Loskop South 53 JS consists of floor rock hornfels and micro-norites at the base (Unit 1). Above this ultramafic-mafic rocks host the basal mineralisation at Sheba's Ridge (Unit 2). The contact is gradual and floor rocks and mafics are inter-layered often causing alteration at the base of the mineralised unit. The hanging wall to the basal mineralisation in all boreholes studied is a norite containing inverted pigeonite. Above this there is a complex interaction of pyroxenites and norites (Unit 3). Field evidence suggests that some of these norite interlayers may be xenoliths within the mafic sequence of pyroxenites. Discontinuous chromitite layers were also found to strike perpendicular to the regional strike and may represent xenoliths within the pyroxenites of Unit 3. Country rock metasedimentary xenoliths also occur sporadically throughout this unit. Towards the top of Unit 3 a number of 'cyclic' units occur comprising pyroxenite-norite-anorthosite but are often incomplete cycles. These are capped by a mottled anorthosite. These 'cyclic' units are a common feature of the upper Critical Zone-lower Main Zone boundary of the BC and can be used as a marker horizon. Finally at the top of the sequence a homogeneous gabbronorite occurs forming Sheba's Ridge (Unit 4). This may potentially correlate with the Main Zone of the BC.

Rock types are discussed in accordance to the four subdivisions (Units 1-4). An attempt is made to correlate these rocks to zones within the main Bushveld Complex and with the rock types on the farm Rietfontein 70 JS, situated to the west of Loskop South 53 JS (Crous, 1995). The 'disorientated' noritic pavement intersected in borehole LPR8/15 is compared petrographically to the noritic unit below and with norites below the Merensky Unit in the main Bushveld Complex. A comparison of the succession of rock types found at Sheba's Ridge with that of typical Bushveld Complex stratigraphy is attempted here using this petrographic data.

Nomenclature is based on the BGS Rock Classification Scheme (Gillespie & Styles, 1999) as shown in Appendix 2.

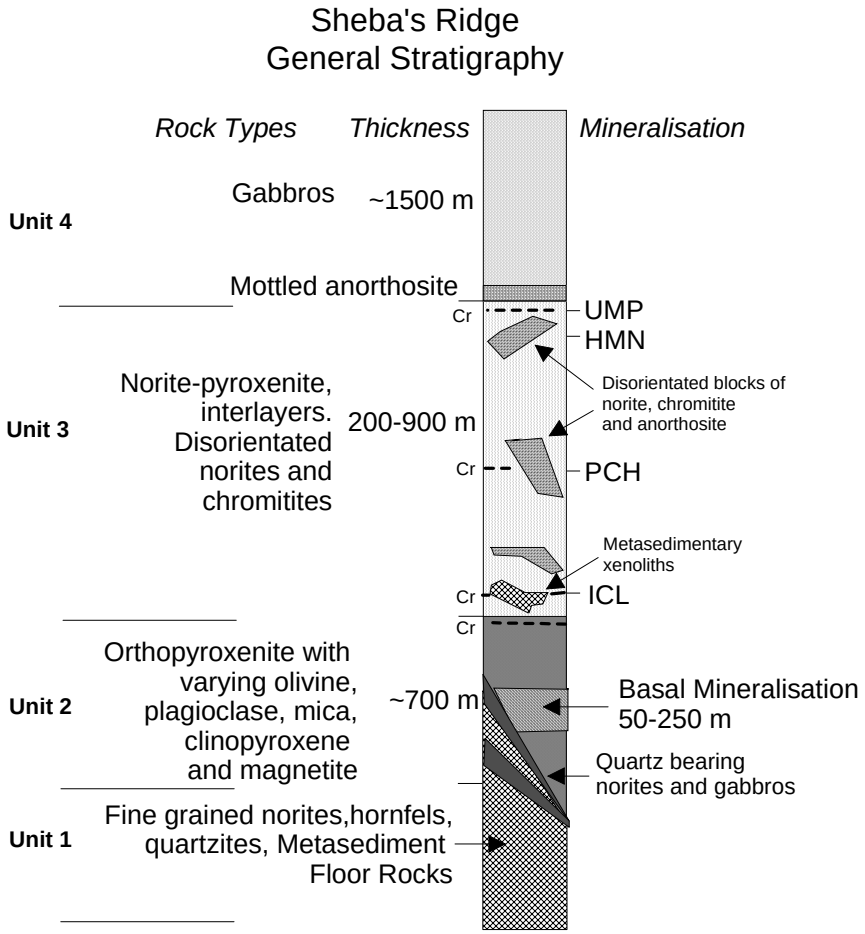

Figure 3.1 Generalised stratigraphy on Loskop South 53 JS. Quartzites, hornfels' and calc-silicates make up the floor rocks in the area (Unit 1). The floor is undulous and as a result onlap of the overlying basic magmatic rocks occur as indicated. Quartz-bearing norites and gabbros intrude the floor and the base of the overlying basal mineralisation (Unit 2). Above Unit 2, discontinuous chromitite layers are hosted by a predominantly noritic zone with pyroxenite interlayers (Unit 3). In this unit 'disorientated' blocks of norite, chromitite and anorthosite occur. These were identified in the field. The base of Unit 4 is marked by the occurrence of a mottled anorthosite that is directly overlain by a thick package of homogeneous gabbronorite that forms Sheba's Ridge.

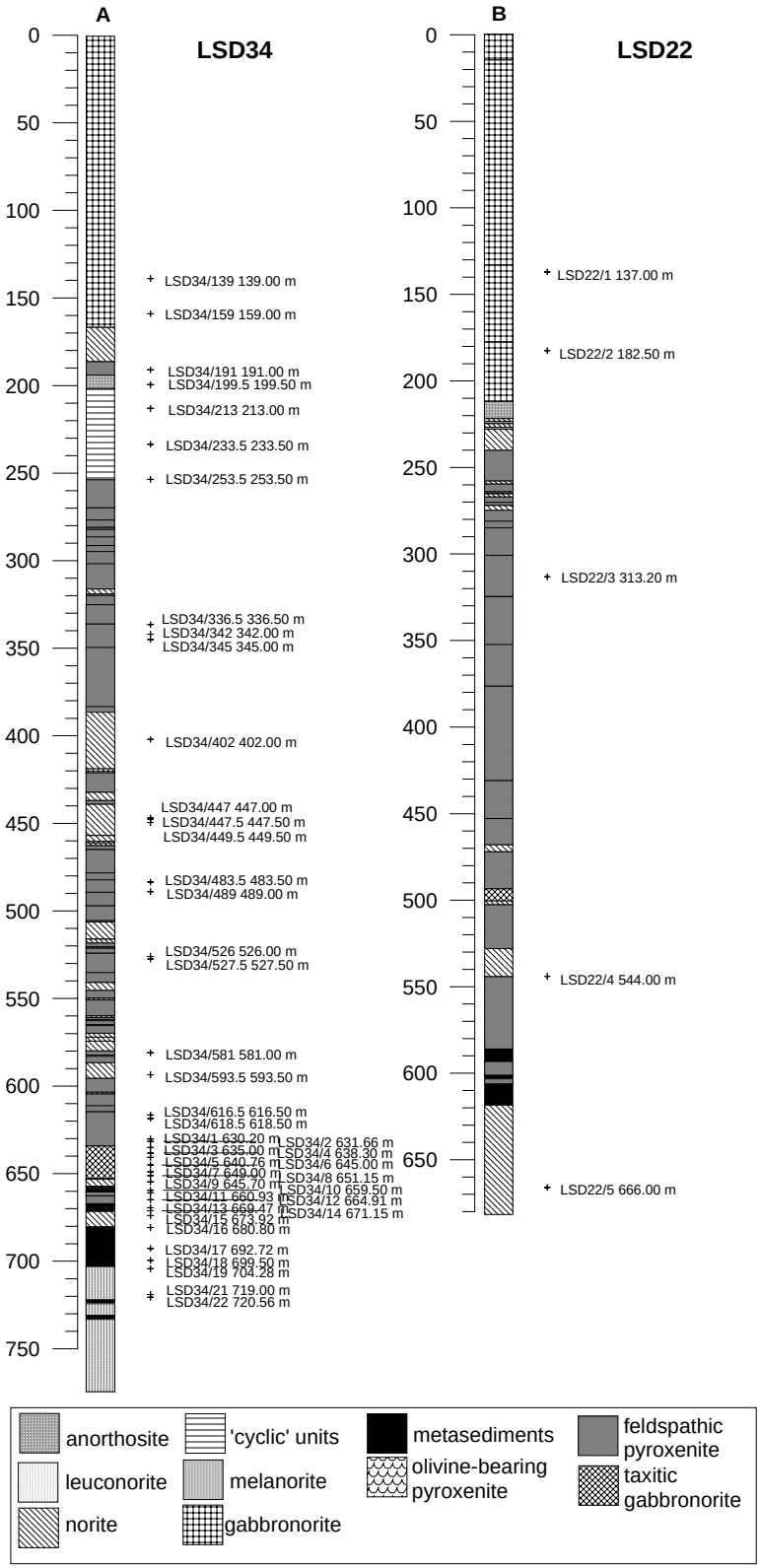

Figure 3.2 Summarised stratigraphic borehole log showing sample number and depth in borehole for A) LSD34 and B) LSD22.

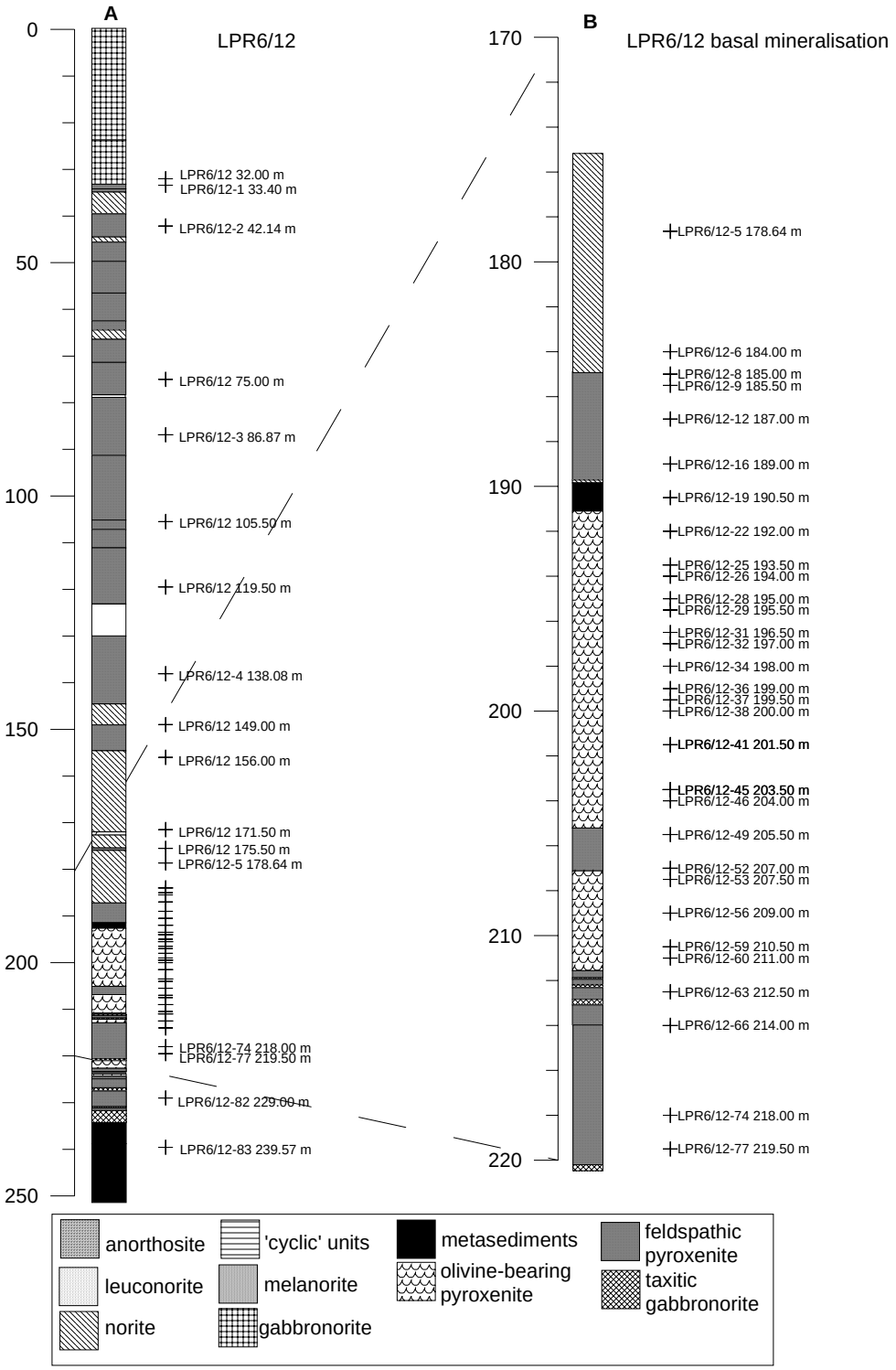

Figure 3.3 Summarised stratigraphic borehole log showing sample number and depth for A) borehole LPR6/12 and B) through the basal mineralisation in borehole LPR6/12.

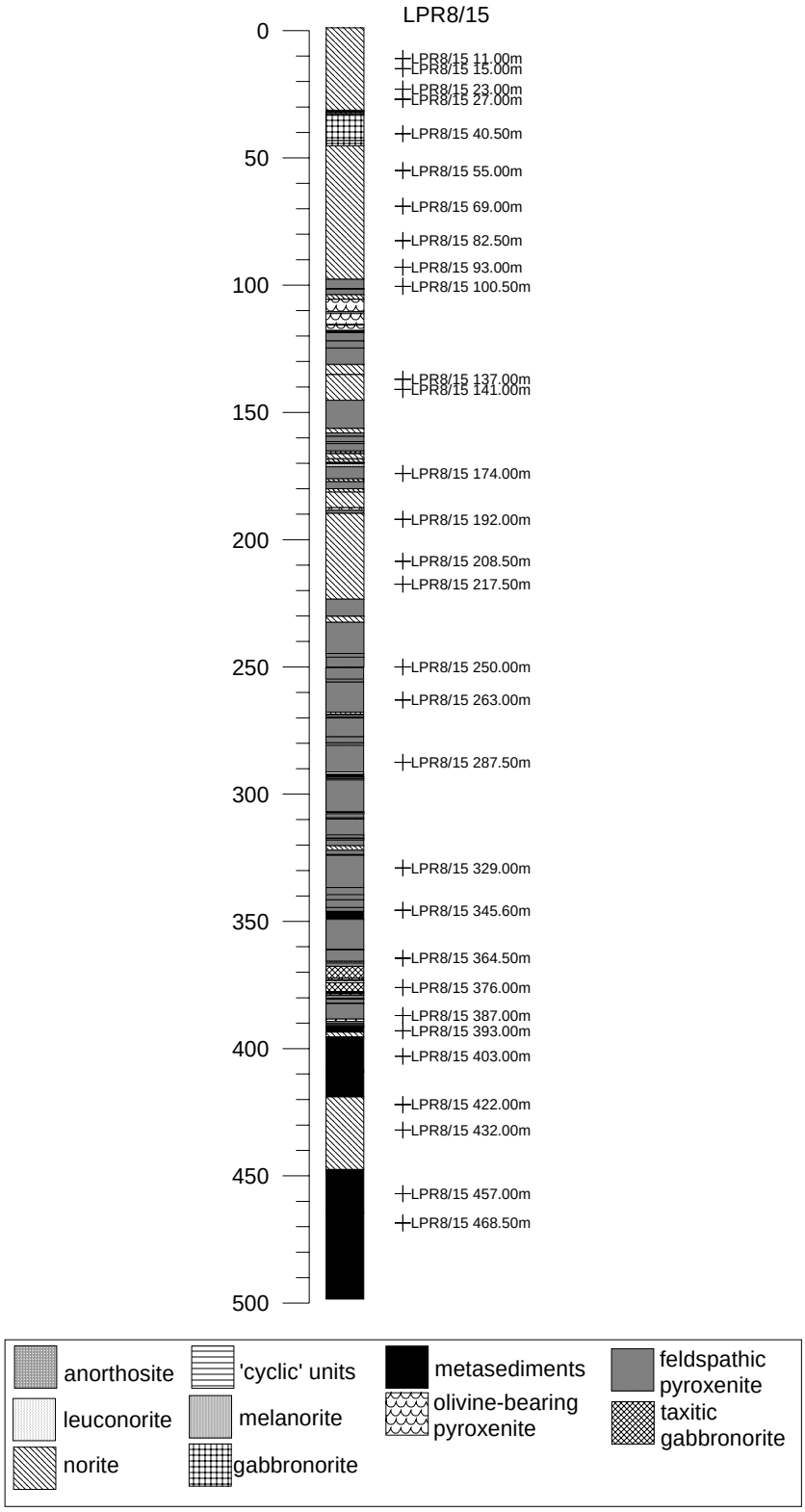

Figure 3.4 Summarised stratigraphic borehole log with sample number and depth for borehole LPR8/15.

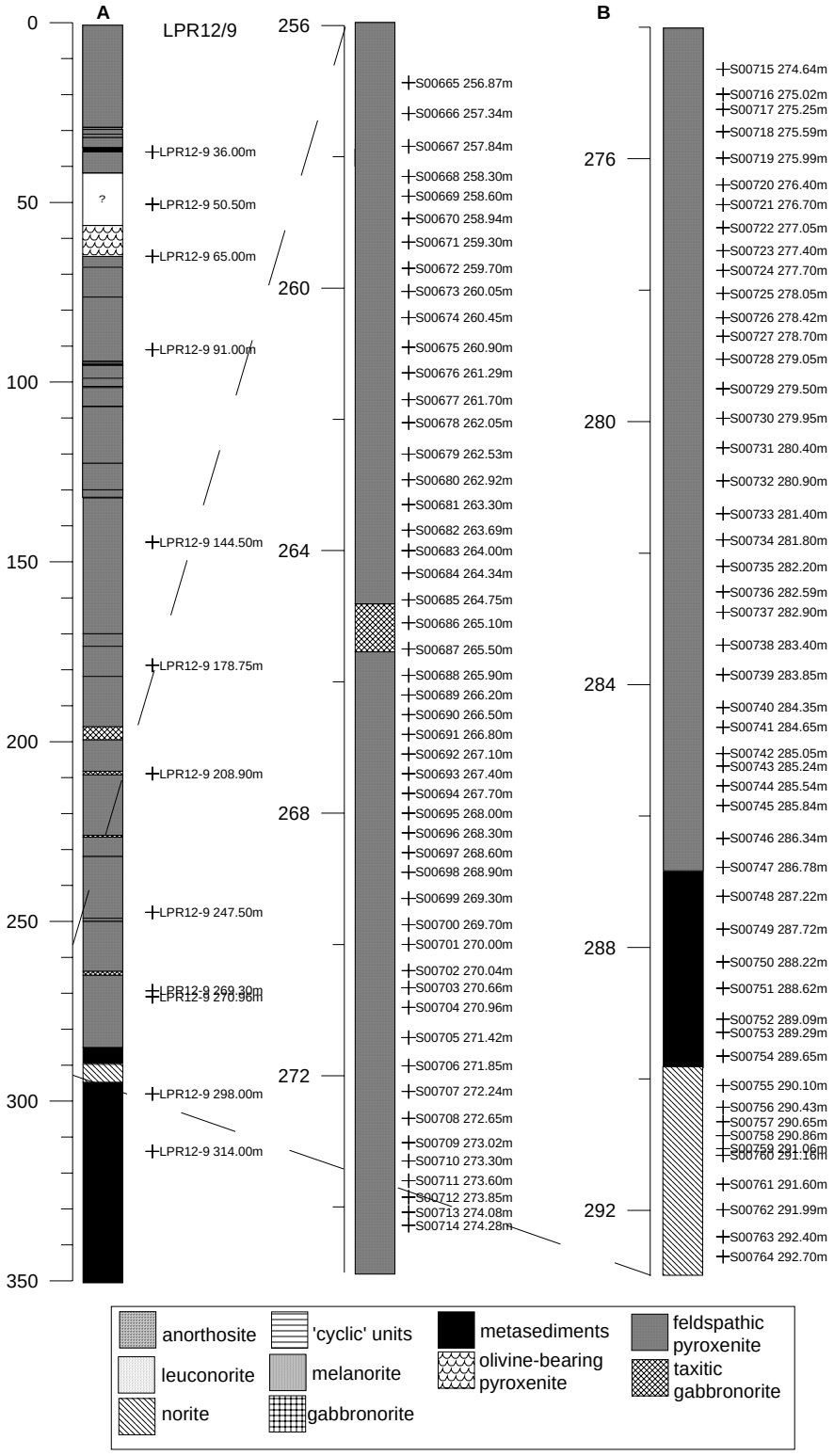

Figure 3.5 Summarised stratigraphic borehole log with sample number and depth for A) borehole LPR12/9, samples taken in this study and B) samples taken by Ridge Mining through the basal mineralisation.

3.2 Floor rocks and Country rock Xenoliths (Unit 1)

A number of metamorphosed shales and calcsilicates occur as floor rocks and xenoliths within the sequence. Sample LPR6/12-82 229.00 m is of a biotite-cordierite hornfels occurring as floor rock on the western sector of Loskop South (Figure 3.3). Whereas, sample LPR8/15 457.00 m is a hornfels xenolith from within a fine-grained norite at the base of the sequence (Figure 3.4).

In thin section porphyroblasts of equant quartz, cordierite and mica are set in a heavily altered very fine-grained greenish coloured cloudy matrix of cordierite (Figure 3.6A). Cordierite is twinned and is distinguished from quartz by the occurrence of pleochroic yellowish halos around inclusions. Pinitisation occurs and forms a cloudy matrix of approximately 40 modal %. A visual estimate of modal proportions is: Quartz 20%, Cordierite 20%, Mica 20%, cloudy fine matrix 40% and minor opaques.

3.3 Quartz-bearing micronorites, micro-gabbronorites (Unit 1)

Norites in the BC predominantly occur in the upper Critical Zone and as marginal rocks to the BC (Eales & Cawthorn, 1996; Sharpe & Hulbert, 1985). Gabbronorites containing cumulus clinopyroxene only occur in the Main Zone (Eales & Cawthorn, 1996). At the base of the sequence on Sheba's Ridge a fine-grained micronorite/gabbronorite occurs and is often seen in drill core interlayered with country rock, as summarised in Figure 3.1. This rock type is recognisable in hand specimen by its fine-grained equigranular, brownish appearance and was termed, from drill core, a micronorite.

In thin section these quartz-bearing micronorites and gabbronorites are characterised by optically continuous interstitial quartz between fine-grained and often elongate and orientated

orthopyroxene and clinopyroxene crystals. Biotite is a major constituent (approx. 20%) with accessory amphibole and minor disseminated base metal sulphides. Plagioclase is sericitised and is apparent as cloudy fine-grained patches (Figure 3.6 B & C).

3.4 Basal Mineralised Pyroxenites (Unit 2)

The sulphide bearing pyroxenites of the basal mineralisation are, in general, altered towards the contact with floor rocks. At the base, the pyroxenites contain country rock xenoliths and the contacts are altered. The basal mineralisation at Sheba's Ridge occurs in a thick 50 – 250 m package of pyroxenites with irregular interlayers of norite and xenoliths of country rock. These pyroxenites are variable in texture and composition throughout. In general the host rocks consist of 2 pyroxenes + interstitial plagioclase + BMS ± olivine ± chromite ± magnetite ± biotite/phlogopite. The composition of the mineralised package varies along strike, up dip and with stratigraphic height. An olivine-bearing, magnetite-rich package occurs in the central to eastern sector on the farm Loskop South 53 JS. In borehole core magnetite is seen as irregular stringers that bifurcate and coalesce. In the central and eastern sectors of Loskop South 53 JS magnetite stringers of this nature occur in bands throughout the mineralised pyroxenite. In the western sector olivine-bearing feldspathic pyroxenites are interlayered within a more pyroxenitic zone with sporadic chromite blebs. Down dip, in the boreholes on the southern side of Sheba's Ridge the mineralised zone thins and comprises relatively unaltered BMS-bearing feldspathic pyroxenites.

In thin section the pyroxenites are generally equigranular 2-pyroxene feldspathic pyroxenites. However, texture can vary with pegmatoidal patches, poikilitic clinopyroxenes, acicular pyroxenes and a presence or absence of micas. Chromite blebs appear to be cumulus and are scattered sporadically in the pyroxenites of the mineralised unit.

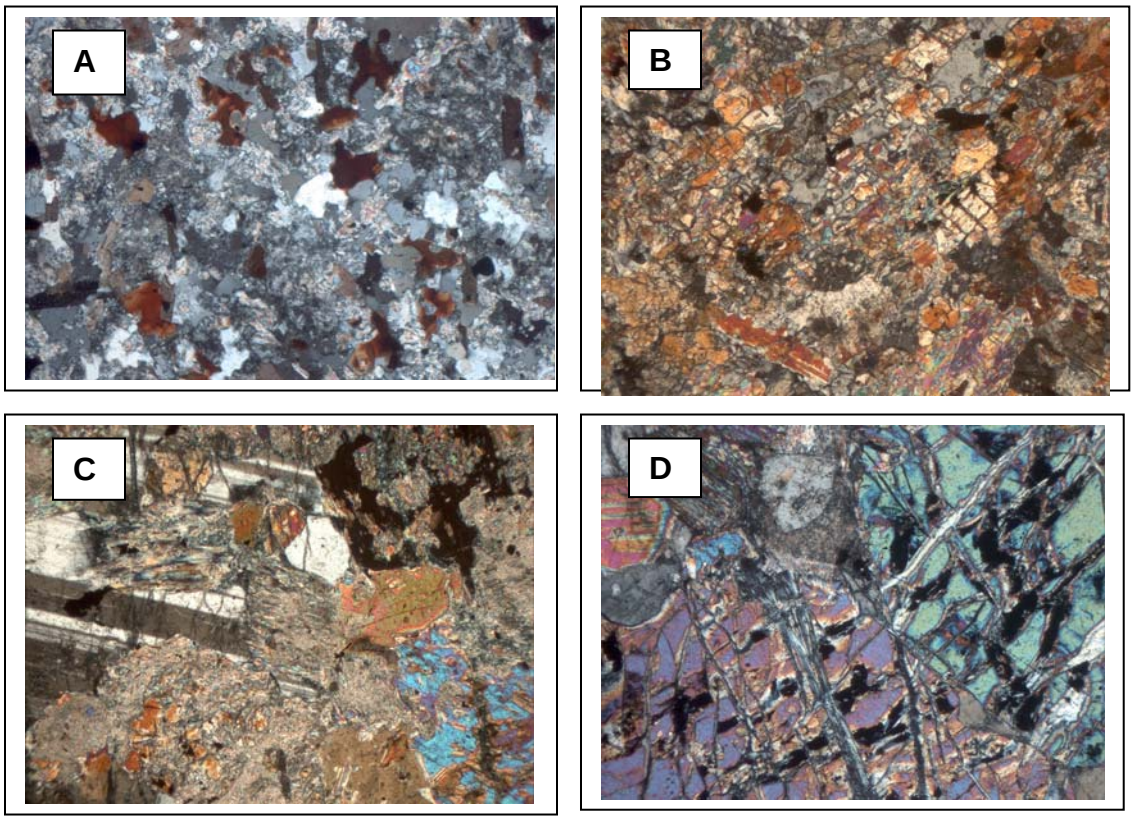

Figure 3.6, Photomicrographs of hornfels and micronorites from Unit 1 and mineralised olivine-bearing pyroxenite from Unit 2. A) A fine-grained equigranular cordierite-biotite-hornfels, with accessory amphibole and opaques, LPR8/15-457.00 m. B) is a heavily altered fine-grained marginal norite; biotite is disseminated throughout, quartz is interstitial and optically continuous, minor sericitisation occurs, LPR8/15 422.00. C) micronorite with sericitised orthopyroxene and optically continuous interstitial plagioclase, LPR8/15 432.00. D) Mineralised olivine-bearing pyroxenite showing cumulus olivine with magnetite permeating fractures and fine-grained subhedral opx and minor interstitial plagioclase, LPR6/12-47. All views are taken with a x4 lens under crossed polars, field of view is 3 mm.

This occurrence is not restricted to the mineralised zone and chromite blebs and stringers occur in pyroxenites that are higher in the sequence.

In the olivine-bearing rocks, subhedral cumulus olivine 0.5 to ~3.5 mm in size is partially altered to serpentine and iddingsite and magnetite permeates fractures within grains (Figure 3.6D). Orthopyroxenes and clinopyroxenes are both cumulus phases which vary in grain size and shape, with rounded to subhedral grains and elongate acicular grains all occurring in the same sample. Alteration of pyroxene to actinolite and tremolite occurs (Figure 3.7A). Plagioclase, showing minor sericitisation, is interstitial and often optically continuous between grains.

Base metal sulphides are interstitial and cumulus. Chalcopyrite, pentlandite, pyrite and pyrrhotite are the predominant sulphide phases (Figure 3.7B). They vary in texture from blebby, massive, disseminated and net-textured to isolated grains or occasionally as minor veins.

Figure 3.7 C is from a gabbronorite in Unit 3. Plagioclase occurs as inclusions in large mottles of opx and interstitial cpx. Embayments occur in the plagioclase grains and included plagioclase grains have a smaller grain size to the cumulus grains in the left of the photomicrograph. Figure 3.7 D is from a micronorite sample close to a hornfels xenolith. Plagioclase and orthopyroxene grains are sub-euhedral and the grains are relatively equigranular. Interstitial cpx is optically continuous.

3.5 Hanging wall Norites

The basal mineralised pyroxenite zone at Sheba's Ridge is directly overlain by a noritic unit which forms the hanging-wall to the basal mineralisation in all of the five boreholes studied.

In thin section plagioclase is cumulus with predominantly carlsbad twinning and minor sericitisation (Figure 3.8A). Interstitial quartz is an accessory phase and shows optical

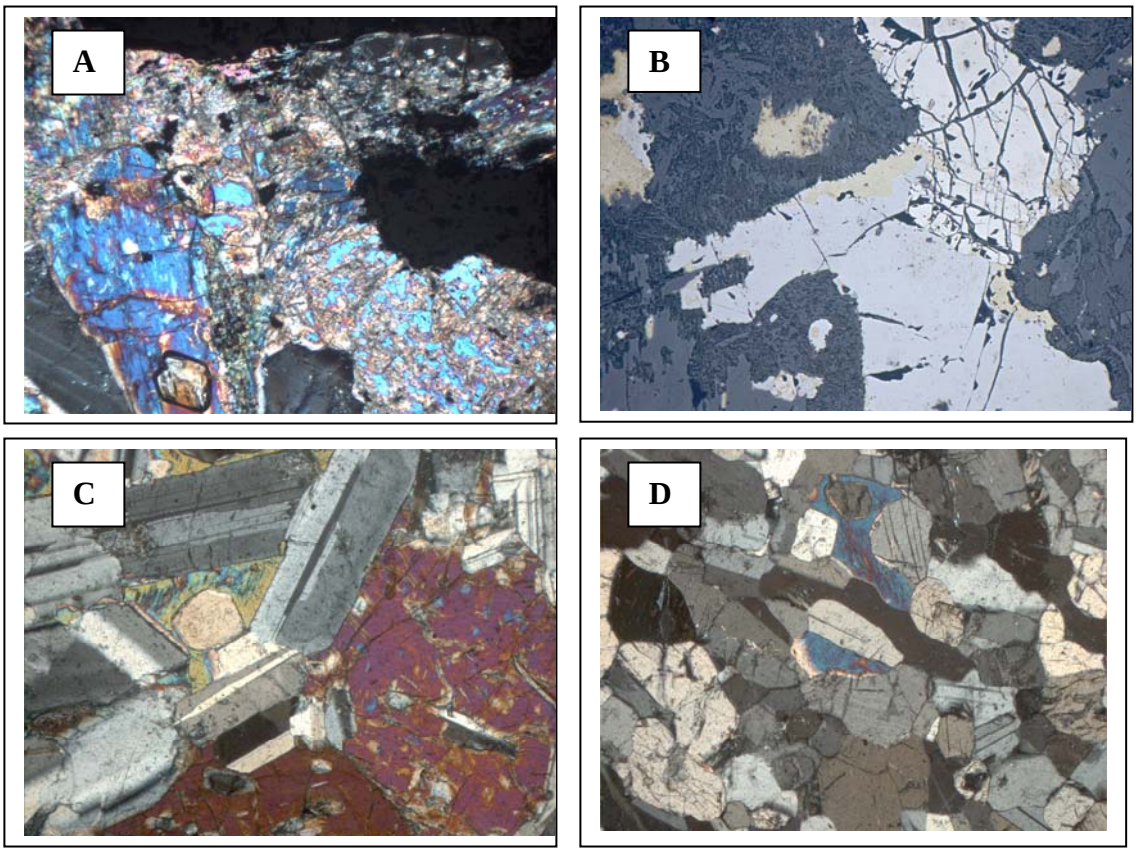

Figure 3.7, Photomicrographs of mineralised pyroxenites from Unit 2 and norites from Unit 3. A) Mineralised pyroxenite with altered pyroxenes, interstitial feldspar and interstitial base metal sulphides, LPR6/12-26. B) Reflected light image of complex sulphides, pentlandite, chalcopyrite and pyrrhotite, occurring as interstitial phases between altered pyroxenes, LPR6/12-26 C) Gabbronorite with interlocking inequigranular cumulus plagioclase with simple albite twins. Opx grains to the right are cumulus and show blebby cpx lamellae and contain inclusions of plagioclase. Interstitial cpx is optically continuous in the top left; LSD 34 489.00. D) Micronorite at the chilled margin of a hornfels xenolith with cumulus plagioclase and opx and interstitial optically continuous cpx, LSD34 447.00. All views are taken with a x4 lens under crossed polars, field of view is 3 mm.

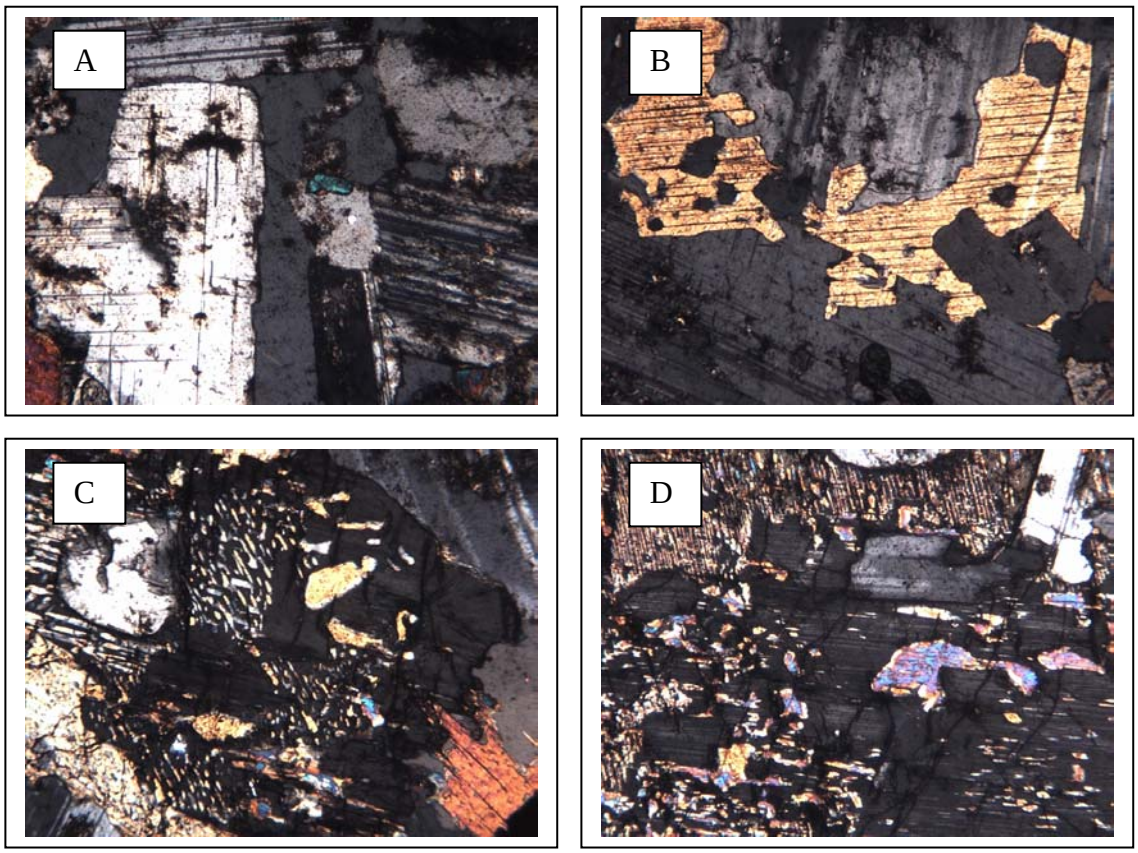

Figure 3.8, Photomicrographs of the hanging wall norite marking the base of Unit 3 from sample LSD34 618.50 m.. A) interstitial optically continuous quartz between cumulate plagioclase and opx grains; B) Optically continuous interstitial cpx between plagioclase and opx grains; C) & D) inverted pigeonite with distinctive two directional blebby lamellae of Ca-cpx. Microprobe data from this sample is outlined in Chapter 5. All views are taken with a x4 lens under crossed polars, field of view is ¬3 mm.

continuity between grains. Clinopyroxene is interstitial and also shows optical continuity between grains (Figure 3.8B). Orthopyroxene forms a minor cumulus phase but predominantly occurs as interstitial mottles of inverted pigeonite with distinctive two directional blebby lamellae of Ca-cpx, (Figure 3.8C & D). Biotite is an accessory phase and often has inclusions of magnetite grains.

3.6 Pyroxenite/Norite Interlayers (Unit 3)

There is a complex interlayered zone of pyroxenites and norites stratigraphically above the mineralised pyroxenites in the north and below the homogenous gabbronorites forming Sheba's Ridge in the south. In borehole core, layers of norite pinch out and contacts between pyroxenites and norites were found to be sharp and in some cases orientated parallel to core axis. In the lower parts, this unit consists of a complex intermix of pyroxenites, with sporadic chromite blebs and stringers, bands of magnetite stringers and irregular interlayers of norite.

Borehole LPR8/15 intersects the suggested 'disorientated' gabbronoritic block with laminations orientated perpendicular to regional strike in outcrop (Figure 3.3). There is little variation in textural features through the gabbronorite of the 'disorientated' block. Plagioclase and opx are both cumulus phases and are euhderal –subedral with little alteration (Figure 3.9 A). Clinopyroxene oikocrysts form interstitial mottles and have inclusions or chadocrysts of orthopyroxene, which in turn have inclusions of plagioclase. This interstitial material constitutes approximately 20% of the thin section. In comparison the leuconorite below the 'disorientated' noritic block has a higher percentage of intercumulus minerals, at ~30 % (Figure 3.9 B & C). There is little variation in this unit with depth and only minor alteration. Oikocrysts of orthopyroxene form mottles with inclusions of plagioclase. Cumulus orthopyroxene and plagioclase form an interlocking framework. Clinopyroxene mottles are less abundant than in the 'disorientated' block. In order to observe differences in the 'disorientated' block and the norite below, samples from each were analysed using a Cameca 355 microprobe and will be discussed in Chapters 4 and 5.

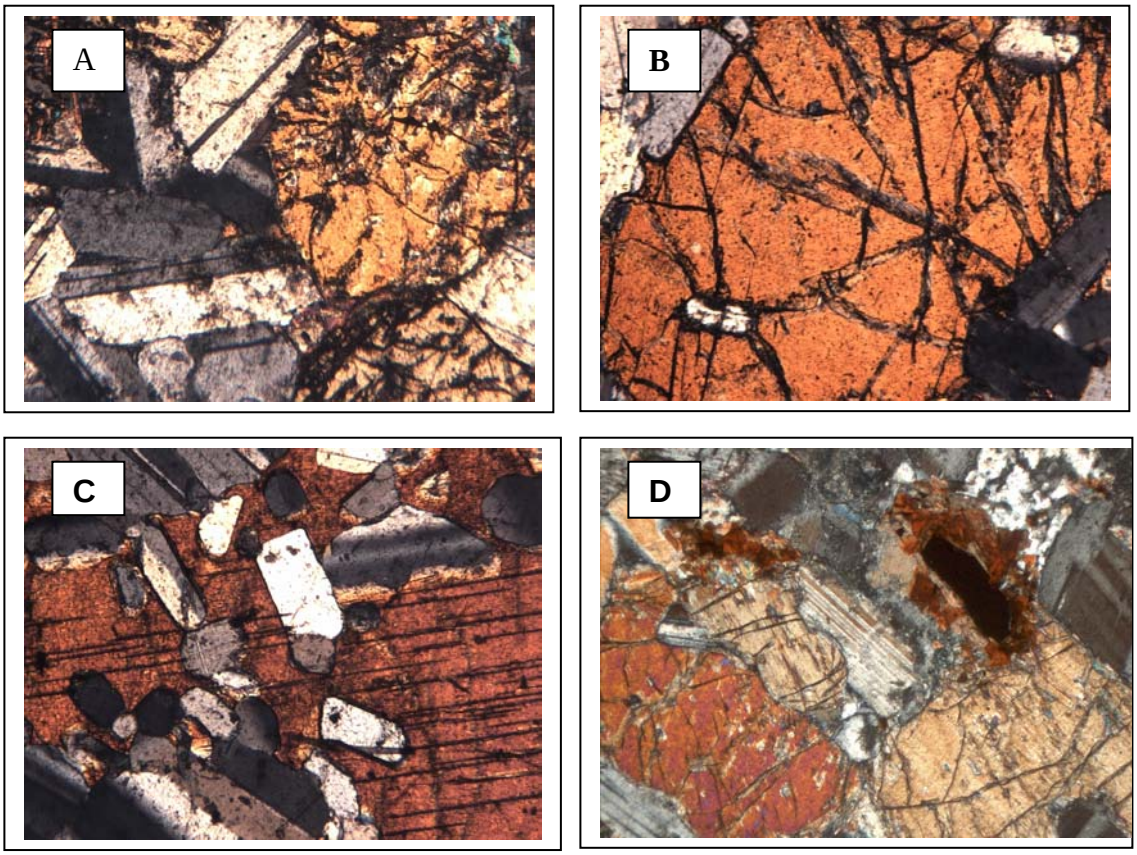

Figure 3.9, Photomicrographs of norites from the 'disorientated' noritic block and below from borehole LPR8/15. A) LPR8/15 27.00 gabbronorite from suggested 'disorientated' noritic block with cumulus opx and plagioclase and minor interstitial cpx, this sample also contains mottles of cpx with inclusions of plag and opx typical of the gabbronorites; B) Leuconorite with large cumulate opx containing plagioclase inclusion, opx forms mottles with sparse mottles of interstitial cpx. LPR8/15 82.50 C) one of the sparse interstitial mottles of cpx with plagioclase inclusions showing simple albite twinning and embayments in LPR8/15 82.50. D) Cumulus opx and plagioclase grains with interstitial plagioclase with Carlsbad twinning and sericitisation at grain boundaries. In the top right a magnetite grain is in association with interstitial biotite LPR8/15 141.00. All views are taken with a x4 lens under crossed polars, field of view is 3 mm

Texturally the pyroxenite interlayers are inhomogeneous. The predominant mineral is orthopyroxene which often comprises ~70% of the rock (Figure 3.9 D). Grain size varies from 0.05 mm to 3 mm. Grain shape is rounded and often grain boundaries form triple points. Elongate orthopyroxene grains occur sporadically. Clinopyroxene if present is interstitial and comprises no more than 25% of the rock. Plagioclase is always interstitial and

is often optically continuous between orthopyroxene grains. Minor alteration of orthopyroxene to tremolite occurs. Biotite is a minor accessory phase. Chromite grains occur as inclusions in orthopyroxene.

At the top of Unit 3 a number of 'cyclic' units occur as outlined in Chapter 2. These consist of pyroxenite-norite-anorthosite layers. It is difficult to define the number of 'cyclic units as no full cycle is present, rather a modal cyclicity occurs between pyroxenite and norites.

A gabbronorite occurs in a cyclic unit below a mottled anorthosite. This gabbronorite has an interlocking framework of inequigranular plagioclase with needle like grains occurring sporadically. Simple albite twinning predominates with minor carlsbad twinning. There are minor cumulus opx grains, although subhedral grains occupy embayments in plagioclase. Orthopyroxene occurs predominantly as interstitial mottles with blebby lamellae of clinopyroxene. Inclusions of plagioclase within the opx are often embayed. In places orthopyroxene grains are rimmed by clinopyroxene causing embayments in the orthopyroxene. Clinopyroxene occurs as an interstitial phase and at opx grain boundaries. Minor interstitial quartz occurs as an accessory mineral.

3.7 Gabbronorites (Unit 4)

The homogeneous package of mottled gabbronorite of Unit 4 marks the top of the stratigraphic sequence on the farm Loskop South 53 JS and forms the predominant ridge in the southern sector known as Sheba's Ridge.

In this unit, plagioclase forms an interlocking framework with up to 50 modal % of grains that are often embayed and which are characterised by carlsbad twinning. Orthopyroxene is

interstitial and forms mottles surrounded by plagioclase (Figures 3.10 A & B). Inclusions within the opx grains are of euhedral-subhedral plagioclase, from which fractures permeate through orthopyroxene (Figure 3.10 C). Clinopyroxene is interstitial with well-developed lamellae and forms oikocrysts showing optical continuity between grains (Figure 3.10 D). Accessory minerals are very minor and include amphibole, tremolite, biotite, sericite and magnetite. These accessory phases typically occur at grain boundaries.

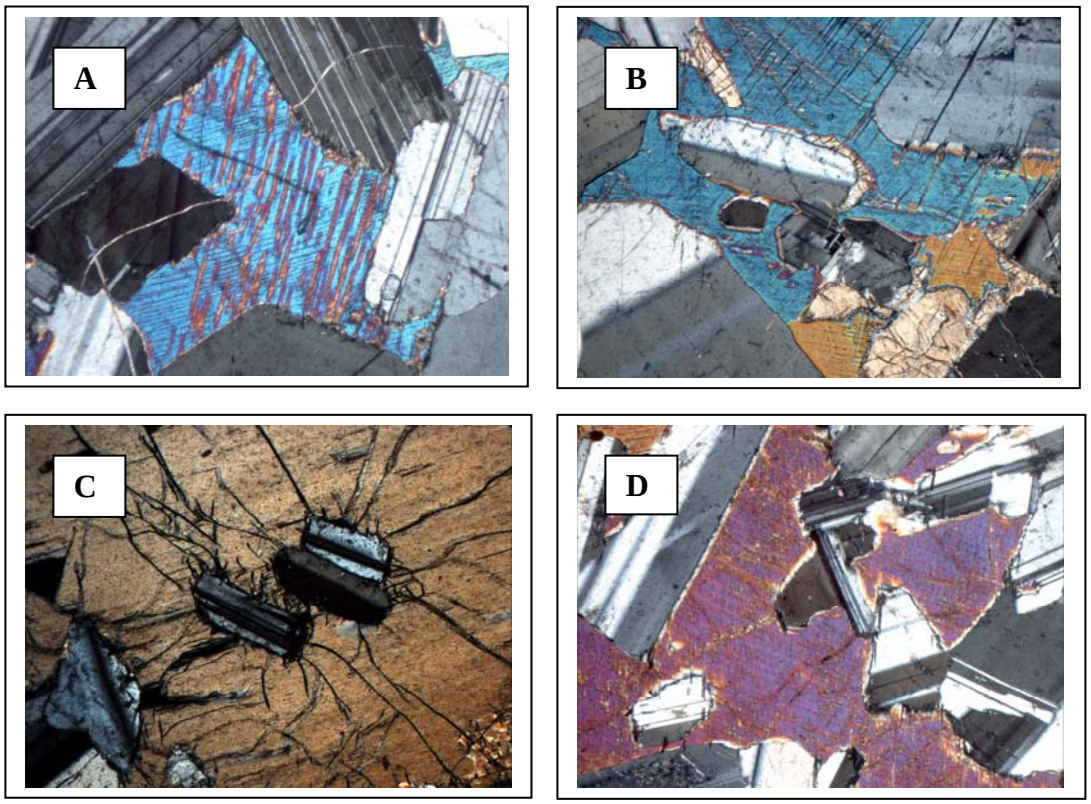

Figure 3.10, Photomicrographs of gabbronorite from Unit 4. A) An interlocking framework of plagioclase and interstitial clinopyroxene with well developed lamellae showing optical continuity; LSD22/1. B) Interstitial clinopyroxene with hornblende developed between cpx and opx grain boundaries and inclusions of plagioclase with reaction rims; LSD22/1. C) Orthopyroxene mottle with inclusions of plagioclase and fractures permeating through the opx grain from the smaller inclusions; LSD22/2. D) An oikocryst of interstitial optically continuous clinopyroxene with anhedral plagioclase with embayments and reaction rims, LSD22/2. All views are taken with a x4 lens under crossed polars, field of view is 3 mm.

3.8 Discussion

Textural features of the Bushveld Rocks

There are a number of processes that may contribute to the final textures in layered intrusions. These may be cumulate and/or postcumulus processes. Cumulus crystals represent early precipitates from a melt dominated system and postcumulus crystals represent intercumulus liquids that occupied the interstices between cumulus crystals, (e.g. Wager *et al*, 1960*;* Wager & Brown, 1968; Irvine, 1982; Hunter, 1996; Zingg, 1996). These can then be subject to a number of postcumulus processes that contribute to the final solidification and composition of the rock. These processes include compaction (McKenzie, 1984; Hunter, 1987; Cawthorn *et al*, 1991; Hunter, 1996), infiltration metasomatism (Irvine, 1982; Cawthorn *et al*, 1991; Hunter, 1996), and compositional convection (Tait *et al*, 1984; Cawthorn *et al*, 1991; Hunter, 1996). A number of textures observed here indicate that post cumulus processes have played a significant role in the final development of the rocks at Sheba's Ridge. Pyroxenes with triple point grain boundaries have been observed. This is attributed to annealing, a texture commonly developed when postcumulus recrystallisation has taken place (Hunter, 1996). Also, in Figures 3.7B 3.9B and 3.9C relatively small sub-euhedral grains of plagioclase are enclosed in large orthopyroxene oikocrysts. Eales *et al*, (1991) suggested that this represents early crystallisation of plagioclase within the melt and that these grains have not undergone recrystallisation. In which case, the grain sizes would be much smaller as seen in Figure 3.7C. Here plagioclase inclusions are of a much smaller grain size than the interlocking framework shown in the top left of the image. Embayments seen in plagioclase (Figure 3.10D) could either represent cotectic crystallisation with pyroxene (Eales *et al*, 1991) or resorbtion of part of that grain by the interstitial liquid (Eales *et al*, 1991; Hunter, 1996). Although this is not supported by the experimental work of

Donaldson (1985, 1988) who suggests embayments in the crystals are due to incomplete crystallisation.

3.8.1 Inverted Pigeonite in the Hanging wall

The occurrence of inverted pigeonite in the sequence indicates, firstly, that the formation of two-directional Ca-rich lamellae has occurred during slow cooling. Uninverted pigeonite only occurs in quickly chilled rocks (Deer *et al*, 1966). Inverted pigeonite is easily recognisable in thin section as during slow cooling monoclinic pigeonite exsolves some excess calcium along planes parallel to 001. On further slow cooling it inverts to an orthorhombic pyroxene which is accompanied by the exsolution of a second generation of augite lamellae parallel to the 100 plane of the orthopyroxene (Deer *et al*, 1966). Therefore inverted pigeonite is distinguished from primary orthopyroxene here by the occurrence of distinctive two-directional exsolution lamellae. Microprobe data from inverted pigeonite grains and augite lamellae are presented in Chapter 5. Secondly, the occurrence of inverted pigeonite in the sequence must represent a position where the phase-change from orthopyroxene to pigeonite takes place (von Gruenewaldt, 1970). This phase-change can be related either to fractionation, rejuvenation of the resident magma (Eales & Cawthorn, 1996) or influx of a more differentiated magma or a magma that has been contaminated by a source containing calcium, e.g. calcsilicates. In the eastern and western limbs of the BC inverted pigeonite is found only in the Main Zone (von Gruenewaldt, 1970; von Gruenewaldt & Weber-Diefenbach, 1977; Cawthorn *et al*, 1991; Eales & Cawthorn; 1996; Nex, *et al*, 1998; Nex *et al* 2002). Von Gruenewaldt (1970; 1973) groups the Main Zone of the eastern limb in to three subzones based on the occurrence of inverted pigeonite. These subzones are further constrained in the western limb by Nex *et al* (1998). The only other occurrence of inverted pigeonite in the BC, to current knowledge, is reported in the northern limb at the Sandsloot

open pit mine, Mokopane (Holwell *et al*, 2004). Here a fine-grained gabbronorite with inverted pigeonite and sulphides occurs at the hanging wall contact of the Platreef. This corresponds to a break in the composition of orthopyroxene from $Mg\#_{77}$ to $Mg\#_{67}$ between the Platreef and the hanging wall. As in the Platreef, the inverted pigeonite also occurs in the hanging wall of the basal mineralisation at Sheba's Ridge. To further investigate this, the occurrence of inverted pigeonite at Sheba's Ridge should be co-incident with a change in geochemical signatures, and is investigated further in chapters 4 and 5 using whole rock geochemical data and mineral chemistry to constrain this marker horizon.

3.8.2 Stratigraphic Correlations

Floor rocks in the area are of the Pretoria Group of the Transvaal Supergroup which is of early-Proterozoic age (Button, 1986; Crous, 1995). The Pretoria Group is represented by the major quartzite ridge of the Daspoort Formation, in the Northern sector of the farm Loskop South 53 JS (Figure 3.11). Here, the country rock hornfels and calcsilicates often occur intermixed with micronorites at the base of the sequence and can contain fine disseminated BMS. This indicates that the ultramafic-mafic rocks in the area intruded into and disrupted the Pretoria Group sediments. The hornfels' as Crous (1995) indicates, may be metamorphosed shales from the Silverstone Shale Formation of the Pretoria Group with an age of 2263 Ma (Burger & Walraven, 1980; Crous, 1995). These rock types form the footwall to the basal mineralisation at Sheba's Ridge. A 'mafic hornfels' was recognised by Crous (1995) which recorded metamorphism and recrystallisation of mafic rocks on a microscopic scale. This mafic hornfels is stratigraphically above the hornfels floor rocks and below the micronorites, (Figure 3.12 & 3.13).

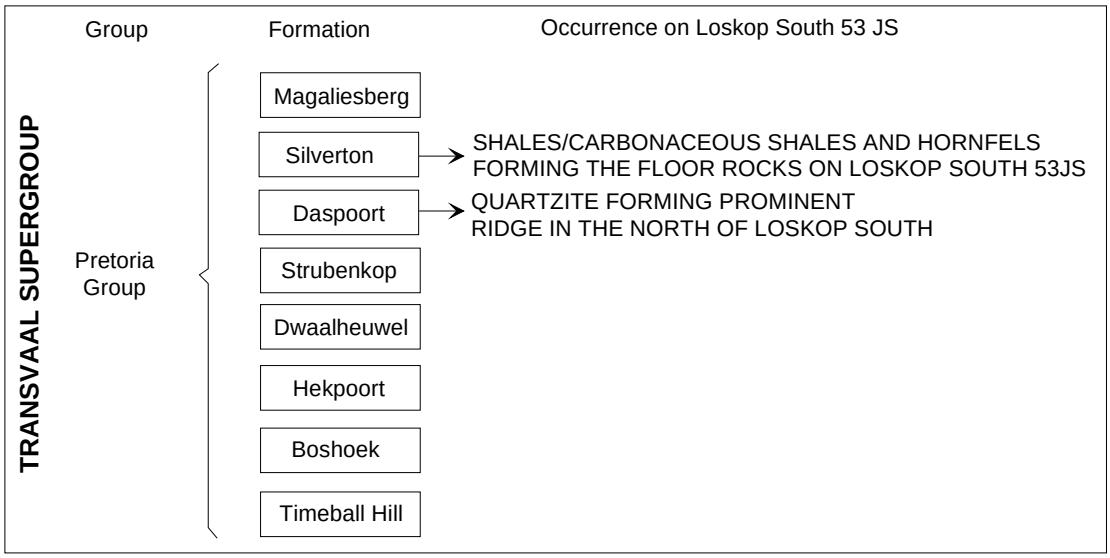

Figure 3.11 Stratigraphy of the Pretoria Group of the Transvaal Super Group showing the occurrence of Transvaal sediments in relation to the mafics on the farm Loskop South 53 JS. Modified from Department of Mines geological Series 2828 Pretoria.

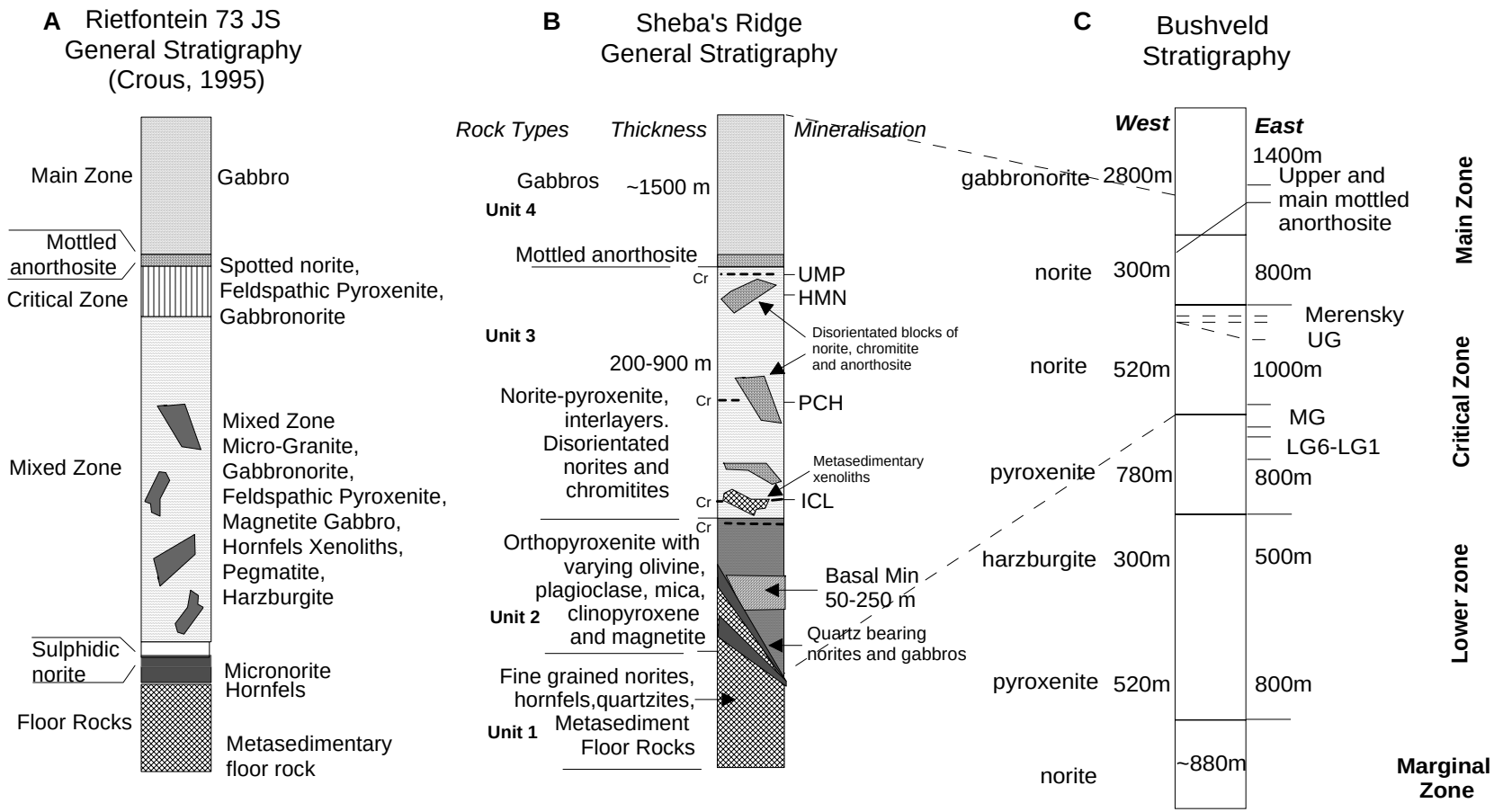

Figure 3.12 General stratigraphy from: A) the farm on the west of Loskop South, Rietfontein 73 JS (Crous, 1995), B) this study, Loskop South 53 JS Sheba's Ridge (modified from Roodt, 2004) and C) general stratigraphy of the Bushveld Complex (Eales & Cawthorn, 1996). The basal mineralisation of Unit 2 correlates to Crous' Lower Mixed Zone, the Critical Zone of Crous' correlates to the 'cyclic units' including the UMP of Sheba's Ridge.

The basal mineralisation described here correlates with the 'lower mixed zone' of Crous (1995). The hanging wall norite to the basal mineralisation at Sheba's Ridge potentially correlates with the norite above the pegmatitic pyroxenites towards the base of the 'middle unit-mixed zone' of Crous (1995). Similarities between the hanging wall norite in this study and that of Crous (1995) occur in the continuity and use as a stratigraphic marker horizon. Norite/pyroxenite interlayers of Unit 3 have been correlated to Crous' 'upper mixed zone'. The cyclic units in Unit 3 correlate to Crous' 'Critical Zone'. Stratigraphic correlation of layers within this zone was not achieved. The homogeneous gabbronorite at the top of the sequence studied can be correlated with Crous' Main Zone.

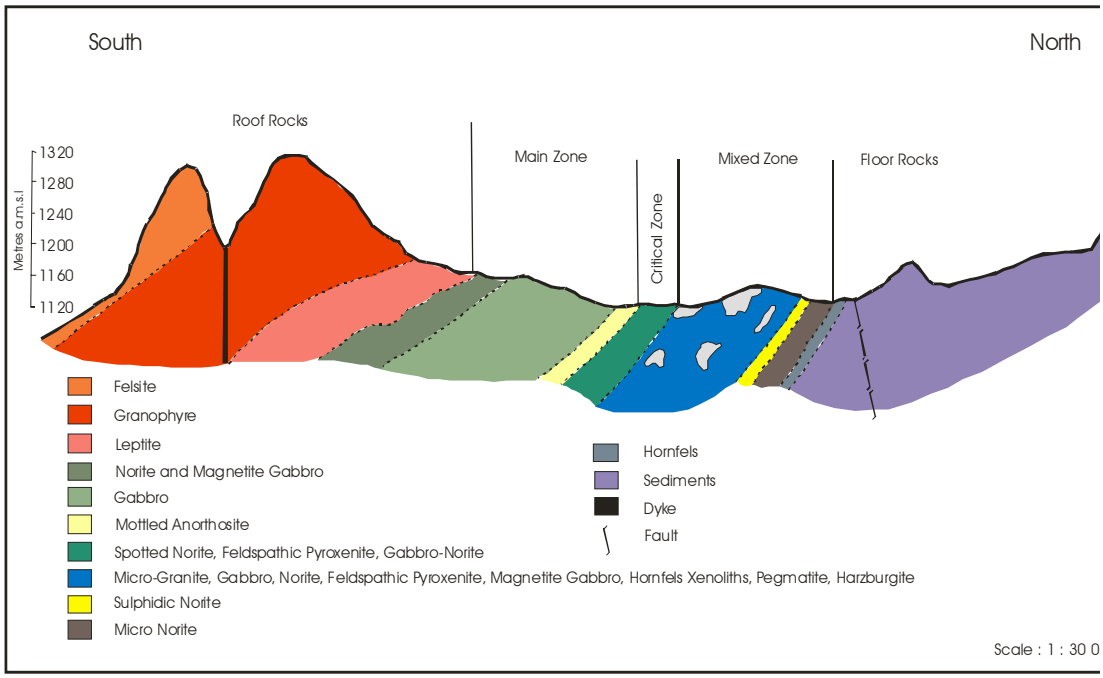

Figure 3.13: Schematic cross section through the farm directly to the west of Loskop South 53 JS, Rietfontein 73 JS, modified from Crous (1995). This shows the mafic rocks in this area dipping to the South. Crous (1995) has correlated units in the area to Zones of the Bushveld Complex and shows the complex and unusual nature of the occurrence of mafic rocks in this area compared to 'typical' layered mafics of the Bushveld Complex. Note the term Leptite refers to country rock that has been subject to regional metamorphism.

The micronorites and gabbronorites are correlated to the Marginal Zone of the Bushveld Complex. No peripheral basal 'contact' style mineralisation has previously been documented in the eastern and western limbs of the BC. Therefore, this contact style mineralisation can be likened only to that of the Platreef proper in the northern limb. The noritic hanging wall horizon bears similarities to that of the Platreef and may suggest similar processes occurred during their formation. Interfingering in Unit 3 may represent two geochemically distinct groupings correlated with Critical Zone and Main Zone signatures (this will be discussed in Chapter 4). Towards the top of Unit 3 the sequence is more typical of upper Critical Zone signatures of the eastern and western limbs of the BC. The homogeneous gabbronorite at the top of the sequence correlates with the Main Zone of the BC.

3.9 Summary

It is clear from the complexity of the area that the rock types and the succession on Loskop South 53 JS are not typical of the layered BC rocks as a whole. Moreover, the mafic rocks dip to the south whereas the eastern compartment dips to the north towards the centre of the Complex. The succession on Sheba's Ridge does not host a strike continuous layered sequence that can be correlated directly with the stratigraphy of the BC, nor can the mineralised units be easily correlated with the Merensky Reef and UG2 layers. The sequence is highly disrupted and the basal mineralisation has not been documented within the BC in the eastern and western limbs. From the data presented suggested correlations of the sequence at Sheba's Ridge with that of the Bushveld Complex and with Crous (1995) data from the farm Rietfontein 73 JS are shown in Table 3.1. As with the Platreef, the LZ and C_lZ is attenuated or absent.

Table 3.1 Suggested correlations of Sheba's Ridge with that of the Bushveld Complex and with the farm Rietfontein 73 JS from Crous (1995).

Sheba's Ridge	Bushveld Complex	Rietfontein 73 JS
Unit 4	Main Zone	Main Zone
Unit 3	Critical Zone	Critical Zone
Unit 2	Similarities to the Platreef	Mixed Zone
Unit 1	Marginal Zone and Transvaal meta-sedimentary floor rocks	Floor Rocks

CHAPTER 4

Whole Rock Geochemistry

4.1 Introduction

In order to investigate the unique ultramafic-mafic sequence of Sheba's Ridge a geochemical study was undertaken. This enabled confirmation of rock identifications and observations made in thin section. Comparisons with data available for typical geochemical profiles for the eastern and western limbs of the Bushveld Complex could then be made. The intrusives of the Sheba's Ridge area are peripheral to the Bushveld Complex and are situated on the flanks of domal features and are unconformable on an undulatory floor sequence. The basal pyroxenite is host to Ni-Cu-PGE mineralisation. In addition, there are suggested xenoliths of noritic and chromitite-bearing units within the mafic sequence. Each of these rock types were included in the geochemical sample suite.

A suite of 135 core samples, were systematically collected from the 5 logged boreholes described in Chapter 2. Samples of 50 cm length quarter core were chosen to represent differing rock types found in each borehole and to systematically cover the stratigraphic range. Areas of basal mineralisation in boreholes LSD34 and LPR6/12 were sampled at 50 cm intervals. Data through the basal mineralisation in LPR12/9 was provided by Ridge Mining. Additionally, a geochemical profile through the stratigraphy was completed to enable a comparison of the 'disorientated' block with the underlying rock types in borehole LPR8/15 to be made. Samples were prepared for whole-rock XRF analysis to provide data to evaluate any systematic geochemical changes with lithological variation or to indicate any abrupt changes in composition through the stratigraphy.

4.2 Sample Preparation and Analysis by Whole Rock X-ray Fluorescence Spectrometry

Samples were processed in a standard jaw crusher and milled to a fine powder in a tungsten mill. The mill was pre-contaminated with a small portion of each new sample to reduce contamination. Samples were submitted for analysis by X-Ray fluorescence spectrometry (XRF) at the University of the Witwatersrand using a PW1400 XRF. Procedures and standards used are given in Appendix 3.

Samples were analysed for the following major element oxides (wt%):

SiO_2, TiO_2, Al_2O_3, Fe_2O_3, MnO, MgO, CaO, Na_2O, K_2O and P_2O_5,.and Loss on Ignition (LOI)

and the following trace elements (ppm): Rb, Sr, Y, Zr, Nb, Co, Ni, Cu, Zn, Ti, V, Cr and Ba.

Results are given in Appendix 4.

4.3 Whole Rock Geochemistry – Major Element Oxides

The intrusive rocks of the Sheba's Ridge area are characterised by variable proportions of orthopyroxene, plagioclase and clinopyroxene. Estimates of modal proportions of the rocks made in Chapter 3 may be inaccurate due to human error and thin sections may not be representative of the whole rock, especially where textures are highly variable. Thus, whole-rock XRF data was used to compare geochemically-based nomenclature with those given during core-logging and petrological study. The compositions of the varying rock types sampled at Sheba's Ridge in each borehole are plotted on graphs in Figures 4.1 and 4.2. The modal ranges are based on the proportions of $MgO+Fe_2O_3$ and Al_2O_3 (Eales *et al* 1986; 1988). Rock types containing orthopyroxene and plagioclase plot on the orthopyroxene-plagioclase tie lines. Rock types containing clinopyroxene plot below the orthopyroxene-plagioclase tie lines whereas olivine-bearing rocks plot as a scatter above the orthopyroxene –

plagioclase tie-line. This is because they have a lower wt % Al_2O_3 and a higher wt% MgO + Fe_2O_3 than the pyroxenites. Figure 4.1 and Figure 4.2 show that the modal proportions of clinopyroxene are highly variable especially in the pyroxenites and mela-norites/gabbronorites whereas olivine does not appear to be a significant phase in the samples studied, bearing out the petrological observations. A summary of values for wt% MgO + Fe_2O_3 and wt % Al_2O_3 subdivisions for the varying rock types sampled at Sheba's Ridge is given in Table 4.1.

Table 4.1 Variation in wt% MgO + Fe_2O_3 and wt% Al_2O_3 for different rock types found at Sheba's Ridge.

Rock Type	**MgO + Fe_2O_3 wt%**	**Al_2O_3 wt%**
Olivine-bearing pyroxenite	>40	<5
Feldspathic pyroxenite	25 - 35	5 - 10
Melanorite	20 - 25	10 - 13
Gabbronorite	15 - 25	5 - 10
Norite	15 - 20	13 - 17
Leuconorite	7 - 12	20 - 25
Anorthosite	<7	>25

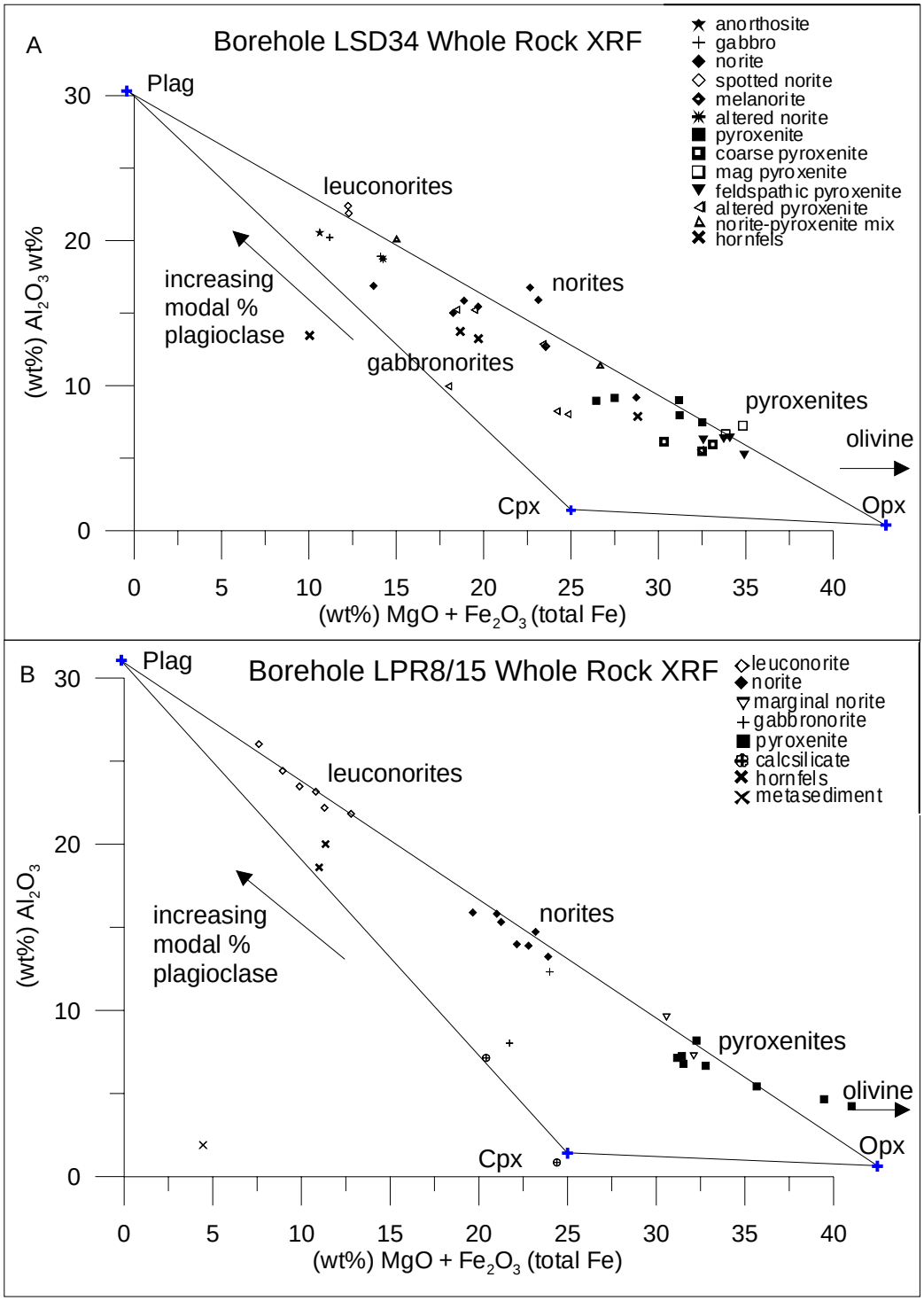

Figure 4.1 Harker plots of whole rock Al_2O_3 plotted against MgO + Fe_2O_3 (representing total Fe) for A) borehole LSD34 and B) LPR8/15. Mineral plots of plagioclase, orthopyroxene and clinopyroxene are taken from averaged microprobe data for each borehole. The plots show that the samples in LSD34 contain higher modal proportions of clinopyroxene than in LPR8/15. Mag pyroxenite refers to pyroxenite that is magnetite bearing.

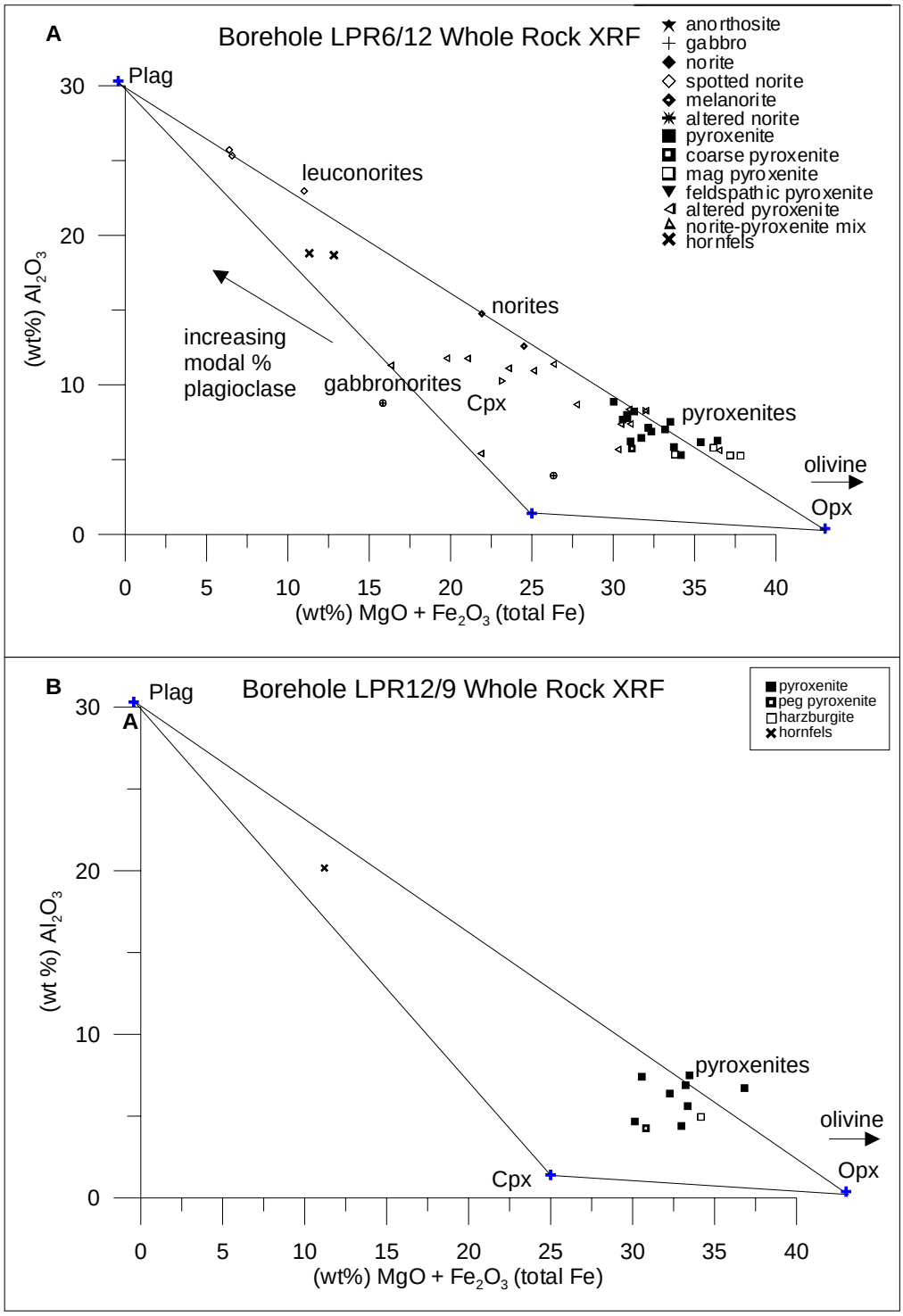

Figure 4.2 Harker plots of whole rock Al_2O_3 plotted against MgO + Fe_2O_3 (representing total Fe) for A) borehole LPR6/12 and B) LPR12/9. Mineral plots of plagioclase, orthopyroxene and clinopyroxene are taken from averaged microprobe data for each borehole. Clinopyroxene is variable in borehole LPR6/12 through the basal reef and hanging wall. Samples in borehole LPR12/9 were taken of reef pyroxenites only. The major element oxides plotted show clinopyroxene, magnetite and olivine are present in these samples.

A further way of demonstrating that the rock types sampled are controlled by modal proportions of minerals is to plot major element oxides against MgO, as shown in Figures 4.3, 4.4, 4.5 and 4.6 for boreholes LSD34 and LSD22, LPR6/12, LPR8/15 and LPR12/9 respectively. Differing geochemical trends are observed for each of the 5 boreholes sampled.

For boreholes LSD34 and LSD22, wt% CaO, Na_2O and Al_2O_3 all show a negative correlation against wt% MgO as plagioclase content increases relative to pyroxene proportions in the rocks (Figure 4.3). In contrast concentrations of Fe_2O_3 and MnO show a positive correlation. This is controlled by the increasing pyroxene to plagioclase proportions in the rocks. There is an iron enrichment occurs towards the base of the basal mineralisation, there is a considerable scatter developed because of varying proportions of biotite/phlogopite present. The scatter of wt% TiO_2 is caused by varying proportions of biotite/phlogopite and varying occurrences of magnetite/ilmenite through the basal mineralisation. The floor rock metasediment is easily recognisable with >65 wt% SiO_2, >0.9 wt% TiO_2, and only ~3 wt% MgO.

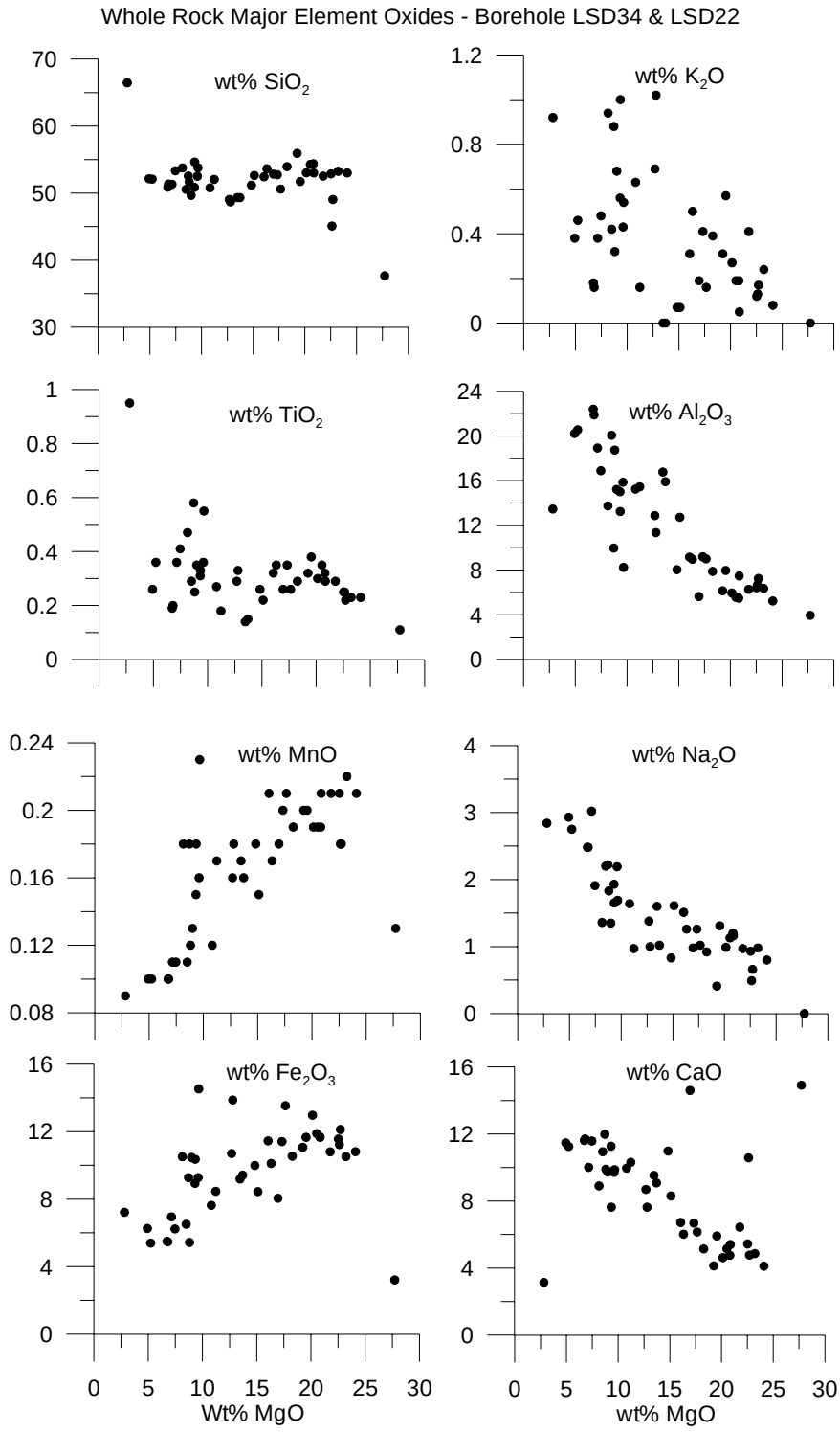

Figure 4.3 Bivariate plots of wt% major element oxides against wt% MgO from boreholes LSD34 and LSD22. Increasing wt% MgO represents increasing pyroxene to plagioclase proportions in the rocks. Wt% Fe_2O_3 and wt% MnO both show positive correlations whilst wt% CaO, Na_2O_3, Al_2O_3 all show a negative correlation against wt% MgO. Wt% SiO_2, TiO_2 and K_2O plots are scattered against wt% MgO. All MgO plots are to the same scale i.e. 0-30.

In borehole LPR6/12, as with boreholes LSD22 & LSD34, the major element oxides CaO, Na_2O, TiO_2 and Al_2O_3 all show negative correlations against wt% MgO controlled by increasing plagioclase to orthopyroxene and clinopyroxene proportions (Figure 4.4). Again, variation in concentrations of wt% K_2O and wt% TiO_2 reflects the occurrence of biotite/phlogopite. Wt% Fe_2O_3 and wt% MnO show a positive correlation which is controlled by the varying pyroxene to plagioclase proportions in the rocks. The hornfels samples are characterised by high wt% SiO_2, K_2O, TiO_2 and low wt% CaO and MnO.

The rocks sampled from borehole LPR8/15 contain much lower proportions of clinopyroxene than the previous 3 boreholes observed as shown in Figure 4.1. This is reflected in the bivariate plots which show little scatter and strong positive trends for wt% Fe_2O_3 and wt% MnO and negative trends for wt% CaO, Na_2O and Al_2O against wt% MgO (Figure 4.5). This shows clearly the varying modal proportions of plagioclase to orthopyroxene present. Again the hornfels is easily recognised by its characteristic high K_2O, SiO_2, and TiO_2 content.

Borehole LPR12/9 was collared into the outcrop of the basal mineralisation so that samples only consist of mineralised pyroxenites. Data analyses for XRF and Fire Assay analyses provided by Ridge Mining supplemented data from this sampling. Major element XRF data from both this study (analysed at the University of the Witwatersrand), and data provided by Ridge Mining, are plotted against wt% MgO in Figure 4.6. In general the trends are similar to those of the previous boreholes. Hornfels and marginal norite are easily distinguished with wt% MgO 2.90 and 12.73 respectively. The cluster of low concentrations of CaO and MgO represent floor rocks and country rock xenoliths.

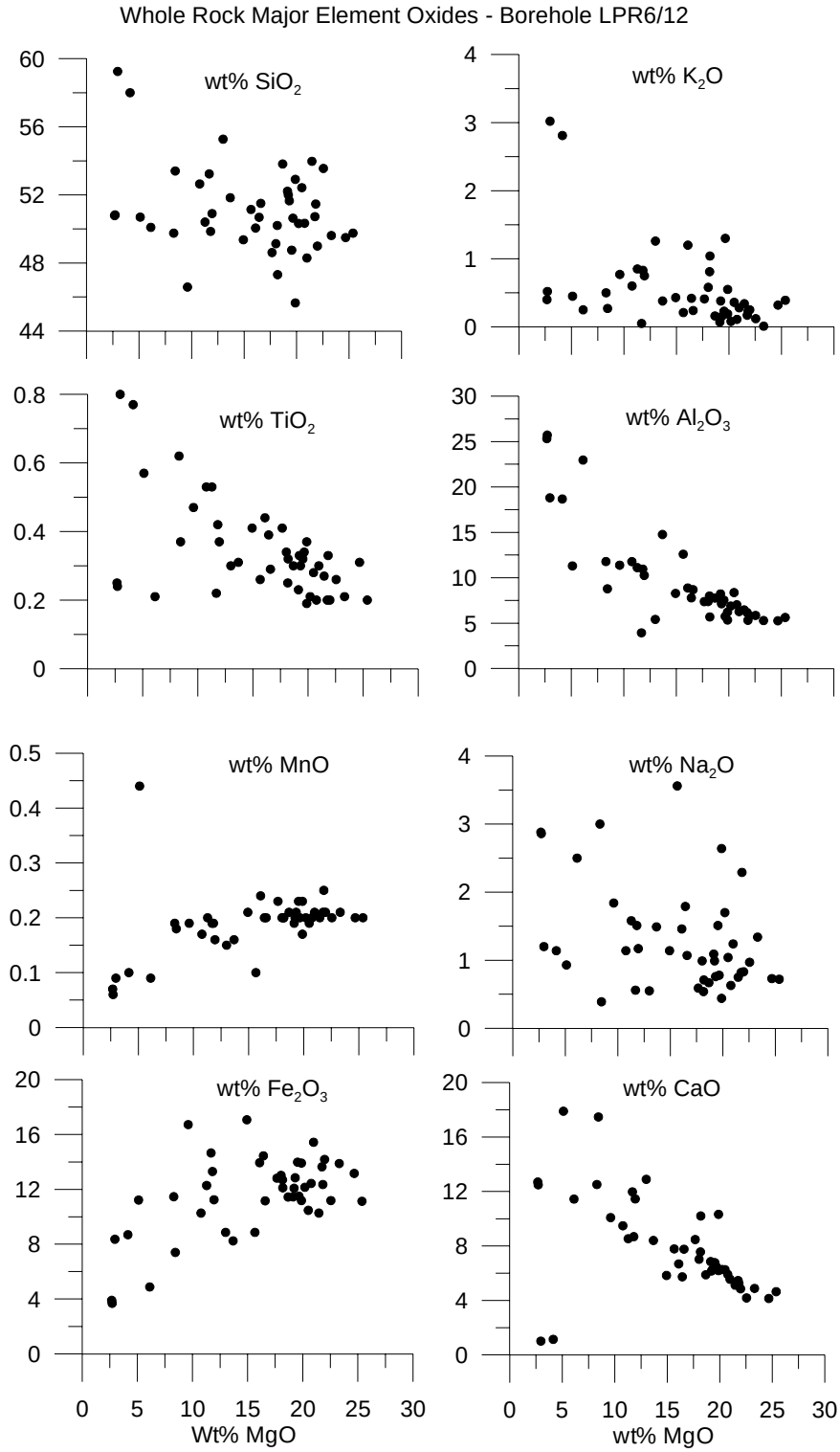

Figure 4.4 Bivariate plots of wt% major element oxides against wt% MgO from borehole LPR6/12. Increasing MgO represents increased pyroxene to plagioclase proportions in the rocks. Generally wt% Fe_2O_3 and wt% MnO both show positive correlations whilst wt% CaO, Na_2O_3, Al_2O_3, TiO_2 all show a negative correlation against wt% MgO. Wt% SiO_2, and K_2O plots are scattered against wt% MgO.

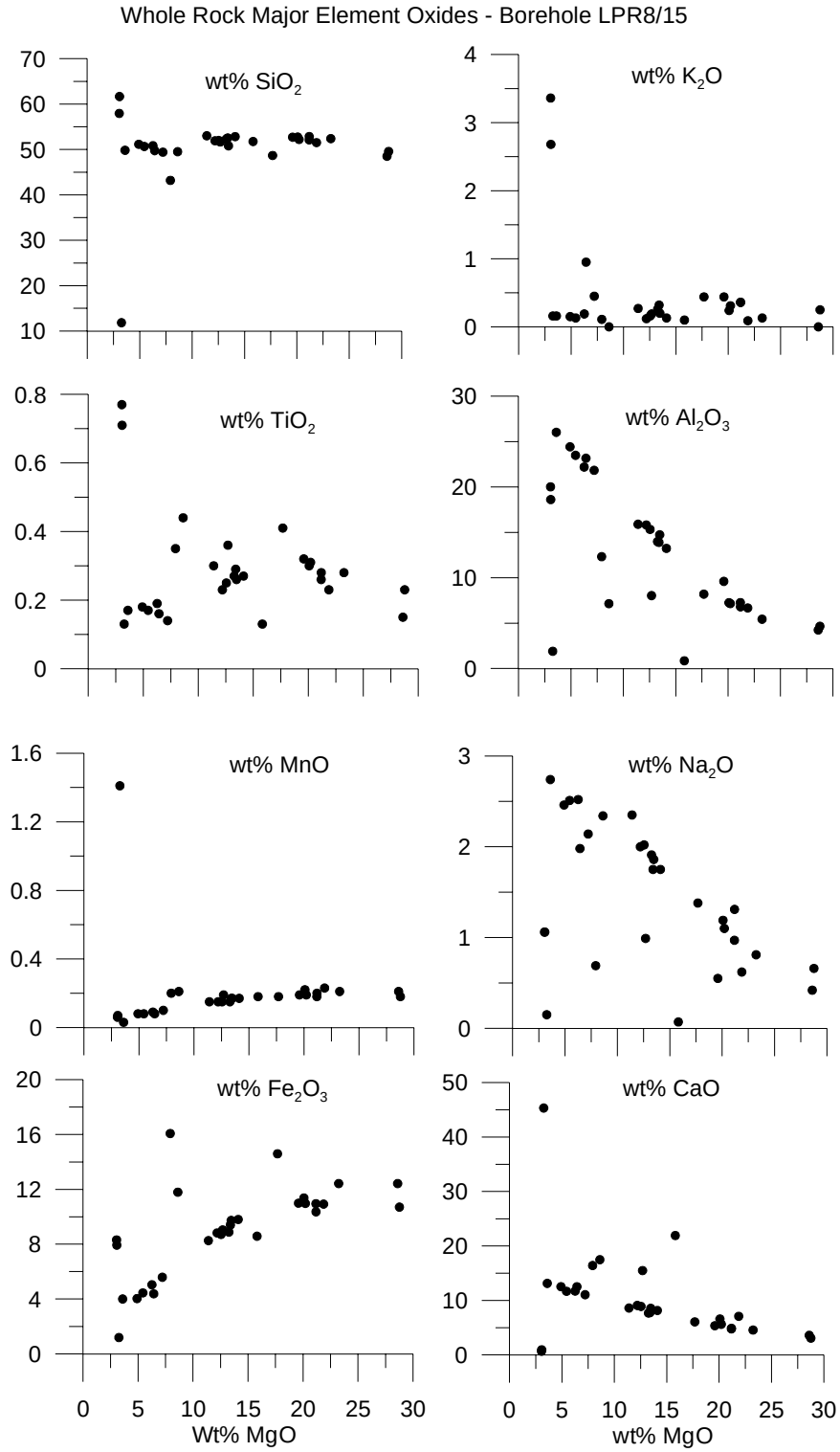

Figure 4.5 Bivariate plots of wt% major element oxides against wt% MgO from borehole LPR8/15. Increasing MgO represents increased pyroxene to plagioclase proportions in the rocks. Generally wt% Fe_2O_3 and wt% MnO both show positive correlations whilst wt% CaO, Na_2O_3, Al_2O_3 all show a negative correlation against wt% MgO. Wt% SiO_2, TiO_2 and K_2O plots are scattered against wt% MgO

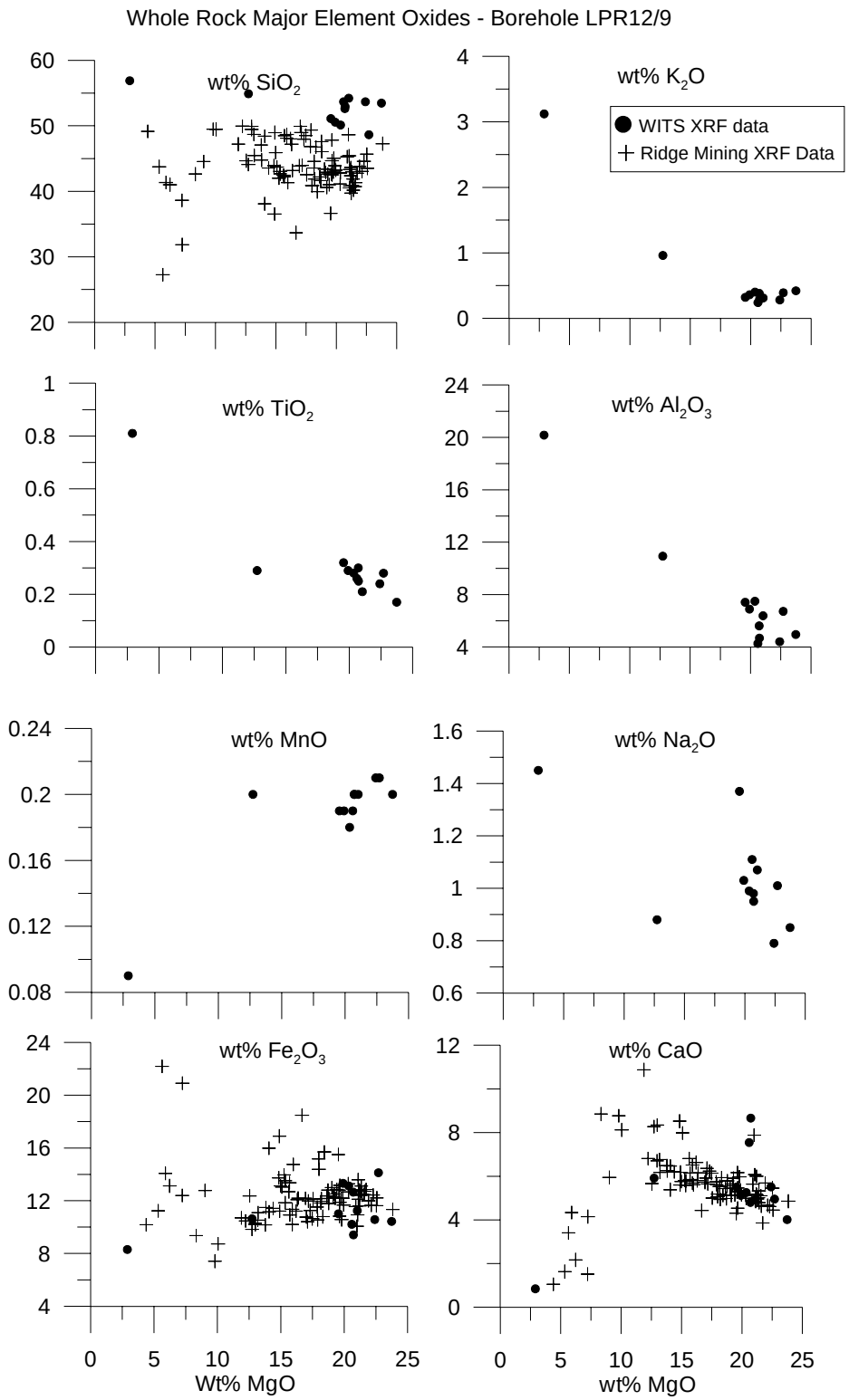

Figure 4.6 Bivariate plots of wt% major element oxides against wt% MgO from borehole LPR12/9. Where data is available results, provided by Ridge Mining have been included. All samples are taken from the basal sulphide zone on Sheba's Ridge.

4.4 Whole rock Mg#

The whole rock Mg# is based on the relative proportions of FeO and MgO and was calculated using equation 4.1.

Equation 4.1

$$Mg\# = 100*(\%MgO/40.3)/(\%MgO/40.3)+((\%Fe_2O_3/158.69)*2)).$$

Fe_2O_3 was converted to Fe^{2+} by multiplication of Fe_2O_3 by 0.8998122 and Fe_2O_3 was assumed to be zero (Eales & Cawthorn, 1996; Seabrook, 2005).

In borehole LSD34, there is a significant break in Mg# at 654.7 m in the mineralised pyroxenite (Figure 4.7). When plotted against depth the Mg# increases with height from 59 at the base of the Fe and sulphide-enriched mineralisation to 80. This corresponds to a decrease in sulphide content upwards from the basal contact with the floor rocks. This trend is also recorded in the southern sector of the Platreef (Kinnaird, 2005). From a depth of 654.7 m the Mg# becomes more constant with a small range in values of ~75 at 654.7 m to 82 at 638 m, decreasing again to 75 just below the hanging wall norite. In general the norites of Unit 3 record a consistently lower Mg# (67 – 77) than the pyroxenites (74 – 83). Another significant break can be seen at 191 m where the gabbronorite forming Sheba's Ridge has lower Mg# (63 - 68) than the units below (73 – 79). Metasedimentary samples have been excluded as they do not record magmatic signatures.

Borehole LPR6/12 again shows high Fe concentrations at the base of the mineralised unit which corresponds to a high sulphide content (Figure 4.8). There is a significant break in the mineralised unit at 203.5 m where the Mg# is scattered below and ranges from 61-80. Above 203.5 m there is a gradual increase from 70 to 80 until the hanging wall norite. There is a decrease in Mg# in the hanging wall norite to ~60. The pyroxenite/melanorites (Unit 3)

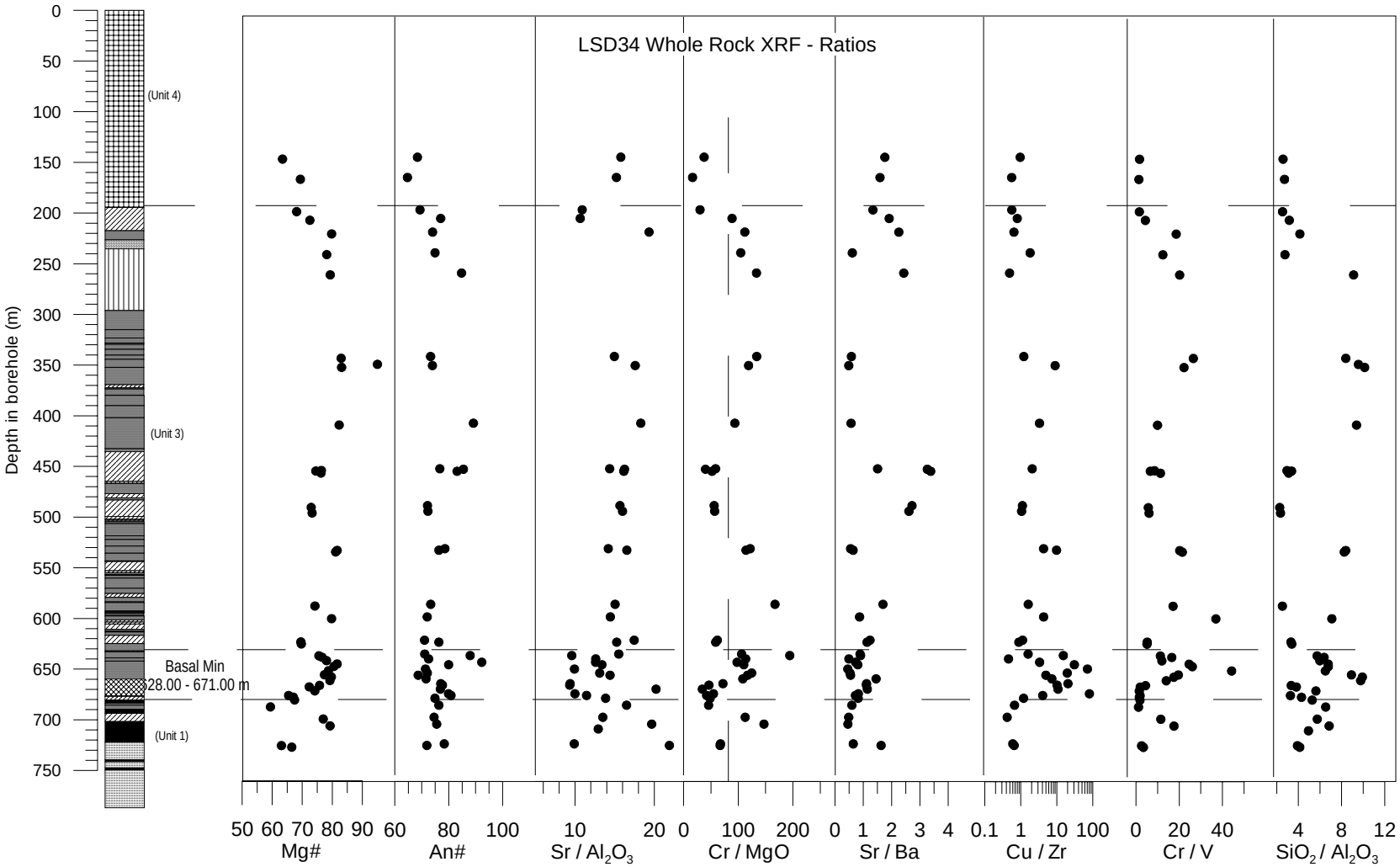

Figure 4.7 Selected whole rock major and trace element ratios plotted against depth in borehole LSD34. Note the significant break recorded at a depth of 654.70 m in the basal mineralisation and the saw tooth pattern with height.

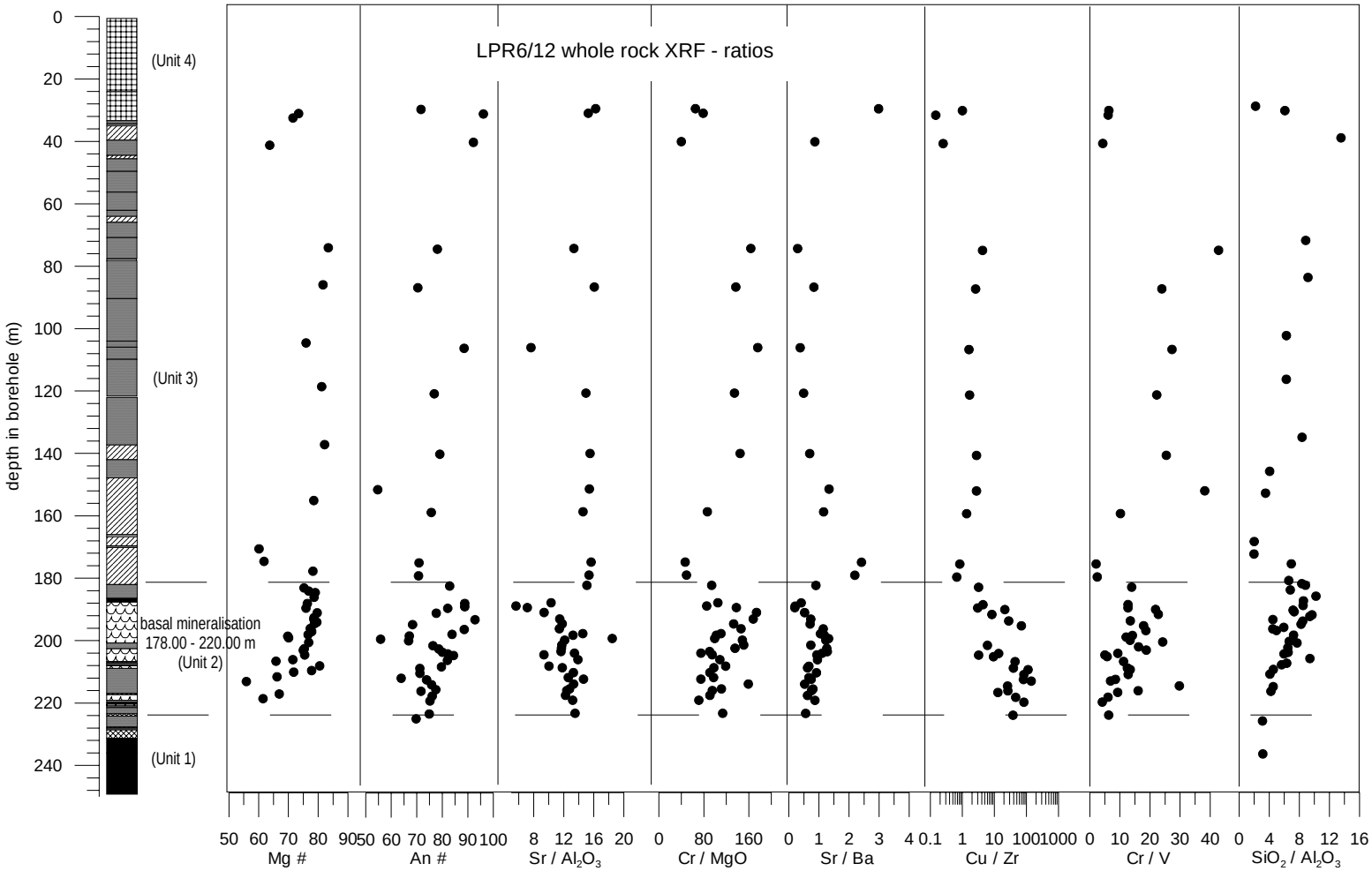

Figure 4.8 Selected whole rock major and trace element ratios plotted against depth in borehole LPR6/12.

above have a consistently higher Mg# (75 – 83) until a break occurs at 42 m with a sharp decrease in Mg# to a range of ~63 – 73.

The sampling in borehole LPR8/15 (Figure 4.9) concentrated on norites and pyroxenites above the mineralised pyroxenite. Therefore, it is unclear if there is Fe-enrichment in the mineralised unit as in other cores, due to the wide sample spacing. The scatter in Mg# at the base of the borehole reflects the presence and assimilation of hornfels and calcsilicate floor rocks. The norites have a consistently lower Mg# (66 – 77) than the pyroxenites (79 – 85). The gabbronorite from the 'disorientated' block has little variation (~75 – 76). The norite below this has a lower Mg# (66 – 73).

Borehole LPR12/9 has a high Mg# (~70 – 83) throughout the mineralised pyroxenite with a decrease again recording high Fe levels at the basal contact that corresponds to an increase in sulphide content (Figure 4.10). The lower Mg# recorded in the sample data provided by Ridge Mining reflects the occurrence of magnetite and sulphides in the sequence.

In summary, for each of these boreholes there is an iron enrichment at the base. Approximately 15 m to 25 m from the base there is a steady increase in Mg# upwards. There is then an abrupt change where the Mg# is variable through the upper part of the basal mineralisation (61-80). The hanging wall norite has a Mg# in all of the boreholes studied of ~70. In general, the Mg# in Unit 3 is interfingered through the sequence, but in part reflects the modal proportions of plagioclase to orthopyroxene. Pyroxenites have a higher Mg# (~75-85) than the norites (65-78). The Mg# is consistently lower in the gabbronorite of Unit 4 (63-68).

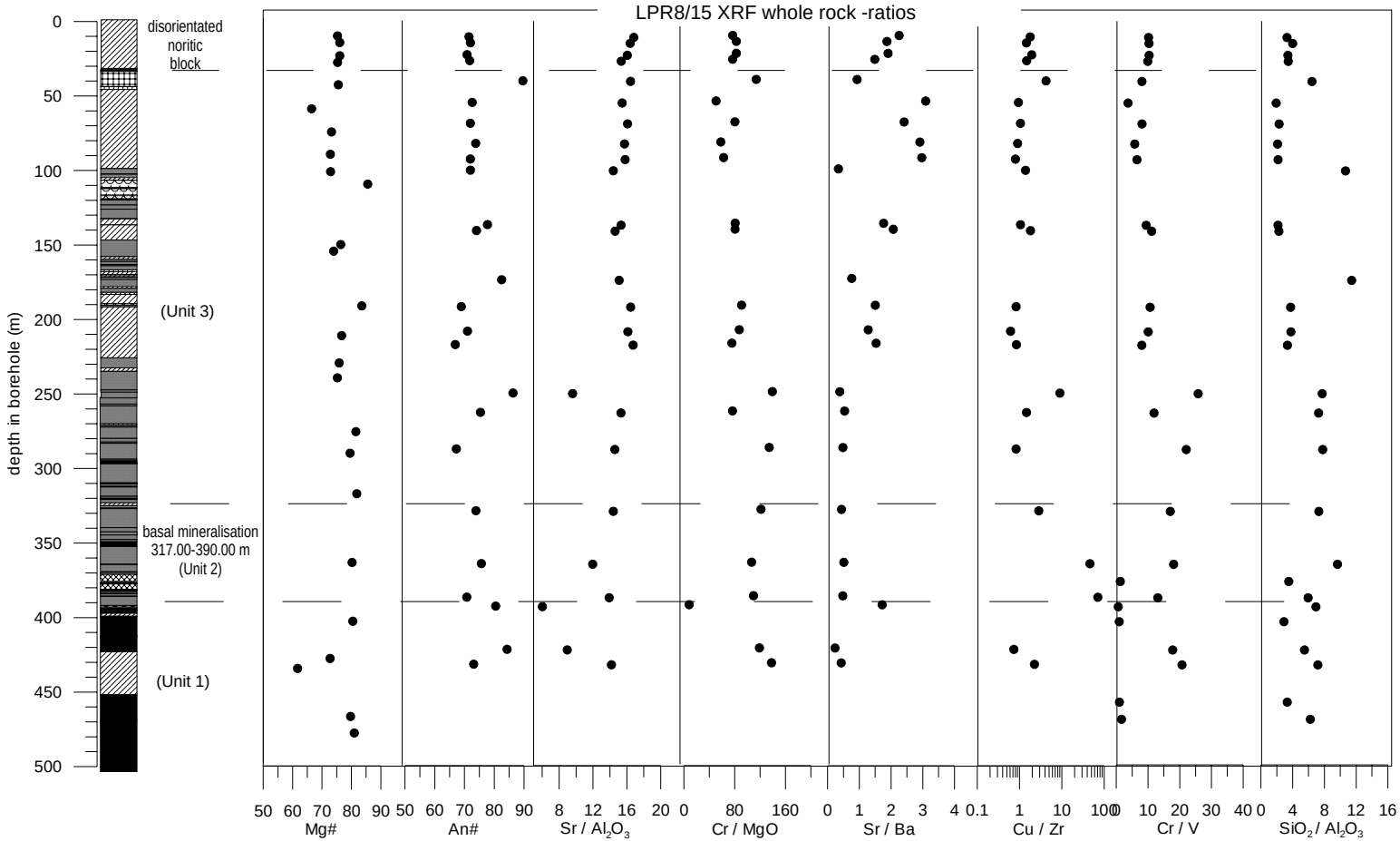

Figure 4.9 Selected whole rock major and trace element ratios plotted against depth in borehole LPR8/15.

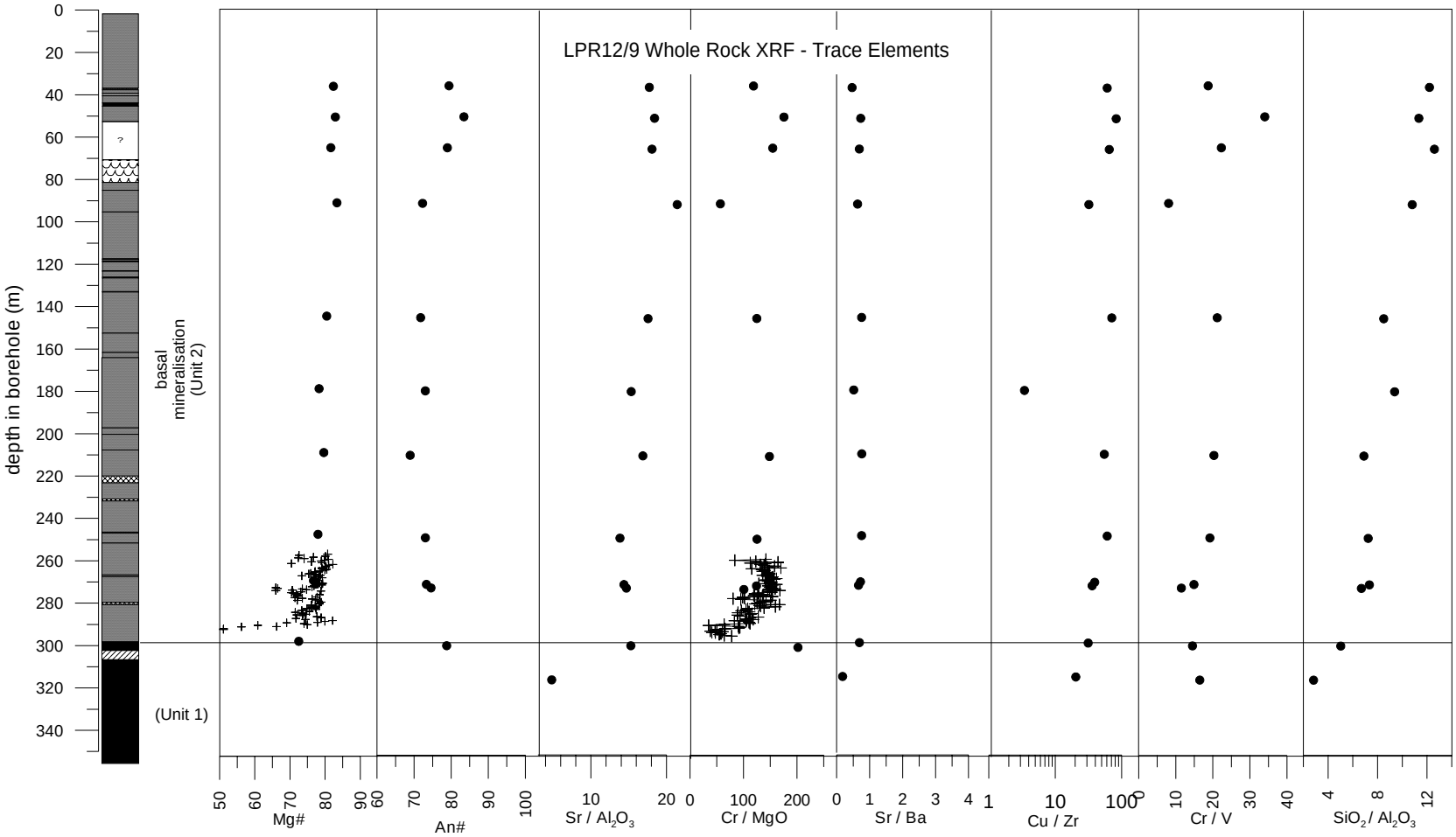

Figure 4.10 Selected whole rock major and trace element ratios plotted against depth in borehole LPR12/9.

4.5 Whole rock An#

Here the An# based on the CaO and Na_2O whole-rock composition is calculated using equation 4.2.

Equation 4.2

$$An\# = 100*(\%CaO/56.08)/((\%CaO/56.08)+((\%Na_2O/61.98)*2)).$$

In borehole LSD34 the An# shows little variation with height (Figure 4.7). Minor breaks are present and can be correlated with the breaks in Mg#. At the base of the mineralised pyroxenite to a depth of 654.7 m the An# ranges from 77 – 80. As with the Mg# the break in An# occurs at 654.7 m where the value drops sharply to 71 and is consistent until a depth of 645 m. This break in the An# profile occurs where the rock type changes from taxitic gabbronorite below to pyroxenite above. Therefore, lower values of An# above 654.7 m may be due to zoning and the intercumulus status of the plagioclase which lowers the An#. Above 645 m the An# becomes variable and increases to >90 indicating contamination by calcsilicate country rock. In the pyroxenite-norite interlayers of Unit 3 above the basal mineralisation variation in An# (71-89) is not controlled by rock type (pyroxenites where plagioclase is interstitial An# 72-89, norites where plagioclase is cumulus 71-85). There is a decrease in An# in the gabbronorites forming Sheba's Ridge (An# 65-69).

In borehole LPR6/12 two apparent trends in An# are recorded through Unit 2 (Figure 4.8). These occur from a depth of 210.5 m to 204 m (77 – 71) and 200 m to 197 m (84 – 76). Above 197 m to the hanging wall norite the An# is highly variable ranging from 91 to 55. This may be due to the interstitial nature of the plagioclase or/and the influence of calcsilicate country rock xenoliths. There is a sharp decrease in An# from 82 in the pyroxenite of Unit 2 to 70 in the hanging wall norite of Unit 3 at 175.5 m. Above this in the pyroxenite/norite interlayers of Unit 3 the An# ranges from 70 to 88. In general the An# in norite samples,

where plagioclase is a cumulus phase, is lower than in the pyroxenites, where plagioclase is intercumulus, of Unit 3 in this borehole. Calcsilicate samples LPR6/12 33.40 and LPR6/12 42.14 have been excluded as the An# (96 & 92) are not a reflection of magmatic processes. Melanorite sample LPR6/12 149 m has also been excluded as it has an anomalously low An# 54.

Sampling in borehole LPR8/15 concentrated on the norite/pyroxenite package of Unit 3 and aimed to enable a comparison to be made between the 'disorientated' block and surrounding rocks (Figure 4.9). Here the An# is controlled by rock type where, in general, pyroxenites have a higher value (70 – 82) than norites (67 – 72). Again very low values in the pyroxenites are caused by the intercumulus nature of the plagioclase. The gabbronorite at 40.5 m has a significantly higher An# (89) than the norites above and below (~70). Calcsilicate samples LPR8/15 345.6 and LPR8/15 468.5 (An# ~99) and hornfels samples LPR8/15 403.00 and LPR8/15 457.00 (An# ~30) have been excluded from the diagram.

In borehole LPR12/9 the An# for Unit 2 is only available for the samples from this study (Figure 4.10). Here the An# varies from 69 to 83 where it increases towards the top of the sequence.

In summary the An# through Unit 2 varies from 74-84. A significant break occurs where the An# decreases from ~71 to 84 in borehole LPR6/12 and from 80 to 71 in borehole LSD34. Although the An# profiles do not mirror the Mg#, significant breaks do occur at the same levels. However, variations in the An# may be a lesser indicator of primary processes due to zoning or the interstitial nature of the plagioclase. As with the Mg# the pyroxenites and norites in Unit 3 appear to have differing An# values although these values are variable. In

the pyroxenites the An# range is 72-89 whereas in the norites the range is lower 67-72. The gabbronorite of Unit 4, as with the Mg# has a significantly lower An# 65-69.

4.6 Whole Rock Geochemistry - Trace Elements

Mineral/melt partition coeffiencts for basaltic and basaltic andesite liquids show that trace elements preferentially partition into specific minerals during the crystallisation of a liquid (Rollinson, 1993 and refs therein). The trace elements are subdivided into compatible, where the element has preference for the mineral phase and therefore has a partition coefficient >1, and incompatible, where the element has preference for the melt and a partition coefficient <1, although this can vary depending on the composition of the melt. Therefore, the abundance of trace elements should be controlled by the modal proportions of minerals present. Abundances may change however, if significant contamination or alteration has occurred.

The low field strength (LFS) elements Rb, Sr, Ba, and the high field strength (HFS) elements Zr, TiO_2 (trace) and Nb have been plotted against depth in Figures 4.11, 4.13, 4.15, and 4.17. The transition metal elements Co, Zn, Cu, Ni, V and Cr are plotted against depth in Figures 4.12, 4.14, 4.16 and 4.18. Rubidium, Ba, and Nb are compatible in accessory phases such as biotite/phlogopite micas and are not controlled by major mineral phases. Yttrium may reflect varying amounts of clinopyroxene in the sequence, or be concentrated where hydrous alteration occurs. Strontium concentrations record proportions of plagioclase feldspar. Zirconium is an incompatible element in olivine, orthopyroxene, plagioclase, and clinopyroxene and indicates the occurrence of varying proportions of trapped liquid. Cobalt, Cu, Ni, V and Cr are all compatible with the pyroxenes and Ni, Cu and Co form sulphides.

However, Ni alone is not a good indicator of sulphides due to its ability to enter the structure of olivine and orthopyroxene (Seabrook, 2005).

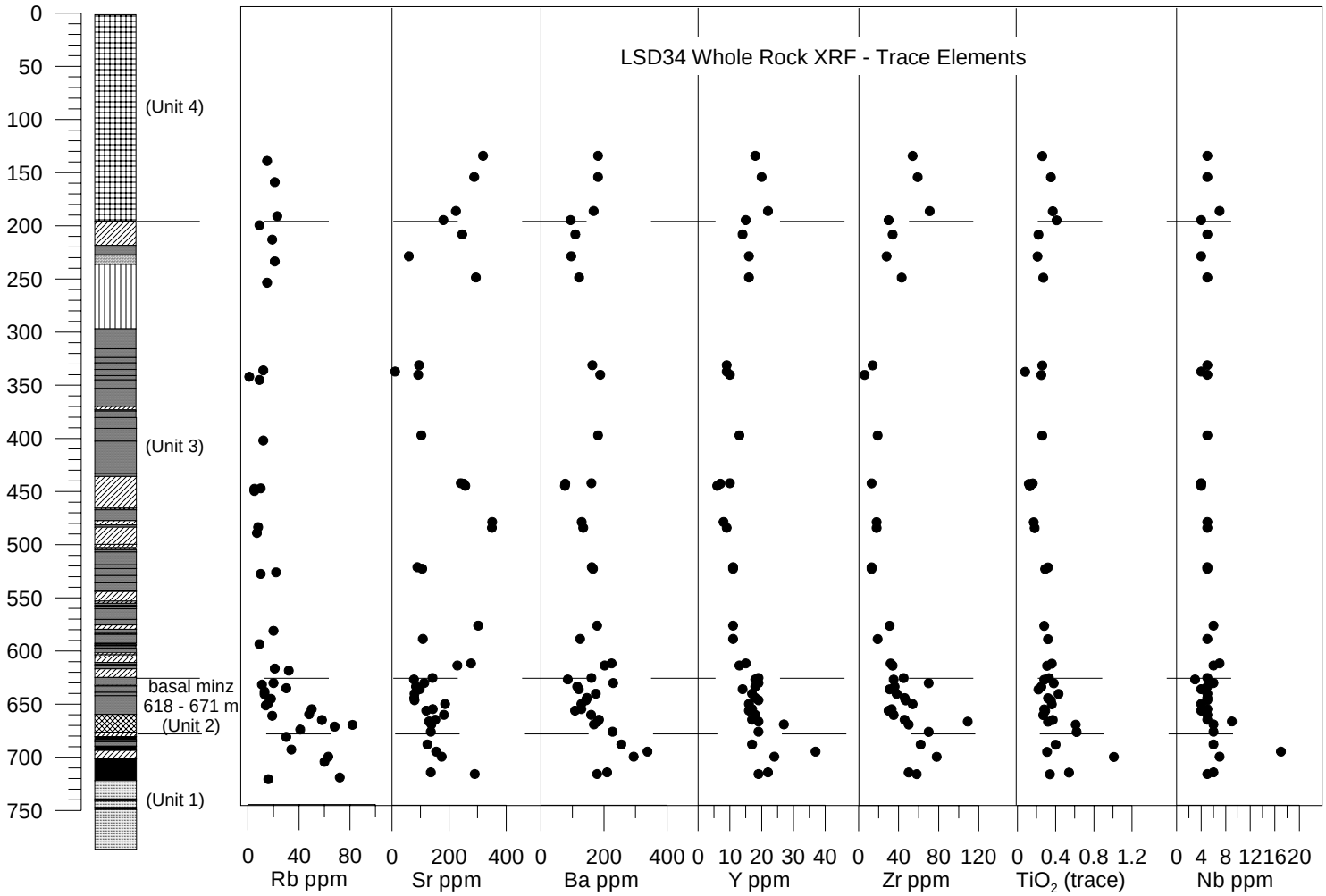

Figure 4.11 Whole Rock XRF trace element data for borehole LSD34. The low field strength incompatible elements Rb, Sr, Ba and the high field strength (HFS) incompatible elements Zr, TiO_2 (trace), and Nb are plotted against depth in borehole. A significant break occurs at a depth of 654.70 m in Rb, Sr, Ba and Zr. This depth is ~16 m above the base of the mineralised unit in this borehole. Another significant break occurs between the top of Unit 3 and the overlying gabbronorite of Unit 4, with higher trace element concentrations in the gabbronorites than in the rocks of Unit 3 below.

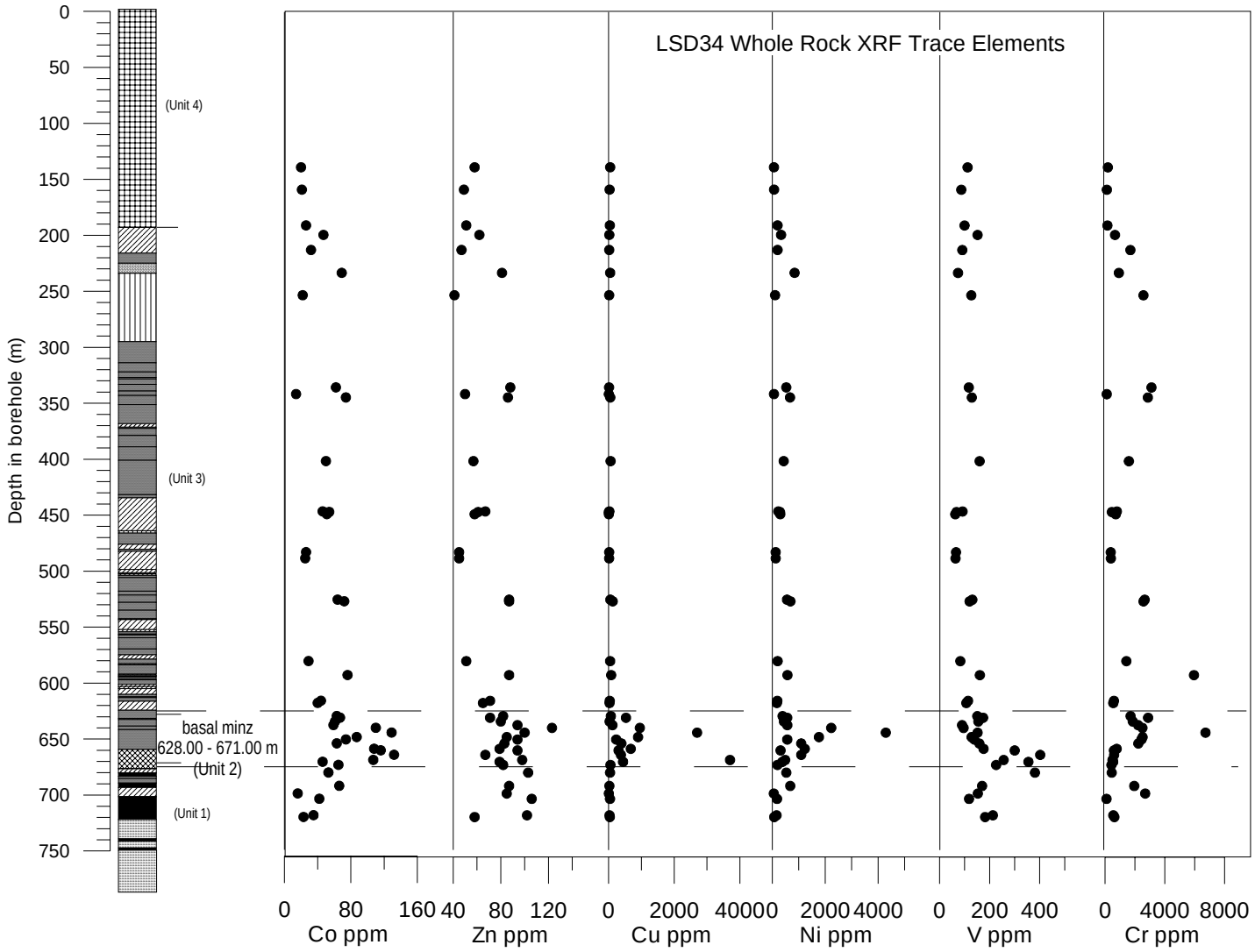

Figure 4.12 Whole rock trace element data for borehole LSD34. The transition metals are plotted against depth - Cu and Ni show peaks where the sulphides occur in the basal mineralisation. Co, V and Cr concentrations show significant breaks at 654.70 m as does Rb, Sr, Ba, and Zr in Figure 4.8.

Borehole LSD34 has elevated Sr levels that correlate with an increase in plagioclase content (Figure 4.11). Thus, Sr concentrations reflect the rock types present, such that high Sr values indicate norites or anorthosites, whereas low Sr concentrations correspond to the occurrence of pyroxenites in the sequence. There are two significant breaks in the trace element profiles of Rb, Sr, Ba, Y, Zr, TiO_2 (trace), Co, V and Cr (Figures 4.11 & 4.12). One significant break occurs between the top of Unit 3 and the base of the gabbronorite of Unit 4, with higher trace element concentrations in the gabbronorites than in the rocks of Unit 3 below. The second break in the trace elements profile occurs at 654.7 m, some 16 m above the base of the mineralised pyroxenite. This break is recorded in Rb, Sr, Ba, Y, Zr, Co, V and Cr and corresponds to a change in composition from taxitic gabbronorite at the base to an orthopyroxene dominant pyroxenite above. Both rock types have elevated Cu and Ni values and contain sulphides. The taxitic gabbronorite has Ni and Cu values of between 312 – 1229 ppm and 305 – 3699 ppm respectively. The pyroxenite above has Cu values of between 72 to 2697 ppm and Ni values of between 388 to 4290 ppm. These values are sporadically distributed through the rock units. For instance, high and low concentrations of Ni alternate with depth in the taxitic gabbronorite but high values are concentrated at the base of the pyroxenite. Conversely, the Cu values increase at the base of the taxitic gabbronorite and peak ~ 10 m above the basal contact of the pyroxenite. Alternating variation of high and low concentrations with stratigraphic height through the entire borehole is recorded in Sr, Co, Zn and Cr.

Borehole LPR6/12 shows a decrease in the trace elements concentrations of Ba, Y, Zr, Nb and TiO_2 with height from the bottom of the base of Unit 2 (Figures 4.13 & 4.14). Changes in the trace element profiles at 200 m and 192 m correspond to a change in the rock type from pyroxenite below to olivine-bearing pyroxenite above. These breaks in the trace elements

and TiO_2 profiles are concomitant with peaks in the transition metals, Co, Cu, and Ni, which reflect sulphide concentrations (Figure 4.14). Barium, Y, Zr, Nb and TiO_2 show a decrease from the base of Unit 2 to a depth of 200 m in the basal mineralisation. All of these elements are incompatible in the major minerals present in pyroxenite and therefore probably reflect the trapped liquid, thus, implying that there is a decrease in the amount of trapped liquid with height in the lowermost pyroxenite. Conversely, Cr increases with height from the base of Unit 2 to this depth of 200 m. Here values decrease rapidly and are scattered through the mineralised unit at values >2000 ppm. The rocks above the basal pyroxenite, in the upper part of the mineralised unit, have undergone varying degrees of alteration and consist of a complex alternating sequence of taxitic gabbronorite, feldspathic pyroxenite and olivine-bearing pyroxenite ± magnetite. Samples taken are predominantly from the olivine-bearing rocks. Some values of Zr were below the detection limit in the olivine-bearing rocks and are therefore omitted from the graph. In general the altered rocks have higher Loss on Ignition and elevated values of Y due to the abundance of hydrous biotite and phlogopite. As with LSD34, the hanging wall norite in this borehole has high Sr levels (>300 ppm) and shows a sharp decrease in Cr content from 1753 ppm to 133 ppm partly due to an increase in the proportion of plagioclase and a decrease in orthopyroxene and partly due to the occurrence of minor chromite grains in the pyroxenite . Floor rock hornfels shows elevated Rb, Ba, Y, Zr, TiO_2, Nb, Zn and V (Figures 4.13 & 4.14).

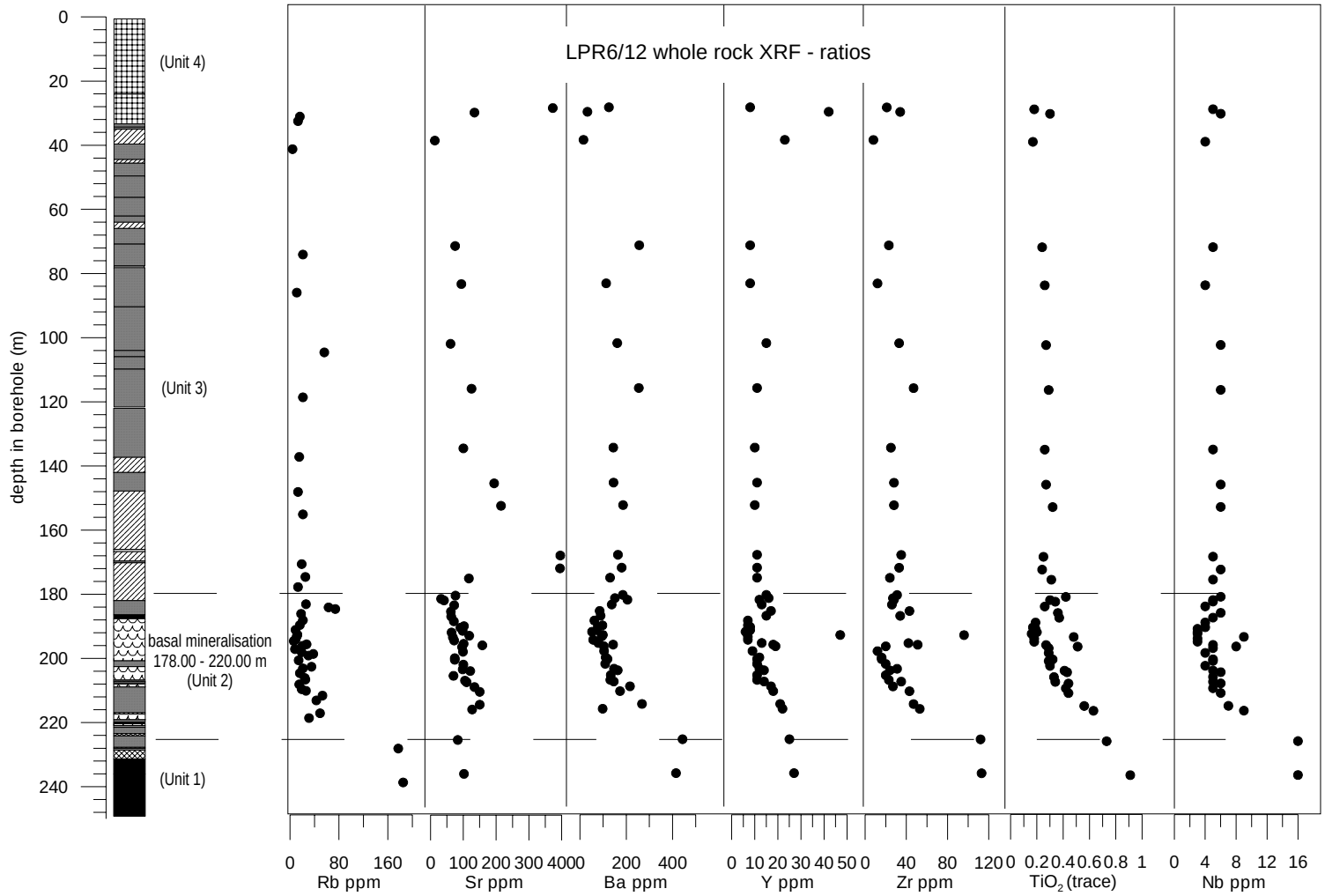

Figure 4.13 Whole Rock XRF trace element data for borehole LPR6/12. The low field strength (LFS) incompatible elements Rb, Sr, Ba and the high field strength (HFS) incompatible elements Zr, TiO_2 (trace) and Nb are plotted against depth in borehole. A significant break occurs at 200.00 m in Zr, TiO_2 and Nb, with another break in the trace element profile at 192.00 m, both within Unit 2.

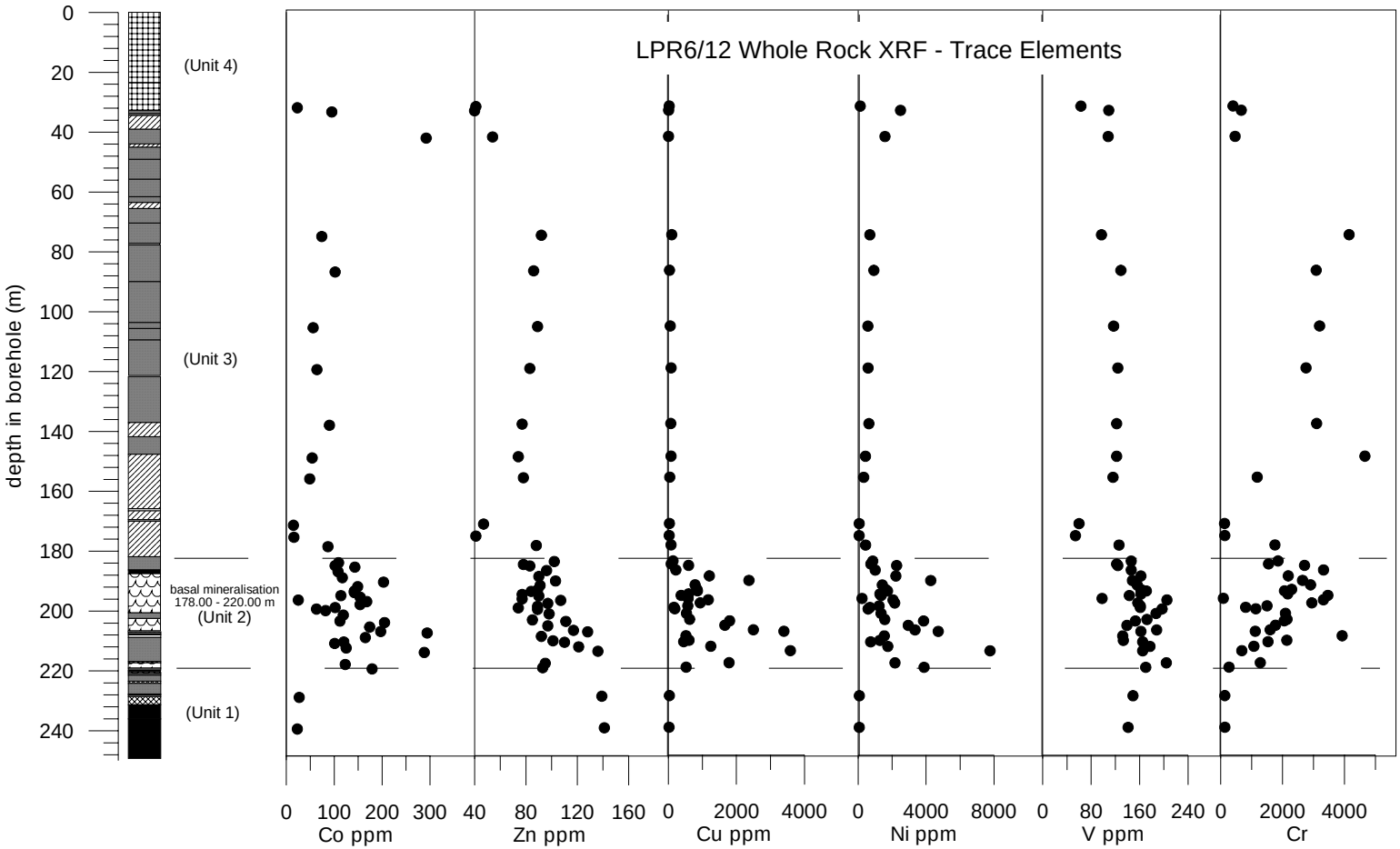

Figure 4.14 Whole rock trace element data for borehole LPR6/12. The transitions metals are plotted against depth - Cu and Ni peaks correspond to sulphide occurrences in the basal mineralisation.

Borehole LPR8/15 shows a break in trace element profiles of Sr, TiO_2, Co, Zn, V and Cr at a depth of 27 m (Figures 4.15 and 4.16) at the top of the 'disorientated' noritic block. Below this at 40.5 m the gabbroic layer (possibly Unit 4) is characterised by increased Y, Zr and V levels. Below the gabbro, the norite package of Unit 3 has differing trace element profiles to the 'norite of the 'disorientated' block, most notably in the higher concentrations of Sr indicating increased proportions of modal plagioclase, and the lower levels of TiO_2, Co, Zn, V and Cr. Samples from pyroxenites at 100.5 m and 174 m both have >3000 ppm Cr recording the presence of Cr-spinel in the samples. Chromium levels plotted against depth show a saw tooth pattern with two general groupings, one containing <1500 ppm and the other >1500 ppm. Strontium also shows a saw tooth pattern with depth and in general with two groups, one with concentrations <300 ppm and the other with >300 ppm. The mineralisation records elevated levels of Cu and Ni at the base of the unit only, but this may be due to the sample spacing rather than a lack of sulphides in the top of the unit. Floor rocks are characterised by elevated levels of Rb, Ba, Y, Zr, TiO_2, Nb, Zn, and V.

Borehole LPR12/9 was collared directly into the basal mineralisation of Unit 2 at Sheba's Ridge and therefore does not include any of the hanging wall rocks of the area. As the rocks contain only interstitial plagioclase, Sr levels are <200 ppm (Figure 4.17). Chromium values are all >2000 ppm with the exception of one sample taken at a depth of 178.5 m (Figure 4.18). This has <200 ppm Cr and elevated concentrations of Y and Nb. These anomalous values reflect alteration or contamination in this sample. Floor rock hornfels are distinct with elevated levels of Rb, Ba, Zr and TiO_2 (trace).

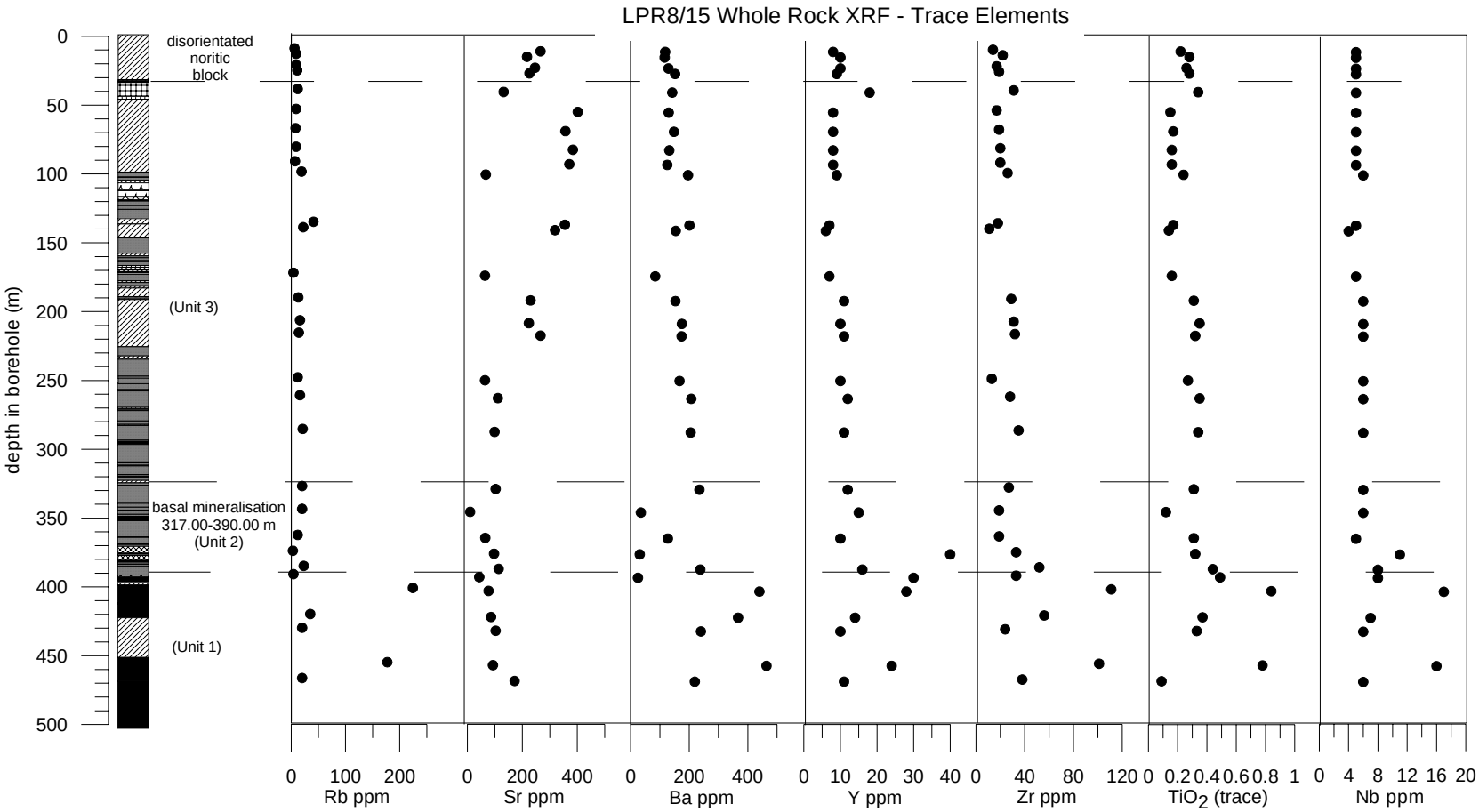

Figure 4.15 Whole rock XRF trace element data for borehole LPR8/15. The low field strength (LFS) incompatible elements Rb, Sr, Ba and the high field strength (HFS) incompatible elements Zr, TiO_2 (trace) and Nb are plotted against depth.

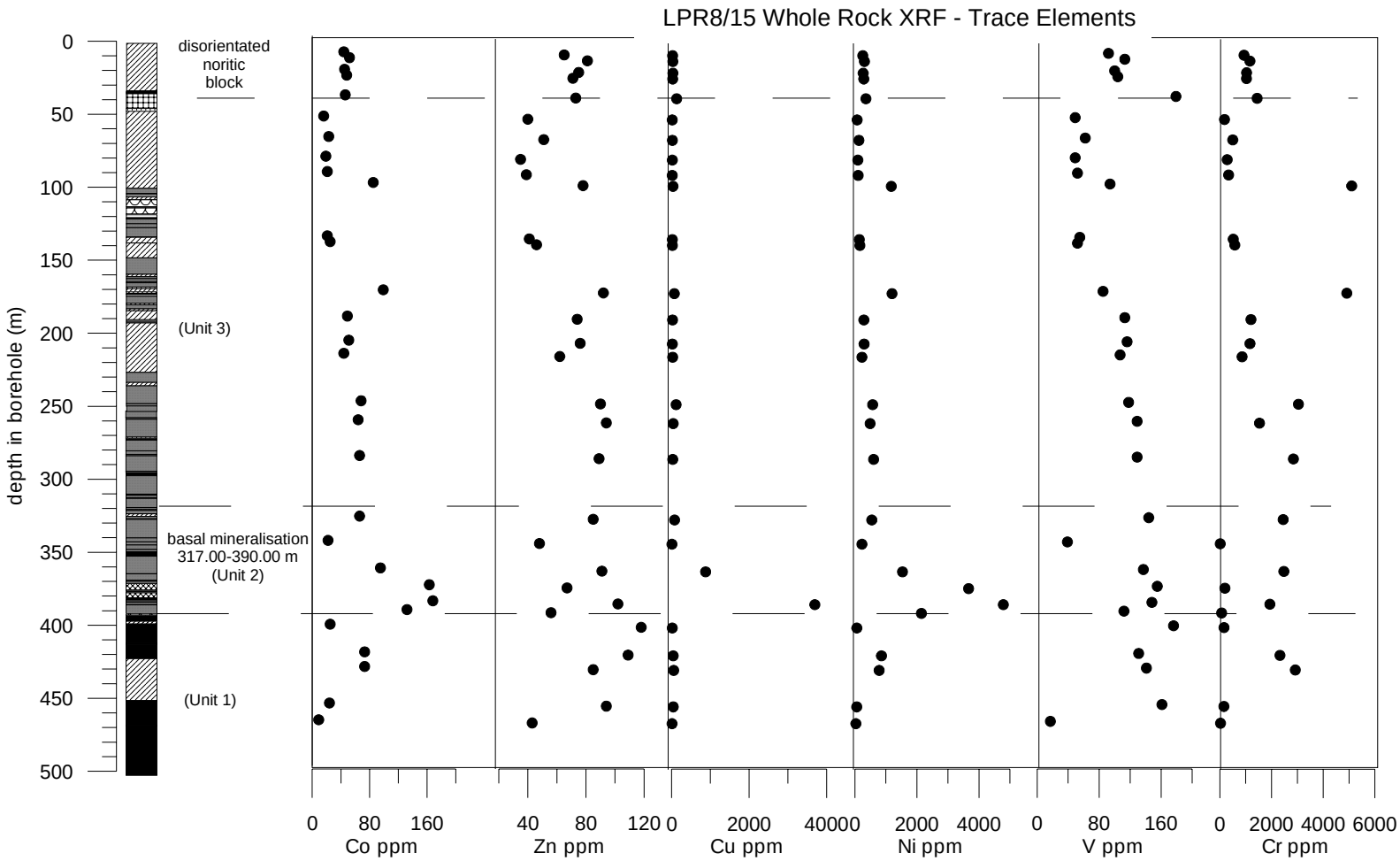

Figure 4.16 Whole rock trace element data for borehole LPR8/15. The transition metals are plotted against depth - Cu and Ni peaks occur where sulphides are present in the basal mineralisation.

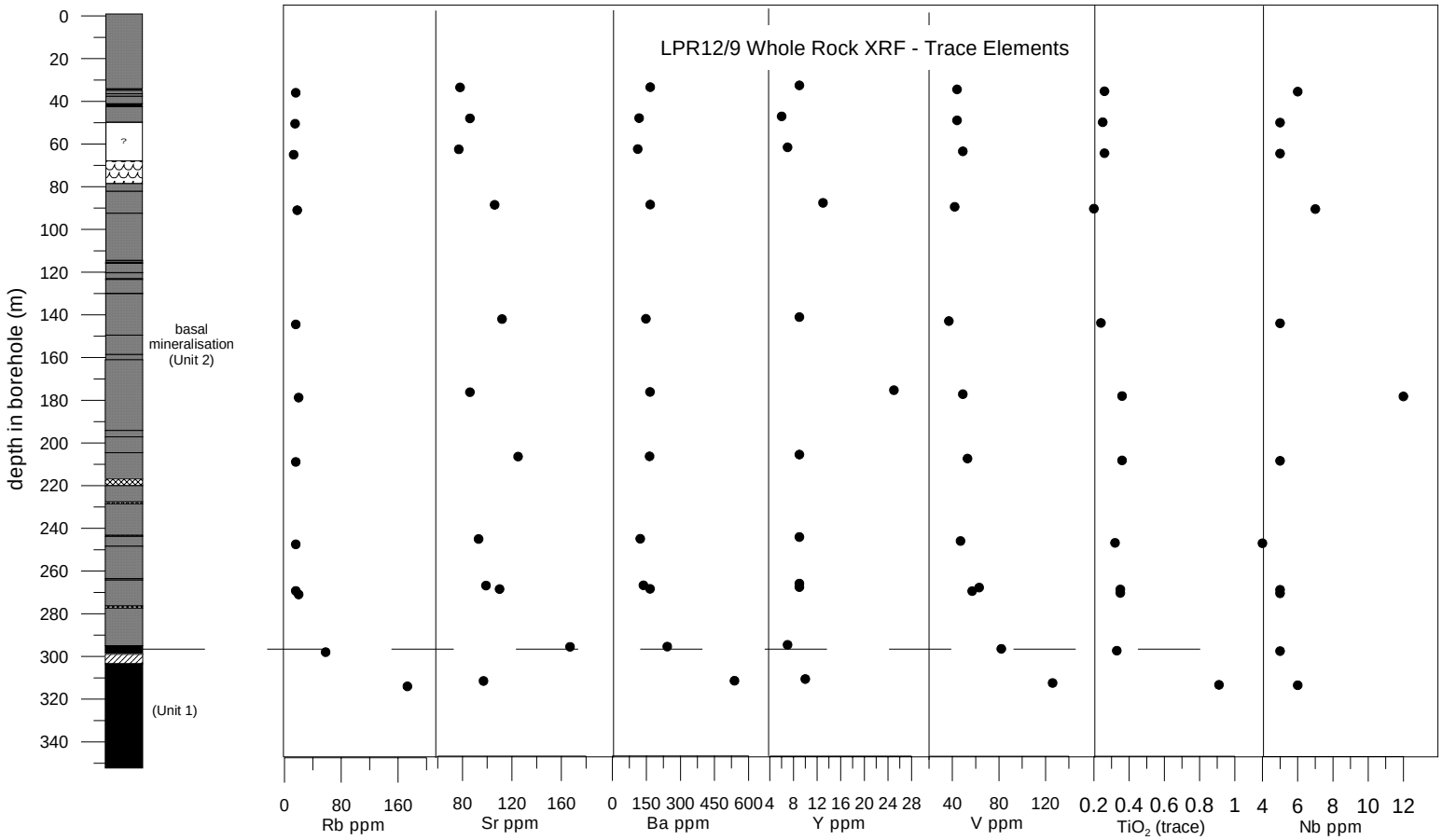

Figure 4.17 Whole rock XRF trace element data for borehole LPR12/9. The low field strength (LFS) incompatible elements Rb, Sr, Ba and the high field strength incompatible elements Zr, TiO_2 (trace) and Nb are plotted against depth in borehole.

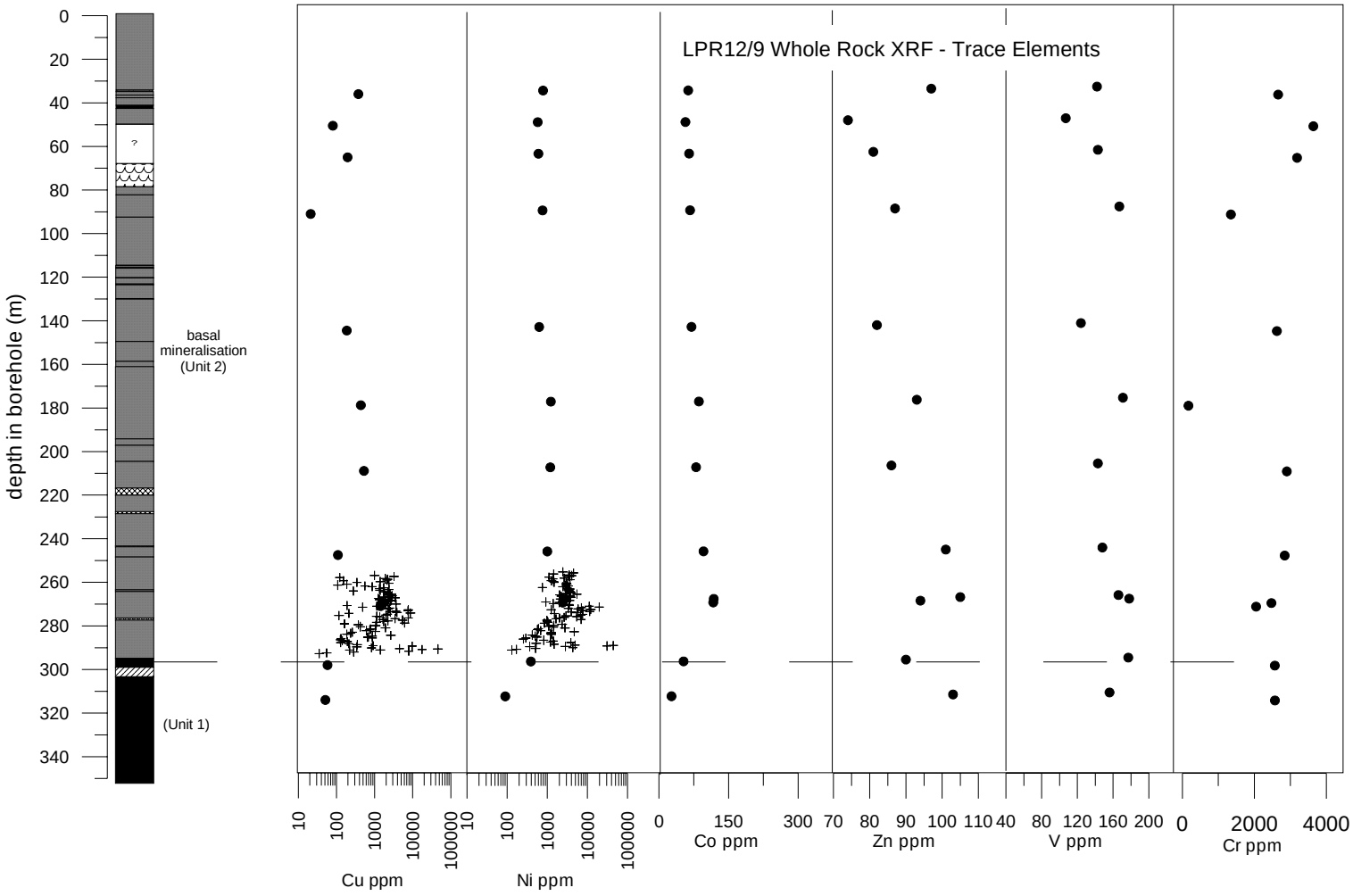

Figure 4.18 Whole rock trace element data for borehole LPR12/9. The transition metals are plotted against depth in borehole - Cu and Ni are plotted using a logarithmic scale. Peaks occur where sulphides are present in the basal mineralisation.

4.7 Element Ratios

Ratios of elements selected for their compatibility in one phase and incompatibility in another should be independent of modal proportions. On this basis the element ratios Sr/Al_2O_3, Cr/MgO, Sr/Ba, Cu/Zr, Cr/V and SiO_2/Al_2O_3 have been plotted against depth in borehole in Figures 4.7, 4.8, 4.9 and 4.10. The Sr/Al_2O_3 and Cr/MgO were chosen to investigate whether there are different magmatic influxes as these ratios are independent of modal proportions in the rock, (Eales *et al,* 1986; Eales *et al,* 1988; Nex *et al,* 2002; Cawthorn & Lee, 2005; Kinnaird, 2005).

Sr/Al_2O_3 ratios are used by Eales *et al* (1986) to identify cyclic units in the C_UZ, of the eastern and western limbs of the Bushveld Complex. As Sr is a compatible element in plagioclase and incompatible in orthopyroxene the ratio of Sr to Al_2O_3 should not vary if derived from the same source. Eales *et al* (1986) recognised fractionation would produce a progressive change but any significant break in the geochemical profile must represent the occurrence of a differing source material, i.e. a new influx of magma or a geochemical hiatus. However, this ratio may be affected by assimilation and later infiltration (Cawthorn & Lee, 2005).

Due to the small amount of Al held in pyroxene, Eales *et al* (1986) used a simple formula to correct for this

Equation 4.3

$$Al_2O_3^{*} = Al_2O_{3\ rock} - (MgO_{\ in\ rock} / MgO_{\ in\ pyroxene} \times Al_2O_{3\ pyroxene})$$

Plots of Sr/Al_2O_3 against depth have not been corrected using this formula as only a limited number of samples were analysed for mineral separate data. However, for those samples

where both whole rock and mineral separate data are available and the correction made, the difference in plotting position is minimal (Figure 4.19).

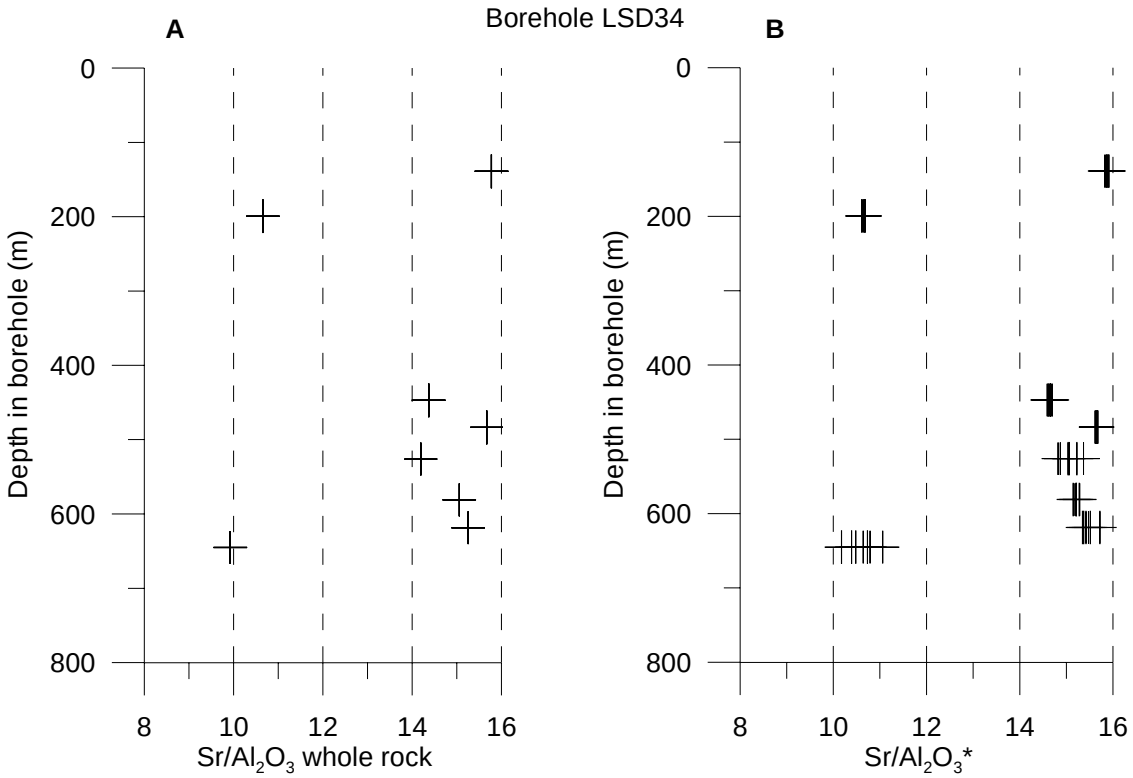

Figure 4.19 Mineral separate data for plagioclase from borehole LSD34 showing A) Sr/Al_2O_3 ratio from whole rock XRF data B) $Sr/Al_2O_3^*$ ratio corrected for the small amount of Al occurring in pyroxene using equation 5.1. Data is taken from microprobe analysis.

As the elements Cr and Mg are relatively immobile they are unaffected by processes of assimilation and overprinting (Cawthorn & Lee, 2005). They are both compatible elements in orthopyroxene and incompatible in plagioclase. Therefore, for samples that contain >5 wt% MgO the Cr/MgO ratio should be unaffected by modal proportions. However, some samples may contain grains of Cr-spinel but these are easily picked out and samples with >3500 ppm have been omitted, following Seabrook (2005). Typical values of Cr/MgO are >80 in the Critical Zone of the BC and <80 in the Main Zone (Seabrook, 2005). Cawthorn & Lee (2005) also record this break in the Northern Limb with the Platreef Cr/MgO >80 and the

Main Zone <80. Therefore, the Cr/MgO ratio can be used to indicate different sources of magma and provide a direct comparison of Bushveld rocks with the rocks at Sheba's Ridge. The ratio of Sr/Ba indicates fractional crystallisation as Sr and Ba are compatible elements in plagioclase and are incompatible elements in all of the major mafic minerals. Therefore, any significant break in the geochemistry should represent the influx of magma or a geochemical hiatus (Eales *et al* 1986). Similarly, the ratio Cr/V is used as these transition metals have differing partition coefficients. Chromium has significantly higher partition coefficients in all of the major minerals than V. However, the ratio will be affected by the occurrence of the spinels chromite and magnetite in the sequence. This is recognisable by a significant increase in Cr content and therefore an elevated ratio. Mitchell *et al* (1998) showed typical values of Cr/V to range from ~6 at the base of the Main Zone in the BC to ~0.1 at 2000 m above the base.

To consider changes in the geochemical profile with depth against the occurrence of peaks in mineralisation, the ratio Cu/Zr is used (Naldrett 2004). Both Cu and Zr are incompatible elements and therefore the concentration of both should increase with increased fractionation but the ratio should remain the same. If sulphide immiscibility is reached, Cu will become compatible and the ratio will decrease as sulphides are removed. If the magma or cumulates acquire more sulphide from elsewhere the ratio will be higher than that of the original sulphide-unsaturated magma (Naldrett, 2004).

The SiO_2/Al_2O_3 ratio is used as a potential indicator of two different magma sources. The ratio should remain unchanged if successive intrusive pulses are from a single source of magma with pyroxene and plagioclase on the liquidus (Kinnaird, 2005).

In borehole LSD34 the Cr/MgO ratio records a break at 654.7 m (Figure 4.7). Above this the ratio varies with height and two distinct geochemical groupings are present: one where Cr/MgO is <80 and one where it is >80. A Cr/MgO of <80 occurs in the taxitic gabbronorite at the base of the mineralisation in Unit 2, in the hanging wall norite to the basal mineralisation, the norite interlayers in Unit 3 and the gabbronorite of Unit 4. Whereas, the pyroxenite in the upper part of Unit 2 and the pyroxenite interlayers of Unit 3 have a Cr/MgO of >80. These distinct groupings of Cr/MgO are concomitant with changes in Cr/V, Sr/Al_2O_3, and SiO_2/Al_2O_3. The Cu/Zr ratio shows that peaks in mineralisation occur at a stratigraphic height where there is a significant break in the element abundances in Unit 2. In borehole LSD34 these geochemical groups are inter-fingered giving repetitive inflexions in the geochemical profile with stratigraphic height. In borehole LPR6/12 breaks in the element ratios also occur at a height where there is a peak in the sulphide content (Figure 4.8). This occurs three times in this borehole in Unit 2 at 192 m, 200 m and at the base of Unit 2. The layers of Unit 3 are again showing an alternating geochemical pattern. Borehole LPR8/15 also records a break in the geochemical element ratios associated with the mineralisation of Unit 2 (Figure 4.9). The 'disorientated' block has the same geochemical signature as the norites of Unit 3 but the gabbronorite directly below has a higher Cr/MgO ratio (113). Borehole LPR12/9 shows little variation with depth which is consistent with the borehole being collared directly into Unit 2 so that only Units 1 and 2 are represented in the geochemical profiles shown in Figure 4.10.

4.8 Discussion

In layered intrusions changes in element abundance is predominantly controlled by modal proportions of minerals in the rocks. As Eales *et al* (1986) indicates, virtually any element will show progressive increase or decrease in the sequence from peridotite through to

anorthosite, with modal variation. This is further complicated in the rocks at Sheba's Ridge by the occurrence of minerals such as magnetite and sulphides which significantly effect the Mg# and the interstitial nature of plagioclase in some of the samples studied. However, ratios of elements selected on the basis of their compatibility with one phase and incompatibility with others should be independent of modal proportions. Therefore, a break in the geochemical signature with depth indicates a hiatus (Eales *et al* 1986). Furthermore, if the ratios differ significantly it is unlikely that they could be derived from the same magma. Here a number of major element oxide and trace element ratios are presented for whole rock data. These ratios have been used in previous studies of the BC and other igneous intrusions as a measure of fractional crystallisation, contamination or assimilation and to indicate the influx of new magma (e.g. Eales *et al*, 1986; Cawthorn, 1999; Kinnaird, 2005). From the major and trace element profiles of the boreholes studied two geochemical groupings can be inferred (Table 4.2). To further constrain these groupings the following discussion attempts to use these methods to interpret possible magmatic processes and compare these rocks to the BC and other ultramafic-mafic intrusions.

Table 4.2 Geochemical characteristics of two geochemically distinct packages at Sheba's Ridge.

	Type A	Type B
Cr ppm whole rock	>800	<800
Wt% MgO whole rock	<15%	>15%
Cr/MgO whole rock	>80	<80
Cr/V whole rock	<10	>10
Sr/Al_2O_3 whole rock	>16	<16
SiO_2/Al_2O_3 whole rock	>4	<4

4.8.1 Whole Rock Mg#

The Mg# is used as a measure of fractional crystallisation in layered intrusions. In the early stages of crystallisation the Mg# will change due to the high Mg-Fe ratio of the liquidus of ferromagnesian minerals (e.g. olivine and orthopyroxene) compared to the host melt (Rollinson, 1993). Thus, with continued fractionation the Mg# should decrease. It is observed at the lower Critical Zone – upper Critical Zone boundary of the Bushveld Complex, that the appearance of cumulus plagioclase corresponds to a change in the Mg#. Eales & Cawthorn (1996) indicated that at an Mg# of 83 the magma starts crystallising cumulus feldspar. The inverse of this ratio may also be used to indicate Fe-enrichment. As Seabrook (2005) notes, although there will be some Fe_2O_3 which will lower the absolute value of Mg#, comparisons using variations in Mg# can still be made. Although the rocks at Sheba's Ridge have ± clinopyroxene ± olivine ± sulphides ± magnetite which vary greatly through the stratigraphic sequence and may significantly effect the Mg#. However, a number of trends are recorded.

The variation in Mg# through the sequence at Sheba's Ridge shows three significant variations. The first is an Fe-enrichment at the base of the mineralised unit which corresponds to an increase in sulphide content towards the contact with the floor rocks. The second is that pyroxenites have a consistently higher Mg# than norites through the sequence. This follows the modal proportions of plagioclase and pyroxene of the rocks sampled. The third is a significant decrease in Mg# in the gabbronorite of Unit 4 forming Sheba's Ridge. Cawthorn (1999) suggests these changes in Mg# cannot be the result of fractional crystallisation only. It can be shown that these variations may be a reflection of the proportion of cumulus pyroxene to interstitial magma. If this is the case the Mg# will be lower with lower values of wt% MgO (taken to represent orthopyroxene as the dominant

mafic mineral) (Figure 4.20). However, as mentioned previously it is inaccurate to apply this method to the rock types at Sheba's Ridge as the rocks often contain ± clinopyroxene ± olivine ± sulphides ± magnetite, which significantly alter the Mg#. The linear trend in borehole LPR8/15 (Figure 4.20 C) records the variation in modal proportions of orthopyroxene to interstitial magma as the samples here are predominantly unaltered orthopyroxenites to leuconorites. Therefore, to suggest that these variations are purely from the fractional crystallisation of a magma is invalid and other methods must be used to determine geochemical groupings.

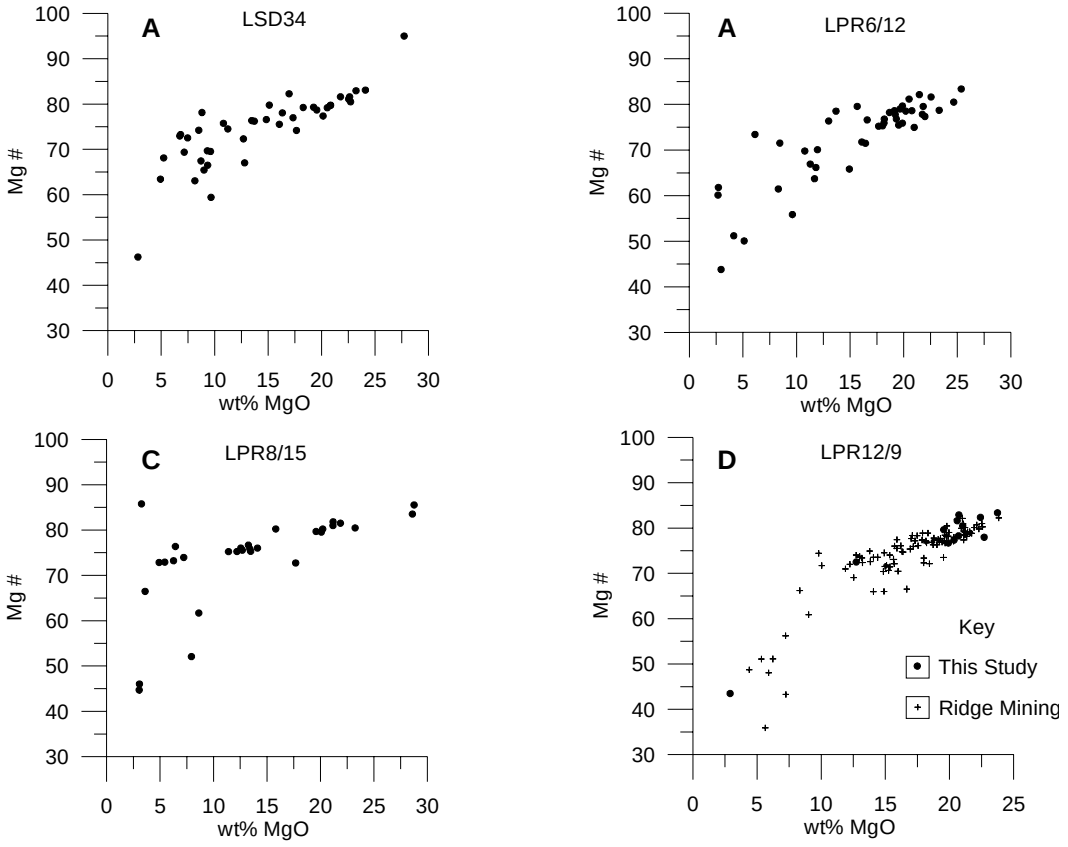

Figure 4.20 Plots of whole rock Mg# *versus* wt% MgO from borehole: A) LSD34, B) LPR6/12, C) LPR8/15 and D) LPR12/9 after Cawthorn (1999) showing lower Mg# values at low wt% MgO (taken to represent orthopyroxene content). This trend is complicated by the occurrence of clinopyroxene, olivine, sulphides and magnetite which all affect the Mg#. Borehole LPR8/15 shows a linear trend in the predominantly unaltered orthopyroxenites to leuconorites sampled in this borehole.

4.8.2 Whole Rock An#

As with Mg#, the An# is used as a measure of crystal fractionation in layered intrusions. In general An# decreases with increased fractionation of a magma. Very low An# values may be due to zoning and the intercumulus nature of the plagioclase which lowers the An#, whereas very high values may be due to contamination or assimilation of Ca-rich country rock (Cawthorn & Lee, 2005). In the Lower and lower Critical Zones of the Bushveld Complex the An# of the interstitial plagioclase ranges between 77 to 50 (Eales & Cawthorn, 1996). At Sheba's Ridge the An# records distinct breaks that are concomitant with breaks in the profiles of Mg# and major and trace element ratios. The An# also shows evidence of assimilation or contamination by country rock and in general records the interstitial and cumulus phases of plagioclase.

4.8.3 Major and Trace Element Ratios

As previously discussed the Sr/Al_2O_3, Cr/MgO, Sr/Ba and SiO_2/Al_2O_3 were chosen to represent different magmatic influxes as these ratios are independent of modal proportions in the rock, (Eales *et al*, 1986; Eales *et al*, 1988; Nex *et al*, 2002; Cawthorn & Lee, 2005; Kinnaird, 2005). Any significant break in the geochemistry should therefore represent the influx of magma or a geochemical hiatus (Eales *et al* 1986). For Sheba's Ridge there are two distinct geochemical groupings that have concomitant breaks in all of the ratios (Table 4.2). These groupings are used here to suggest that there were two geochemically different magmas that intruded to form the sequence at Sheba's Ridge designated types A and B. From the Cu/Zr profile it can also be suggested that peaks in the basal mineralisation occur where there is a transition from type A to type B in the sequence.

4.8.4 Comparison with the Bushveld Complex

There are a number of geochemical criteria that defines the Bushveld Complex stratigraphic sequence. This has been summarised by Eales & Cawthorn (1996) and is shown in Figure 4.21. As introduced in Chapter one, previous studies of the Bushveld Complex have shown that the CZ and the MZ have distinctive geochemical signatures. In recent years it has become increasingly recognised that this marked change in geochemistry represents two different magmas (e.g. Sharpe, 1981; Davies & Tredoux, 1985; Eales *et* al, 1986; Kruger, 1990; Cawthorn *et al*, 1991; Kruger, 1994; Eales *et* al, 1993*;* Mitchell *et al*, 1998). However, the stratigraphic sequence at Sheba's Ridge has geochemical variations that differ significantly from those of the main eastern limb of the Bushveld Complex. They do not follow a simple fractional crystallisation trend with upward Fe-enrichment. Eales & Cawthorn (1996), summarising the general fractionation trend for the eastern and western limbs of the Bushveld Complex, show that Mg# in opx varies from ~90-70 in the LZ and CZ and is only below 60 in the Upper Zone (Figure 4.21). There is a concomitant decrease in An# in plagioclase from ~80-60 through the C_UZ and MZ, reaching ~40 in the Upper Zone. However, this trend through the Bushveld stratigraphy is on a macro scale and several minor breaks in geochemistry have been used to postulate multiple magma influxes or replenishment through the differing zones (e.g.; Cawthorn *et al*, 1991; Kruger, 1990; 1994; Eales *et al*, 1993; Mitchell, 1996; Kinnaird *et al*, 2002).

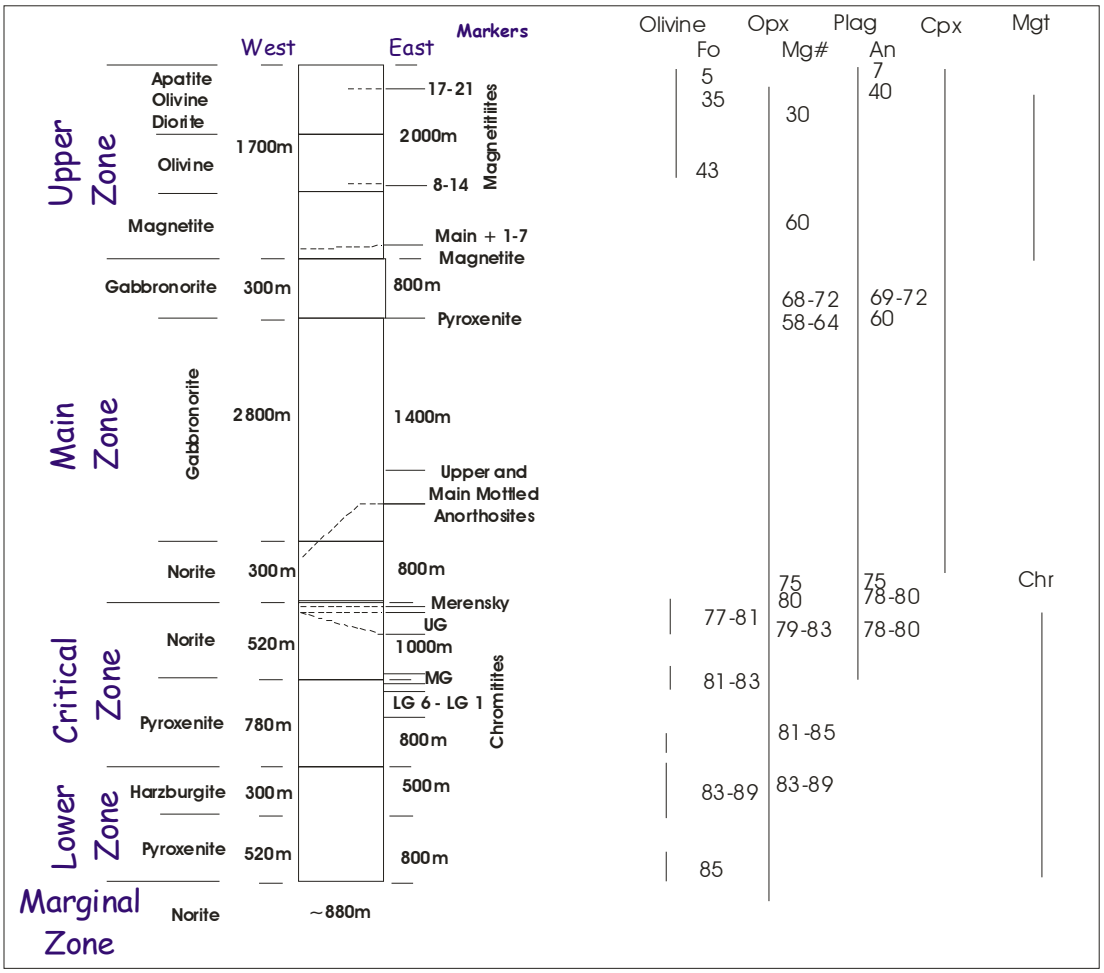

Figure 4.21 Stratigraphic succession of the Bushveld Complex, showing mineralised intervals, geochemical variation with height and Zones of the Complex. Modified from Eales & Cawthorn (1996).

Sheba's Ridge rocks on the basis of Mg# and An# suggest affinities to both the CZ znd MZ of the main Bushveld Complex. However, the CZ-type and MZ-type which have been equated to Group A nd Group B in Table 4.2 do not show a fractionating sequence upward but are rather inter-fingered. Unit 3 which has affinities to the CZ, has a saw tooth pattern displaying the interfingered nature of these two magma types. By comparison, the gabbronorites of Unit 4 have a distinct geochemical signature which has an affinity to the Main Zone of the BC. The inter-fingering in Units 2 and 3 shows similarities to the Platreef of the northern limb. Kinnaird (2005) shows 4 geochemically distinct packages through the

Platreef. These packages do not display a fractionating sequence from bottom to top but are also inter-fingered. From this Kinnaird (2005) suggests the Platreef is a complex zone of multiphase emplacement of pyroxenitic sills sometimes interlayered with country rocks. It can, therefore, be postulated here that Unit 2 at Sheba's Ridge formed from the mixing of two geochemically distinct packages with peaks in mineralisation that are concomitant to the boundary between these two magma types.

4.9 Summary

- Two distinct geochemical groupings are present in the basal mineralisation and peaks in the mineralisation occur at the boundary between them.
- There is an Fe-enrichment at the base of the mineralised Unit 2 towards the contact with floor rocks. This is concomitant with an increase in sulphide content.
- The hanging wall norite to the basal mineralisation shows a marked change in geochemistry and marks the base of Unit 3.
- In general the norites of Unit 3 have a lower Mg# and An# than the pyroxenites.
- There is a distinct break in the geochemical profile from Unit 3 to the gabbronorite of Unit 4.
- Unit 4 is correlated with the MZ of the Bushveld Complex whereas in Units 2 and 3 rocks that seem to have a CZ affinity and those that have a MZ affinity are interfingered.

CHAPTER 5

Mineral Chemistry

5.1 Introduction

Data from mineral separate analyses are the classic way to document trends in the magmatic evolution of layered intrusions (e.g. Wager & Brown, 1968; Parsons, 1987; Nex *et al*, 2002). In the previous Chapter, the whole rock An# was discussed. This reflects behaviour of plagioclase in the magmas. Variations in An# were concomitant with changes in Mg#. In this Chapter plagioclase and pyroxenes were analysed by microprobe in 12 samples in order to evaluate whether minerals are zoned, and if so how such variations might compare with the whole rock An#. A further 19 plagioclase mineral separate samples were analysed by XRF from 3 boreholes over demarcated stratigraphic boundaries betweens Units 1-4. In addition Rb-Sr isotope analysis of 10 plagioclases were undertaken in an attempt to correlate the Sheba's Ridge succession with that of the isotope stratigraphy of the eastern limb of the BC, proposed by Kruger (1990, 1994).

Eight samples chosen for microprobe analysis were from borehole LSD34 on the southern side of Sheba's Ridge. These were selected to represent variation with stratigraphic height (Appendix 5). Four samples were chosen from the norite of the 'disorientated' block to compare with the noritic unit below in LPR8/15 (Appendix 5). Within each sample the pyroxene chosen for analysis was selected on the basis of its cumulus nature and lack of any alteration. For each grain between four and eight analyses were run from the core of the grain to the outer rim. For plagioclase, unaltered cumulus crystals were chosen from norites and gabbronorites. In pyroxenites the plagioclase grains chosen were intercumulus and unaltered.

A further 19 samples of pure plagioclase mineral separates from boreholes LSD22. LSD34 and LPR6/12 were analysed using XRF to compare with the analyses obtained by microprobe and in order to determine whether there is any systematic change in plagioclase composition from base to top of the stratigraphy, or whether any sudden geochemical changes occur (Appendix 6).

5.2 Mineral Separate analytical techniques

Energy-Dispersive Electron Microprobe Analysis

Analyses were carried out at SPECTRAU, University of Johannesburg (previously Rand Afrikaans University) with a Cameca 355 electron microprobe. Polished thin sections were carbon coated and loaded into the Cameca 355 and pumped to a high vacuum. The applied accelerating voltage was 15 KeV and the diameter of the electron beam 10μm. A certified MAC standard was used as an internal standard throughout the run.

All pyroxene grains were analysed for FeO, MnO, TiO_2, CaO, Na_2O, SiO_2, Al_2O_3, MgO, Cr_2O_3, K_2O and are expressed as oxide weight %.

All plagioclase grains were analysed for MnO, Na_2O, K_2O, SiO_2, Al_2O_3, MgO, FeO, CaO and are expressed as oxide weight %.

As zoning in orthopyroxene and plagioclase grains occurs due to reaction with interstitial liquid or sub-solidus equilibrium (Eales & Cawthorn, 1996), a number of analyses were made for each grain.

X-ray Fluorescence Spectrometry

A further 19 whole rock samples were crushed, milled and sieved to a fraction size of 95 – 120µm. This material was then washed to remove any fines and dried in pans at ~100˚C. A hand magnet was used to remove any magnetite in the sample. Samples were then processed through a Franz Electromagnetic separator at various amperages to separate plagioclase from orthopyroxene and other minerals. Any impurities were removed by hand under a binocular microscope. Each plagioclase separate was then crushed to a fine powder using a manual agate pestle and mortar. The separates were then analysed for major and trace elements by X-Ray fluorescence spectrometry (XRF) at the University of the Witwatersrand using a PW1400 XRFS. As with whole rock analysis samples were analysed for major element oxides (wt%):

SiO_2, TiO_2, Al_2O_3, Fe_2O_3, MnO, MgO, CaO, Na_2O, K_2O and P_2O.and Loss on Ignition (LOI) and trace elements (ppm):

Rb, Sr, Y, Zr, Nb, Co, Ni, Cu, Zn, Ti, V, Cr and Ba.

The full results of these analyses are shown in Appendix 6.

Isotope Dilution Mass Spectrometry

The five samples from borehole LSD22 chosen to represent the rock types at Sheba's Ridge were selected because they had undergone minimal alteration. Three samples from LSD34 were chosen to correlate with those of LSD22 and to show any variation in $^{87}Sr/^{86}Sr$ values in Units 3 and 4. Two samples from LPR6/12 were chosen to determine $^{87}Sr/^{86}Sr$ values in Unit 2. Analysis was undertaken at the Hugh Allsop Laboratories, University of the Witwatersrand under the supervision of Prof Johan Kruger following the techniques of Eales *et al.* (1990), outlined by Seabrook (2005) as follows:

The samples were crushed, milled and sieved to a fraction size of 95 – 120µm. This material was then washed to remove any fines and dried in pans at ~100˚C. A hand magnet was used to remove any magnetic material in the sample. Samples were then run through a Franz Electromagnetic separator at various settings to separate plagioclase. Any impurities were removed by hand from the pure plagioclase under a binocular microscope. The pure plagioclase separate was then washed with acetone to remove any surface contaminants and then crushed to a fine powder in a agate mortar. Approximately 0.05g of each plagioclase sample was placed in a Teflon beaker. Spikes of ^{84}Sr (99%) and 99% Rb were added prior to dissolution. Samples were then dissolved in a mixture of concentrated hydrofluoric acid (HF) and 8N nitric acid (HNO_3). The lids were then removed to evaporate the silica-saturated acid. The residue was dissolved in 2.5N hydrochloric acid (HCl) and placed in teflon tubes. These were placed on a centrifuge for 10 minutes at 7000 rpm. Each sample was loaded in 1ml of HCl and filtered through a standard cation-exchange chromatographic quartz-glass column filled with Bio-Rad AG50W 8x200-200 mesh cation exchange resin to achieve bulk separation of Sr. An eluant of 2.5N HCl was used and the last 7 ml was collected and dried. Sr taken from the original samples was retained in the remaining portion. Samples of Sr were loaded on to single Ta filaments with 1 drop H_2PO_4 and 1 drop HNO_3. Rubidium samples were loaded on to a side filament with a central Ta filament. Rubidium was analysed using a MM30 solid-source mass spectrometer and Sr using a Thermal Ionisation Mass Spectrometer (TIMS) VG354 multi-collector instrument using Pyramid TIMS software. Sr-isotopic data were normalized to $^{86}Sr/^{87}Sr = 0.1194$. Runs of SRM-987 $SrCo_3$ standard yielded an $^{86}Sr/^{87}Sr$ ratio of 0.71023±20 (2σ). Sr isotopic ratios were then calculated and the results and calculations used are shown in Table 5.1.

Table 5.1 Results of Isotope Dilution Mass Spectrometry of plagioclase separates for 10 selected samples.

Sample Number	Depth (m) from top of borehole	Mineral	Rock type	Rb ppm	87Rb	Sr ppm	86Sr	87Rb/87Sr	87Sr/86Sr	±	2se	R 2,055	±	2σ
Borehole LSD 34														
LSD34 139.00	139.00	Plag	gabbronorite	10.50	2.96	404.2	39.0753	0.07488	0.710755	±	42	0.70854	±	16
LSD34 234.50	234.50	Plag	gabbronorite	21.09	5.94	301.6	29.1575	0.20142	0.710685	±	25	0.70472	±	20
LSD34 253.50	253.50	Plag	gabbronorite	38.86	10.95	429.7	41.5241	0.26065	0.713834	±	58	0.70612	±	22
Borehole LPR 6/12														
LPR6/12-5	178.64	Plag	pyroxenite	5.01	1.41	471.1	45.5537	0.03065	0.707549	±	66	0.70664	±	15
LPR6/12-29	195.50	Plag	pyroxenite	3.23	0.91	432.1	41.7866	0.02155	0.707404	±	21	0.70677	±	15
Borehole LSD 22														
LSD22/1	137.00	Plag	gabbronorite	12.24	3.45	597.0	57.72	0.05909	0.708189	±	52	0.70644	±	16
LSD22/2	182.50	Plag	gabbronorite	21.35	6.02	273.4	36.1	0.16478	0.712155	±	40	0.70728	±	19
LSD22/3	313.20	Plag	pyroxenite	11.41	3.21	402.3	38.8912	0.08169	0.710103	±	18	0.70768	±	17
LSD22/4	544.00	Plag	norite	14.02	3.95	479.4	46.3549	0.08422	0.708746	±	34	0.70625	±	17
LSD22/5	666.00	Plag	norite	10.88	3.07	180.0	17.4	0.17416	0.7138	±	2	0.70864	±	19

(Equation 5.1)

To calculate the $^{87}Sr/^{86}Sr$ ratio the following equation is used with an assumed intrusion date of 2055.

$$^{87}Sr/^{86}Sr_{(initial)} = {}^{87}Sr/^{86}Sr_{(present)} - [(^{87}Sr/^{86}Sr)*(e\lambda^{t}-1)]$$

$^{87}Sr/^{86}Sr_{(initial)}$	=	initial ratio
$^{87}Sr/^{86}Sr_{(present)}$	=	measured ratio
e	=	constant
λ	=	$1.42 \times 10^{-11}\ y^{-1}$
t	=	2055×10^{6}

5.3 Pyroxenes

Compositional data of pyroxenes from the microprobe analyses are presented in a ternary diagram (Figure 5.1). Data from previous studies of the BC, data are also plotted on the ternary diagram. Pyroxenes from the gabbronorites of Sheba's Ridge Unit 4 are of ferrohypersthene compositions (En_{30-50}). Pyroxenes from the pyroxenites below in Unit 3 and Unit 2 are more magnesian in comparison and have orthopyroxene compositions of hypersthene (En_{50-70}) to bronzite (En_{70-90}). These are similar in composition to the average values for pyroxenes from the Platreef (Harris and Chaumba, 2001), and also those from the Lower and Critical Zones (Eales *et al,* 1993) as indicated. Norites have an orthopyroxene composition of hypersthene. These are grouped with Main Zone samples from Cawthorn *et al* (1991) and the Critical Zone from Eales *et al* (1993).

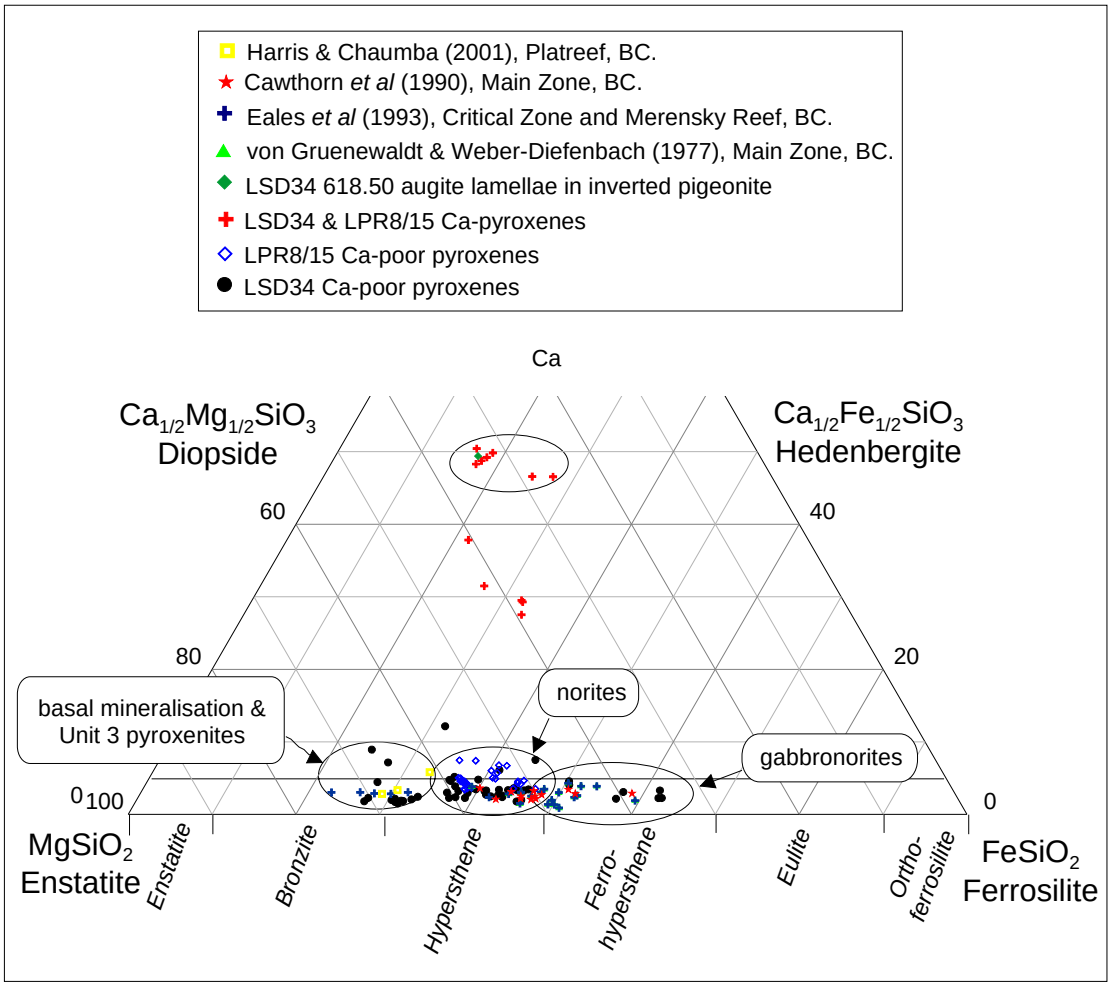

Figure 5.1 Microprobe data plotted on a ternary diagram of average pyroxene compositions for this study, the Critical and Main Zones, and the Platreef, BC. Interstitial clinopyroxenes and augite lamellae from inverted pigeonite are also plotted.

Microprobe data shows significant variation in individual grains as shown in Figure 5.2. The Cr/MgO and Mg# has been plotted against depth in borehole and shows that due to low values of Cr in opx and the detection limit of the microprobe, Cr/MgO ratio can not be used accurately in the interpretation of this data.

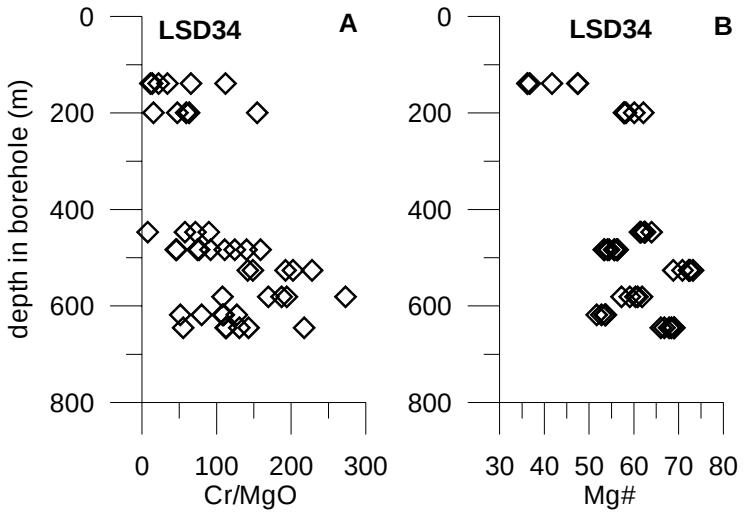

Figure 5.2 Microprobe data for orthopyroxene grains in samples from borehole LSD34 showing element ratios: A) Cr/MgO and B) Mg#. Data shows significant compositional variation within individual grains.

5.4 Plagioclase

Mineral separate data (Appendix 6) of plagioclase analysed using XRF from boreholes LSD34, LSD22 and LPR6/12 are plotted on ternary diagrams in Figures 5.3A, B & C respectively (after Seabrook, 2005). Microprobe data from boreholes LSD34 and LPR8/15 are plotted in Figure 5.3D. These plots were chosen to indicate that the samples chosen contained no contamination or alteration and that the samples were pure plagioclase mineral separate grains. XRF analyses indicate that, with the exception of sample LSD22/5 and LPR6/12 28 195 m, the samples analysed are pure plagioclase (labradorite-bytownite) in composition and that the bulk composition from the XRF analysis is the same as that obtained for the averaged microprobe analysis. Samples LSD22/5 and LPR6/12 28 have high %CaO (35.08 and 48.41 respectively) and low silica and clearly cannot be plagioclase. However, it is not clear what the mineral could be, since calcite alteration would be reflected in high LOI. Therefore, these samples are disregarded in the interpretation of the data set.

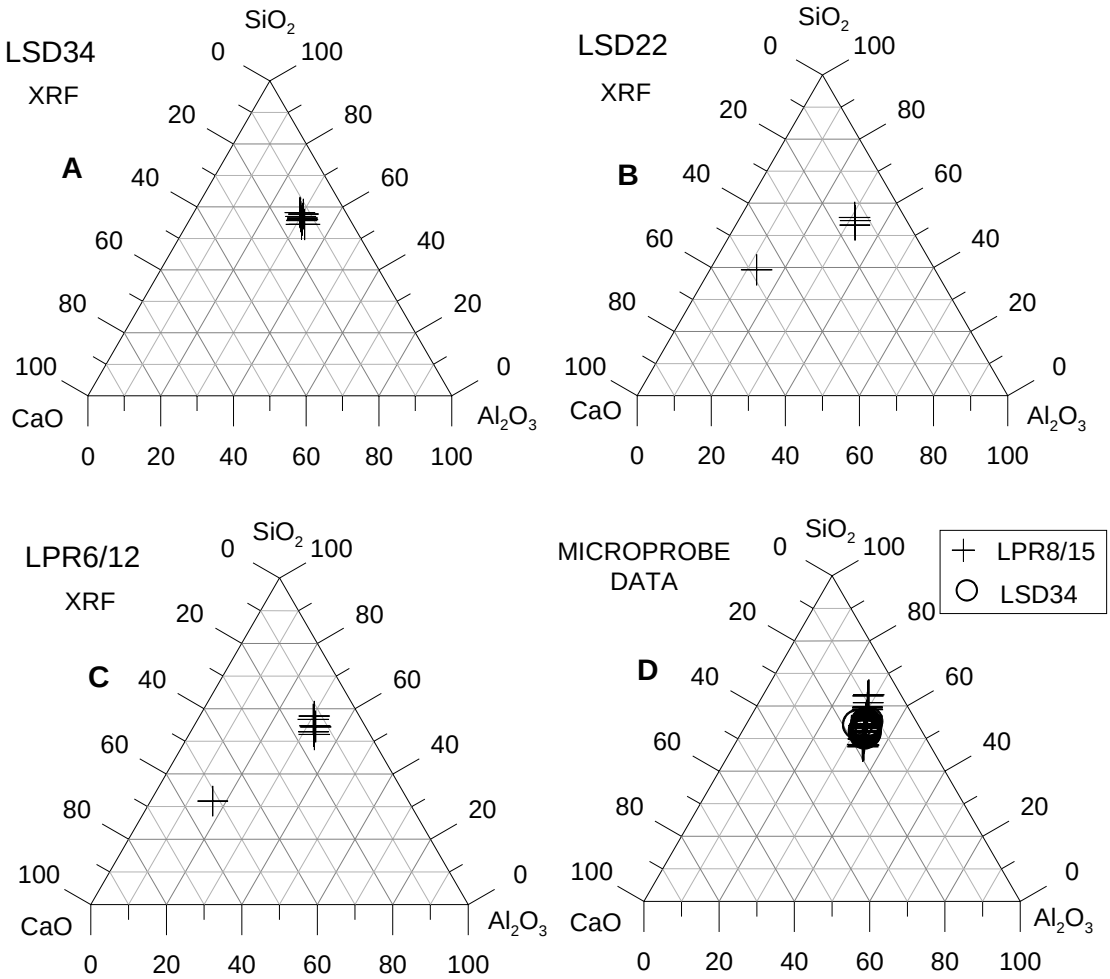

Figure 5.3 Ternary diagrams of major element oxides in plagioclase from microprobe data: A) borehole LSD34, B) LSD22 and C) LPR6/12 and D) XRF plagioclase mineral separate data from boreholes LSD34 and LPR8/15.

The An# has been plotted against depth in borehole in Figures 5.4. Data is taken from whole rock and plagioclase mineral separates and microprobe analyses for each of the 3 boreholes. The compositional range exhibited by single grain plagioclase microprobe analysis in each sample shows that there is a significant variation in the plagioclase grains. As presented in Chapter 4 there is significant variability in the An# which does not follow the Mg# profiles suggests either zoning and/or the interstitial nature of the plagioclase. In borehole LPR6/12 between a depth of 195 to 200 m there are elevated Zr levels in whole rock analyses suggesting that the variation in the An# is due to the trapped liquid shift effect.

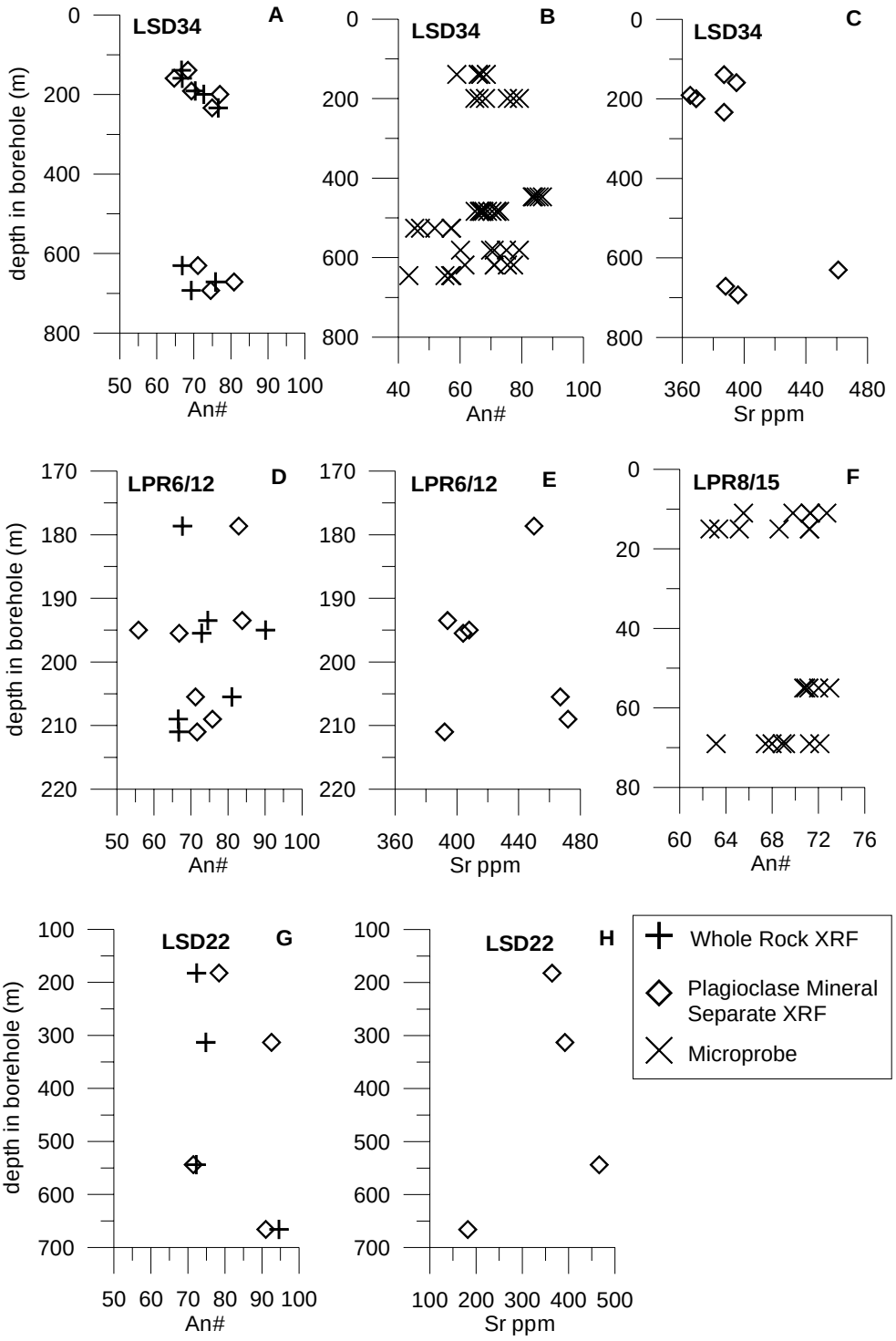

Figure 5.4 An# from whole rock and plagioclase mineral separate data plotted against depth from boreholes: A) LSD34, D) LPR6/12 and G) LSD22 and Sr ppm values from plagioclase mineral separate data from boreholes: C) LSD34, E) LPR6/12 and H) LSD22. Note the different scale for Sr ppm on 5.3F due to contamination in sampleLSD22-5 causing low Sr concentrations. An# from microprobe data are plotted against depth from boreholes: B) LSD34 and F) LPR8/15.

Eales & Cawthorn (1996) give An# values for plagioclase from the Critical Zone of 78-80 with lower values in the Main Zone of ~75. In borehole LSD34, values range from 64-80, with a decrease in An# notably occurring from Unit 3 to Unit 4. Plagioclase from pyroxenite in Unit 2 has an An# of 71, more typical of Upper Zone Bushveld signatures in the eastern and western limbs (Figures 4.21). The other two boreholes sampled show similar anomalies. At the base of the sequence in Unit 3, the norite has an An# of 80 where the plagioclase is cumulus. Above this in the feldspathic pyroxenite where the plagioclase is intercumulus the An# decreases to 74.

Absolute Sr values are also used to distinguish between Main and Critical Zones in the BC (Kruger 1990; Kruger 1994). The Critical Zone typically has values <400 ppm whereas Main Zone values are >400 ppm. In Figure 5.5 Sr concentrations from mineral separate data shows a variation in pattern with values of <400 ppm for Unit 4 and Unit 1 footwall rocks whereas samples from the Unit 2 have values >400 ppm from borehole LPR6/12 where the two geochemical groups are also apparent (Figure 5.4E). This data is consistent with the interfingered nature of the sequence evident from previous chapters and also suggests two geochemically distinct packages are present in the sequence.

5.5 LPR8/15 'disorientated' block

In order to determine if there were any geochemical differences between the norite of the 'disorientated' block with that of underlying units, four samples were chosen from borehole LPR8/15. These were chosen to represent the norite of the disorientated block and the norite stratigraphically below this in the sequence (Figure 5.5). The Mg# in orthopyroxene grains from the norite of the 'disorientated' block show little compositional variation (Mg# 59-61). Samples taken from the norite below show a much wider range of Mg# in orthopyroxene (50-

58 and 53-60). The Cr/MgO ratio has been plotted (Figure 5.5B) and shows no difference between the norite block and norites below. However, this may be due to the low Cr content of the orthopyroxene which is close to the detection limit.

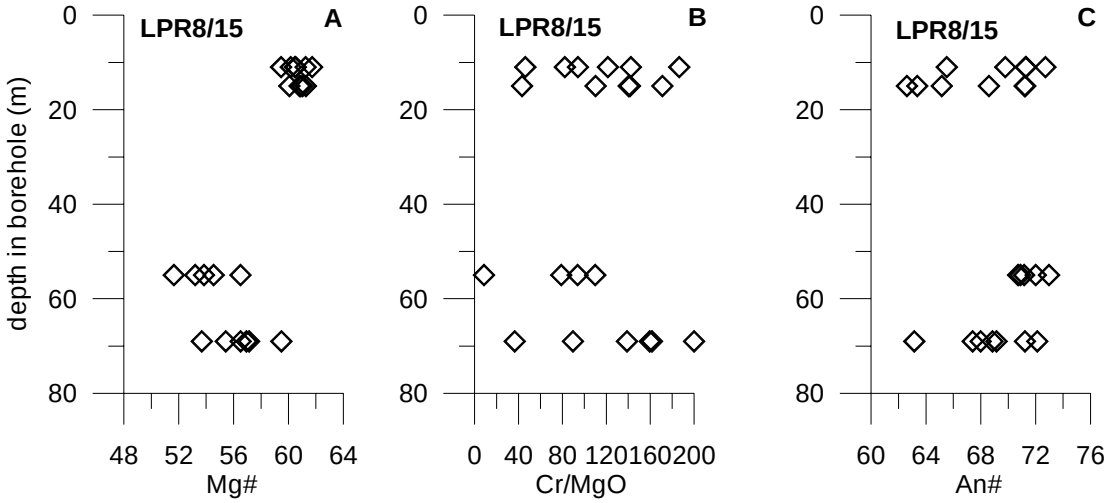

Figure 5.5 Microprobe data for orthopyroxene grains in borehole LSD8/15from the 'disorientated' block and the norites below showing: A) Mg# in orthopyroxene with depth, B) Cr/MgO in orthopyroxene with depth and C) An# in plagioclase with depth. Note Cr values have been converted from % to ppm from the microprobe data obtained.

The An# is plotted in Figure 5.5C and suggests that some plagioclase is zoned as indicated by the spread of data for samples LPR8/15 11.00 (66-74), LPR8/15 15.00 (62-72) and LPR8/15 69.00 (63-71). No systematic variation from core to rim was observed. Sample LPR8/15 55.00 shows little compositional variation (71-73). No clear conclusions can be drawn from this data regarding the nature of the 'disorientated' block and further investigation is necessary.

5.6 Strontium isotope analyses of plagioclase separates

In terms of igneous processes, variations in $^{87}Sr/^{86}Sr$ are unaffected by fractional crystallisation and partial melting. Thus, variations are considered to be the result of

contamination from isotopically different sources. Each of the major zones of the BC is characterised by differences in overall Sr content and in initial $^{87}Sr/^{86}Sr$ ratios: Critical Zone, magmas typically have Sr values <400ppm and initial $^{87}Sr/^{86}Sr$ ratios of <0.7070, whereas Main Zone magmas have Sr values of >400ppm and $^{87}Sr/^{86}Sr$ ratios of >0.7070 (Kruger & Marsh, 1982), (Figure 5.6). Here 10 samples from 3 boreholes were analysed by thermal ionisation mass spectrometry to compare the results with those for samples from the eastern and western limbs of the Bushveld Complex and the Platreef. The results are shown in Table 5.1. The initial Sr isotopic ratios are plotted against depth in borehole to show variation with stratigraphic height (Figure 5.7).

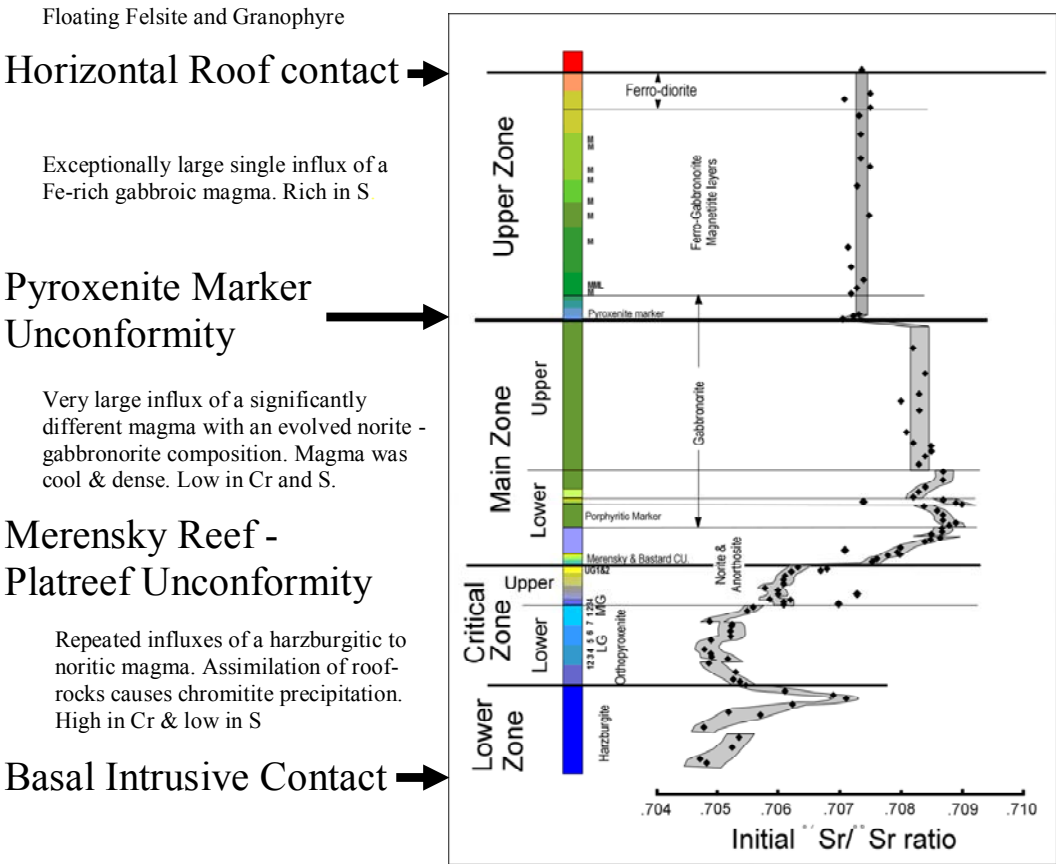

Figure 5.6 Average $^{87}Sr/^{86}Sr$ ratios for the zones of the Bushveld Complex. There are distinct isotopic breaks in the ratio that are concomitant with the zone boundaries. The Upper Critical Zone has values of between 0.7060 – 0.7065 with slightly higher values at the level of the Merensky Reef i.e. 0.7065-0.7070. It can clearly be seen here that $^{87}Sr/^{86}Sr$ ratios <0.7070 represent Critical and Lower Zone rocks and values >0.7070 represent Main and Upper Zone rocks (Kruger, 2003)

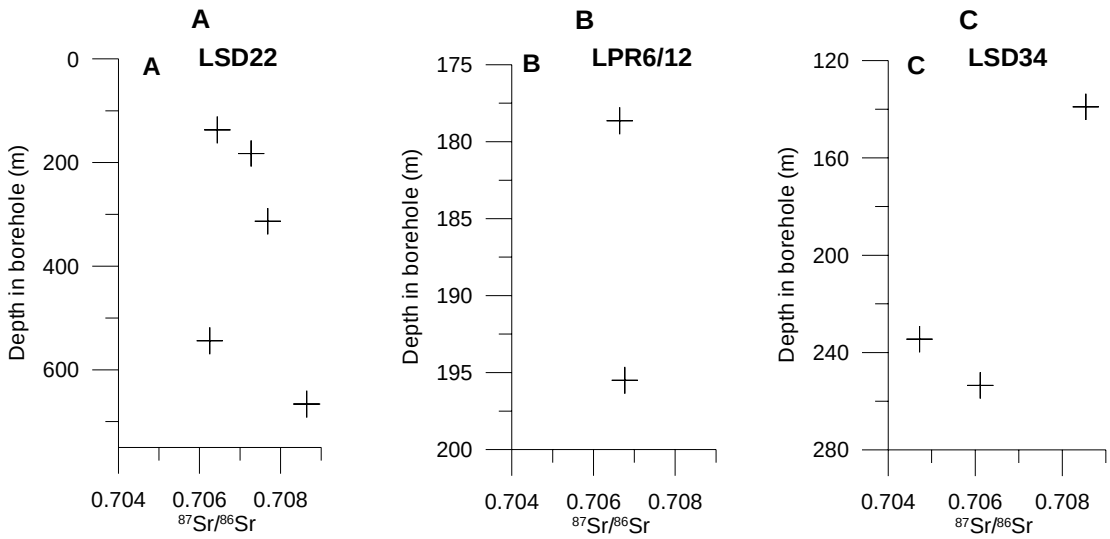

Figure 5.7 Initial Sr isotopic ratios plotted against depth in boreholes: A) LSD22, B) LPR6/12 and C) LSD34. Note the differing scales for depth. The Sr initial ratio has been calculated at 2055 Ma.

In borehole LSD22 the gabbronorite of Unit 4 and the norite which is the hanging wall to the basal mineralisation have similar Sr isotope initial ratios (0.7064 and 0.7062 respectively). The pyroxenites in Unit 3 have a significantly higher isotopic signature (0.70768). As shown in Chapter 4, sample LSD22 at the base of the sequence has anomalously high SiO_2. The $^{87}Sr/^{86}Sr$ ratio is also anomalously high for this sample which implies contamination. The two data points shown in LPR6/12 chosen to represent the basal mineralisation of Unit 2 have similar $^{87}Sr/^{86}Sr$ ratios of 0.70664 and 0.70667. These values suggest minor contamination has occurred. In borehole LSD34 the samples taken from Unit 3 have values <0.7070 whereas the sample taken from the overlying gabbronorites of Unit 4 has a significantly higher $^{87}Sr/^{86}Sr$ ratio of 0.70854.

5.7 Discussion

Kruger (1994) has demarcated the stratigraphic boundaries of the BC using $^{87}Sr/^{86}Sr$ ratios as shown in Figure 5.7. Initial Sr isotope ratios <0.7070 represent Critical and Lower Zone rocks and values >0.7070 represent Main and Upper Zone rocks (e.g. Hamilton, 1977; Kruger and Marsh, 1982; Sharpe, 1985; Kruger, 1994; Kinnaird & Nex, 2003). Seabrook (2005) shows however, that the boundary between the Critical and Main Zone is more complex as previously discussed by Lee & Butcher (1990). The upper Critical Zone has values of between 0.7060 – 0.7065 with slightly higher values at the level of the Merensky Reef i.e. 0.7065-0.7070. Instead of a sudden break in isotopic signature at the level of the Merensky reef there is a transitional zone where initial Sr ratios vary between 0.7064 – 0.7075. Seabrook (2005) also shows that this trend is followed by values of Sr. In the transitional zone between the Main Zone and Critical Zone Sr values do not show a sudden break in the geochemical profile. Instead Sr values range in this unit between 380 ppm to 460 ppm. However, it remains clear that the isotopic break at the base of the Merensky Reef is consistent throughout the entire Bushveld Complex, and has been used to indicate the introduction of a new magma (Seabrook, 2005 and refs therein). In the Platreef, which has been postulated to be the northern limb equivalent of the Merensky Reef (Viljeon & Schürmann, 1998; Kruger 2005), the initial Sr ratio is also variable. Values range from 0.707-0.709 in samples with little contamination and from 0.711-0.722 in samples which, Cawthorn & Lee (2005) suggest, may have elevated values due to invasion by a later melt or fluid from the floor. In comparison the samples taken from the basal mineralisation in this study have initial Sr ratios of 0.7064 and 0.7067 and absolute Sr levels of 471 ppm and 432 ppm. These values correlate with Seabrook's Transitional Unit rather than being unequivocally Main Zone or Critical Zone signatures. In borehole LSD34 a clear distinction can be made from Unit 3 to Unit 4. Values of < 0.707 in Unit 3 can be correlated to values of

BC Critical Zone and values of >0.707 in Unit 4 can be correlated to BC Main Zone signatures. In addition mineral compositions of orthopyroxene grains analysed by microprobe from the basal mineralisation of Unit 2 and pyroxenites from Unit 3 also correlate with compositions from the Platreef, Merensky Reef and Critical Zone, as shown previously in Figure 5.1. In borehole LSD22 the initial Sr ratio has an alternating profile which as suggested in Chapter 4 may indicate inter-fingering of units rather than simple fractionation of the sequence. Absolute Sr values from plagioclase grains and mineral separate data also confirm that two geochemically distinct groupings, also interfinger through the succession. If these parameters are to be correlated with Main Zone and Critical Zone values as outlined, it might be anticipated that the Cr/MgO ratio and Mg# could be similarly used. However, microprobe analyses of orthopyroxenes show significant compositional zoning in the grains which makes this parameter an inaccurate ratio for correlation with whole-rock analytical data. However, it can be seen that the average An# can be correlated to the MZ, of the Bushveld Complex.

CHAPTER 6

Basal Mineralisation

6.1 Introduction

Mineralisation at Sheba's Ridge occurs in a number of stratigraphic horizons in the sequence (Figure 6.1). These show lateral variation along strike and in some cases are discontinuous or even 'disorientated' in outcrop, where strike is perpendicular to the regional strike. Within the basal mineralisation Ridge Mining defined an 'Lower Platreef', 'Platreef' and 'Upper Platreef' based on fire assay analyses of PGE's from extensive drilling which demarcated a three peaked profile of the mineralised zone of Unit 2. Above the basal mineralisation in Unit 2 other mineralised intervals include the intermediate chromitite layer (ICL), possibly equivalent to the lower or middle group chromitites of the BC; the Platchro (PCH), possibly analogous to the middle group chromitite of the BC; the hanging wall mineralised norite (HMN) and the upper mineralised pyroxenite (UMP) possibly analogous to the Merensky Reef (Sharpe *et al.*, 2002). Here research focuses on the basal mineralisation of Unit 2.

Unit 2 is arcuate in outcrop and strikes approximately E-W in the north of the farm Loskop South 53 JS (Figure 6.2). This unit is a ~50 - 250m thick strike continuous basal Ni-Cu-PGE deposit. The contact with the Transvaal Supergroup quartzite and shale floor rocks is undulatory. The mafic intrusives accumulated in a basin on the periphery of the Dennilton and Rietfontein domes. The mineralisation is not hosted in a stratiform ore body, as are for example, the UG2 or Merensky Reefs. It is a sulphide-bearing zone where sulphides are hosted in a package of ultramafic-mafic rocks with variable thickness and composition (i.e. norite, pyroxenite, taxitic-gabbronorite). These host rocks also include metasedimentary xenoliths. As postulated in previous chapters, evidence presented in this dissertation indicates that there are two geochemically distinct magmas present in the sequence.

Furthermore, the peaks in the enrichment of the basal mineralisation occur at the boundary between these two packages. Here the geology of the basal mineralised unit is summarised for each borehole and a schematic cross section through the package is presented. Sample LPR6/12-19 is analysed using scanning electron microscopy and reflected light microscopy to examine the relationship of sulphides and PGE's to host cumulates of the basal mineralisation. The geochemistry provided by Ridge Mining is presented and compared to that of previous studies to determine if PGE and sulphide signatures from the basal mineralisation have affinities to the rest of the Bushveld Complex.

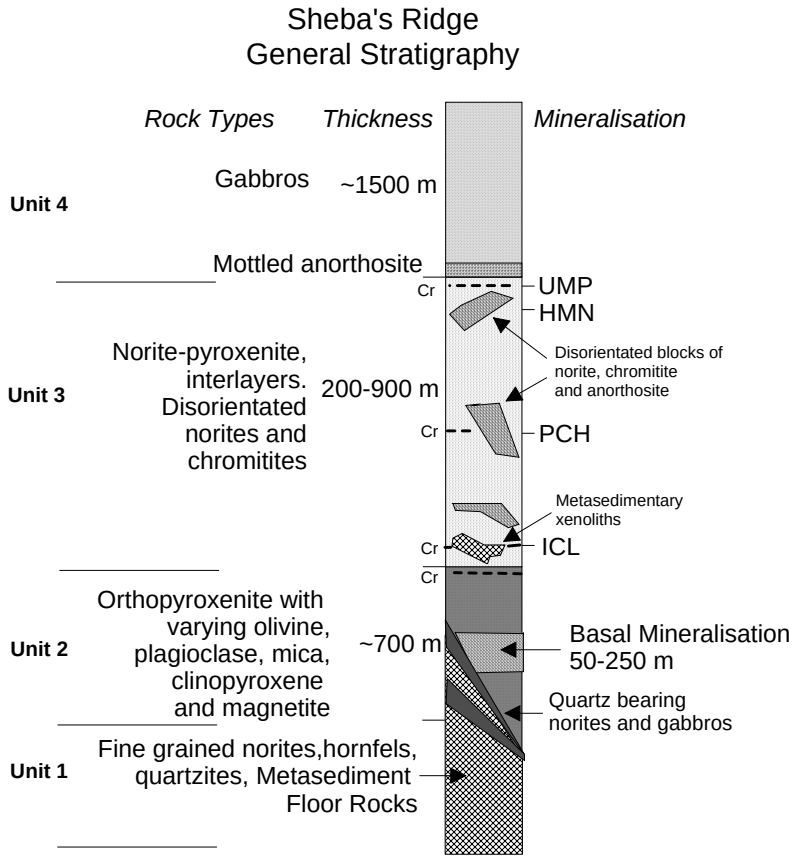

Figure 6.1 Generalised stratigraphy showing mineralisation within the stratigraphic sequence on the farm Loskop South 53 JS. The focus of this study, the basal mineralisation of Unit 2, onlaps floor rocks in the west and is variable in composition and texture up dip and along strike. The hanging wall norite and varying footwall lithologies are often sulphide-bearing. Chromitite layers in Unit 3 are often discontinuous and were found in outcrop to be orientated perpendicular to the regional strike. The mineralised cyclic units towards the top of Unit 3 are bimodal rather than complete cycles and it is unclear if layers within the unit correlate along strike. Modified from Roodt (2004).

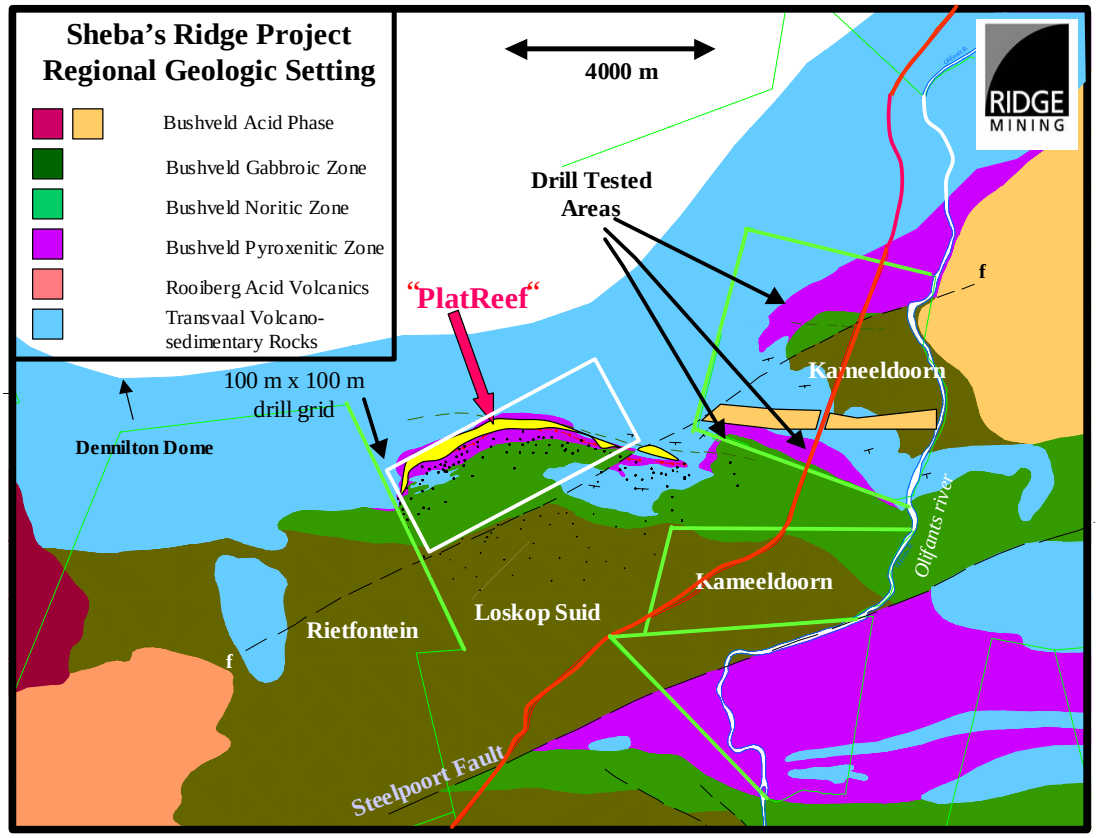

Figure 6.2 Regional geology of the project area. The Ni-Cu-PGE basal mineralisation is shown in yellow striking approximately E-W and outcropping in an arcuate nature. The term 'Platreef' was introduced by Ridge Mining during exploration and refers to the mineralisation in Unit 2 described in this dissertation. North of outcrop steeply dipping quartzites form a ridge in the north and gabbros form Sheba's Ridge to the south. Domal features in the area include the Dennilton Dome to the northeast and the Rietfontein Dome to the west (Map courtesy of Roodt, 2004).

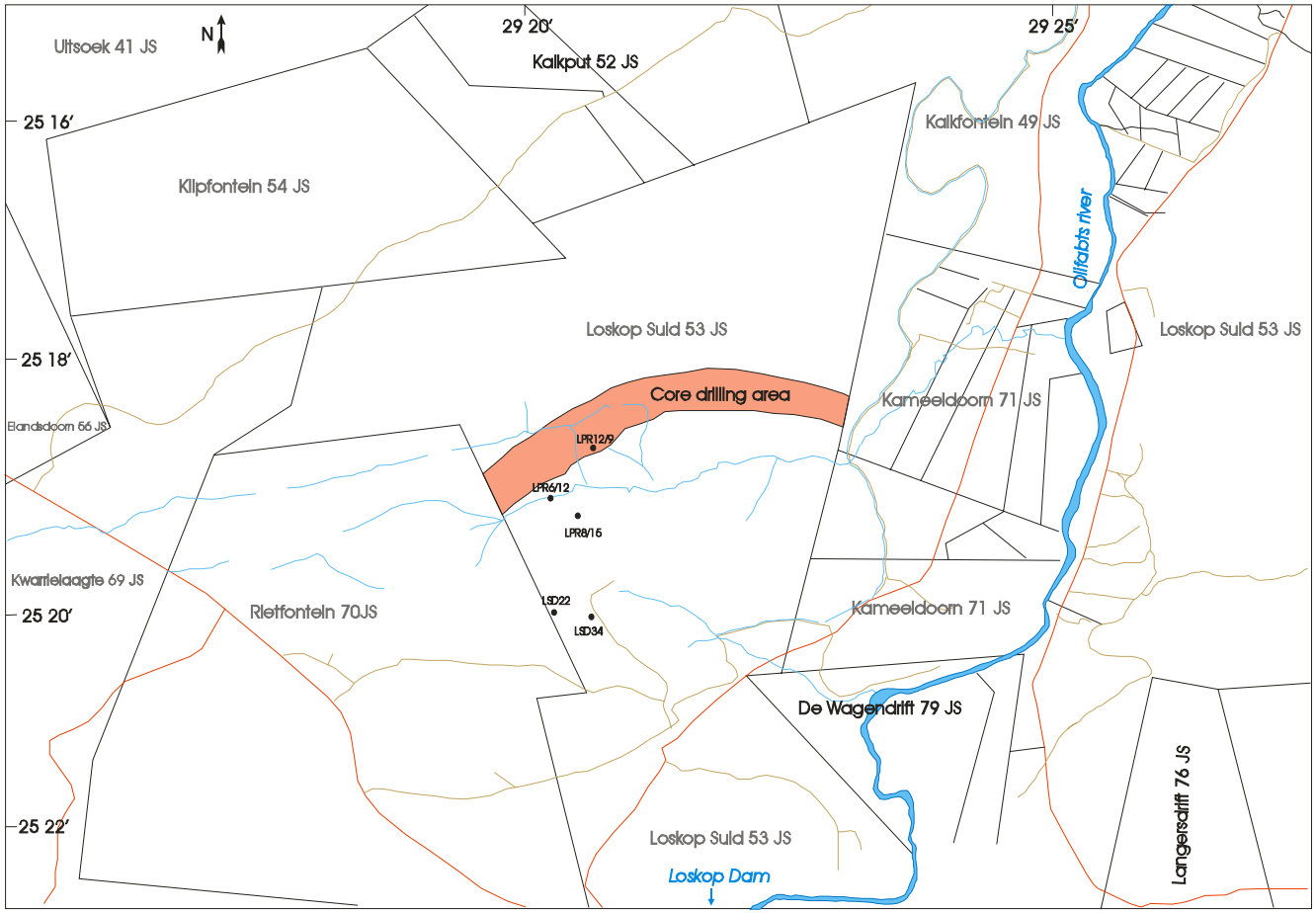

Figure 6.3 Positions of boreholes on the farm Loskop South 53 JS. LSD34 and LSD22 are located on the southern side of Sheba's Ridge. LPR6/12, LPR8/15 and LPR12/9 are located updip through the ultramafic-mafic layered rocks. The perennial Olifants river has ephemeral eastwardly-flowing tributaries through the field area. The main access road to the farm Loskop South 53 JS is the N11 running NE-SW to the East of the farm.

6.2 Basal Mineralisation

The host rock and floor rocks to the basal mineralisation are variable up dip and along strike. Boreholes LSD34 and LSD22 are situated on the southern side of Sheba's Ridge where the basal reef is relatively thin at 46 m and 73 m respectively. Further north, the reef thickens so that in borehole LPR8/15 the reef is 70 m thick and in the most northern sector of the farm, in borehole LPR12/09 the reef must be at least 300 m thick as the borehole was collared in the reef itself. However, since the field team observed that the regional dip increases in the north, this has the effect of slightly increasing the apparent thickness of the reef. In the central sector of Loskop South 53 JS, the reef is anomalously thin (46 m) in borehole LPR6/12 due to the occurrence of a floor rock high. The floor rocks in these boreholes include hornfels, cordierite-hornfels, and calc-silicates. A 4 m thick layer of graphite is in contact with the host pyroxenite in LSD22 and a cordierite-hornfels occurs at the base of borehole LPR8/15. In all of the boreholes studied, excluding borehole LSD22, the mafic rocks at the base are fine-grained quartz-bearing gabbronorites and norites. These basal mafic rocks interdigitate with the metasedimentary floor rocks. The host rocks in the 2 boreholes to the south are feldspathic pyroxenite and taxitic gabbronorite (Figure 6.5 B & C). Hornfels and calc-silicate xenoliths occur within the mineralised package. In the central sector an olivine-bearing feldspathic pyroxenite occurs with the taxitic gabbronorite and feldspathic pyroxenite in borehole LPR8/15 (Figure 6.5D).

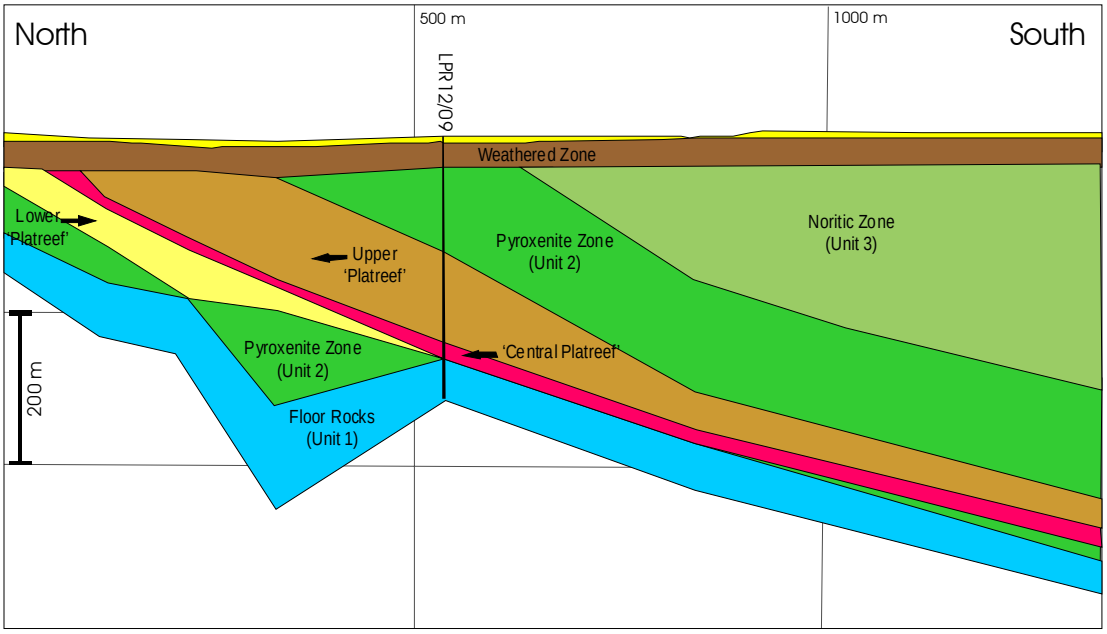

Figure 6.4 A schematic cross section of the basal mineralisation (Unit 2)-'Platreef'. The nature of the undulous floor rock is shown. The position of the demarcated zones 'Upper Platreef', 'Central Platreef' and 'Lower Platreef' are shown and were extrapolated from exploration borehole data, modified from Roodt (2004).

In borehole LPR6/12 the host rock is an equigranular orthopyroxene dominant feldspathic pyroxenite with clinopyroxene phenocrysts. Minor olivine-bearing units are present and often altered where magnetite stringers occur. In borehole LPR12/09 the host rock is predominantly an olivine-bearing feldspathic pyroxenite with magnetite layers and stringers occurring throughout. Norite containing inverted pigeonite is the hanging wall to the basal mineralisation of Unit 2 in all of the boreholes studied (Figure 6.5A).

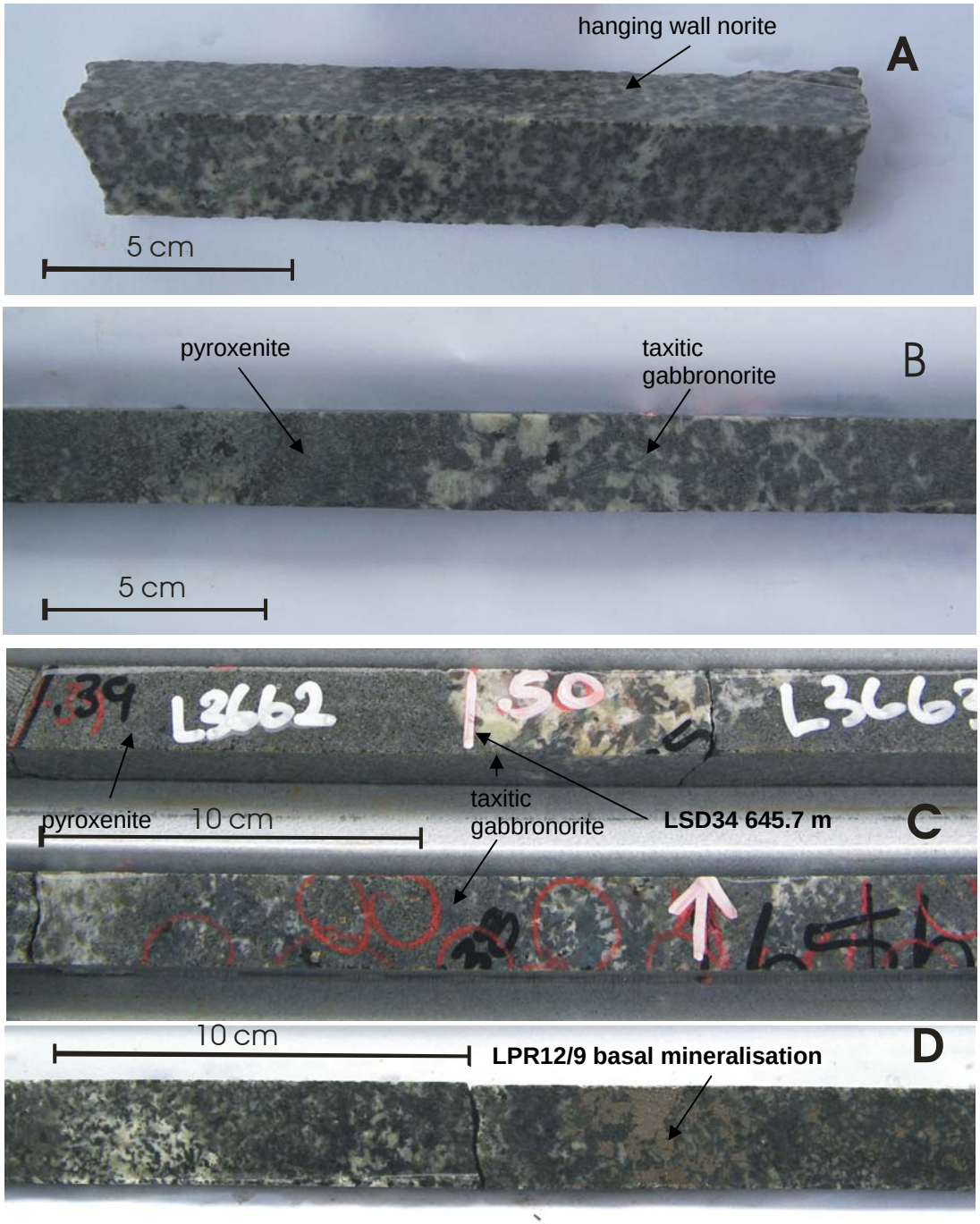

Figure 6.5 Photographs of typical mineralised cores: A) Hanging wall norite to the basal mineralisation at Sheba's Ridge. B) & C) the boundary between heterogeneous taxitic gabbronorite and feldspathic pyroxenite above at 654.7 m in borehole LSD34, disseminated sulphides are circled in red. D) Olivine-bearing feldspathic pyroxenite with interstitial blebby and net-textured sulphides and magnetite as an alteration mineral in borehole LPR12/9.

6.3 Sulphides in the Basal Mineralisation, Unit 2

The basal mineralisation of Unit 2 at Sheba's Ridge is unusual for the Bushveld Complex, in that it is enriched in sulphides. These are predominantly pyrrhotite and pentlandite with lesser chalcopyrite and minor pyrite and bornite. Grades of Cu and Ni are typically within the range of 4000 to 16000 pmm with associated PGE enrichment. Similar basal sulphide enrichment occurs in the Uikomst Complex at Nkomati and in the central and southern Platreef (Hornsey, 1999; Hutchinson & Kinnaird, 2005; Nyama *et al.*, 2005). Sulphide occurrence is variable and may be disseminated, net-textured (usually associated with altered olivine-bearing horizons), interstitial and blebby, or with a combination of textures.

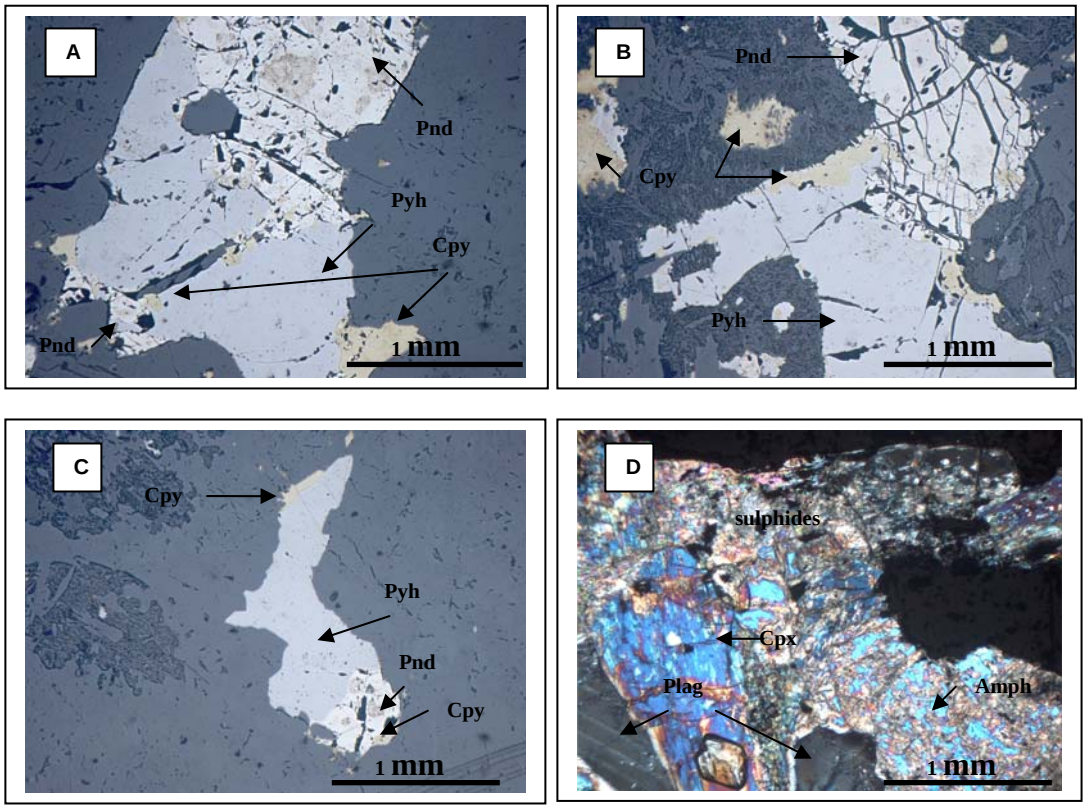

Figure 6.6 Photomicrographs of the basal mineralised pyroxenite from sample LPR6/12-19: A), B) & C) Interstitial multiphase sulphides. Pyrrhotite and pentlandite are the major sulphides with minor chalcopyrite occurring at grain boundaries. Pentlandite is characteristically fractured. In A) pentlandite has a sharp planar contact with the surrounding unaltered silicate gangue, whereas B) & C) show irregular grain boundaries with surrounding silicates and alteration minerals actinolite and sericite. D) Altered silicate gangue; pyroxenes are altered to actinolite, interstitial plagioclase is unaltered in this sample. A, B & C are taken in reflected light and D) in cross polars. Abbreviations: Pnd, Pentlandite; Pyh, Pyrrohtite; Cpy, Chalcopyrite; Cpx, Clinopyroxene; Plag, Plagioclase; Amph, Amphiboles.

Sulphides commonly occur as large multiphase blebs along with smaller disseminated monomineralic grains (Figures 6.5A, B and C). The sulphides show planar contacts with silicates and occur interstitially between altered secondary minerals such as actinolite and sericite (Figure 6.5D).

6.4 PGE's

The association of PGE's with the basal sulphides was first documented by JCI in the early 1980's. The discovery of this sulphide zone refocused the target for exploration from base metals to platinum-group metals (PGM) and the project was taken over by Rustenburg Platinum Holdings (then part of the JCI group). A continuous zone of low-grade mineralisation 13.4 m thick along 4 km of strike and a 7.7 to 39 m thick 'Platreef' were documented during exploration and became the target of exploration by Ridge Mining (formally Cluff Mining) in early 2001.

In order to investigate the association between the PGE's and sulphides at Sheba's Ridge which often occur at the margins of chalcopyrite or hosted within pentlandite, sample LPR6/12-19 was chosen for detailed study. This sample was selected to be representative of the differing textural features within the basal mineralisation. The polished thin section was mounted into the vacuum tube of the JEOL JXA840A scanning electron probe microanalyser equipped with a Noran Norvar EDS detector and Voyager EDS software. EDS data were collected over 200 s (dead time corrected) with an accelerating voltage of 15 kV and a 1 nA probe current. Pure element standards for the PGMs (including Pt, Pd, Bi, Te, Sb and As) were supplied by Micro-Analysis Consultants Ltd. Analyses were conducted under the supervision of Dr Dave Hutchinson at SPECTRAU laboratory of the University of Johannesburg.

Results show that different platinum group minerals (PGM's) occur in different sulphides. For example, in sample LPR6/12 palladium bismuthide is found as an inclusion in a grain of chalcopyrite (Figure 6.7A). Argentopentlandite and nickel arsenide occur as discrete grains included in pyrrhotite (Figure 6.7B). Palladium tellurium bismuthide occurs in association with altered olivine close to the edge of a pentlandite grain (Figure 6.7C), and is also seen as an inclusion within a grain of pentlandite (Figure 6.7D). No platinum-bearing minerals were found in this sample.

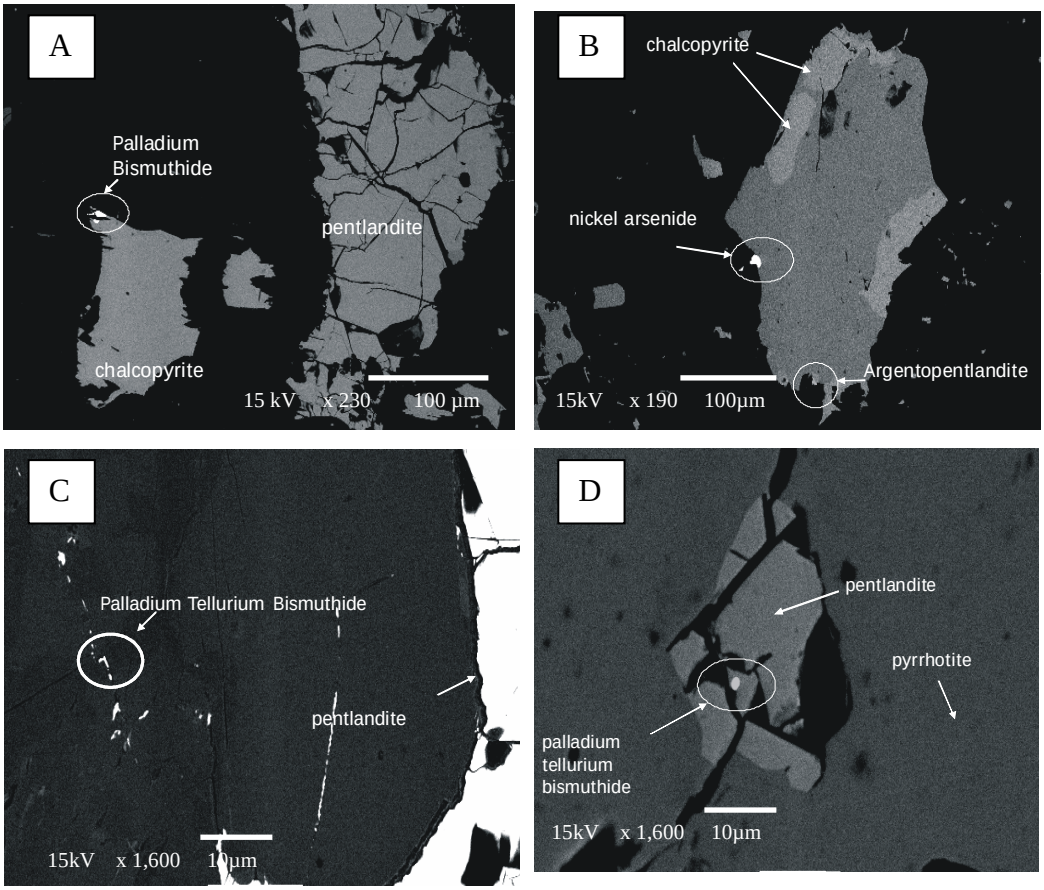

Figure 6.7 Backscatter electron photomicrographs: A) cumulate sulphides, chalcopyrite and pentlandite with a discrete palladium telluride in association with a chalcopyrite grain, B) Multiphase sulphides pyrrhotite and chalcopyrite with nickel arsenide and argentopentlandite occurring in association with the sulphides; C) & D) Multiphase sulphides pentlandite and pyrrhotite with a discrete grain of palladium tellurium bismuthide in association with pentlandite. All images taken from sample number LPR 6/12-19.

6.5 Geochemistry of the basal mineralisation

Data has been provided by Ridge Mining from borehole LPR12/09 (Appendix 4). This data only covers the 'Central Platreef' sector as defined by Ridge Mining and does not include 'Upper' or 'Lower' Platreef. This can be seen in Figure 6.4 where in borehole LPR12/9 the 'main Platreef' is in contact with the floor rocks. However, within this assay data for the 'Platreef' there appears to be 3 peaks of 2PGE+Au enrichment with concomitant increased sulphur. These have been designated as sub-divisional Zones 1, 2 and 3 (Figure 6.8).

Sub-divisional Zone 1 of the 'Central Platreef' at the base which occurs between 289.30-291.60 m, has a low Mg# which correlates with Fe-enrichment associated with an increase in sulphide content. The zone is defined by a change in the Cr/MgO ratio which exhibits a ratio of <80 whereas at the top of the zone Cr/MgO ratios increase sharply to >80. This has been used to demarcate the top of Zone 1. There are elevated levels of 2 PGE+Au, S and Ni+Cu content and the Zone is characterised by the highest Pt:Pd ratios (Figure 6.8A, 6.8C, & 6.8E).

Sub-divisional Zone 2 of the 'Central Platreef' occurs between 273.02-278.78 m. The Zone is characterised by the highest concentrations of 2 PGE+Au, S and Cu+Ni. Within the zone there is an abrupt compositional break which is characterised by a change is Cr/MgO ratio from >150 to <105 and elevated PGE enrichment at the same level (Figure 6.8D).

Sub-divisional Zone 3 of the 'Central Platreef' occurs between 255- 262.5 m. It is characterised by lower S concentrations and a very different Ni:Cu ratio from other parts of the basal mineralisation. Whereas in Zones 1 and 2 the typical Ni:Cu ratio is <4, in this upper zone the Ni:Cu ratio is quite variable and may reach 12. The high Ni values reflect both an increase in pentlandite and olivine content in the top portion of Zone 1, with a corresponding

increase in PGE's, especially in Pd, although the grade does not reach that of Zones 1 and 2 (Figure 6.8).

Figure 6.8 Plots of geochemical data with depth in borehole LPR12/9: A) 2 PGE+Au, B) Sulphur (S), and C) Nickel + Copper (Ni+Cu) show three zones of increased mineralisation with depth in borehole. Zone 3 is between a depth of 255- 262.5 m, Zone 2 is between a depth of 273.02-278.78 m and Zone 1 is between a depth of 289.30-291.60 m. D) Cr/MgO ratios show significant breaks in geochemistry that is concomitant with peaks in grade as indicated in zones 2 and 3. The Cr/MgO value of 80 has been used by Seabrook (2005) to distinguish between Critical and Main Zone magmas. E) Pt/Pd ratios show that there are increased concentrations of Pt compared to Pd in Zone 1, towards the base of the mineralised unit. F) Ni/Cu ratios indicates an increase of Ni and olivine content in Zone 3 towards the top of the mineralised unit. G) & H) show the concentrations of Pt and Pd respectively. I) Mg# may suggest basal reversal and there are breaks in this profile that are concomitant with breaks in the Cr/MgO which demarcate Zone 2.

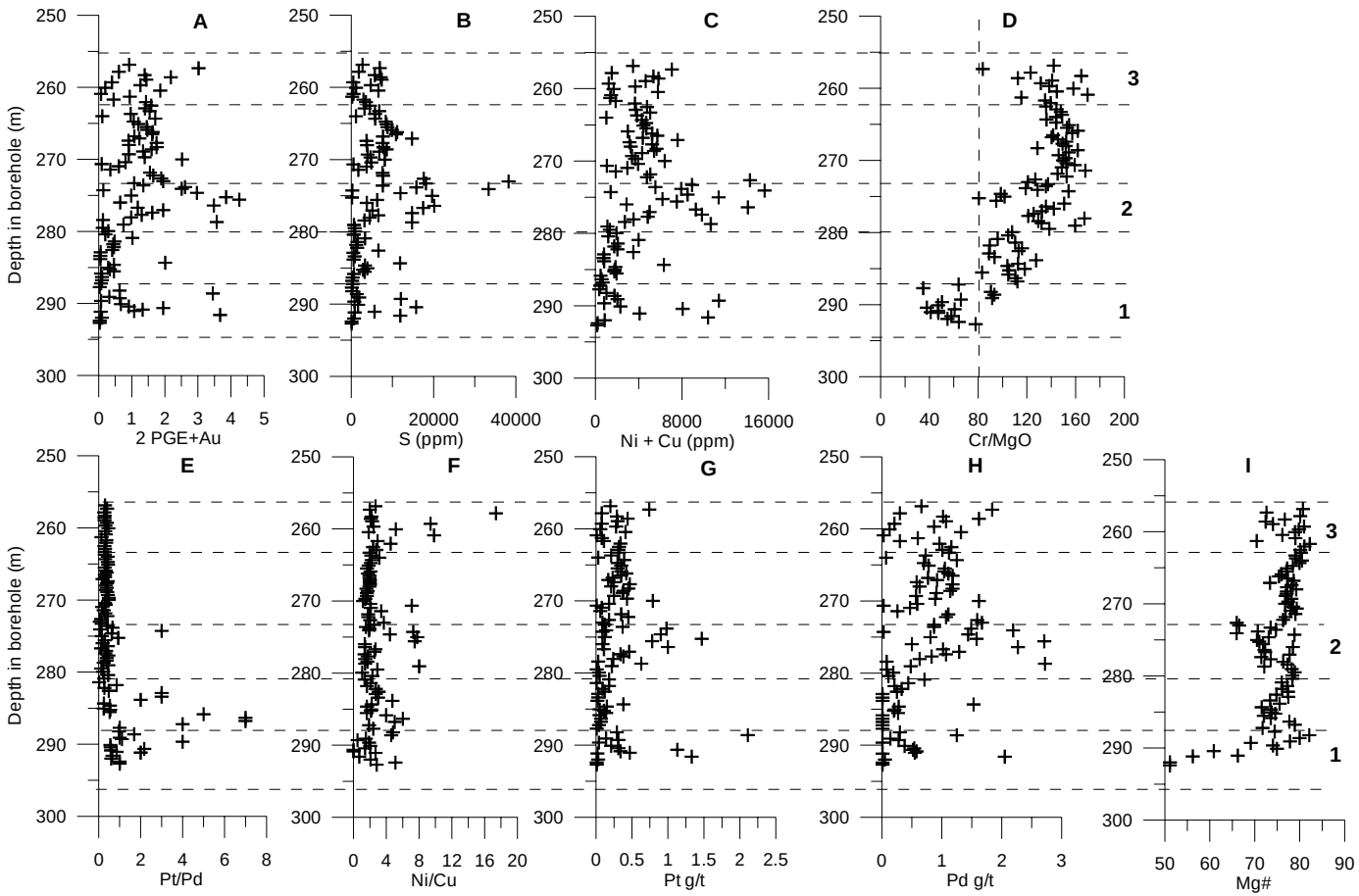

Figure 6.8 Plots of geochemical data with depth in borehole LPR12/9. See page 132 for full figure caption.

Pt+Pd and S have been plotted against Ni+Cu in Figures 6.9A and B. There is a positive correlation between Ni+Cu and S indicating that Ni+Cu levels are associated with sulphides in the rocks sampled. Pt+Pd shows a positive correlation with Ni+Cu for samples with up to 6000 ppm Cu+Ni and up to 2g/t Pt+Pd. However, for high levels of Ni+Cu or Pt+Pd this correlation is not valid implying that higher concentrations of the PGE's are not associated with sulphides. The Pt:Pd ratio of the samples in this borehole are ~0.5. However, values of Pt:Pd are variable in Zone 1 locally exceeding 7 (Figure 6.8E).

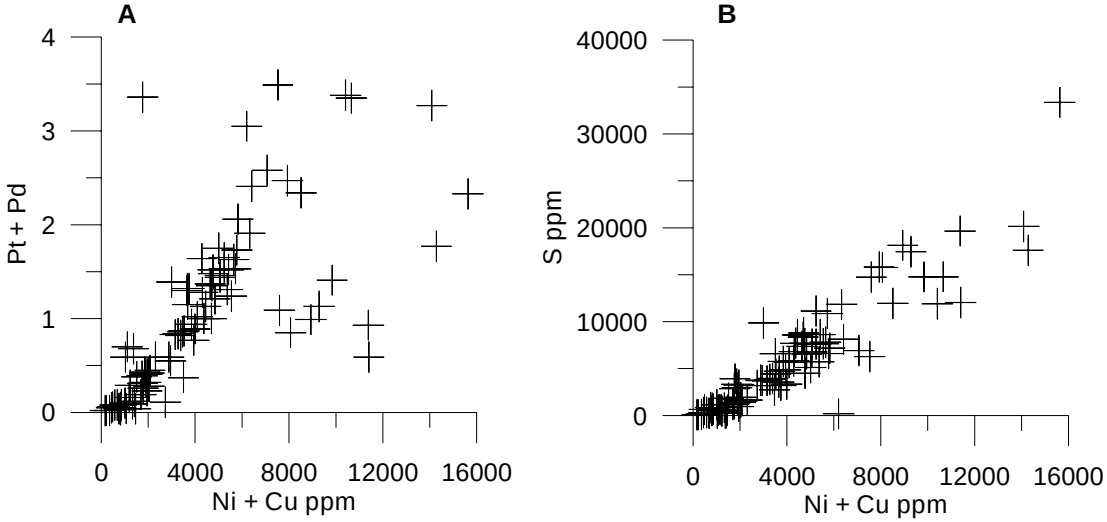

Figure 6.9 Bivariate plots of whole rock XRF data from borehole LPR12/9: A) Ni + Cu vs Pt + Pd and B) Ni + Cu vs S. The linear trend confirms that both Ni and Cu are associated with sulphides in the sequence and predominantly PGE's are associated with sulphides.

6.6 Discussion

Sulphides occur as an immiscible liquid in reduced magmatic systems when sulphur saturation is achieved (e.g. Naldrett, 1989). PGE, Cu and Ni partition into the immiscible sulphide liquid. An immiscible sulphide liquid forms once the silicate magma becomes saturated in sulphur, as summarised by Seabrook (2005), which is triggered by:

- Fractionation (e.g. Andersen *et al*, 1998; Miller & Andersen 2002)
- Changing temperature and pressure (Haughton *et al*., 1974)

- Magma Mixing (Li *et al.*, 2001)
- Addition of S or crustal material (e.g. Ripley, 1986; Naldrett, 1989, 1999)

Magma mixing has been suggested as the trigger for sulphur-saturation during the formation of the Merensky Reef (e.g. Naldrett & von Gruenewaldt, 1989). Contamination by crustal rocks through the assimilation of siliceous material has been suggested to induce sulphide saturation in many large magmatic Ni-Cu-(PGE) sulphide deposits (Irvine, 1975; Ripley & Alawi, 1988). For the Platreef, Hutchinson & Kinnaird (2005) suggest that a number of these mechanisms may have contributed to the current distribution of sulphides and PGE's. They show that extensive modification of the original magmatic PGE-bearing sulphide assemblage must have taken place. They suggest that mechanisms such as footwall/hornfels-magma interaction, devolitisation and partial melting, infiltration of felsic magmas and later alteration processes are evident in the Platreef. The sulphide minerals examined in this study possess cumulate textures and are PGM-bearing suggesting that much of the sulphide population and PGM's are of magmatic origin. However, the sulphides also occur as an intercumulus phase, notably net-textured, which indicates an intercumulus phase of sulphide formation in the reef. This together with the hydrothermal alteration of primary silicates to sericite, amphibole and chlorite (Figure 6.7D and Chapter 3) suggests that significant alteration has occurred to redistribute a minor proportion of the magmatic sulphides and PGE's in the reef. Furthermore, from the geochemical data presented here it is suggested that the peaks in mineralisation through the basal mineralised unit at Sheba's Ridge occur at a level where two magmas have interacted.

Similarities and differences exist between the mineralised rocks studied at Sheba's Ridge to that of signatures from the Merensky Reef and the Platreef:

- The Merensky Reef is enriched in PGE but not Cu+Ni (Seabrook, 2005) compared to Sheba's Ridge. The Pt:Pd ratio also differs, in the Merensky Reef it is ~2:1 across both the eastern and western limbs, whereas at Sheba's Ridge the Pt:Pd ratio is 1:2 with enrichment in Cu+Ni. However the Merensky Reef occurs at a level where the interaction of two magmas has taken place, although the exact process that took place during this interaction is still under dispute i.e. magma 'mixing' or magma 'mingling'.
- For the UG2 in the western and eastern limbs of the Bushveld Complex south of the Steelpoort Fault the Pt:Pd ratio is 2:1. Whereas north of the Steelpoort Fault the Pt:Pd ratio is 1:1 similar to the Platreef in the northern limb.
- For the Platreef as a whole the Pt:Pd through the reef is 1. However, in the basal Platreef the Pt:Pd ratio is also 1:2 (Kinnaird, 2005) with associated enrichment of pyrrhotite, and pentlandite. Hutchinson & Kinnaird (2005) have also proposed that a number of geochemically distinct pyroxenitic sills were emplaced to form the Platreef. Other comparisons with the Platreef and BC signatures are shown in Table 6.1 where similarities and differences are apparent.

There are therefore considerable similarities between the basal mineralisation and the Platreef in the northern limb, although the Platreef is directly overlain by the Main Zone and does not possess any upper mineralised layers.

Table 6.1 A comparison of Sheba's Ridge basal mineralised Unit 2 and the Platreef (Cawthorn & Lee, 2005; Kinnaird 2005).

Sheba's Ridge **Basal mineralisation**	**Platreef** (Cawthorn & Lee, 2005; Kinnaird 2005)
Pt:Pd ratio of ~1:2	Pt:Pd ratio ~1:1
Good correlation between Pt+Pd v Ni+Cu, and Cu+Ni v S at low concentrations.	Shows good correlation of PGE v S at low concentrations but not at high levels.
It is generally bottom loaded but shows a two/three-peaked profile.	The reef has a variation of bottom loaded, mixed and top loaded mineralisation
Sr isotopic signature in host pyroxenite interstitial plagioclase is ~0.7066.	The Sr isotopic signature in plagioclase is ~0.707-0.722.
Sulphides are hosted by an olivine bearing orthopyroxenitic unit with varying olivine, plagioclase, mica, clinopyroxene and magnetite.	Sulphides are hosted in orthopyroxene dominant cumulates with variable proportions of plagioclase, clinopyroxene, quartz, biotite, sulphides, chromite.

CHAPTER 7

Discussion and Conclusions

7.1 Introduction

The link between the stratigraphy of Sheba's Ridge area and that of the main Bushveld Complex has not yet been established unequivocally. Whilst there are a number of similarities that can be compared with the known stratigraphy there are also a number of contrasts. This MSc research project was sponsored by Ridge Mining in order to gain a greater understanding of the mineralogy and geochemistry of the Sheba's Ridge deposit. In order to add to Ridge Mining's existing database, this research concentrated on rock types below, within and above the basal 'sulphide-bearing' mineralisation. As this 'contact' style of mineralisation in the BC is only known to occur in the Platreef proper of the northern limb this study aimed to log and document the stratigraphic sequence at Sheba's Ridge and make comparisons not only with the eastern and western limbs but also with the Platreef. The mineralisation is also compared to other layered igneous intrusions.

7.2 Stratigraphic Correlations at Sheba's Ridge

The mafic succession at Sheba's Ridge dips to the south whereas the eastern limb dips to the north towards the centre of the Complex. The unusual stratigraphic succession at Sheba's Ridge comprises a sequence that can be subdivided into 4 units (Table 7.1). This succession does not host a strike continuous layered sequence that can be correlated directly with the stratigraphy of the BC, nor with the Merensky and UG2 layers. The sequence is highly disrupted. From the data presented, suggested correlations of the sequence at Sheba's Ridge with that of the Bushveld Complex and with Crous (1995) data from the farm Rietfontein 73 JS are shown in Table 7.2.

Table 7.1 Key characteristics of the subdivisions of the mafic succession at Sheba's Ridge.

Unit 4	is marked by a distinctive mottled anorthosite at the base, with thick gabbronorites
Unit 3	comprises norite-pyroxenite interlayers with 'enclaves' of disoriented blocks of norite, chromitite and anorthosite. Thickness is variable. It is host to a number of mineralised intervals that do not appear to be strike-continuous.
Unit 2	varies from olivine-bearing feldspathic pyroxenite to orthopyroxene dominant pyroxenite to taxitic gabbronorite. This unit hosts the sulphide-PGE basal mineralisation. There is a hanging wall norite to the mineralised unit in all boreholes.
Unit 1	includes floor rocks interlayered by fine-grained quartz-bearing norites and gabbronorites. The top of the unit is marked by the appearance of the sulphide-bearing pyroxenites of Unit 2.

Unit 1

The floor rocks in the area are of the Pretoria Group of the Transvaal Supergroup which is of early-Proterozoic age (Button, 1986; Crous, 1995). The major quartzite ridge of the farm Loskop South 53 JS is correlated with the Daaspoort Formation (Figure 3.11). The hornfels' may be metamorphosed shales from the Silverton Shale Formation of the Pretoria Group with an age of 2263 Ma (Burger & Walraven, 1980; Crous, 1995). The mafic rocks in the area intruded into, and disrupted, the Pretoria Group sediments. The fine-grained norites and gabbronorites are equated with the Marginal Zone elsewhere in the eastern and western limbs. This is based on the fact that they are consistently fine-grained implying that they were intruded into cool country rock and rapidly cooled (after Kinnaird, 2005).

Unit 2

The pyroxenites of the lower part of Unit 2 correlate with the 'lower mixed zone' of Crous (1995). Sharpe *et al.* (2002) suggested that the succeeding mineralised layers in Unit 3 are analogous to the Lower, Middle and Upper Group chromitites and to the Merensky Reef. Therefore, based on this the pyroxenites of the basal mineralisation in Unit 2 must correlate

to lower Critical Zone of the Bushveld Complex. However geochemical data in this study shows that these pyroxenites have more affinity with the upper Critical Zone, e.g. $Mg\#_{75-85}$, Cr/MgO >80. The range in An# which is caused in part by the development of the taxitic gabbronorite in this Unit, could have developed by the mixing or mingling of the earlier pulse of Marginal Zone magma with the later more fractionated magma. However, purely the occurrence of cumulus plagioclase suggests that this unit must correlate with the Upper Critical Zone of the Bushveld Complex.

The occurrence of an inverted pigeonite-bearing norite hanging wall to the reef implies that the formation of two-directional Ca-rich lamellae occurred during slow cooling as uninverted pigeonite only occurs in quickly chilled rocks (Deer *et al*, 1966). This must represent a position where the phase-change from orthopyroxene to pigeonite takes place (von Gruenewaldt, 1970). This phase-change could be due either to fractionation, rejuvenation of the resident magma (Eales & Cawthorn, 1996) or influx of a more differentiated magma. In the eastern and western limbs of the Bushveld Complex inverted pigeonite is found only in the Main Zone (von Gruenewaldt, 1970; von Gruenewaldt & Weber-Diefenbach, 1977; Cawthorn *et al*, 1991; Eales & Cawthorn; 1996; Nex, *et al,* 1998; Nex *et al* 2002). The only other occurrence of inverted pigeonite in the BC, to current knowledge, is reported in the northern limb at the Sandsloot open pit mine (Holwell *et al*, 2004). Here a fine-grained gabbronorite with inverted pigeonite and sulphides occurs at the hanging wall contact of the Platreef.

Unit 3

Norite/pyroxenite interlayers of Unit 3 have been correlated to Crous' 'upper mixed zone'. The cyclic sequence towards the top of Unit 3 are more typical of upper Critical Zone

signatures of the eastern and western limbs of the BC. These correlate to Crous' 'Critical Zone'. Stratigraphic correlation of 'cyclic units' in the boreholes studied was not achieved.

Unit 4

The homogeneous gabbronorite (Unit 4) at the top of the sequence can be correlated with Crous' Main Zone, which he correlates with the Main Zone of the BC. The mottled anorthosite at the base may be the equivalent of the Bastard Succession of the eastern and western limbs. Von Gruenewaldt (1970; 1973) groups the Main Zone of the eastern limb into three subzones based on the occurrence of inverted pigeonite. In contrast, Nex et al (1998) subdivided the Main Zone of the western lobe of the Bushveld Complex into five subzones which can be recognized in the field. The homogenous texture of the two pyroxene-bearing gabbronorite and lack of inverted pigeonite suggests that it might be correlated with subzone B of the Main Zone of Nex et al (1998) rather than with the basal subzone A which is noritic.

Table 7.2 Suggested correlations of Sheba's Ridge with that of the Bushveld Complex in column B and with the farm Rietfontein 73 JS from Crous (1995).

Sheba's Ridge	Bushveld Complex	Rietfontein 73 JS
Unit 4	Main Zone	Main Zone
Unit 3	upper Critical Zone	Critical Zone
Unit 2	Similarities to the Platreef Lower Critical Zone?	Mixed Zone
Unit 1	Marginal Zone and Transvaal meta-sedimentary floor rocks	Floor Rocks

7.3 Geochemical correlations at Sheba's Ridge

From the major and trace element profiles of the boreholes studied two geochemical groupings of magmas has been inferred based on Mg#, Cr ppm and selected element ratios (Table 7.3). Important conclusions can be inferred for the origin of these two groups.

The Mg# which is used as a measure of fractional crystallisation in layered intrusions changes at the boundary from lower Critical Zone to upper Critical Zone in the eastern and western limbs of the Bushveld Complex from >$Mg\#_{83}$ to <$Mg\#_{83}$ (Eales & Cawthorn, 1996). This change corresponds to the appearance of cumulus plagioclase. Although the Mg# in the stratigraphic

Table 7.3 Geochemical characteristics of two geochemically distinct packages at Sheba's Ridge

	Type A	Type B
Cr ppm whole rock	>800	<800
Wt% MgO whole rock	<15%	>15%
Cr/MgO whole rock	>80	<80
Cr/V whole rock	<10	>10
Sr/Al_2O_3 whole rock	>16	<16
SiO_2/Al_2O_3 whole rock	>4	<4
Mg#	75-85	65-78

sequence at Sheba's may be significantly affected by the occurrence of clinopyroxene ± olivine ± sulphides ± magnetite, three significant variations occur in the Mg# through the sequence at Sheba's Ridge: The first is an Fe-enrichment at the base of the mineralisation in Unit 2 which corresponds to an increase in sulphide content towards the contact with the floor rocks. The second is the higher Mg# in pyroxenites ($Mg\#_{75}$-$Mg\#_{85}$) compared to the norites ($Mg\#_{65}$-$Mg\#_{78}$) through the sequence. This is reflected in An# of the which is higher in the pyroxenites (An $\#_{72-89}$) than in the norites (An $\#_{67-72}$). The third is a significant decrease in Mg# in the gabbronorite of Unit 4 which varies from $Mg\#_{63}$-$Mg\#_{68}$. For the Platreef the boundary between the Platreef and the overlying Main Zone norite corresponds to a break in

the composition of orthopyroxene from $Mg\#_{77}$ to $Mg\#_{67}$. By comparison, this might imply that the pyroxenites of Sheba's Ridge are of Critical Zone affinity and the norites and gabbronorites are of Main Zone lineage.

The parameter Cr/MgO has been used by Seabrook (2005) to distinguish between Main Zone and Critical Zone sequences. Values are typically >80 in the Critical Zone and <80 in the Main Zone. Based on this parameter the Type A package of Table 6.3 has affinities with the Critical Zone whereas Type B shows typical Main Zone ratios.

Element ratios of Sr/Al_2O_3, Cr/MgO, Sr/Ba and SiO_2/Al_2O_3 help indicate different magmatic influxes as these ratios are independent of modal proportions in the rock, (Eales *et al,* 1986; Eales *et al,* 1988; Nex *et al,* 2002; Cawthorn & Lee, 2005; Kinnaird, 2005). Again, for the rocks studied from Sheba's Ridge there are two distinct geochemical groupings that have concomitant breaks in all of these ratios (Table 7.3).

7.4 Comparison of mineralised layers at Sheba's Ridge with the eastern and western limbs, Bushveld Complex

The basal Ni-Cu-PGE mineralisation of Unit 2 occurs in a 50-250 m thick interval along ~7 km of strike in the pyroxenites of the lower part of the intrusive succession. From the data provided by Ridge Mining three zones were identified:

- Zone 1 at the base, has a low Mg# which correlates with Fe-enrichment due to an increased sulphide content. The zone is characterised by a Cr/MgO ratio <80. There are elevated levels of 2 PGE+Au, S and Ni+Cu content and the Zone is characterised by the highest Pt:Pd ratios (Figure 6.8). At the top of the zone, Cr/MgO ratios increase sharply to >80.

- Zone 2 is characterised by the highest concentrations of 2 PGE+Au, S and Cu+Ni. There is an abrupt compositional break which is characterised by a change in Cr/MgO ratio from >150 below to <105 above and concomitant elevated PGE enrichment (Figure 6.8).
- Zone 3 is characterised by a very different Ni:Cu ratio from other mineralised zones. Whereas in Zones 1 and 2 the typical Ni:Cu ratio is <4, in this upper zone the Ni:Cu ratio is quite variable and may reach 12. The high Ni values reflect both an increase in pentlandite and olivine content in the top portion of Zone 1, with a corresponding increase in PGE's, especially in Pd, although the grade does not reach that of Zones 1 and 2 (Figure 6.8).

The cumulus nature of the PGM-bearing sulphide minerals suggests that much of the sulphide and PGM's are of magmatic origin although there is also an intercumulus phase of sulphide formation in the reef. This together with the hydrothermal alteration of primary silicates to sericite, amphibole and chlorite suggests that significant alteration has occurred to redistribute a minor proportion of the magmatic sulphides and PGE's. The peripheral basal 'contact' style mineralisation has close analogies to the southern part of Platreef in the northern limb rather than to any mineralisation of the eastern and western limbs of the Bushveld Complex. Another comparison with the Platreef is the occurrence of an inverted pigeonite-bearing noritic hanging wall to the reef.

Succeeding mineralised layers have been equated by Sharpe *et al* (2002) to the Lower, Middle and Upper Group chromitites of the BC and to the Merensky Reef. These are in ascending order the intermediate chromite layer (ICL), which was suggested to be equivalent to the lower or middle group chromitites of the BC; the Platchro (PCH), possibly analogous to the middle group chromitite of the BC; the hanging wall mineralised norite (HMN) and the

upper mineralised pyroxenite (UMP) possibly analogous to the Merensky Reef (Sharpe *et al.*, 2002). However, the work of this thesis casts doubt on these correlations. If the ICL in Unit 3 is equivalent to the lower or middle group chromitites of the BC as suggested by Sharpe et al (2002) then Unit 2 and associated mineralisation must be of Lower- or lower Critical Zone affinity since the MG2 chromitite occurs at the top of the lower Critical Zone in the eastern and western limbs. However, based on geochemical parameters discussed above, the pyroxenites of Unit 2 and the norite-pyroxenites of Unit 3, have more affinity with the upper rather than the lower Critical Zone.

7.5 Model for the formation of the succession at Sheba's Ridge

Combining the petrographic, geochemical and mineralisation data, it would appear that at Sheba's Ridge two different magmas have been emplaced as interfingering sills. One (Type A) has upper Critical Zone characteristics, the other (Type B) has Main Zone affinities. From the Cu/Zr profile it can also be suggested that peaks in the basal mineralisation of Unit 2 occur where there is a transition from type A Critical Zone magma to type B Main Zone magma in the sequence. The world's largest PGE deposits occur as intrusions which are characterised by an early magma with a distinctive Al_2O_3-poor and MgO, Cr- and SiO_2- rich (U-type) composition (Sharpe, 1981; Davies & Tredoux, 1985; Naldrett, 2004). This U-type magma is typically followed by a more tholeiitic magma and in many of these intrusions mineralised intervals occur at levels where these two magmas have mixed or 'mingled' (e.g. Kruger, 2005; Kinnaird, 2005, Seabrook, 2005). By analogy to the model for Bushveld magmatism of Sharpe (1981) it is suggested that two magmas were also involved in the formation of the stratigraphic sequence at Sheba's Ridge, one of a 'U-type and one of a 'tholeiitic type'.

For Sheba's Ridge, the following sequence of emplacement events is envisaged as shown in Figure 7.1.

- Unit 1 – a 'Marginal Zone' magma, which crystallized the norites, was probably the earliest phase of intrusion. The norites are consistently fine-grained implying that they were intruded into cool country rock and rapidly cooled (after Kinnaird, 2005). These Marginal Zone rocks which may have incorporated xenoliths of floor rock hornfels are equated with the Marginal Zone sills in the eastern and western limbs (Sharpe & Hulbert, 1985).

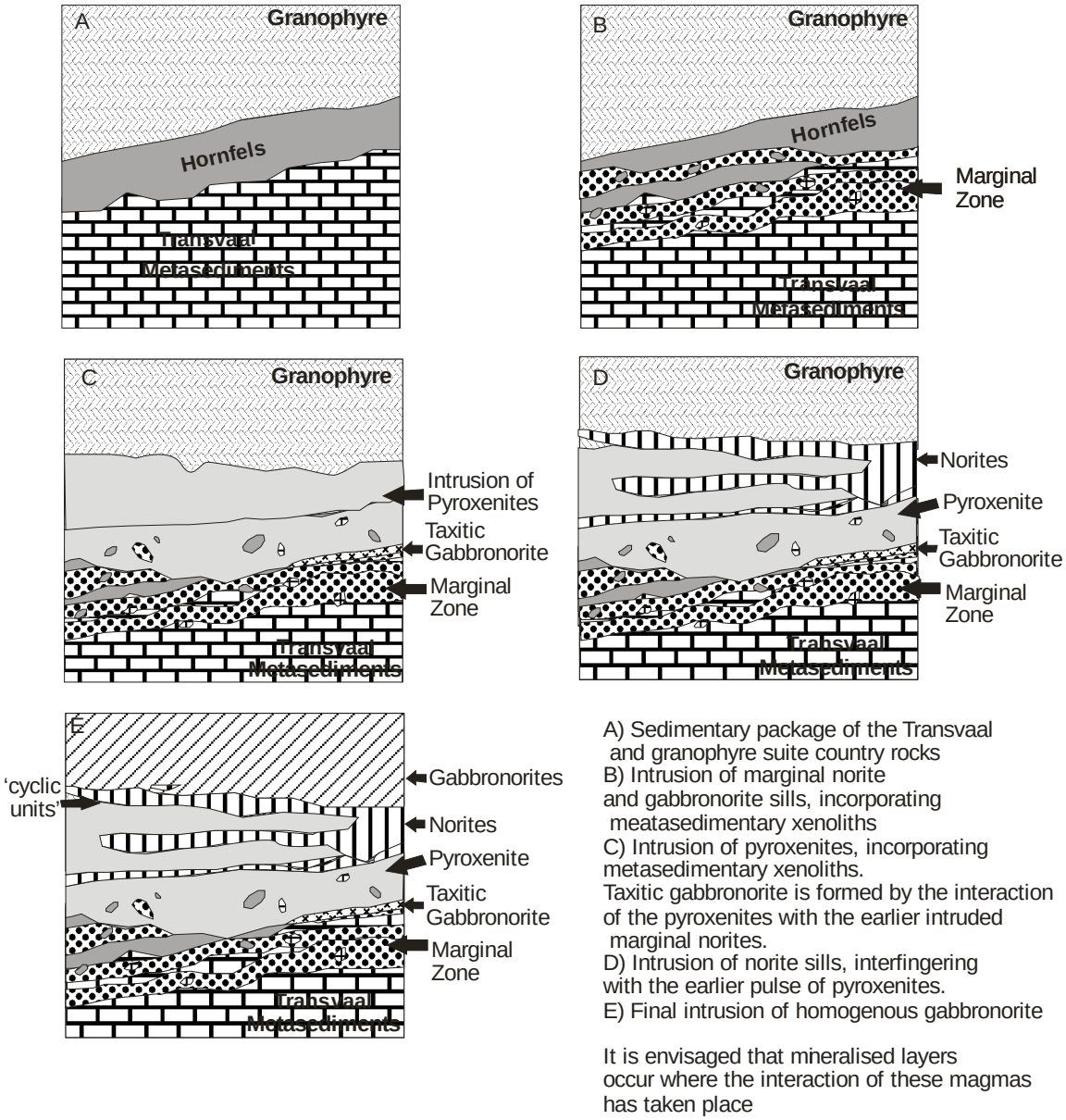

Figure 7.1 Suggested sequence of events for the emplacement of the mafic rocks at Sheba's Ridge.

- The successive intrusion of pyroxenitic layers of Unit 2 is likely to have followed also with the incorporation both of country rock xenoliths and earlier 'Marginal zone' intrusives. This magma is regarded as of upper Critical Zone affinity. The development of the taxitic gabbronorite in this Unit could have been caused by a mixing or mingling of the earlier pulse of Marginal Zone magma with the later more fractionated magma, which was lower in MgO and Cr_2O_3 and relatively iron enriched compared to the earlier magma, before complete consolidation of the earlier intrusion as has been inferred for the Federov-Pansky intrusion by Schissel *et al* (2002). The Cr/MgO ratio and Mg# of the basal section is geochemically distinct but this may be due to the interaction with floor rocks and assimilation of country rock xenoliths.

- The norite package of Unit 3 was probably the next phase of magma influx at Sheba's Ridge, disrupting the pyroxenite package and forming as sills causing a discontinuous interfingering in the package.

- The latest stage influx of magma was the gabbronorite of Unit 4. This intrusion, which may have disrupted some of the already layered norite packages and chromitite layers, is equated with the Main Zone elsewhere in the Bushveld Complex as a whole.

For the Bushveld Complex as a whole, it is still under dispute as to whether it was the Main Zone or the Critical Zone magma which was enriched in PGE at the time of the formation of the Merensky Reef (e.g. Kruger, 2005). For the Platreef, Kinnaird (2005) postulates multiple influxes of a Critical Zone-type magma. This magma was the source of the PGE-enriched source rather than the overlying Main Zone. A similar scenario is envisaged for the basal mineralisation at Sheba's Ridge.

The basin and dome setting of Sheba's Ridge and undulous nature of the floor rock must have contributed to the complex geology in the area. It is suggested by the field team that

onlap onto the domal features to the west and northwest occurred and that the stratigraphic sequence is incomplete in areas of floor rock highs. As with the Platreef the Lower Zone and lower Critical Zone are either attenuated or missing.

7.6 A comparison with the Bushveld Complex and other Ni-Cu-PGE deposits

The concept of multiple magma influxes in the Bushveld is well established (e.g. Eales *et* al, 1986; Eales *et* al, 1993; Eales *et al,* 1998*;* Kruger, 1990; Cawthorn *et al*, 1991; Kruger, 1994; Mitchell, 1998; Nex, 1998; Kinnaird, 2002; Nex, *et al* 2002; Arndt *et al*, 2005; Hutchinson & Kinnaird, 2005; Kinnaird, 2005; Kruger 2005; McDonald *et al*, 2005). For the Platreef the occurrence of multiphase magma influx has also been suggested (Hutchinson & Kinnaird, 2005; Kinnaird, 2005). They suggest that the Platreef comprises 4 pyroxenitic sills which assimilated sulphur from the footwall and country rock xenoliths (Sharman-Harris, 2005). The mineralisation within the Platreef, is not concentrated at one particular horizon in fact grade is variable with stratigraphic height and along strike. Kinnaird (2005) used geochemical data to further define these variations within the southern Platreef as follows: A top pyroxenite package with high Pt:Pd ratios of 2 or greater. An upper middle pyroxenite package where PGE content is the lowest and the Pt:Pd ratio is ~1:2 and increases from the base upward. A lower middle pyroxenite package which has the lowest Pt:Pd ratios of the pyroxenites and a lower pyroxenite which has a Pt:Pd of ~1 and carries the highest PGE's. The northern limb transgresses differing Transvaal metasedimentary floor rock northwards, from quartzites, Duitschland shales and dolomites, Penge banded iron formations, Malmani dolomites and Archaean granites in the north. Abundant sedimentary xenoliths are present. Sulphur isotopes from bulk samples indicate a non-mantle input (Buchanan *et al*, 1981) and recent sulphur isotope studies from the sulphide separates indicate a significant input by crustal rocks (Sharman-Harris & Kinnaird, 2004). This process of contamination is also supported by Harris & Chaumba (2001) who suggest post-magmatic fluid interaction.

The interaction of magma with crustal rocks is also suggested for the Noril'sk deposit in Siberia where $\delta^{34}S$ ranges between +8 to +12 and abrupt changes in Sr, Nd and wt% SiO_2 indicate the ingestion of crustal sulphur from surrounding anhydrite evaporates and contamination by granitic mid-crustal gneisses respectively (Naldrett, 1999). In contrast, the Federov-Pansky intrusion in the Kola Peninsular, Russia shows a very narrow range of $\delta^{34}S$ (-0.2 - + 1.4 per mil) in whole rock, indicating a dominant magmatic source even when sulphur content increases significantly (Schissel *et al*, 2002). Magma mixing is suggested for the Konttijärvi and Ahmavaara areas of the Portimo layered igneous complex, Finland. Iljina & Hanski (2002) suggest that this marginal series hosting a basal Ni, Cu, PGE deposit is similar only to the Platreef of the Bushveld Complex and that this unusual placing of PGE enrichment is the result of magma injection into areas that were not totally solidified allowing the two magmas to mix. More importantly they demonstrate that the small size of a mafic body does not make it non-prospective when it is related to large volumes of magma of the whole intrusion belt. This is very much the case at the Uitkomst Complex a Ni-rich Cr-Cu-PGE-bearing satellite body to the Bushveld Complex in South Africa where highly variable $\delta^{34}S$ values indicate crustal contamination (Gauert *et al*, 1996).

7.7 Current Progress in Exploration at Sheba's Ridge

Since this research project began, Ridge Mining has completed the pre-feasibility study at Sheba's Ridge, with the feasibility study due for completion in 2007. The Sulphide Mineral Resource (basal mineralised Unit 2) is stated at: 1.4 million tonnes nickel, 19 million ounces 3PGE and 0.5 million tonnes copper. The exploration and resource statement states that the Phase 1 drilling on Loskop South identified three distinct units of mineralisation: a layer similar to the UG2 termed the Platchro; an upper mineralized pyroxenite (UMP) analogous to the Merensky Reef and a thick basal sulphide zone similar to that of the Platreef of the

northern limb. However, due to the discontinuity of the Platchro and UMP the Phase 1 drilling concentrated on the basal sulphide mineralisation. The resource is now stated to be within a 30 m thick 'bulk sulphide zone' which lies within an 80 m thick sulphide horizon. The pre-feasibility study, completed in March 2005, projected an open pit mine of 3 km long, one km wide and 400 m deep (www.ridgemining.com, 21/12/2006). In addition to the activities of Ridge Mining, Lonmin and Platinum Ltd are in a joint venture currently undertaking exploration in the Loskop area. The project termed the 'Loskop Project' includes exploration on the farms Rietfontein 70JS, Kameeldoorn 71JS, De Wagendrift 79JS and Loskop South 53JS. However, unlike the pre-feasibility of Ridge Mining on Loskop South 53JS early exploration infers a continuous UMP through the farm Rietfontein 70JS with an estimated grade of 4.4 g/t 3PGE+Au. Unlike the basal mineralisation this has a Pt:Pd of 2:1 similar to that of the Merensky Reef in the main eastern limb of the Bushveld Complex.

7.8 Conclusions

For Sheba's Ridge the following conclusions can be made:

- A lithologically variable sequence has been formed from the interfingering of sills formed from two geochemically distinct magmas, one of Critical Zone affinity and one with Main Zone characteristics.
- One of these magma contained sufficient concentrations of Ni, Cu and PGE so that, when immiscible sulphides developed, these sulphides became enriched in these metals according to the model of Naldrett (2004).
- For Sheba's Ridge, the reason for sulphide immiscibility has not been established. In the Bushveld Complex at the level of the Merensky Reef sulphide immiscibility may have been caused by magma mixing or magma mingling (e.g. Seabrook, 2005, Naldrett, 2004); For the Platreef, the addition of crustal sulphur has been suggested

as the cause (Sharman Harris & Kinnaird, 2004). At Sheba's Ridge magma mixing or mingling may have been important but there are also sufficient sulphide-bearing hornfels xenoliths to suggest that some addition of sulphur may have occurred through migration from the footwall and country rock xenoliths.

7.9 Suggestions for further work in the Loskop area

It is suggested that more detailed geochemical analysis of samples through the stratigraphic sequence would provide a more comprehensive study of the area as a whole especially with regard to the interfingering of different magmas. It is also considered important to undertake a sulphur isotope study to help to constrain the source of sulphur and the processes involved in the formation of the ore-body at Sheba's Ridge. An oxygen isotope study on silicate rock samples from the mineralised pyroxenite and possibly floor rock and country rock xenoliths may also help to indicate if there was significant contamination of crustal material that could have caused sulphur saturation.

It is evident that the stratigraphic sequence at Sheba's Ridge has many similarities with the eastern and western limbs of the Bushveld Complex. However, the sequence is atypical in the Bushveld Complex and although similarities occur, there are also significant differences. It is unclear whether the deposit at Sheba's Ridge formed from a separate feeder to the main limbs of the Bushveld Complex or whether perhaps the basin and dome setting acted to restrict the igneous rocks in this area. Nevertheless, peripheral areas to the eastern and western limbs of the Bushveld Complex are becoming recognized as potential prospects for the mining and exploration industry, and further exploration can only add to the knowledge of the largest igneous layered intrusion known on Earth.

References

Andersen, J.C.O., Rasmussen, H., Nielsen, T.F.D. & Ronsbo, J.G., (1998). The Triple Group and the Platinova gold and palladium reefs in the Skaergaard intrusions: Stratigraphic and Petrographic relations. *Economic Geology,* **93**, 488-509.

Armitage, P.E.B., McDonald, I., Edwards, S.J., Manby, G.M., (2000). PGE Mineralization in the Platreef and Calc-Silicate Footwall at Sandsloot, Potgietersrus District, South Africa. *Transactions of the institute of mining and metallurgy,* **111,** B36-B45.

Arndt, N., Jenner, G., Ohnenstetter, M., Deloule, E., & Wilson, A.H., (2005). Trace elements in the Merensky Reef and adjacent norites Bushveld Complex South Africa. *Mineralium Deposita*, **40**, 550-575.

Barker & Associates, (2004). Platinum map of Southern Africa. 2nd Edition. *Bruma 2026*, South Africa.

Brown, G. M. (1968). Experimental Studies in Inversion Relations in Natural Pigeonitic Pyroxenes. *Carnegie Institute of WashingtonYearbook.* 347-359.

Buchanan, D.L., Nolan, J., Suddaby, P., Rouse, J.E., Viljoen, M.J. & Davenport, W.J. (1981). The genesis of Sulphide Mineralization in a Portion of the Potgietersrus Limb of the Bushveld Complex. *Economic Geology,* **76,** 568-579.

Burger, A.J. & Walraven, F. (1980). Summary of age determinations carried out during the period April 1978 to March 1979. *Annual Geological Survey of South Africa*, **14,** 109-118.

Button, A. (1986). The Transvaal sub-basin of the Transvaal Sequence. *In*: Anhaeusser, C.R. and Maske, S. (Editors.). *Mineral Deposits of South Africa, (Geological Society of South Africa) II*, 811-817.

Cawthorn, R.G., Meyer, P.S. & Kruger, F.J. (1991). Major Addition of Magma at the Pyroxenite Marker in the Western Bushveld Complex, South Africa. *Journal of Petrology*, **32**, 739-763.

Cawthorn R.G. (1999). The platinum and palladium resources of the Bushveld Complex. *South African Journal of Science*, **95**, 481-489.

Cawthorn, R.G. & Webb, S.J. (2000). Connectivity between the western and eastern limbs of the Bushveld Complex. *Tectonophysics*, **330,** 195-209.

Cawthorn, R.G. & Lee, C.A. (2005). Lateral Geochemical Variability of Host Rocks to PGE Mineralisation in the Platreef, Bushveld Complex. 'Platinum-Group Elements-from Genesis to Beneficiation and Environmental Impact'. Extended abstract volume, 10th International Platinum Symposium, Oulo, Finland, August 2005. 300-303.

Crous, S.P. (1995). The geology, geochemistry and stratigraphic correlations of the farm Rietfontein 70 JS on the south-eastern flank of the Dennilton dome, Transvaal, South Africa. M.Sc. dissertation, Rhodes University, Grahamstown, South Africa.

Davies, R.G. & Tredoux, M. (1985). The platinum group elements and gold content of the marginal rocks and sills of the Bushveld Complex. *Economic Geology*, **80,** 838-848.

Deer, W.A., Howie, R.A. & Zussman, J. (1966). An introduction to rock forming minerals. *Longman Scientific & Technical, Essex, UK.*

Donaldson, C. H. (1985). A comment on crystal shapes resulting from dissolution in magmas. *Mineralogical Magazine*, **49**: 129-132.

Donaldson, C.H, & Henderson, C.M.B. (1988). A New Interpretation of round embayments in quartz crystals. *Mineralogical Magazine.* **52 (364)**: 27-33 Part 1.

Eales, H.V. & Reynolds, I.M. (1986). Cryptic Variations within Chromitites of the Upper Critical Zone, Northwestern Bushveld Complex. *Economic Geology*, **81,** 1056-1066.

Eales, H.V., Marsh, J.S., Mitchell, A.A., de Klerk, W.J., Kruger, F.J. & Field, M. (1986). Some geochemical constraints upon models for the crystallization of the upper Critical Zone-Main Zone interval, northwestern Bushveld Complex. *Mineralogical Magazine*, **50,** 567-582.

Eales, H.V., Field, M., De Klerk, W.J. & Scoon, R.N. (1988). Regional trends of chemical variation and thermal erosion in the upper Critical Zone, western Bushveld Complex. *Mineralogical Magazine*, **52,** 63-79.

Eales, H.V., De Klerk, W.J., Butcher A.R. & Kruger, F.J. (1990). The cyclic unit beneath the UG1 chromitite (UG1FW unit) at RPM Union Section Platinum Mine – Rosetta stone of the Bushveld Upper Critical Zone. *Mineralogical Magazine.* **54,** 23-43.

Eales, H.V., Maier, W.D. & Teigler, B. (1991). Corroded plagioclase feldspar inclusions in orthopyroxene and olivine of the Lower and Critical zones, Western Bushveld Complex. *Mineralogical Magazine*, **55,** 479-486.

Eales, H.V., Botha, W.J., Hattingh, P.J., De Klerk, W.J., Maier, W.D. & Odgers, A.T.R. (1993). The mafic rocks of the Bushveld Complex: a review of emplacement and crystallisation history, and mineralisation, in light of recent data. *Journal of African Earth Science.* **16,** 121-142.

Eales , H.V. & Cawthorn, R.G. (1996). *The Bushveld Complex*. In Cawthorn, R.G. (Editor.) Layered Intrusions. *Elsevier Science*, 181-229.

Faure, G. (1986). Principles of Isotope Geology, Second Edition. *John Wiley & Sons, New York.*

Gauert, O.D.K., Jordaan, L.J., de Waal, S.A. & Wallmach, T. (1996). Isotopic constraints on the source of sulphur for the base metal sulphides of the Uitkomst Complex, Badplaas, South Africa. *South African Journal of Geology,* **99 (1):** 41-50.

Gillespie & Styles, (1999). Rock classification Scheme. British Geological Society. www.bgs.ac.uk/data/dictionaries.html, view in 2003.

Hamilton, J. (1977). Sr isotope and trace element studies of the Great Dyke and Bushveld mafic phase and their relation to early Proterozoic magma genesis in Southern Africa. *Journal of Petrology,* **18**, 24-52.

Harris, C. & Chaumba, J.B. (2001). Crustal contamination and Fluid-Rock Interaction during the Formation of the Platreef, Northern Limb of the Bushveld Complex, South Africa. *Journal of Petrolog,*. **42 (7),** 1321-1347.

Hatton, C.J. & von Gruenewaldt, G., (1987). The geological setting and petrogenesis of the Bushveld chromitite layers. In: Stowe, C.W. (Editor) Evolution of chromium ore fields. *New York: Van Nostrand Reinhold Co.*, 109-43.

Haughton, D.R., Roeder, P.L. & Skinner, B.J. (1974). Solubility of Sulfur in Mafic Magmas. *Economic Geology*, **69**, 451-462.

Holwell, D.A., McDonald, I. & Armitage, P.E.B. (2004). Platinum-group mineral assemblages in the Platreef at Sandsloot mine, Limpopo Province, South Africa.

Geoscience Africa, *Abstract volume*, University of the Witwatersrand, Johannesburg, South Africa. 282-283.

Hornsey, R.A. (1999). The genesis and evolution of the Nkomati Mine Ni-sulphide deposit, Mpumalanga Province, South Africa. MSc, University of Natal, Durban, South Africa, pp 224.

Hunter, R.H., (1987). Textural equilibrium in layered igneous rocks. In: Parsons, I., (Editor) Origins of Igneous Layering. *Dordrecht: Reidel*, 473-503.

Hunter, R.H., (1996). Texture Development in Cumulate Rocks. .In Cawthorn, R.G., (Editor) Layered Intrusions, *Elsevier Science*. 77-101.

Hutchinson, D. & Kinnaird, J.A. (2005). Complex multistage genesis for the Ni-Cu-PGE mineralization in the southern region of the Platreef, Bushveld Complex, South Africa. *Applied Earth Science Trans. Inst. Min. Metall. B,* **114,** B208-B224.

Ijina, M. & Hanski, E. (2002). Multimillion-Ounce PGE deposits of the Portimo Layered Igneous Complex, Finland. In *9th Platinum Symposium*, Stillwater 2002.

Irvine, T. N. (1975). Crystallisation sequences in the Muskox intrusion and other layered intrusion-II. Origin of chromitite layers and similar deposits of other magmatic ores. *Geochimica et Cosmochimica Acta*, **39**: 991-1020.

Irvine, T.N. (1982). Terminology for Layered Intrusions. *J. Petrology*, **23**, 127-162.

Kinloch, E.D. (1982). Regional Trends in the Platinum-Group Mineralogy of the Critical Zone of the Bushveld Complex, South Africa. *Economic Geology*, **77**, 1328-1347.

Kinnaird, J.A., Kruger, F.J., Nex, P.A.M. & Cawthorn, R.G. (2002). Chromitite formation - a key to understanding processes of platinum enrichment. *Transactions of the Institution of Mining and Metallurgy,* **111,** 23-35.

Kinnaird, J. & Nex, P. (2003). Mechanisms of marginal mineralisation in the Bushveld Complex. *Transactions of the Institution of Mining and Metallurgy.* **112 (2),** 206-208.

Kinnaird, J.A. (2005). Geochemical evidence for multiple phase emplacement in the southern Platreef. *Transactions of the Institute of Mining and Metallurgy,* **114,** B225-B242.

Kruger , F.J. & Marsh, J.S. (1982). Significance of $^{87}Sr/^{86}Sr$ ratios in the Merensky cyclic unit of the Bushveld Complex. *Nature,* **298,** 53-55.

Kruger, F.J. (1990). The stratigraphy of the Bushveld Complex: a reappraisal and the relocation of the Main Zone boundaries. *South African Journal of Geology,* **93 (2),** 376-381.

Kruger, F.J. (1994). The Sr-isotopic stratigraphy of the Western Bushveld Complex. *South African Journal of Geology.* **97,** 393-398.

Kruger, F.J. (2005). Filling the Bushveld Complex magma chamber: lateral expansion, roof and floor interaction, magmatic unconformities, and the formation of giant chromitite, PGE and Ti-V-Magnetite Deposits. *Mineralium Deposita,* **40, (5)**, 451-472.

Lee, C.A. & Butcher, A.R. (1990). Cyclicity in the Sr Isotope stratigraphy through the Merensky and Bastard Reef units, Atok Section, Eastern Bushveld Complex. *Economic Geology,* **85**, 877-883.

Li, C., Maier, W. & de Waal, S. (2001). The role of magma mixing in the genesis of PGE mineralisation in the Bushveld Complex: Thermodynamic calculations and new interpretations. *Economic Geology,* **96,** 653-662.

Lomberg, K.G., Martin, E.S., Patterson, M.A. & Venter, J.E. (1999). The morphology of potholes in the UG2 chromitite layer and the Merensky Reef (pothole reef facies) at Union Section, Rustenburg Platinum Mines. *South African Journal of Geology,* **102,** 209-220.

McDonald, I., Howell, D.A. & Armitage, P.E.B. (2005). Geochemistry and mineralogy of the Platreef and "Critical Zone" of the northern limb of the Bushveld Complex, South Africa. *Mineralium Deposita,* **40 (5),** 526-549.

McKenzie, D. (1984). The generation and compaction of partially molten rock. *Journal of Petrology,* **25**, 713-765.

Miller, J.D. Jr & Andersen, J.C.O. (2002). Attributes of Skaergaard-type PGE reefs. *9th International Platinum Symposium Abstracts*. Billings, Montana.

Mitchell, A.A. (1990). The stratigraphy, petrography and mineralogy of the Main Zone of the northwestern Bushveld Complex. *South African Journal of Geology*, **93,** 818-831.

Mitchell, A.A. (1996). Compositional Cyclicity in a pyroxenitic layer from the Main Zone of the Western Bushveld Complex: evidence for repeated magma influx. *Mineralogical Magazine*, **60,** 149-161.

Mitchell, A.A., Eales, H.V. & Kruger, F.J. (1998). Magma replenishment, and the significance of poikilitic textures, in the Lower Main Zone of the western Bushveld Complex, South Africa. *Mineralogical Magazine*, **62(4)**, 435-450.

Molyneux, T.G. (1974). A geological investigation of the Bushveld complex in Sekhukuneland and part of the Steelpoort Valley. *Transactions of the Geological Society of South Africa*, **77,** 329-338.

Naldrett, A.J. (1989). *Magmatic Sulfide Deposits*. Oxford University Press, Oxford, pp186.

Naldrett, A. J. and von Gruenewaldt, G., (1989). Association of platinum-group elements with chromitite in layered intrusions and ophiolite complexes. *Economic Geology*, **84**: 180-187.

Naldrett, A.J. (1999). World-class Ni-Cu-PGE deposits: key factors in their genesis. In: *Mineralium Deposita.* 34, 227-240.

Naldrett, A.J. (2004). *Magmatic Sulphide Deposits*. Springer. Berlin Heidelberg New York, pp 727.

Nex, P.A., Kinnaird, J.A., Ingle, L.J., van der Vyer, B.A. & Cawthorn, R.G. (1998). A new stratigraphy for the Main Zone of the Bushveld Complex, in the Rustenburg area. *South African Journal of Geology,* **101(3),** 215-223.

Nex, P.A.M., Cawthorn, R.G. & Kinnaird, J.A. (2002). Geochemical effects of magma addition: compositional reversals and decoupling of trends in the Main Zone of the western Bushveld Complex. *Mineralogical Magazine,* **66, (6),** 833-856.

Norish, K. & Hutton, J.T. (1969). An accurate X-ray spectrographic method for the analysis of a wide range of geological samples. *Geochim Cosmochin Acta,* **33,** 431-453.

Nyama, N., Nex, P. & Yao, Y. (2005). Preliminary Petrological Studies of the Platreef on Tweefontein Hill, Bushveld Igneous Complex, South Africa. 2nd Platreef Workshop, Mokopane 28th-30th October 2005. University of the Witwatersrand, South Africa.

Parsons, I. (1987). *Origins of Igneous Layering.* Reidel Publishing Company, Dordrecht, The Netherlands, pp 666.

Ripley, E.M. (1986). Applications of stable isotope studies to problems of magmatic sulfide ore genesis with special reference to the Duluth Complex, Minnesota. In: 'Geology and Metallogeny of Copper Deposits'. Friedrich, G.H., Genkin, A.D., Naldrett, A.J., Ridge, J.D., Sillitoe, R.H., and Vokes, F.M. (Editors). Society for Geology Applied to Ore Deposits, Spec. Publ. No. 4, Berlin, Heidelberg: Springer-Verlag. Pp 25-42.

Ripley, E. M., and Alawi, J.A. (1988). Petrogenesis of pelitic xenoliths at the Babbitt Cu-Ni deposit, Duluth Complex, Minnesota, USA. *Lithos.* **21**, 143-159.

Rollinson, H.R. (1993). *Using geochemical data: evaluation, presentation, interpretation.* Longman Group UK Ltd, pp 352.

Roodt, E. (2004). *Geological Report on Sheba's Ridge, Groblersdal, Mpumalanga, South Africa*. Cluff Platinum Management S.A. Pty. Ltd. Internal Report.

Schissel, D., Tsvetkov, A.A., Mitrofanov, F.P. & Korchagin, A.U. (2002). Basal Platinum-Group element Mineralization in the Federov Pansky Layered Mafic Intrusion, Kola Penninsula, Russia. *Economic Geology,* **97,** 1657-1677.

Schoenberg, R., Kruger, F.J., Nagler, T,F., Meisel, T. and Kramers, J.D. (1999). PGE enrichment in chromitite layers and the Merensky Reef of the western Bushveld Complex; a Re-Os and Rb-Sr isotope study. *Earth and Planetary Science Letters*, **172**: 49-64.

Scoon, R.N. & Teigler, B. (1994). Platinum-Group Element Mineralization in the Critical Zone of the Western Bushveld Complex: I. Sulphide Poor-Chromitites below the UG-2. *Economic Geology*, **89,** 1094-1121.

Scoon, R.N. & Teigler, B. (1995). A New LG-6 Chromite Reserve at Eerste Geluk in the Boundary Zone between the Central and Southern Sectors of the Eastern Bushveld Complex. *Economic Geology*, **90,** 969-982.

Seabrook, C.L. (2005). The Upper Critical and Lower Main Zones of the Bushveld Complex. Ph.D. Thesis, University of the Witwatersrand, Johannesburg, South Africa.

Seabrook, C.L., Cawthorn, R.G. & Kruger, F.J. (2005). The Merensky Reef, Bushveld Complex: Mixing of Minerals not Mixing of Magmas. *Economic Geology*, **100**, 1191-1205.

Sharkov, E.V., Bogatikov, O.A., Grokhovskaya, T.L., Chistyakov, A.V., Ganin, V.A., Grincvich, N.G., Snyder, G.A. & Taylor, L.A. (1995). Petrology and Ni-Cu-Cr-PGM mineralisation of the largest mafic pluton in Europe: The early Proterozoic Burakovsky layered intrusion, Karelia, Russia. *International Geology Review*, **37**, 509-525.

Sharman-Harris, E.R. & Kinnaird, J.A. (2004). Into the new millennium: Sulphur isotope studies of the southern Platreef, Northern Limb, Bushveld Igneous Complex. 2nd

Platreef Workshop, Mokopane 16th-19th July 2004, University of the Witwatersrand, South Africa.

Sharpe, M.R. (1981). The chronology of magma influxes to the eastern compartment of the Bushveld Complex as exemplified by its marginal border groups. *Journal of the Geological Society London*, **138,** 307-326.

Sharpe, M.R. (1985). Strontium isotope evidence for preserved density stratification in the Main Zone of the Bushveld Complex, South Africa. *Nature*, **316**, 119-126.

Sharpe, M.R. & Hulbert, L.J. (1985). Ultramafic Sills beneath the Eastern Bushveld Complex: Mobilized Suspensions of Early Lower Cumulates in a Parental Magma with Boninitic Affinities. *Economic Geology*, **80**, 849-871.

Sharpe, M.R., Crous, S.P., Gain, S.B., Chunnett, G.K. & Lee, C.A. (2002). Sheba's Ridge – An Unconventional Setting for Platreef, UG2 and Merensky-Style PGE-BMS Deposits in the Bushveld Complex. In: *9th Platinum Symposium.* Stillwater 2002.

Streckeisen, A. (1976). To each plutonic rock its proper name. *Earth Science Review*, **12,** 1-33.

Tait, S.R., Huppert, H.E., & Sparks, R.S.J. (1984). The role of compositional convection in the formation of adcumulus rocks. *Lithos*, **17,** 139-146.

Viljoen, M.J. & Schürmann, L.W. (1998). Platinum Group Metals. In: Wilson, M.G.C. & Anhaeusser, C.R., (Editors). *The mineral resources of South Africa.* Council for Geosciences Handbook, **16,** 533-568**.**

von Gruenewaldt, H.G. (1970). On the phase-change orthopyroxene-pigeonite and the resulting textures in the Main and Upper Zones of the Bushveld Complex in the eastern Transvaal. *Special Publication of the Geological Society of South Africa*, **1**, 67-73.

von Gruenewaldt, H.G. (1973). The Main and Upper Zones of the Bushveld Complex in the Roossenkal area, Eastern Transvaal. *Transactions of the Geological Society of South Africa*, **76,** 207-227.

von Gruenewaldt, H.G. & Weber-Diefenbach, K. (1977). Coexisting Ca-poor pyroxenes in the Main Zone of the Bushveld complex. *Contributions to Mineralogy and Petrology*, **65,** 11-18.

Wager, L.R., Brown, G.M. & Wadsworth, W.J. (1960). Types of igneous cumulates. *Journal of Petrology*, **1**, 73-85.

Wager, L.R. & Brown, G.M., (1968). Layered Igneous Rocks. *Oliver & Boyd, Ltd. Edinburgh*, pp 588.

Walraven, F., Armstrong, R.A. & Kruger, F.J. (1990). A chronostratigraphic framework for the north-central Kaapvaal Craton, the Bushveld Complex, and Vredefort structure. *Tectonophysics*, **171,** 23-48.

Zingg, A.J. (1996). Recrystallization and origin of layering in the Bushveld Complex. *Lithos*, **37,** 15-37.

www.ridgemining.com, 21/12/2006

Appendix 1A - LSD34 Borehole Log

Magnetite	Chromite	BMS	BH ID	FROM	TO	LITHOLOGY	DESCRIPTION
			LSD34	0.00	140.00	Gabbro	
			LSD34	140.00	193.00	Gabbro	
			LSD34	193.00	216.00	Norite	
			LSD34	216.00	218.00	Feldspathic Pyroxenite	
			LSD34	225.00	233.50	Anorthosite	Gradual basal contact.
			LSD34	233.50	233.73	Feldspathic Pyroxenite	Coarse grained and fractured with a sharp basal contact.
			LSD34	233.73	235.20	Norite	Spotted, altered at base.
			LSD34	235.20	235.70	Feldspathic Pyroxenite	Coarse grained and fractured with a sharp basal contact.
			LSD34	235.70	236.90	Norite	Spotted norite, altered around minor felsic veins.
			LSD34	236.90	237.00	Feldspathic Pyroxenite	Fine grained, fractured and altered towards base.
			LSD34	237.00	238.50	Norite	Heavily altered with abundant felsic veins.
			LSD34	238.50	238.55	Chlorite	Chlorite parting.
			LSD34	238.55	239.60	Norite	Sharp basal contact dipping at 30˚.
			LSD34	239.60	239.70	Anorthosite	Sharp basal contact dipping at 30˚.
			LSD34	239.70	240.30	Norite	Sharp basal contact dipping at 10˚.
			LSD34	240.30	240.50	Anorthosite	Mottle anorthosite with a sharp basal contact dipping at 20˚.
			LSD34	240.50	240.65	Feldspathic Pyroxenite	Sharp basal contact dipping at 20˚.
			LSD34	240.65	240.70	Anorthosite	Sharp basal contact dipping at 20˚.
			LSD34	240.70	240.80	Feldspathic Pyroxenite	
			LSD34	240.80	241.00	Anorthosite	Mottled anorthosite with gradual basal contact.
			LSD34	241.00	241.10	Norite	
			LSD34	241.10	241.20	Anorthosite	Mottled with gradual basal contact.
			LSD34	241.20	241.25	Norite	
			LSD34	241.25	241.30	Anorthosite	
		BMS	LSD34	241.30	241.60	Feldspathic Pyroxenite	Fine scattered base metal sulphides.
		BMS	LSD34	241.40	241.45	Norite	Fine scattered base metal sulphides.
		BMS	LSD34	241.45	241.60	Feldspathic Pyroxenite	Fine scattered base metal sulphides.
		BMS	LSD34	241.60	242.60	Norite	Spotted norite, altered around minor felsic veins.
		BMS	LSD34	242.60	242.70	Feldspathic Pyroxenite	Fine disseminated BMS.
		BMS	LSD34	242.70	243.30	Norite	Fine disseminated BMS.
		BMS	LSD34	243.30	243.45	Feldspathic Pyroxenite	Fine disseminated BMS.
		BMS	LSD34	243.45	244.40	Norite	Fine disseminated BMS.

Appendix 1A - LSD34 Borehole Log continued

Magnetite	Chromite	BMS	BH ID	FROM	TO	LITHOLOGY	DESCRIPTION
		BMS	LSD34	244.40	244.65	Melanorite	Melanorite with ~10% biotite and fine disseminated BMS
		BMS	LSD34	244.65	245.40	Norite	Fine disseminated BMS.
		BMS	LSD34	245.50	245.60	Feldspathic Pyroxenite	With a sharp basal contact at 0˚ bedding angle. Fine disseminated BMS.
		BMS	LSD34	245.60	246.07	Melanorite	Recrystallised at basal contact. Fine disseminated BMS.
		BMS	LSD34	246.07	246.13	Felsic Vein	
		BMS	LSD34	246.13	246.30	Melanorite	Recrystallised at top contact. Fine disseminated BMS.
		BMS	LSD34	246.30	246.40	Norite	Spotted norite. Fine disseminated BMS.
		BMS	LSD34	246.40	246.88	Melanorite	Fine disseminated BMS.
		BMS	LSD34	246.88	247.10	Norite	Fine disseminated BMS.
		BMS	LSD34	247.10	247.55	Melanorite	Fine disseminated BMS.
		BMS	LSD34	247.55	248.00	Feldspathic Pyroxenite	Fine disseminated BMS.
		BMS	LSD34	248.00	249.18	Norite	Altered towards base with an increase in biotite. Fine disseminated BMS.
		BMS	LSD34	249.18	250.70	Feldspathic Pyroxenite	Fine disseminated BMS.
		BMS	LSD34	250.70	250.80	Felsic Vein	Fine disseminated BMS.
		BMS	LSD34	250.80	254.10	Feldspathic Pyroxenite	Medium grained with ~10% biotite. Fine disseminated BMS.
		BMS	LSD34	254.10	254.42	Norite	Spotted norite with fine disseminated BMS.
		BMS	LSD34	254.42	259.10	Feldspathic Pyroxenite	Medium grained with ~10% biotite. Fine disseminated BMS.
		BMS	LSD34	259.10	259.20	Calcsilicate	Very fine-grained and heavily altered.
		BMS	LSD34	259.20	259.30	Gabbronorite	
		BMS	LSD34	259.30	261.10	Feldspathic Pyroxenite	Fine disseminated BMS.
			LSD34	261.10	261.50	Gabbronorite	Fine-grained quartz-bearing gabbronorite.
		BMS	LSD34	261.50	262.30	Feldspathic Pyroxenite	Fine disseminated BMS.
			LSD34	262.30	262.50	Gabbronorite	Quartz-bearing gabbronorite with 5 cm quartz vein.
		BMS	LSD34	262.50	263.30	Feldspathic Pyroxenite	Fine disseminated BMS.
			LSD34	263.30	263.50	Melanorite	Fine disseminated BMS.
		BMS	LSD34	263.50	266.70	Feldspathic Pyroxenite	Medium-grained woth disseminated BMS, predominantly pentlandite, chalcopyrite and pyrrhotite. Gradual basal contact.
		BMS	LSD34	266.70	267.30	Norite	Spotted norite with a gradual basal contact. Fine disseminated BMS.
		BMS	LSD34	267.30	267.70	Feldspathic Pyroxenite	Fine disseminated BMS.
		BMS	LSD34	267.70	267.78	Norite	Spotted norite. Fine disseminated BMS.
		BMS	LSD34	267.78	268.00	Feldspathic Pyroxenite	Fine disseminated BMS.

Appendix 1A - LSD34 Borehole Log continued

Magnetite	Chromite	BMS	BH ID	FROM	TO	LITHOLOGY	DESCRIPTION
		BMS	LSD34	268.00	268.20	Melanorite	Fine disseminated BMS.
			LSD34	268.20	269.20	Anorthosite	Mottled anorthosite.
		BMS	LSD34	269.20	271.00	Norite	Spotted norite. Fine disseminated BMS.
		BMS	LSD34	271.00	271.15	Leuconorite	
		BMS	LSD34	271.15	274.40	Melanorite	
		BMS	LSD34	274.40	275.10	Norite	Sharp basal contact dipping at 70˚.
		BMS	LSD34	275.10	275.20	Leuconorite	Sharp basal contact dipping at 70˚.
		BMS	LSD34	275.20	276.05	Norite	Sharp basal contact dipping at 70˚.
		BMS	LSD34	276.05	276.10	Leuconorite	Sharp basal contact dipping at 70˚.
		BMS	LSD34	276.10	276.70	Norite	Sharp basal contact dipping at 70˚.
		BMS	LSD34	276.70	277.10	Leuconorite	Sharp basal contact dipping at 70˚.
		BMS	LSD34	277.10	277.40	Norite	
		BMS	LSD34	277.40	281.40	Melanorite	Sharp basal contact dipping at 80˚.
		BMS	LSD34	281.40	281.80	Leuconorite	Sharp basal contact dipping at 80˚.
		BMS	LSD34	281.80	281.90	Norite	
		BMS	LSD34	281.90	282.30	Leuconorite	
		BMS	LSD34	282.30	282.65	Norite	Sharp basal contact dipping at 40˚.
		BMS	LSD34	282.65	282.70	Anorthosite	Sharp basal contact dipping at 40˚.
		BMS	LSD34	282.70	283.40	Leuconorite	
		BMS	LSD34	283.40	283.46	Anorthosite	Mottled anorthosite.
		BMS	LSD34	283.46	286.60	Norite	Spotted norite with a sharp basal contact dipping at 45˚.
		BMS	LSD34	286.60	287.00	Feldspathic Pyroxenite	
		BMS	LSD34	287.00	288.66	Norite	Spotted norite. Fine disseminated BMS.
		BMS	LSD34	288.66	288.70	Feldspathic Pyroxenite	
		BMS	LSD34	288.70	288.90	Norite	
		BMS	LSD34	288.90	289.00	Feldspathic Pyroxenite	
		BMS	LSD34	289.00	289.08	Norite	
		BMS	LSD34	289.08	289.65	Feldspathic Pyroxenite	
		BMS	LSD34	289.65	289.90	Leuconorite	Altered towards the base. Sharp basal contact dipping at 20˚.
		BMS	LSD34	289.90	289.92	Anorthosite	Sharp basal contact dipping at 20˚.
		BMS	LSD34	289.92	290.00	Leuconorite	

Appendix 1A - LSD34 Borehole Log continued

Magnetite	Chromite	BMS	BH ID	FROM	TO	LITHOLOGY	DESCRIPTION
		BMS	LSD34	290.00	290.40	Feldspathic Pyroxenite	
		BMS	LSD34	290.40	290.45	Anorthosite	Sharp basal contact dipping at 30˚.
		BMS	LSD34	290.45	290.70	Norite	
		BMS	LSD34	290.70	290.80	Anorthosite	
		BMS	LSD34	290.80	292.70	Norite	
		BMS	LSD34	292.70	292.77	Anorthosite	
		BMS	LSD34	292.77	293.15	Norite	
		BMS	LSD34	29.15	293.17	Anorthosite	
		BMS	LSD34	293.17	294.10	Norite	
			LSD34	294.10	313.00	Feldspathic Pyroxenite	
			LSD34	313.00	321.00	Feldspathic Pyroxenite	20% mica, 20% interstitial plagioclase. Phenocrysts of opx with cpx chadocrysts
Mag		BMS	LSD34	321.00	326.00	Pegmatoidal Pyroxenite	Magnetite stringers at 324m, BMS throughout pegmatoidal pyroxenite with a decrease in concentration at basal magnetite (324 m).
Mag		BMS	LSD34	326.00	327.00	Feldspathic Pyroxenite	Fine grained with magnetite stringers.
		BMS	LSD34	327.00	332.00	Feldspathic Pyroxenite	Varying grain size from medium to coarse with minor BMS and fractures common at 60°.
		BMS	LSD34	332.00	338.00	Feldspathic Pyroxenite	Medium grained with intermittent pegmatoidal texture, trace BMS and 1 cm chromite blebs. Magnetite stringers and blebs.
Mag			LSD34	338.00	342.00	Pegmatoidal Pyroxenite	pink/orange alteration of feldspar, magnetite stringers and blebs.
Mag			LSD34	342.00	342.50	Magnetite	
		BMS	LSD34	342.50	350.00	Feldspathic Pyroxenite	Fine grained, 10% mica. Disseminated BMS at top of unit. Phenocrysts of pyroxene crystals occur at top and base of unit. Calcsilicate xenolith.
Mag		BMS	LSD34	350.00	367.00	Feldspathic Pyroxenite	Pegmatoidal patches dip at 70° with sharp contacts. Magnetitite veins bifurcate. Bottom contact marked by magnetite vein. BMS is sparse and disseminated at base of unit.
		BMS	LSD34	367.00	370.00	Norite	Fine grained with 20-30% interstitial plagioclase, 1.5 cm phenocrysts of cpx, 5% mica. Disseminated BMS occurs towards base of unit.
Mag			LSD34	370.00	371.00	Pyroxenite	Dense magnetite stringers obscure original texture, gradational contact at base.

Appendix 1A - LSD34 Borehole Log continued

Magnetite	Chromite	BMS	BH ID	FROM	TO	LITHOLOGY	DESCRIPTION
Mag		BMS	LSD34	378.00	388.00	Feldspathic Pyroxenite	Dense magnetite stringers obscure original texture, sporadic pegmatoidal texture in pyroxenite. Trace BMS throughout. Towards base of unit
Mag		BMS	LSD34	388.00	400.00	Feldspathic Pyroxenite	20% mica. Chlorite veins are common and dip at 60°. Grain size varies from fine to medium. 1 cm bleb of BMS occurs in association with minor magnetite vein.
Mag		BMS	LSD34	371.00	377.00	Feldspathic Pyroxenite	Fine grained equigranular. 23 cm of magnetite stringers at 373 m and 25 cm at 374 m associated with increased grained size and increase in BMS concentration. Base marked by disappearance of magnetite.
			LSD34	377.00	378.00	Feldspathic Pyroxenite	Medium grained, no BMS or magnetite.
Mag		BMS	LSD34	400.00	430.00	Feldspathic Pyroxenite	Fine grained equigranular, 20% interstitial plagioclase, 10% mica. Magnetite stringers and BMS at 417.00 for 10 cm, chromite bleb at 418.00 m. Minor sporadic increases in grain size and minor chlorite veins.
Mag			LSD34	430.00	433.00	Feldspathic Pyroxenite	Magnetite stringers. Original texture obscured. Unit is heavily altered by calcsilicate xenolith. Contact is heavily fractured.
			LSD34	433.00	462.00	Norite	Top contact at 60°. Hornfels xenolith at 435.00 m with associated fracturing at contacts. Grain size varies from fine to medium. Bottom contact is undulous.
			LSD34	462.00	464.00	Harzburgite	Medium grained with 20% interstitial plagioclase. Discontinous fine grained pxroxenitic layers occur.
	Chromite		LSD34	464.00	474.00	Feldspathic Pyroxenite	Fine to medium grained. Interlayers of norite/melanorite with gradational contacts. Orthopyroxenitic xenolith with sugary texture occurs until 468 m. Chromite bleb at 469 m.
			LSD34	474.00	478.00	Norite	Mixed zone with interlayers of anorthosite and pyroxenite with wedging or pinching. Dips between 45°-60° with sharp contacts. Siliceous veining occurs at 80°. <5% mica.
Mag	Chromite	BMS	LSD34	478.00	480.00	Feldspathic Pyroxenite	Noritic interlayers. Siliceous contamination with magnetite stringers. 1-2 mm blebs of BMS occur below chromite bleb at 479 m. Sharp basal contact at 25°.
			LSD34	480.00	496.00	Norite	Medium grained equigranular, with 5% cpx, 60% cumulate plagioclase and 35-40% opx. Gradual increase in cpx with depth.
			LSD34	496.00	499.00	Norite	Mottled with clustered opx with cpx rimming, <5% mica.
			LSD34	499.00	499.75	Norite	Sharp upper contact.

Appendix 1A - LSD34 Borehole Log continued

Magnetite	Chromite	BMS	BH ID	FROM	TO	LITHOLOGY	DESCRIPTION
Mag			LSD34	503.00	515.00	Feldspathic Pyroxenite	Minor olivine. Varying grain size predominantly cpx, 15% mica, 10% interstitial plagioclase. Magnetite stringers at 506.50 m and 2 cm vein at 506.90 m dips at 65°. Siliceous xenolith at 507.75 m with crystalline
Mag		BMS	LSD34	515.00	518.50	Feldspathic Pyroxenite	Heavily altered mixed zone with magnetite stringers and appearance of interstital blebby and disseminated BMS. Chlorite veining dips at 70°.
			LSD34	499.75	501.00	Norite	Mottled with decreasing grain size and feldspar content with depth. 2 Chlorite veins dip at 35°.
	Chromite		LSD34	501.00	503.00	Feldspathic Pyroxenite	Fine grained with 10% mica. Chromite stringers.
		BMS	LSD34	518.50	518.55	Chromitite	Bifurcates and becomes stringers towards base. Increase in BMS above and below.
Mag		BMS	LSD34	518.55	525.00	Feldspathic Pyroxenite	Magnetite stringers, chromite blebs and disseminated BMS.
			LSD34	525.00	532.00	Pyroxenite	Fine grained equigranular, with <5% interstital plagioclase and 50:50 opx:cpx. Fractures are common and dip at 60°.
Mag		BMS	LSD34	532.00	539.50	Feldspathic Pyroxenite	Fine grained 5-10% plagioclase and 10% mica, trace disseminated BMS. 25 cm Magnetite stringers at 537.75 m with increased BMS.
		BMS	LSD34	539.50	540.00	Norite	Spotted with sharp upper contact and no BMS.
			LSD34	540.00	549.00	Norite	Mottled leuconorite. Gradual basal contact.
			LSD34	549.00	551.00	Norite	Medium grained melanorite, 20% mica.
Mag		BMS	LSD34	551.00	553.00	Pyroxenite	Heavily altered with varying grain size. Magnetite stringers dip at 70°, BMS occurs in association.
			LSD34	553.00	553.25	Norite	
			LSD34	553.25	556.00	Pyroxenite	Gradual loss of original structure, dense magnetite stringers with increased BMS.
Mag			LSD34	556.00	566.00	Pyroxenite	Sporadic chromite blebs and magnetite stringers, unit heavily altered with ~15 cm interlayers of norite and anorthosite, sharp contacts dip at 60°.
	Chromite	BMS	LSD34	566.00	571.00	Feldspathic Pyroxenite	Heavily altered, saussuritised plagioclase and chlorite fractures common. Serpentinised mafics with remnant crystal structure. Interstitial disseminated BMS occurs from 567.60 m. Chromite bleb occurs towards base.
			LSD34	571.00	575.00	Norite	Mottled and spotted. Opx is fine grained and equigranular. Dense fracturing and chlorite veins.
	Chromite		LSD34	590.50	592.50	Feldspathic Pyroxenite	Chromite blebs
			LSD34	592.50	593.00	Norite	
	Chromite	BMS	LSD34	593.00	597.00	Feldspathic Pyroxenite	Clustered chromite blebs. Gradational basal contact.

Appendix 1A - LSD34 Borehole Log continued

Magnetite	Chromite	BMS	BH ID	FROM	TO	LITHOLOGY	DESCRIPTION
			LSD34	597.00	599.00	Norite	Altered with interstitial BMS at top of unit. Intermixing with fine grained pyroxenite occurs towards base, sharp irregular contacts.
			LSD34	599.00	601.00	Norite	
			LSD34	601.00	606.00	Norite	Norite-pyroxenite mixing, heavily fractured with intense alteration towards bsae.
			LSD34	575.00	579.00	Feldspathic Pyroxenite	Fine grained, decrease in alteration with depth. 10% mica, increase in plagioclase with depth. Heavily fractured between 20°-60°. Sharp basal contact.
			LSD34	579.00	580.00	Norite	Gradational basal contact.
	Chromite	BMS	LSD34	580.00	588.00	Feldspathic Pyroxenite	Sporadic chromite blebs and BMS in areas of less intense alteration.
			LSD34	588.00	589.00	Norite	
	Chromite	BMS	LSD34	589.00	590.00	Feldspathic Pyroxenite	Fine grained with chromite blebs and interstital BMS.
			LSD34	590.00	590.50	Norite	
			LSD34	606.00	608.00	Feldspathic Pyroxenite	
			LSD34	608.00	608.50	Norite	No BMS.
	Chromite	BMS	LSD34	608.50	612.00	Feldspathic Pyroxenite	Interstitial BMS and sporadic chromtie blebs, gradual basal contact.
			LSD34	612.00	620.00	Norite	Melanorite, mottled with 15% mica. No BMS.
	Chromite		LSD34	620.00	627.00	Feldspathic Pyroxenite	Fine grained,sporadic chromite blebs. 10% mica, no BMS. Increase in feldspar content with depth.
			LSD34	627.00	628.00	Norite	Sharp chilled basal contact. Minor alteration.
	Chromite	BMS	LSD34	628.00	634.00	Feldspathic Pyroxenite	Fine grained with sporadic chromite blebs ~1 cm. Interstitial disseminated BMS throughout. Occassional chlorite fractures dip 60°
		BMS	LSD34	634.00	637.00	Pyroxenite	Fine grained with disseminated interstitial BMS.20% mica gives spotted appearance.
Mag		BMS	LSD34	637.00	654.50	Pyroxenite	Magnetite veins occur at 639.00-639.10 m and 641.00-641.10 m with massive BMS. Disseminated and massive BMS occurs throughtout but decreases in areas of intense alteration. Dense magnetite stringers and serpentinisation.
		BMS	LSD34	654.50	671.00	Taxitic Gabbronorite	Veins and blebs of coarse grained feldspar and pyroxene occur sporadically. BMS present throughout but decreases in areas of intense alteration. Plagioclase is cumulus in pegmatoidal patches and can be 50% in patches.

Appendix 1A - LSD34 Borehole Log continued

Magnetite	Chromite	BMS	BH ID	FROM	TO	LITHOLOGY	DESCRIPTION
		BMS	LSD34	671.00	671.50	Norite	Mixing of norite and pyroxenite. Disseminated BMS throughout.
		BMS	LSD34	671.50	675.00	Norite	Sharp contacts dip at 70°, trace BMS.
			LSD34	675.00	678.00	Meta-sediment	Very fine grained xenolith.
			LSD34	678.00	680.00	Feldspathic Pyroxenite	Fine grained with 15% mica orthopyroxenite, interstitial plagioclase.
		BMS	LSD34	680.00	684.00	Pyroxenite	Coarse graine norite interlayer with metasedimentary xenolith. 20% mica, BMS disseminated throughout pyroxenite.
		BMS	LSD34	684.00	688.00	Mixed Zone	Heavily altered with sparse BMS. Varying grain size.
			LSD34	688.00	696.00	Norite	Fine grained with 20% mica. Upper contact is gradational from norite.
		BMS	LSD34	696.00	716.00	Metasediment	Calcsilicate. Interlayers of fine grained pyroxenite with chilled margins dip at 25°-40°. 3 cm rounded norite inclusion. Sparse BMS occurs in pyroxenitic layers. Gradational basal contact.
			LSD34	716.00	733.00	Quartz Gabbro	60% plagioclase, 15% mica, minor opx. Sharp basal contact.
			LSD34	733.00	735.00	Metasediment	Calcsilicate.
		BMS	LSD34	735.00	741.00	Quartz Gabbro	60% plagioclase, 15% mica, minor opx, acicular texture. Trace BMS is sporadic.
			LSD34	741.00	743.00	Metasediment	
			LSD34	743.00	760.00	Quartz Gabbro	metasediment and gabbronorite mixed interlayers to end of hole.

Appendix 1B - LSD22 Borehole Log

Magnetite	Chromite	BMS	BH ID	FROM	TO	LITHOLOGY	DESCRIPTION
			LSD22	0.00	15.00	Gabbro	Coarse 2mm plagioclase with minor orthopyroxene
			LSD22	15.00	135.00	Gabbro	Mottled texture. Clinopyroxene clusters give mottled appearance. 2 mm laths of plagioclase chadocrysts in clinopyroxene oikicrysts, minor orthopyroxene.
			LSD22	135.00	180.00	Gabbronorite	Medium grained, occasional fractures dip at 70°.
			LSD22	180.00	215.00	Gabbro	Mottled texture. Gradual increase in orthopyroxene with depth. Sub vertical fracture veins towards base.
		BMS	LSD22	215.00	225.00	Anorthosite	Mottled texture. Trace Base Metal Sulphides (BMS)
			LSD22	225.00	244.00	Cyclic Unit	Norite-Anorthosite minor cyclic units of Norite 2-3 cm width
	Chromite		LSD22	244.00	285.00	Cyclic Unit	Anorthosite-Norite-Pyroxenite cyclic units with BMS and plagioclase in pyroxenite increasing with depth. Irregular chromite blebs in pyroxenite towards base.
Mag		BMS	LSD22	285.00	289.00	Pyroxenite	Dense magnetite veining occur within a varied textured pyroxenite. Marked increase in BMS in association with magnetite.
		BMS	LSD22	289.00	305.00	Feldspathic Pyroxenite	Decrease in plagioclase and BMS with depth
Mag		BMS	LSD22	305.00	329.00	Feldspathic Pyroxenite	Magnetite stringers and veins. BMS decrease with depth.
Mag		BMS	LSD22	329.00	356.00	Pyroxenite	Magnetite stringers and veins. Trace BMS and mica.
Mag	Chromite	BMS	LSD22	356.00	380.00	Feldspathic Pyroxenite	Chromitite vein at 360.50 m with chromite blebs and stringers between 364 m-368 m and disseminated magnetite and BMS throughout.
Mag	Chromite		LSD22	380.00	433.50	Feldspathic Pyroxenite	Phenocrysts of clinopyroxene, abundant fractures with random orientation. 3 cm magnetite vein at 414 m.
Mag	Chromite		LSD22	433.50	455.00	Pyroxenite	Calcsilicate xenolith. Irregular blebs of chromite and magnetite.
Mag			LSD22	455.00	470.00	Feldspathic Pyroxenite	Magnetite stringers and gradual increase in plagioclase with depth.
			LSD22	470.00	474.00	Norite	Xenoliths of pyroxenite as rounded blebs with cumulus plagioclase in medium grained leuconorite.
Mag			LSD22	474.00	495.00	Feldspathic Pyroxenite	Magnetite as stringers and blebs. Varying grain size of pyroxenes and varying feldspar content. Phenocrysts of cpx.
Mag			LSD22	495.00	502.00	Mixed Zone	Magnetite stringers and xenoliths of pyroxenite in a varying feldspathic pyroxenite.
			LSD22	502.00	504.00	Norite	Mottled and spotted leuconorite with increasing opx content with depth. Sharp contact at base.
	Chromite		LSD22	504.00	529.00	Feldspathic Pyroxenite	Grain size and feldspar content vary sporadically. Chromite bleb at 524 m.
			LSD22	529.00	545.00	Norite	Mottled and spotted with rimmed opx. Gradational change into mixed zone with chlorite alteration. 1-5% mica.
Mag		BMS	LSD22	545.00	586.00	Feldspathic Pyroxenite	Disseminated and blebby BMS throughout. Medium to fine grained with magnetite stringers and moderate alteration of pyroxenes.

Appendix 1B - LSD22 Borehole Log continued

Magnetite	Chromite	BMS	BH ID	FROM	TO	LITHOLOGY	DESCRIPTION
		BMS	LSD22	586.00	593.00	Hornfels	Blebby BMS throughout. Fine grained with abundant fluid veining. 5-10% mica. Sharp basal contact.
		BMS	LSD22	593.00	601.00	Feldspathic Pyroxenite	Medium grained with varying feldspar content. 5-7% mica and no BMS.
		BMS	LSD22	601.00	603.00	Hornfels	Fine grained dark grey with disseminated BMS throughout.
			LSD22	603.00	606.00	Pyroxenite	Medium grained.
		BMS	LSD22	606.00	614.00	Hornfels	Xenoliths of feldspathic pyroxenite in mixed zone at top of unit. BMS is disseminated
		BMS	LSD22	614.00	618.00	Graphite	Minor BMS in mixed zones.
			LSD22	618.00	680.00	Norite	Fine grained with >20% mica. Vertical fractures are common.

Appendix 1C- LPR6/12 Borehole Log

Magnetite	Chromite	BMS	BH ID	FROM	TO	LITHOLOGY	DESCRIPTION
			LPR6/12	0.00	24.00	Gabbronorite	Mottled texture. Decreasing plagioclase with depth. 5 mm chlorite/amphibole. 3 mm cpx.
			LPR6/12	24.00	33.50	Gabbronorite	Spotted and mottled with decreasing plagioclase content with depth, no mica.
Mag			LPR6/12	33.50	34.50	Feldspathic Pyroxenite	Magnetite stringers
			LPR6/12	34.50	35.20	Quartz Vein	
		BMS	LPR6/12	35.20	35.40	Feldspathic Pyroxenite	Pegmatitic, 2.5-1 cm blebs of chalcopyrite and pentlandite. Gradational contact.
			LPR6/12	35.40	40.00	Norite	Mottled and spotted.
		BMS	LPR6/12	40.00	45.00	Feldspathic Pyroxenite	Fine grained with minor disseminated BMS.
		BMS	LPR6/12	45.00	46.00	Norite	Mottled and spotted with blebby BMS at upper contact.
Mag			LPR6/12	46.00	50.00	Feldspathic Pyroxenite	Magnetite stringers and decreasing feldspar content with depth. Norite xenolith.
			LPR6/12	50.00	57.00	Pyroxenite	Acicular texture at 45° trend to core axis. Cpx oikocryts give spotted appearance.
Mag			LPR6/12	57.00	63.00	Pyroxenite	Orthopyroxenite with sugary texture. Magnetite stringers for 1.3 m with increased feldspar content and grain size with increasing magnetite.
Mag			LPR6/12	63.00	65.00	Pyroxenite	Textures obscured by magnetite stringers. Heavily fractured with gradual contact at base.
			LPR6/12	65.00	67.00	Norite	Spotted texture. Contact dips at 60°.
	Chromite		LPR6/12	67.00	72.00	Pyroxenite	1.5 cm rounded chromite bleb. Medium grained norite intermixed with pyroxenite.
Mag			LPR6/12	72.00	79.00	Pyroxenite	Fine grained with acicular texture. circa 2 cm micas give spotted appearance. One bleb of magnetite.
			LPR6/12	79.00	79.50	Quartz Vein	Slight increase in grain size in lithologies above and below.
Mag			LPR6/12	79.50	92.00	Pyroxenite	Spotted by mica and acicular texture. Cpx dominant-diopside? Magnetite stringers surround coarse grained pyroxenite towards base with some serpentinisation.
Mag			LPR6/12	92.00	106.00	Pyroxenite	Varying gran size from fine to medium with magnetite abundant in areas of increased grain size
			LPR6/12	106.00	108.00	Pyroxenite	
			LPR6/12	108.00	112.00	Pyroxenite	Pegmatitic texture with serpentinite and quartz veining
Mag	Chromite		LPR6/12	112.00	124.00	Pyroxenite	Altered with sugary texture. Predominantly opx with minor amphibole. Sporadic rounded chromite blebs . Chlorite veins common. Magnetite stringers towards base dip at 78°.
Mag			LPR6/12	124.00	127.00	Magnetite	Dense stringers obscuring any original texture.

Appendix 1C- LPR6/12 Borehole Log continued

Magnetite	Chromite	BMS	BH ID	FROM	TO	LITHOLOGY	DESCRIPTION
	Chromite		LPR6/12	127.00	140.00	Pyroxenite	Fine grained with minor alteration and sporadic chromite blebs. Chlorite veins dip at 60°. <5% interlocking plagioclase. Basal contact is intermixed and dips at 75°.
			LPR6/12	140.00	144.00	Norite	Leuconorite with pyroxene xenoliths? 80% plagioclase fine grained with minor alteration.
			LPR6/12	144.00	149.00	Pyroxenite	Fine grained with 15% mica giving spotted appearance. Minor alteration and acicular texture with vertical orientation.
	Chromite		LPR6/12	149.00	164.50	Norite	Spotted texture. Sporadic chromite blebs. Gradual increase in elongate opx giving acicular texture at 45°. 2 minor interlayers of gabbro norite approx 40 cm thick. 14 cm calcsilcate dips at 65°.
			LPR6/12	164.50	165.00	Mixed	Highly altered pyroxenite grades into feldspathic pyroxenite with coarse graned norite at base.
		BMS	LPR6/12	165.00	167.50	Norite	Mottled. medium grained. 15% mica. Minor disseminated BMS.
		BMS	LPR6/12	167.50	168.00	Pyroxenite	Coarse grained with BMS blebs. Contacts dip at 80°.
			LPR6/12	168.00	178.00	Norite	Mottled. Decrease in plagioclase content and increase in cpx with depth. Pyroxene show rimming. Gradual basal contact.
			LPR6/12	178.00	181.80	Feldspathic Pyroxenite	
			LPR6/12	181.80	181.90	Norite	
Mag			LPR6/12	181.90	182.90	Magnetite	Dense stringers
Mag		BMS	LPR6/12	182.90	194.00	Olivine-bearing Feldspathic Pyroxenite	Olivine crystals are altered to magnetite. Densely mineralised with disseminated, blebby and often combined pentlandite, chalcopyrite and pyrrhotite.
		BMS	LPR6/12	194.00	195.50	Feldspathic Pyroxenite	Sparsely mineralised with disseminated BMS.
		BMS	LPR6/12	195.50	199.00	Olivine-bearing Feldspathic Pyroxenite	Heavily mineralised with blebby and disseminated BMS. Gradual basal contact.
		BMS	LPR6/12	199.00	199.25	Feldspathic Pyroxenite	Sparsely mineralised with disseminated BMS.
		BMS	LPR6/12	199.25	199.30	Gabbronorite	Sharp top and bottom contact dip at 20°. Sparsely mineralised with disseminated BMS.
		BMS	LPR6/12	199.30	199.50	Feldspathic Pyroxenite	Sparsely mineralised with disseminated BMS.
		BMS	LPR6/12	199.50	199.60	Taxitic Gabbronorite	Sharp top and bottom contact dip at 20°. Sparsely mineralised with disseminated BMS.
		BMS	LPR6/12	199.60	200.00	Feldspathic Pyroxenite	Sparsely mineralised with disseminated BMS.
		BMS	LPR6/12	200.00	200.20	Taxitic Gabbronorite	Sparsely mineralised with disseminated BMS.
		BMS	LPR6/12	200.20	200.90	Feldspathic Pyroxenite	Sparsely mineralised with disseminated BMS.
		BMS	LPR6/12	200.90	201.00	Olivine-bearing Feldspathic Pyroxenite	Sparsely mineralised with disseminated BMS.

Appendix 1C- LPR6/12 Borehole Log continued

Magnetite	Chromite	BMS	BH ID	FROM	TO	LITHOLOGY	DESCRIPTION
		BMS	LPR6/12	201.00	207.80	Feldspathic Pyroxenite	Disseminated sulphides throught out with sporadic multiphase blebs of sulphides.
		BMS	LPR6/12	207.80	208.10	Taxitic Gabbronorite	Sharp top and bottom contacts dipping at 50°. Sulphides are blebby and combined.
		BMS	LPR6/12	208.10	209.60	Olivine-bearing Feldspathic Pyroxenite	Sparsely mineralised with disseminated BMS.
		BMS	LPR6/12	209.60	210.15	Feldspathic Pyroxenite	Sparsely mineralised with disseminated BMS.
		BMS	LPR6/12	210.15	210.22	Taxitic Gabbronorite	Sharp top and bottom contact dipping at 50°. Sparsely mineralised with disseminated BMS.
		BMS	LPR6/12	210.22	210.35	Feldspathic Pyroxenite	Sparsely mineralised with disseminated BMS.
		BMS	LPR6/12	210.35	210.42	Taxitic Gabbronorite	Sharp top and bottom contacts dipping at 50°. Sparsely mineralised with disseminated BMS.
		BMS	LPR6/12	210.42	210.70	Feldspathic Pyroxenite	Sparsely mineralised with disseminated BMS.
		BMS	LPR6/12	210.70	211.15	Olivine-bearing Feldspathic Pyroxenite	Sparsely mineralised with disseminated BMS.
		BMS	LPR6/12	211.15	211.60	Feldspathic Pyroxenite	Sparsely mineralised with disseminated BMS.
		BMS	LPR6/12	211.60	211.63	Felsic Vein	Sharp top and bottom contacts dip at 70°.
		BMS	LPR6/12	211.63	213.30	Feldspathic Pyroxenite	Sparsely mineralised with disseminated BMS.
		BMS	LPR6/12	213.30	213.90	Taxitic Gabbronorite	Sparsely mineralised with disseminated BMS.
		BMS	LPR6/12	213.90	216.90	Feldspathic Pyroxenite	Sparsely mineralised with disseminated BMS.
		BMS	LPR6/12	216.90	217.20	Taxitic Gabbronorite	Sparsely mineralised with disseminated BMS.
		BMS	LPR6/12	217.20	217.70	Feldspathic Pyroxenite	Sparsely mineralised with disseminated BMS.
		BMS	LPR6/12	217.7	219.50	Taxitic Gabbronorite	Sparsely mineralised with disseminated BMS.
		BMS	LPR6/12	220.00	224.00	Mixed Zone	Gradual upper contact. Calcsilicate intermixed with heavily altered taxitic gabbronorite. Veining abundant. BMS becomes sparse at 221 m.
		BMS	LPR6/12	224.00	254.00	Hornfels	Abundant fractures occur at 70-90°. Disseminated BMS occurs at 240 m where calc-silicate vein cuts at 70°.

Appendix 1D - LPR8/15 Borehole Log

Magnetite	Chromite	BMS	BH ID	FROM	TO	LITHOLOGY	DESCRIPTION
			LPR8/15	0.00	32.52	Norite	Granular subhedral opx floating in plagioclase matrix, spotted appearance. Sparse chlorite fractures dip at 15°. Plagioclase content varies. Vertical margins of increased plagioclase and faint layering can be picked out dipping at 15°. Heavily fractured between 9.07-9.10 m and 9.22-9.26 m. Chlorite fractures and veining are sparse and also dip at 15°. 1 cm plagioclase vein at 14.60 m.
			LPR8/15	32.52	32.83	Norite	Leucocratic with minor chlorite alteration. Bottom contact is irregular and dips at ~50°.
			LPR8/15	32.83	33.42	Norite	Gradational bottom contact.
			LPR8/15	33.42	33.93	Gabbronorite	Coarse grained almost pegmatoidal, with gradational bottom contact.
			LPR8/15	33.93	34.47	Norite	Bottom contact is sharp and dips at 20°.
		BMS	LPR8/15	34.47	44.42	Gabbronorite	Coarse grained and 40% alteration of plagioclase gives a mesocratic appearance. BMS (0.5%) occur as combined and blebby (~0.5 cm) and are sparsely distributed. 3 cm plagioclase/quartz vein at 35.50 m. A fine-grained norite vein with a chilled margin occurs with a coarse grained vertical gabbronorite. Plagioclase has a glassy appearance towards base with acicular pyroxenes floating in matrix.
			LPR8/15	44.42	46.46	Gabbronorite	Plagioclase and pyroxenes are altered to dark amphiboles. Sharp basal contact dips at 50°.
			LPR8/15	46.46	99.00	Norite	Chilled margin at top of unit for 22 cm. Appears spotted with alteration of pyroxenes to dark green amphiboles/chlorite? Sparse chlorite fractures dip at 55°. Mottling occurs for 50 cm towards base where appearance is more of a mottled anorthosite. White massive plagioclase at base with glassy appearance at base for 48 cm.
			LPR8/15	99.00	102.57	Pyroxenite	Medium grained with 10% mica, an acicular texture and 20% alteration. Sharp basal contact dips at 40°.
			LPR8/15	102.57	102.82	Norite	Gradational bottom contact dips at 65°.
	Chromite		LPR8/15	102.82	104.97	Feldspathic Pyroxenite	Medium grained with an acicular texture. Chromite stringers occur between 103.29-103.35 m and 104.80-104.90 m .
			LPR8/15	104.97	106.76	Norite	40% alteration of pyroxenes. Gradational contact at base.
Mag			LPR8/15	106.76	111.66	Olivine Pyroxenite	Interlayers of norite 1-2 cm wide with sharp and undulose contacts occur. Zones with dense stringers of magnetite occur. Overall 50% alteration.
			LPR8/15	111.66	112.47	Pyroxenite	Feldspathic with minor norite interlayers.

Appendix 1D - LPR8/15 Borehole Log continued

Magnetite	Chromite	BMS	BH ID	FROM	TO	LITHOLOGY	DESCRIPTION
			LPR8/15	112.47	116.61	Olivine Pyroxenite	60% alteration with irregular interlayers of norite and unaltered feldspathic pyroxenite.
	Chromite		LPR8/15	116.61	117.03	Chromitite	Dense stringers of chromite with contacts dipping at 45°.
			LPR8/15	117.03	119.09	Pyroxenite	10-15% serpentinisation.
			LPR8/15	119.09	119.92	Serpentinite	Very fine grained with soapy feel. Dark green in colour and translucent, weakly magnetic.
			LPR8/15	119.92	123.22	Pyroxenite	10% alteration, serpentinisation.
		BMS	LPR8/15	123.22	125.96	Pyroxenite	Chromitite stringers at top and bottom contacts with sparse BMS in between.
			LPR8/15	125.96	132.36	Pyroxenite	Acicular texture with 20% alteration.
			LPR8/15	132.36	132.51	Fractured zone	Heavily fractured at 40°.
			LPR8/15	132.51	136.35	Norite	Interlayers of pyroxenite with sharp contacts dipping at 15°.
			LPR8/15	136.35	146.51	Norite	Irregular interlayer of pyroxenite at 140.30 m and pegmatoidal at 142.70 m for 30 cm. 40% alteration of pyroxenes in norite.
			LPR8/15	146.51	157.58	Pyroxenite	Medium grained with spotted appearance and acicular texture. Bottom contact is sharp but irregular. 60% alteration.
			LPR8/15	157.58	159.29	Norite	Medium grained equigranular with a gradational bottom contact.
			LPR8/15	159.29	160.70	Pyroxenite	Medium grained and equigranular with 50% alteration to chlorite. Gradational bottom contact.
	Chromite		LPR8/15	160.70	162.76	Pyroxenite	Medium grained and equigranular with 30% alteration to chlorite. 3 cm chromite bleb.
	Chromite		LPR8/15	162.76	163.56	Pyroxenite	Medium grained equigranular with 80% alteration to chlorite. Heavily fractured with irregular 4 cm chromite vein at 163.47 m.
			LPR8/15	163.56	166.46	Pyroxenite	Medium grained equigranular and orthopyroxene dominant. Occasional fractures.
			LPR8/15	166.46	167.56	Gabbronorite	Medium to coarse grained equigranular with 20% alteration and a gradational bottom contact.
			LPR8/15	167.56	169.53	Norite	Medium grained equigranular with irregular bottom contact.
	Chromite		LPR8/15	169.53	169.66	Chromitite	Very fine grained equigranular with irregular contacts.
			LPR8/15	169.66	170.90	Norite	Medium grained equigranular and orthopyroxene dominant with interstitial plagioclase.
			LPR8/15	170.90	170.96	Chromitite	Very fine grained equigranular with irregular contacts.
			LPR8/15	170.96	171.10	Norite	Medium grained equigranular with sharp but irregular contacts.

Appendix 1D - LPR8/15 Borehole Log continued

Magnetite	Chromite	BMS	BH ID	FROM	TO	LITHOLOGY	DESCRIPTION
	Chromite		LPR8/15	171.10	171.36	Norite	Medium grained with a varied texture. Chromite stringers throughout. Irregular bottom contact.
	Chromie		LPR8/15	171.36	172.69	Melanorite	Medium grained equigranular with interstitial plagioclase. Gradational bottom contact. 3 cm chromite bleb at 172.44 m
			LPR8/15	172.69	177.38	Pyroxenite	Olivine-bearing with acicular texture and interstitial plagioclase. 10% Mica and sharp bottom contact dipping at 55°.
Mag			LPR8/15	177.38	178.47	Norite	Medium grained equigranular with 20 % mica and occasional fractures. Bottom contact dips at 70°. 2 cm magnetite vein at base.
			LPR8/15	178.47	181.27	Pyroxenite	Medium grained equigranular with 10% mica. Acicular texture and a gradational bottom contact.
			LPR8/15	181.27	182.63	Norite	Medium grained with a spotted appearance and acicular texture. 30% alteration of interstitial plagioclase.
	Chromite		LPR8/15	182.63	182.69	Chromitite	Very fine grained equigranular with chromite stringers and irregular bottom contact.
	Chromite		LPR8/15	182.69	188.70	Norite	Medium grained equigranular with acicular texture. 10 cm chromite bleb at base.
			LPR8/15	188.70	189.78	Olivine-bearing Pyroxenite	Medium to coarse grained olivine bearing with interstitial feldspar. Irregular bottom contact.
			LPR8/15	189.78	190.97	Pyroxenite	Olivine-bearing fine grained with a varied texture. Coarse patches of norite at top contact dense stringers throughout. 70% alteration.
			LPR8/15	190.97	224.78	Norite	Leucocratic, medium grained, equigranular with chlorite alteration. Occasional 2 cm chlorite vein dips at 30°. Irregular increase in plagioclase. Sharp contact at base dips at 30°.
Mag			LPR8/15	224.78	231.42	Pyroxenite	Fine to medium grained with varied texture and serpentinite alteration. 80% alteration. Interlayers of fine grained norite. Heavily fractured between 228.46 m-228.67 m. Acicular texture in less altered zones. Magnetite vein at 226.19 m-226.24 m.
			LPR8/15	231.42	233.87	Norite	Leucocratic, medium grained, equigranular with irregular interlayers of fine grained norite and mica rich (~20%) pyroxenite.
Mag			LPR8/15	233.87	246.00	Pyroxenite	Medium grained with spotted appearance, acicular texture and serpentinite alteration. Magnetite stringers and weakly magnetic throughout. 70% alteration and heavily fractured between 246.77 m-247.00 m.
Mag			LPR8/15	246.00	247.67	Pyroxenite	Olivine-bearing fine grained with a varied texture. Dense magnetite stringers with zones of serpentinite. 90% alteration.
Mag			LPR8/15	247.67	254.90	Pyroxenite	Medium grained spotted appearance and acicular texture. Magnetite stringers and 40% alteration.

Appendix 1D - LPR8/15 Borehole Log continued

Magnetite	Chromite	BMS	BH ID	FROM	TO	LITHOLOGY	DESCRIPTION
Mag			LPR8/15	254.90	255.90	Pyroxenite	Fine grained with a varied texture. 90% serpentinisation.
			LPR8/15	255.90	267.76	Pyroxenite	Medium grained with spotted appearance and ~20% mica.. Occasional magnetite bleb and stringer. Occasional chlorite fractures.
			LPR8/15	267.76	268.88	Gabbronorite	Medium to coarse grained equigranular with 20% mica. Pyroxenes altered to amphiboles, clinopyroxene rich, with cumulus plagioclase. Chilled margins on units above and below.
			LPR8/15	268.88	269.73	Pyroxenite	Medium grained with spotted appearance and acicular texture. Bottom contact is sharp and dips at 55°.
			LPR8/15	269.73	270.05	Gabbronorite	Medium to coarse grained equigranular with minor saussuritisation of plagioclase. 20% mica and clinopyroxene dominant.
	Chromite	BMS	LPR8/15	270.05	277.19	Pyroxenite	Medium grained equigranular with 10% serpentinisation. Acicular texture. Chromite bleb at 273.47 m sulphide zone between 274.10-274.80 m
			LPR8/15	277.19	277.49	Pegmatoid	Very coaser grained pegmatoid. Clinopyroxene, feldspar and quartz are major constituent minerals.
			LPR8/15	277.49	279.97	Pyroxenite	Medium grained with acicular texture and spotted appearance. 20% mica with minor chlorite alteration. Gradational basal contact.
Mag			LPR8/15	279.97	280.80	Pyroxenite	Variable grain size and texture. 90% serpentinisation with dense magnetite stringers throughout.
Mag			LPR8/15	280.80	291.47	Pyroxenite	Medium grained equigranular with 15% mica. Acicular with spotted appearance. Magnetic in patches. Irregular bleb of norite at 286.64 m-286.87 m. Dense magnetite stringers at base.
			LPR8/15	291.47	292.33	Acid Intrusion	Medium grained with varible texture. 20 % mica, feldspar and quartz are major constiuents. Granitic vein. Basal contact is sharp and dips at 70°.
			LPR8/15	292.33	293.52	Chromitite	Very fine-grained equigranular. Irregular basal contact dips at 50°.
			LPR8/15	293.52	294.05	Acid Intrusion	Medium grained with varible texture. 20 % mica, feldspar and quartz are major constiuents. Granitic vein. Basal contact is sharp and dips at 45°.
			LPR8/15	294.05	294.51	Chromitite	Very fine grained equigranular with interlayers of pyroxenite.
			LPR8/15	294.51	307.13	Pyroxenite	Medium grained equigranular with interstitial feldspar. Spotted appearance and gradational basal contact.
Mag			LPR8/15	307.13	307.48	Olivine Pyroxenite	Medium to coarse grained olivine-bearing with interstitial feldspar. 60% alteration, weakly magnetic with gradational basal contact.
Mag			LPR8/15	307.48	307.67	Pyroxenite	Medium grained equigranular with 10% mica and minor serpentinisation. 8 cm serpentinite-magnetite alteration at base. Irregular basal contact.
		BMS	LPR8/15	307.67	307.88	Gabbronorite	Medium grained equigranular with minor saussuritisation. 0.05% BMS occur, fine and clustered. Pyroxenites above and below have chilled margin.

Appendix 1D - LPR8/15 Borehole Log continued

Magnetite	Chromite	BMS	BH ID	FROM	TO	LITHOLOGY	DESCRIPTION
			LPR8/15	307.88	309.50	Pyroxenite	Medium equigranular with interstitial plagioclase and 10% mica as 3 cm flakes. Gradational basal contact.
Mag			LPR8/15	309.50	309.97	Pyroxenite	Very fine grained banded texture with chlorite and serpentinite alteration. Leucocratic with 90% alteration. Magnetite occurs towards top of unit.
		BMS	LPR8/15	309.97	316.27	Pyroxenite	Medium grained spotted appearance with acicular texture. 15% mica and trace BMS at base. Gradational bottom contact.
Mag		BMS	LPR8/15	316.27	316.52	Pyroxenite	Very fine grained banded texture with serpentinisation. Magnetite occurs as bands of stringers and BMS are clustered in Magnetite layers. Bottom contact is irregular and gradual.
		BMS	LPR8/15	316.52	317.27	Pyroxenite	Medium grained equigranular with 15% mica. Acicular texture and sharp basal contact dipping at 65°. 0.05% BMS is fine and scattered.
			LPR8/15	317.27	317.35	Norite	Medium grained equigranular and leucocratic. Basal contact is sharp dipping at 40°.
			LPR8/15	317.35	317.61	Pyroxenite	Medium grained equigranular with 10% mica. ~1.5 cm rounded blebs of plagioclase occur. Basal contact is sharp dipping at 50°.
			LPR8/15	317.61	318.25	Pyroxenite	Medium to coarse grained equigranular with saussuritisation. 10% mica. Leucocratic grey translucent with 80% alteration.
	Chromite	BMS	LPR8/15	318.25	320.50	Pyroxenite	Medium grained equigranular and 20% mica. Varying degrees af alteration. ~1 cm chromite blebs occur sporadically. 5 cm plagioclase vein with coarse grained pyroxenes occurs at 319.27 m. 0.1% BMS are fine and scattered.
			LPR8/15	320.50	322.28	Norite	Medium grained with a varied texture. 5% mica with varying orthopyroxene content. Interlayered with a spotted pyroxenite.
			LPR8/15	322.28	323.98	Pyroxenite	Medium grained equigranular with interstitial plagioclase. Heavily serpentinised at 323.15 m for 10 cm.
		BMS	LPR8/15	323.98	324.27	Pyroxenite	Fine grained with a varied texture.10% mica and interlayers of coarse grained plagioclase. 0.1% BMS is fine and scattered.
		BMS	LPR8/15	324.27	337.04	Pyroxenite	Medium grained equigranular with 40% chlorite alteration. 10% mica and 1% BMS fine and clustered sporadically. Basal contact is marked by chlorite fracture.
		BMS	LPR8/15	341.82	344.90	Pyroxenite	Medium to coarse grained with varied texture. Acicular texture with 80% alteration. Heavily fractured. 4% BMS are blebby throughout unit.
			LPR8/15	344.90	346.50	Hornfels	Fine grained hornfels with altered interlayers of pyroxenite.
		BMS	LPR8/15	346.50	349.60	Feldspathic Pyroxenite	Sparse disseminated BMS.

Appendix 1D - LPR8/15 Borehole Log continued

Magnetite	Chromite	BMS	BH ID	FROM	TO	LITHOLOGY	DESCRIPTION
			LPR8/15	349.60	349.63	Chlorite	Chlorite parting dipping at 40°.
			LPR8/15	337.04	339.80	Pyroxenite	Medium grained with a varied texture. 80% Serpentinisation and dense chlorite fractures and veins. Basal contact is marked by fracture.
		BMS	LPR8/15	339.80	341.82	Pyroxenite	Medium grained with a varied texture. 20% mica and acicular texture with 0.1% fine clustered BMS. Bottom contact marked by increase in alteration.
		BMS	LPR8/15	349.63	361.50	Feldspathic Pyroxenite	Sparse disseminated BMS with ~20% biotite.
			LPR8/15	361.50	361.60	Taxitic Gabbronorite	Irregular top and bottom contacts.
		BMS	LPR8/15	361.60	366.20	Feldspathic Pyroxenite	Sparse disseminated BMS and ~20% biotite. Sulphides are blebby and combined towards the base.
		BMS	LPR8/15	366.20	366.78	Taxitic Gabbronorite	Sparse disseminated BMS.
		BMS	LPR8/15	366.78	368.20	Feldspathic Pyroxenite	Blebby combined and disseminated BMS.
		BMS	LPR8/15	368.20	372.80	Taxitic Gabbronorite	Sparse disseminated BMS.
		BMS	LPR8/15	372.80	373.60	Olivine-bearing Feldspathic Pyroxenite	Blebby combined BMS.
		BMS	LPR8/15	373.60	373.80	Taxitic Gabbronorite	Disseminated BMS with combined blebs towards the base.
		BMS	LPR8/15	373.80	374.60	Olivine-bearing Feldspathic Pyroxenite	Disseminated BMS.
		BMS	LPR8/15	374.60	378.10	Taxitic Gabbronorite	Sporadic scattered blebs of pentlandite, chalcopyrite and pyrrhotite often combined.
			LPR8/15	378.10	378.70	Calcsilicate	Taxitic gabbronorite and calcsilicate mixing heavily altered.
			LPR8/15	378.70	379.00	Taxitic Gabbronorite	Heavily altered.
		BMS	LPR8/15	379.00	379.50	Olivine-bearing Feldspathic Pyroxenite	Magnetite stringers dipping at 70°. Disseminated BMS.

Appendix 1D - LPR8/15 Borehole Log continued

Magnetite	Chromite	BMS	BH ID	FROM	TO	LITHOLOGY	DESCRIPTION
		BMS	LPR8/15	379.50	380.90	Feldspathic Pyroxenite	Disseminated BMS.
		BMS	LPR8/15	380.90	381.10	Taxitic Gabbronorite	Disseminated BMS.
		BMS	LPR8/15	381.10	382.65	Feldspathic Pyroxenite	Disseminated BMS.
		BMS	LPR8/15	382.65	382.80	Taxitic Gabbronorite	Disseminated BMS.
		BMS	LPR8/15	382.80	389.90	Feldspathic Pyroxenite	Heavily mineralised with blebby combined and disseminated pentlandite, chalcopyrite and pyrrhotite.
			LPR8/15	389.90	388.95	Micronorite	Very fine-grained equigranular light brown micronorite with sharp top and bottom contacts dipping at 30°.
		BMS	LPR8/15	388.95	389.90	Olivine-bearing Feldspathic Pyroxenite	Sparse BMS.
		BMS	LPR8/15	389.90	390.80	Feldspathic Pyroxenite	Sparse BMS.
			LPR8/15	390.80	391.10	Taxitic Gabbronorite	Quartz-bearing taxitic gabbronorite, medium to coarse.
			LPR8/15	391.10	391.60	Feldspathic Pyroxenite	Fine-grained with no BMS.
			LPR8/15	391.60	391.80	Micronorite	
			LPR8/15	391.80	392.50	Calcsilicate	
			LPR8/15	392.50	392.60	Hornfels	
			LPR8/15	392.60	394.10	Calcsilicate	
			LPR8/15	394.10	396.00	Micronorite	
			LPR8/15	396.00	409.05	Hornfels	Very fine grained equigranular melanocratic cordierite-hornfels with very fine sulphides. Sharp basal contact dips at 60°.
			LPR8/15	409.05	409.40	Calc-Silicate	Leucocratic equigranular very fine grained pale green chalky calcsilicate xenolith with irregular basal contact.
		BMS	LPR8/15	409.40	409.94	Meta-Sediment	Leucocratic very fine grained with a varied texture and irregular basal contact. Calcareous green/grey meta-sediment. 1% fine sulphides.
		BMS	LPR8/15	409.94	419.71	Hornfels	Very fine grained with a varied texture. Interlayered with calcsilicates. Mica-rich in hornfels with fine BMS and occasional bleb. Varying degrees of alteration.

Appendix 1D - LPR8/15 Borehole Log continued

Magnetite	Chromite	BMS	BH ID	FROM	TO	LITHOLOGY	DESCRIPTION
		BMS	LPR8/15	419.71	448.35	Micronorite	Fine grained equigranular melanocratic with 20% mica and trace BMS fine and scattered. Quartz vein at 421.20 m-421.45 m showing internal brecciation of norite. Interlayers of very fine-grained hornfels and heavily fractured zone between 424.00 m-426.50 m.
			LPR8/15	448.35	465.32	Meta-Sediment	Fine grained leucocratic with calc-silicate interlayers and norite. Banded appearance. Quartz vein at 455.50 m-460.40 m.
			LPR8/15	465.32	499.38	Hornfels	Very fine grained equigranular melanocratic cordierite-hornfels to end of hole.
					EOH		

Appendix 1E - LPR12/9 Borehole Log

Magnetite	Chromite	BMS	BH ID	FROM	TO	LITHOLOGY	DESCRIPTION
			LPR12/09	0.00	34.64	Pyroxenite	Medium grained, equigranular and intensely weathered. Broken core in weathered bed rock.
			LPR12/09	34.64	35.36	Pyroxenite	Dense magnetite stringers, saussuritisation, interstitial plagioclase with cumulate olivine.
			LPR12/09	35.36	36.85	Pyroxenite	Medium grained, equigranular with interstital plagioclase, cumulate orthopyroxene rich with elongate pyroxenes and minor interstital sulphides.
			LPR12/09	36.85	38.13	Pyroxenite	Fine to medium-grained, equigranular, with light grey saussuritised plagioclase, magnetite stringers associated with BMS. Serpentinite at base in an olivine bearing feldspathic pyroxenite.
			LPR12/09	38.13	41.52	Pyroxenite	Medium to coares-grained and equigranular. Cumulate olivine and orthopyroxene with interstitial quartz? Feldspar. Elongate pyroxenes and cumulate magnetite?
			LPR12/09	41.52	42.94	Calcsilicate	55 cm pyroxene xenolith with chlorite alteration at margins enclosed in calcsilicate.
Mag			LPR12/09	42.94	50.10	Pyroxenite	Varied texture and grain size with chlorite alteration, moderate fracturing, magnetite stringers and pegmatoidal patches.
			LPR12/09	50.10	67.95	Pyroxenite	Medium to coarse-grained, light green, quartz and clinopyroxene, orthopyroxene patches? Pegmatoidal pyroxene?
Mag			LPR12/09	67.95	78.40	Olivine-bearing Feldspathic Pyroxenite	Medium grained, equigranular with cumulate orthopyroxene and olivine, magnetite stringers, interstitial feldspar with suassuritisation and chlortie alteration. Cumulate magnetite??
Mag			LPR12/09	78.40	82.00	Pyroxenite	90% alteration to serpentinite with pegmatoidal patch and magnetite stringers towards base.
Mag			LPR12/09	82.00	92.20	Pyroxenite	Interstitial plagioclase, acicular texture (quenched?) with 15% mica and minor magnetite.
Mag		BMS	LPR12/09	92.20	114.00	Pyroxenite	Varible texture with minor magnetite stringers. Sparse BMS towards base.
Mag			LPR12/09	114.00	114.17	Magnetite	
Mag		BMS	LPR12/09	114.17	114.96	Pyroxenite	Acicular texture with sparse disseminated BMS.
Mag		BMS	LPR12/09	114.96	115.37	Magnetite	
			LPR12/09	115.37	116.88	Pyroxenite	
Mag			LPR12/09	119.56	119.72	Magnetite	
			LPR12/09	119.72	122.44	Pyroxenite	Increase in plagioclase content with medium to coarse grain size.
Mag			LPR12/09	122.44	122.84	Magnetite	
		BMS	LPR12/09	122.84	129.20	Pyroxenite	Disseminated BMS in clusters throughout.

Appendix 1E - LPR12/9 Borehole Log continued

Magnetite	Chromite	BMS	BH ID	FROM	TO	LITHOLOGY	DESCRIPTION
Mag			LPR12/09	129.20	129.30	Magnetite	
		BMS	LPR12/09	129.30	148.49	Pyroxenite	Light green alteration, mica rich giving spotted appearance. Minor disseminated BMS at 130.00 m.
		BMS	LPR12/09	148.49	157.45	Pyroxenite	Variable texture with minor disseminated BMS.
Mag			LPR12/09	157.45	160.00	Pyroxenite	Fine grained with saussuritisation magnetite stringers, heavily veined and fractured.
		BMS	LPR12/09	160.00	193.00	Pyroxenite	Medium grained with a variable texture and disseminated clusters of BMS
		BMS	LPR12/09	193.00	195.90	Pyroxenite	Heavily fractured with a decrease in plagioclase with depth and loss in sulphide content.
		BMS	LPR12/09	195.90	203.30	Pyroxenite	Variable texture with minor disseminated BMS.
		BMS	LPR12/09	203.30	215.50	Pyroxenite	Variable texture with sericitisation of plagioclase, mica rich and minor plagioclase veining. Sporadic magnetite stringers and fine disseminated BMS.
			LPR12/09	215.50	218.70	Taxitic Gabbronorite	
		BMS	LPR12/09	218.70	226.15	Pyroxenite	Scattered BMS throughout.
			LPR12/09	226.15	227.05	Taxitic Gabbronorite	
		BMS	LPR12/09	227.05	241.75	Feldspathic Pyroxenite	Disseminated and scattered BMS throughout.
			LPR12/09	241.75	242.15	Taxitic Gabbronorite	
		BMS	LPR12/09	242.15	246.78	Pyroxenite	Sparse disseminated BMS.
			LPR12/09	246.78	246.90	Quartz Vein	
			LPR12/09	246.90	261.78	Pyroxenite	Magnetite stringers at 253 m and 258.50 m.
		BMS	LPR12/09	261.78	262.58	Pyroxenite	Saussuritisation, decrease in BMS content.
		BMS	LPR12/09	262.58	274.64	Pyroxenite	Disseminated and blebby BMS throughout.
		BMS	LPR12/09	274.64	275.59	Taxitic Gabbronorite	Blebby sulphides.
		BMS	LPR12/09	275.59	293.00	Pyroxenite	Disseminated and blebby BMS throughout.
			LPR12/09	293.00	297.13	Hornfels	
			LPR12/09	297.13	301.47	Norite	
			LPR12/09	301.47	350.00	Hornfels	
					EOH		

Appendix 2 - Triangular diagrams for the classification and nomenclature of gabbroic rocks based on modal proportions of plagioclase (Plag), pyroxenes (Px), Olivine (Ol), clinopyroxene (Cpx) and Orthopyroxene (Opx) modified from Gillespie & Styles, (1999), (after Streckeisen, 1976).

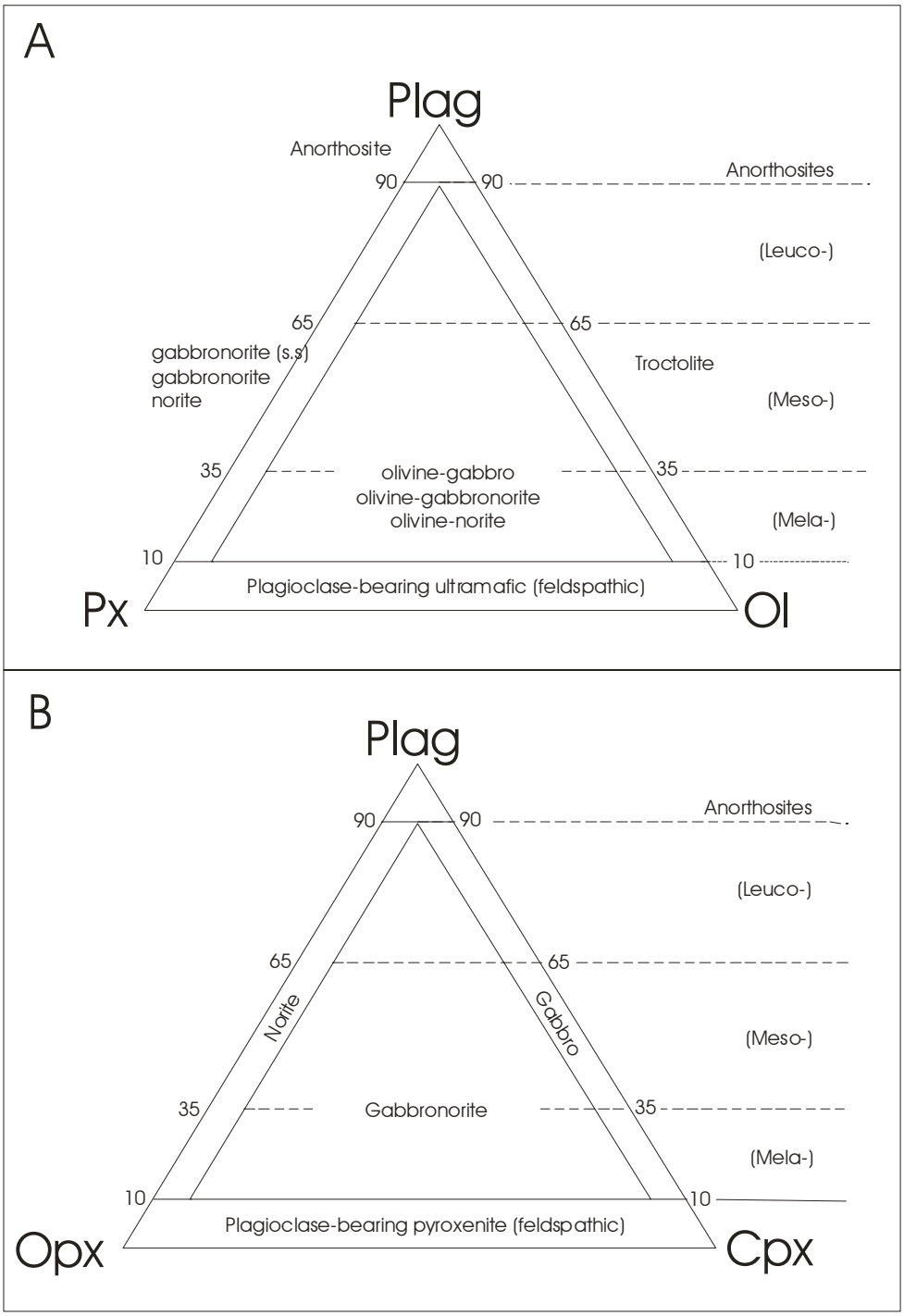

Appendix 3 – XRF Procedures and Standards

Major and trace element compositions of each sample were determined using X-ray fluorescence spectrometry. The samples were crushed and then milled to talcum-powder fineness. The crushing and milling instruments were pre-contaminated by each sample for each sample. Samples were milled in tungsten metal carbide swing mills. For trace element analyses pressed powder pellets were prepared from the sample powder combined with Mowiol glue and placed into aluminium cups. For major element analyses fusion discs were made using 1.28 g of sample with 1.5 g flux (a mixture of lithium tetraborate, lithium carbonate and lanthanum oxide) and sodium nitrate (an oxidising agent). Analyses were run in a PW 1400 XRF machine with a Rhodium X-ray tube at 50 kV and 50 mA at the University of the Witwatersrand, Johannesburg. Loss on ignition was measured by placing a known weight (typically ~ 10g) of sample in a dried crucible. The crucible was then placed in a furnace at 900˚C and left over night. The sample was cooled in a dessicator and re-weighed. The LOI was calculated as the weight loss relative to the original weight of the sample.

Standards used for major element analysis were NIM-P (pyroxenite), and NIM-G (granite) and standards for trace elements were NIM-D (dunite), NIM-N (norite).

Results of standard runs and analytical precision for major and trace element analysis are shown in the tables below

Appendix 3 – XRF Procedures and Standards continued

Results for standards during analyses of samples for this study on the PW 1400 XRF

		Run A					Run B				
Element	ppm / %	LLD (ppm)	NIM-D (ref)	NIM-D	NIM-P (ref)	NIM-P	LLD (ppm)	NIM G (ref)	NIM-G	NIM N (ref)	NIM-N
Rb	(ppm)	3	nd	2	4	5	3	325	320	5	5
Sr	(ppm)	3	3	6	32	37	3	10	11	260	259
Y	(ppm)	3	nd	2	5	5	3	143	143	7	10
Zr	(ppm)	8	8	11	15	21	8	300	288	14	12
Nb	(ppm)	3	nd	1	nd	1	3	53	55	nd	4
Co	(ppm)	6	208	213	110	114	6	nd	3	58	50
Ni	(ppm)	6	2040	2031	555	560	6	8	7	120	114
Cu	(ppm)	6	10	8	18	18	6	12	12	14	14
Zn	(ppm)	6	90	83	100	98	6	50	52	68	65
TiO2	(%)	12	0.02	0.04	0.20	0.23	0.10	0.09	0.12	0.20	0.19
V	(ppm)	12	40	39	230	216	12	2	3	220	211
Cr	(ppm)	20	2870	2895	23950	22009	12	12	9	30	28
Ba	(ppm)	9	10	11	46	59	20	120	125	102	104

	Run A				Run B	
Element	NIM P (ref)	NIM P	MA-N (ref)	MA-N	NIM P (ref)	NIM P
%SiO2	51.10	50.74	66.60	66.30	51.10	50.88
%TiO2	0.20	0.20	0.01	0.02	0.20	0.22
%Al2O3	4.18	4.13	17.62	17.84	4.18	3.99
%Fe2O3	12.70	12.66	0.47	0.40	12.70	12.76
%MnO	0.22	0.24	0.04	0.04	0.22	0.23
%MgO	25.33	25.43	0.04	0.12	25.33	25.46
%CaO	2.66	2.68	0.59	0.64	2.66	2.68
%Na2O	0.37	0.41	5.84	5.73	0.37	0.40
%K2O	0.09	0.10	3.18	3.13	0.09	0.06
%P2O5	0.02	0.03	1.39	1.42	0.02	0.03
%LOI	-0.84	-0.56	1.82	1.70	-0.84	-0.56
%TOTAL	96.03	96.06	97.60	97.34	96.03	96.15

Appendix 3 – XRF Procedures and Standards continued

Standards used for calibration of PW 1400 XRF for silicate analysis.

The X-Ray tube used is a Rhodium tube and is run at 50KV and 50 mA. The method used is from the paper "An accurate X-Ray spectrographic method for the analysis of a wide range of geological samples by K. Norrish and J.T. Hutton." Published in Geochimica et Cosmochimica Acta, 1969, Vol 33, pp. 431 to 453

Standard	%Fe2O3	%MnO	%TiO2	%CaO	%K2O	%P2O5	%SiO2	%Al2O3	%MgO	%Na2O	%LOI	%Total
NIM-G	2.02	0.02	0	0.79	5.03	0.01	76.31	12.18	0.06	3.39	0.45	100.42
NIM-S	1.41	0.01	0	0.68	15.4	0.12	63.85	17.4	0.46	0.43	0.28	99.7
NIM-N	8.96	0.18	0.2	11.49	0.25	0.03	52.57	16.48	7.49	2.46	-0.4	99.83
NIM-D	16.87	0.22	0.02	0.28	0.01	0.01	38.66	0.3	43.18	0.04	-0.93	99.42
NIM-P	12.77	0.22	0.2	2.67	0.09	0.02	51.39	4.2	25.47	0.37	-0.84	96.03
AN-G	3.39	0.04	0.22	16.03	0.13	0.01	46.67	30.04	1.81	1.64	0.65	99.84
AC-E	2.54	0.06	0.11	0.34	4.51	0.01	70.63	14.76	0.03	6.57	0.37	99.53
MA-N	0.47	0.04	0.01	0.59	3.19	1.4	66.86	17.69	0.04	5.86	1.82	97.6
AGV-2	6.69	0.1	1.05	5.2	2.88	0.48	59.3	16.91	1.79	4.19	1.59	100.18
FK-N	0.09	0.01	0.02	0.11	12.88	0.02	65.37	18.71	0.01	2.59	0.54	99.82
BHVO-2	12.3	0.17	2.73	11.4	0.52	0.27	49.9	13.5	7.23	2.22	-0.71	99.53
MICA-FE	25.65	0.35	2.5	0.43	8.75	0.45	34.4	19.5	4.55	0.3	2	98.88

Analytical precision for major element analysis.

The analysis is based on duplicate samples representing 5 calibrations.

Element	Standard deviation	Absolute % error	Relative Error - %	Standard Range %
Fe2O3	0.09	-0.03	-3.7	0.09 - 26.65
MnO	0.01	-0.009	4.8	0.01 - 0.35
TiO2	0.07	-0.04	13.7	0.00 - 2.69
CaO	0.04	0.003	0.2	0.11 - 16.03
K2O	0.07	0.005	-5.6	0.01 - 15.40
P2O5	0.02	-0.02	14.2	0.01 - 1.40
SiO2	0.36	0.06	-0.09	34.40 - 76.31
Al2O3	0.07	0.07	1.3	0.30 - 30.04
MgO	0.18	-0.05	-6.1	0.03 - 43.18
Na2O	0.13	-0.05	-6.8	0.04 - 6.57
LOI	0.26	-0.21	7.1	
Total	0.58	-0.18	0.2	

Appendix 3 – XRF Procedures and Standards continued

Standards used for calibration of PW 1400 XRF for trace element analysis.

Sample preparation: 6g Pellets + 6 drops 2% Mowiol solution, backed with an aluminum cup. Regression lines are calculated using SuperQ software with the De Jongh model for matrix correction (α-coefficients). We used a rhodium x-ray tube (4KW)

Standard	ppm Rb	ppm Sr	ppm Y	ppm Zr	ppm Nb	ppm Co	ppm Ni	ppm Cu	ppm Zn	% TIO2	ppm V	ppm Cr	ppm Ba
AGV-1	67	662	21	225	15	15	17	60	88	1.06	123	12	1221
GA	175	310	21	150	12	5	7	16	80	0.38	38	12	840
GH	390	10	75	150	85	1	3	14	85	0.08	5	6	20
G-2	170	478	11	300	13	5	5	11	85	0.49	36	9	1880
NIM-G	325	10	143	300	53	0	8	12	50	0	2	12	120
NIM-S	530	62	1	20	0	3	7	19	10	0	10	12	2420
NIM-P	4	32	5	15	0	110	555	18	100	0.2	230	23950	46
NIM-N	5	260	7	14	0	58	120	14	68	0.2	220	30	102
NIM-D	0	3	0	8	0	208	2040	10	90	0.02	40	2870	10
PCC-1	0	0	0	0	1	110	2400	10	42	0.01	30	2730	1
BR	47	1320	30	250	98	52	260	72	160	2.6	235	380	1050
BHVO-1	11	403	28	179	19	45	121	136	105	2.71	317	289	139
MAG-1	149	146	28	126	12	20	53	30	130	0.75	140	97	479
SGR-1	83	420	13	53	5	12	29	66	74	0.26	128	30	290
SCO-1	112	174	26	160	11	11	27	29	103	0.63	131	68	570
QLO-1	74	336	24	185	10	7	6	29	61	0.62	54	3	1370
STM-1	118	700	46	1210	268	1	3	5	235	0.14	9	4	560
RGM-1	149	108	25	219	9	2	4	12	32	0.27	13	4	807
SDC-1	127	183	40	290	18	18	38	30	103	1.01	102	64	630
DR-N	73	400	28	125	8	35	15	50	145	1.09	220	42	385
GS-N	185	570	19	235	21	65	34	20	48	0.68	65	55	1400
MICA-FE	2200	5	50	800	270	23	35	5	1300	2.5	135	90	150

Appendix 3 – XRF Procedures and Standards continued

Standards used for calibration of PW 1400 XRF for trace element analysis continued

Standard	ppm Rb	ppm Sr	ppm Y	ppm Zr	ppm Nb	ppm Co	ppm Ni	ppm Cu	ppm Zn	% TIO2	ppm V	ppm Cr	ppm Ba
MICA-MG	1300	27	0	20	120	24	110	4	290	1.63	90	100	4000
FK-N	860	39	0	13	0	16	3	2	10	0.02	3	5	200
BX-N	10	110	114	520	58	35	190	18	75	2.37	310	290	34
DT-N	5	27	10	370	0	12	16	9	28	1.4	150	240	130
UB-N	6	10	3	8	0	100	2000	28	85	0.11	75	2300	30
GXR-1	14	259	0	38	1	8	41	1110	760	0.06	76	13	680
GXR-2	78	160	17	269	11	9	21	76	530	0.5	52	36	2240
GXR-3	92	950	15	63	2	43	60	15	207	0.17	42	19	5000
GXR-4	160	221	14	186	10	15	42	6520	73	0.48	87	64	1640
Standard	ppm Rb	ppm Sr	ppm Y	ppm Zr	ppm Nb	ppm Co	ppm Ni	ppm Cu	ppm Zn	% TIO2	ppm V	ppm Cr	ppm Ba
GXR-6	90	35	14	110	8	14	27	66	118	0.83	186	96	1300
GSP-1	254	234	29	530	26	7	10	34	103	0.66	53	13	1310
MA-N	3600	84	1	27	173	1	3	140	220	0.01	5	3	42
AN-G	0	76	8	15	2	25	35	19	20	0.22	70	50	34

Analytical precision for trace element analysis.

The analysis represents 5 calibrations.

Element	LLD-ppm	Standard deviation	Absolute error-ppm	Relative Error - %
Rb	3	2	1	-1.9
Sr	3	2	1.3	0.4
Y	3	2	-0.7	-3.7
Zr	8	3	4.3	1.2
Nb	3	1	-2.4	-8.5
V	12	9	-3.8	-12.7
Cr	12	7	0.7	5.2
Co	6	2	0.7	-10.7
Ni	6	2	0.6	-9.3
Cu	6	5	1.9	-0.3
Zn	6	2	2.8	-6.2
Ba	20	7	12	3.1
Pb	10	2	3.1	-
As	15	2	4.7	-

Appendix 4A - LSD22 XRF Whole Rock Analyses

Sample Number	Rock Type	Depth (m) from top of borehole	%SiO2	%TiO2	%Al2O3	%Fe2O3	%MnO	%MgO	%CaO	Na2O	%K2O	%P2O5	%LOI	%total
LSD22/1	gabbro	137.00	52.29	0.26	19.70	5.77	0.10	6.82	11.43	2.46	0.32	0.04	0.22	99.41
LSD22/2	gabbro	182.50	50.37	0.46	18.38	6.92	0.19	3.56	14.12	2.15	0.53	0.45	1.65	98.78
LSD22/3	pyroxenite	313.20	47.36	0.20	4.23	10.78	0.19	23.91	8.33	0.37	0.04	0.03	3.85	99.29
LSD22/4	norite	544.00	50.16	0.32	20.20	6.25	0.14	5.80	12.46	2.75	0.29	0.16	0.22	98.75
LSD22/5	norite	666.00	41.03	0.69	12.14	9.95	0.42	3.33	22.24	1.21	0.17	1.02	6.59	98.79

Sample Number	Rock Type	Depth (m) from top of borehole	Rb	Sr	Y	Zr	Nb	Co	Ni	Cu	Zn	TiO2	V	Cr	Ba
LSD22/1	gabbro	137.00	18	267	36	80	8	21	69	29	59	0.24	87	206	131
LSD22/2	gabbro	182.50	8	66	14	26	4	67	572	62	83	0.45	99	158	70
LSD22/3	pyroxenite	313.20	14	342	16	44	5	26	121	39	48	0.18	97	1963	158
LSD22/4	norite	544.00	23	217	69	146	13	16	47	1	61	0.27	87	411	122
LSD22/5	norite	666.00	23	218	69	146	14	16	45	1	61	0.77	97	94	127

Appendix 4B - LSD34 XRF Whole Rock Analyses

Sample Number	Rock Type	Depth (m) from top of borehole	%SiO2	%TiO2	%Al2O3	%Fe2O3	%MnO	%MgO	%CaO	Na2O	%K2O	%P2O5	%LOI	%Total
LSD34/139	gabbro	139.00	52.15	0.26	20.22	6.26	0.10	4.93	11.47	2.93	0.38	0.07	0.51	99.28
LSD34/159	gabbro	159.00	51.32	0.36	18.92	6.95	0.11	7.15	10.01	3.02	0.38	0.05	0.45	98.72
LSD34/191	anorthosite	191.00	52.08	0.36	20.55	5.39	0.10	5.23	11.25	2.75	0.46	0.07	0.52	98.76
LSD34/199.5	gabbro	199.50	53.33	0.41	16.89	6.23	0.11	7.47	11.58	1.91	0.48	0.06	1.07	99.54
LSD34/213	gabbronorite	213.00	52.63	0.22	12.72	8.44	0.15	15.11	8.30	1.61	0.07	0.03	0.04	99.32
LSD34/233.5	gabbro	233.50	51.69	0.25	18.74	5.43	0.12	8.81	9.89	1.83	0.32	0.10	1.47	98.65
LSD34/253.5	gabbro	253.50	55.93	0.32	6.14	11.07	0.20	19.25	4.13	0.41	0.31	0.03	1.56	99.35
LSD34 336.00	feldspathic pyroxenite	336.00	53.26	0.23	6.35	10.52	0.22	23.22	4.86	0.98	0.24	0.02	0.63	100.53
LSD34 342.00	pegmatoidal pyroxenite	342.00	37.65	0.11	3.94	3.21	0.13	27.72	14.91	0.00	0.00	0.01	12.26	99.94
LSD34 345.00	feldspathic pyroxenite	345.00	53.00	0.23	5.23	10.81	0.21	24.10	4.11	0.80	0.08	0.04	0.12	98.73
LSD34 402.00	feldspathic pyroxenite	402.00	52.83	0.26	5.63	8.05	0.18	16.96	14.60	0.98	0.19	0.04	0.60	100.32
LSD34 447.00	norite	447.00	49.33	0.14	16.77	9.19	0.17	13.47	9.53	1.60	0.00	0.02	-0.17	100.05
LSD34 447.50	norite	447.50	52.04	0.18	15.45	8.46	0.17	11.23	10.31	0.97	0.16	0.04	0.08	99.09
LSD34 449.50	norite	449.50	49.32	0.15	15.91	9.42	0.16	13.71	9.08	1.02	0.00	0.03	-0.15	98.65
LSD34 483.50	norite	483.50	50.89	0.19	22.40	5.50	0.10	6.74	11.61	2.48	0.18	0.03	0.27	100.39
LSD34 489.00	norite	489.00	51.35	0.20	21.89	5.47	0.10	6.81	11.70	2.48	0.16	0.04	0.15	100.35
LSD34 526.00	pyroxenite	526.00	52.54	0.29	6.27	10.80	0.21	21.77	6.44	0.97	0.41	0.04	0.70	100.44
LSD34 527.50	pyroxenite	527.50	52.87	0.25	6.41	11.56	0.21	22.53	5.44	0.93	0.12	0.05	0.11	100.48
LSD34 581.00	feldspathic pyroxenite	581.00	50.55	0.29	20.06	6.51	0.11	8.51	10.94	2.20	0.42	0.06	0.58	100.23
LSD34 593.50	feldspathic pyroxenite	593.50	53.00	0.29	7.47	11.66	0.21	20.85	5.40	1.16	0.05	0.04	-0.07	100.06
LSD34 616.50	norite	616.50	52.52	0.36	15.86	9.27	0.16	9.61	9.71	2.19	0.43	0.06	0.12	100.29
LSD34 618.50	norite	618.50	50.86	0.31	15.01	8.93	0.15	9.32	11.27	1.93	0.56	0.04	0.86	99.24
LSD34/1	feldspathic pyroxenite	630.20	52.43	0.32	9.15	11.45	0.21	16.05	6.72	1.51	0.31	0.05	0.50	98.70
LSD34/2	feldspathic pyroxenite	631.66	51.18	0.26	8.03	9.99	0.18	14.83	10.98	0.83	0.07	0.04	2.22	98.61
LSD34/3	pyroxenite	635.00	53.63	0.35	8.96	10.11	0.17	16.33	6.02	1.26	0.50	0.07	1.30	98.70
LSD34/4	pyroxenite	638.30	45.09	0.25	6.67	11.23	0.18	22.62	10.58	0.49	0.13	0.04	3.09	100.37
LSD34/5	pyroxenite	640.76	49.04	0.22	7.24	12.12	0.18	22.71	4.77	0.66	0.17	0.05	2.14	99.30
LSD34/6	pyroxenite	645.00	51.72	0.38	7.96	11.66	0.20	19.55	5.91	1.31	0.57	0.07	0.52	99.85
LSD34/7	pyroxenite	649.00	53.03	0.30	5.95	12.97	0.19	20.14	4.62	0.99	0.27	0.04	0.63	99.13
LSD34/8	pyroxenite	651.15	54.38	0.32	5.48	11.69	0.19	20.81	4.76	1.20	0.19	0.05	0.24	99.31
LSD34/9	pyroxenite	654.70	54.28	0.35	5.56	11.88	0.19	20.53	5.15	1.13	0.19	0.05	-0.02	99.29
LSD34/10	pyroxenite	659.50	50.79	0.27	15.24	7.63	0.12	10.82	9.96	1.64	0.63	0.04	2.62	99.76
LSD34/11	pyroxenite	660.93	49.05	0.29	12.87	10.70	0.16	12.69	8.69	1.38	0.69	0.04	2.47	99.03
LSD34/12	pyroxenite	664.91	50.60	0.26	9.00	13.53	0.21	17.65	6.15	1.02	0.16	0.05	0.64	99.27
LSD34/13	pyroxenite	669.47	49.67	0.35	15.22	10.47	0.13	9.00	9.73	1.35	0.68	0.04	2.37	99.01
LSD34/14	norite	671.15	48.68	0.33	11.35	13.87	0.18	12.80	7.63	1.00	1.02	0.06	2.02	98.94
LSD34/15	norite	673.92	52.55	0.58	9.96	9.27	0.18	8.72	11.98	2.22	0.88	0.03	2.20	98.57
LSD34/16	pyroxenite	680.80	53.78	0.55	8.24	14.53	0.23	9.66	9.87	1.69	0.54	0.05	0.10	99.24
LSD34/17	norite	692.72	52.74	0.35	9.18	11.41	0.20	17.33	6.68	1.26	0.41	0.06	0.83	100.45

Appendix 4B - LSD34 XRF Whole Rock Analyses continued

Sample Number	Rock Type	Depth (m) from top of borehole	%SiO2	%TiO2	%Al2O3	%Fe2O3	%MnO	%MgO	%CaO	Na2O	%K2O	%P2O5	%LOI	%Total
LSD34/18	meta-sediment	699.50	53.95	0.29	7.88	10.54	0.19	18.28	5.14	0.92	0.39	0.07	1.01	98.66
LSD34/19	meta-sediment	704.28	66.45	0.95	13.46	7.22	0.09	2.82	3.14	2.84	0.92	0.11	1.02	99.02
LSD34/21	gabbro	719.00	53.76	0.47	13.74	10.51	0.18	8.15	8.90	1.36	0.94	0.10	1.05	99.16
LSD34/22	gabbro	720.56	54.64	0.33	13.24	10.36	0.18	9.34	7.63	1.65	1.00	0.09	1.90	100.36

Appendix 4B - LSD34 XRF Whole Rock Analyses continued

Sample Number	Rock Type	Depth (m) from top of borehole	Rb	Sr	Y	Zr	Nb	Co	Ni	Cu	Zn	TiO2	V	Cr	Ba
LSD34/139	gabbro	139.00	15	319	18	54	5	20	62	52	58	0.26	112	185	181
LSD34/159	gabbro	159.00	21	288	20	59	5	21	67	33	49	0.35	87	117	181
LSD34/191	anorthosite	191.00	23	224	22	71	7	26	197	40	51	0.37	100	157	167
LSD34/199.5	gabbro	199.50	9	180	15	30	4	47	333	24	62	0.41	152	662	94
LSD34/213	gabbronorite	213.00	19	246	14	34	5	32	198	22	47	0.22	91	1693	109
LSD34/233.5	gabbro	233.50	21	59	16	28	4	69	842	51	81	0.21	74	921	96
LSD34/253.5	gabbro	253.50	15	294	16	43	5	22	107	21	41	0.27	127	2567	121
LSD34 336.00	feldspathic pyroxenite	336.00	12	95	9	14	5	62	528	17	88	0.26	117	3107	163
LSD34 342.00	pegmatoidal pyroxenite	342.00	1	11	9	<8	4	14	63	9	50	0.08	<12	109	<20
LSD34 345.00	feldspathic pyroxenite	345.00	9	92	10	6	5	74	669	54	86	0.25	129	2865	188
LSD34 402.00	feldspathic pyroxenite	402.00	12	103	13	19	5	50	430	63	57	0.26	160	1591	181
LSD34 447.00	norite	447.00	10	241	10	13	4	46	228	27	67	0.16	92	788	160
LSD34 447.50	norite	447.50	5	251	7	<8	4	54	290	9	61	0.12	68	450	77
LSD34 449.50	norite	449.50	5	257	6	<8	4	51	301	10	58	0.13	63	713	76
LSD34 483.50	norite	483.50	8	351	8	18	5	26	128	20	45	0.17	66	377	129
LSD34 489.00	norite	489.00	7	350	9	18	5	25	130	19	45	0.18	64	387	134
LSD34 526.00	pyroxenite	526.00	22	89	11	13	5	64	556	56	87	0.32	131	2654	161
LSD34 527.50	pyroxenite	527.50	10	106	11	13	5	72	685	128	87	0.29	120	2571	165
LSD34 581.00	feldspathic pyroxenite	581.00	20	302	11	31	6	29	201	50	51	0.28	83	1423	178
LSD34 593.50	feldspathic pyroxenite	593.50	9	108	11	19	5	76	573	82	87	0.32	161	5952	124
LSD34 616.50	norite	616.50	21	277	15	32	7	44	189	36	71	0.36	114	593	224
LSD34 618.50	norite	618.50	32	229	13	34	6	40	172	30	65	0.31	107	547	202
LSD34/1	feldspathic pyroxenite	630.20	20	142	19	45	5	63	388	72	82	0.33	151	1704	160
LSD34/2	feldspathic pyroxenite	631.66	11	77	18	35	3	67	562	532	71	0.28	174	2881	85
LSD34/3	pyroxenite	635.00	30	113	19	70	6	61	440	32	80	0.38	155	1855	229
LSD34/4	pyroxenite	638.30	13	84	18	36	5	59	567	120	94	0.25	90	2212	115
LSD34/5	pyroxenite	640.76	13	97	14	31	4	110	2227	954	123	0.22	96	2502	120
LSD34/6	pyroxenite	645.00	18	79	17	38	5	129	4290	2697	100	0.43	152	6728	174
LSD34/7	pyroxenite	649.00	16	78	18	46	5	87	1763	899	85	0.32	128	2509	146
LSD34/8	pyroxenite	651.15	14	79	19	47	5	74	566	234	94	0.35	139	2434	143
LSD34/9	pyroxenite	654.70	50	186	16	54	4	63	1093	393	83	0.36	159	2225	128
LSD34/10	pyroxenite	659.50	48	143	17	33	5	108	1229	678	79	0.28	176	778	128
LSD34/11	pyroxenite	660.93	19	120	16	30	4	116	312	305	94	0.29	300	589	108
LSD34/12	pyroxenite	664.91	58	182	18	35	5	132	1094	379	67	0.27	402	604	159
LSD34/13	pyroxenite	669.47	82	152	17	46	5	107	487	3699	98	0.37	256	492	184
LSD34/14	norite	671.15	68	130	19	109	9	46	379	443	79	0.32	355	540	180
LSD34/15	norite	673.92	41	138	27	50	6	65	196	60	82	0.61	226	423	168
LSD34/16	pyroxenite	680.80	30	136	19	70	6	53	529	47	103	0.62	381	442	227
LSD34/17	norite	692.72	34	124	17	62	6	66	678	26	87	0.4	170	1952	255

Appendix 4B - LSD34 XRF Whole Rock Analyses continued

Sample Number	Rock Type	Depth (m) from top of borehole	Rb	Sr	Y	Zr	Nb	Co	Ni	Cu	Zn	TiO2	V	Cr	Ba
LSD34/18	meta-sediment	699.50	63	155	37	265	17	16	56	10	85	0.31	153	2687	338
LSD34/19	meta-sediment	704.28	60	174	24	78	7	42	179	45	106	1.01	118	93	294
LSD34/21	gabbro	719.00	72	136	22	50	6	35	161	30	102	0.54	213	550	210
LSD34/22	gabbro	720.56	16	290	19	58	5	23	74	38	58	0.34	182	624	178

Appendix 4C - LPR6/12 XRF Whole Rock Analyses

Sample Number	Rock Type	Depth (m) from top of borehole	%SiO2	%TiO2	%Al2O3	%Fe2O3	%MnO	%MgO	%CaO	Na2O	%K2O	%P2O5	%LOI	%Total
LPR6/12 32.00	leuco-norite	32.00	50.09	0.21	22.96	4.88	0.09	6.12	11.44	2.50	0.25	0.05	1.28	99.87
LPR6/12-1	calc-silicate	33.40	53.40	0.37	8.78	7.40	0.18	8.44	17.47	0.39	0.27	1.29	0.78	98.77
LPR6/12-2	calc-silicate	42.14	53.23	0.22	3.93	14.65	0.19	11.68	11.97	0.56	0.05	0.16	2.68	99.32
LPR6/12 75.00	altered pyroxenite	75.00	49.75	0.20	5.62	11.13	0.20	25.37	4.64	0.72	0.39	0.04	1.07	99.13
LPR6/12-3	pyroxenite	86.87	53.55	0.26	5.85	11.18	0.20	22.55	4.18	0.97	0.12	0.04	0.09	98.99
LPR6/12 105.50	pyroxenite	105.50	50.20	0.25	7.99	12.69	0.20	18.16	7.56	0.54	0.81	0.05	1.89	100.34
LPR6/12 119.50	altered pyroxenite	119.50	52.42	0.28	8.36	10.47	0.19	20.50	6.25	1.04	0.36	0.10	0.25	100.22
LPR6/12-4	mela-norite	138.08	53.97	0.27	6.45	10.27	0.20	21.46	5.12	0.75	0.34	0.05	0.34	99.22
LPR6/12 149.00	mela-norite	149.00	51.14	0.26	12.59	8.86	0.10	15.66	7.78	3.56	0.21	0.05	0.31	100.52
LPR6/12 156.00	pyroxenite	156.00	51.83	0.31	14.76	8.24	0.16	13.68	8.40	1.49	0.38	0.06	0.77	100.08
LPR6/12 171.50	leuco-norite	171.50	50.78	0.25	25.32	3.90	0.07	2.67	12.69	2.88	0.40	0.05	0.99	100.00
LPR6/12 175.50	leuco-norite	175.50	50.82	0.24	25.71	3.69	0.06	2.71	12.49	2.86	0.52	0.06	1.28	100.44
LPR6/12-5	norite pyroxenite	178.64	53.81	0.30	7.76	11.44	0.21	18.67	5.88	0.67	0.16	0.05	0.10	99.05
LPR6/12-6	altered pyroxenite	184.00	48.61	0.41	7.37	12.81	0.23	17.66	8.47	0.59	0.41	0.07	3.82	100.45
LPR6/12-8	altered pyroxenite	185.00	47.31	0.32	5.68	12.11	0.20	18.19	10.20	0.71	1.04	0.10	3.51	99.37
LPR6/12-9	pegmatoidal pyroxenite	185.50	50.63	0.34	5.74	11.50	0.20	19.65	6.49	0.78	1.30	0.06	2.51	99.20
LPR6/12-12	pyroxenite	187.00	52.21	0.23	7.68	11.45	0.19	19.13	6.85	1.09	0.07	0.04	0.51	99.45
LPR6/12-16	altered pyroxenite	189.00	55.27	0.30	5.41	8.86	0.15	13.00	12.89	0.55	1.26	0.07	2.05	99.81
LPR6/12-19	mag pyroxenite	190.50	45.65	0.37	5.34	13.91	0.23	19.88	10.32	2.64	0.19	0.06	1.69	100.28
LPR6/12-22	pyroxenite	192.00	52.91	0.19	6.22	11.18	0.17	19.88	6.19	0.44	0.55	0.03	2.00	99.76
LPR6/12-25	pyroxenite	193.50	50.33	0.20	7.02	12.43	0.20	20.76	5.91	0.63	0.11	0.03	1.16	98.78
LPR6/12-26	pyroxenite	194.00	50.32	0.21	6.88	12.15	0.20	20.19	6.27	1.70	0.08	0.03	0.88	98.91
LPR6/12-28	pyroxenite	195.00	51.46	0.33	5.31	12.35	0.25	21.82	5.24	2.29	0.23	0.04	0.40	99.72
LPR6/12-29	mag pyroxenite	195.50	49.61	0.21	5.28	13.88	0.21	23.31	4.88	1.34	0.01	0.03	0.77	99.53
LPR6/12-31	altered pyroxenite	196.50	50.69	0.57	11.30	11.22	0.44	5.11	17.89	0.93	0.45	0.47	1.41	100.48
LPR6/12-32	mag pyroxenite	197.00	48.99	0.20	5.79	14.18	0.21	21.98	4.85	0.83	0.25	0.03	1.61	98.92
LPR6/12-34	pyroxenite	198.00	50.72	0.20	6.16	13.64	0.21	21.74	5.46	0.82	0.17	0.03	1.11	100.26
LPR6/12-36	altered pyroxenite	199.00	51.50	0.29	8.68	11.16	0.20	16.59	7.76	1.07	0.24	0.04	1.30	98.83
LPR6/12-37	altered pyroxenite	199.50	52.64	0.53	11.77	10.27	0.17	10.77	9.48	1.14	0.60	0.11	1.92	99.40
LPR6/12-38	taxitic pyroxenite	200.00	50.90	0.37	10.26	11.24	0.16	11.95	11.45	1.17	0.75	0.04	2.15	100.41
LPR6/12-41	pyroxenite	201.50	51.65	0.30	7.13	12.84	0.21	19.31	6.27	0.76	0.15	0.04	0.70	99.36
LPR6/12-45	altered pyroxenite	203.50	49.13	0.34	7.38	13.02	0.20	18.03	7.02	0.99	0.58	0.05	2.11	98.85
LPR6/12-46	pyroxenite	204.00	48.29	0.30	6.27	15.43	0.21	20.98	5.55	1.24	0.28	0.06	1.86	100.47
LPR6/12-49	pyroxenite	205.50	48.75	0.32	7.53	13.98	0.23	19.53	6.77	1.51	0.23	0.05	0.56	99.46
LPR6/12-52	pyroxenite	207.00	50.68	0.39	7.78	14.44	0.20	16.43	5.73	1.79	0.42	0.05	1.67	99.58
LPR6/12-53	taxitic pyroxenite	207.50	49.36	0.41	8.27	17.07	0.21	14.93	5.83	1.14	0.43	0.07	1.50	99.22
LPR6/12-56	mag pyroxenite	209.00	49.49	0.31	5.26	13.16	0.20	24.67	4.14	0.73	0.32	0.06	0.63	98.97
LPR6/12-59	pyroxenite	210.50	51.99	0.33	8.22	12.08	0.20	19.21	6.16	0.99	0.38	0.05	0.94	100.55
LPR6/12-60	pyroxenite	211.00	50.05	0.44	8.87	13.94	0.24	16.09	6.68	1.46	1.20	0.06	1.15	100.18
LPR6/12-63	altered pyroxenite	212.50	49.85	0.42	10.95	13.30	0.19	11.81	8.68	1.51	0.83	0.06	1.64	99.24

Appendix 4C - LPR6/12 XRF Whole Rock Analyses continued

Sample Number	Rock Type	Depth (m) from top of borehole	%SiO2	%TiO2	%Al2O3	%Fe2O3	%MnO	%MgO	%CaO	Na2O	%K2O	%P2O5	%LOI	%Total
LPR6/12-66	pyroxenite	214.00	46.58	0.47	11.38	16.72	0.19	9.61	10.08	1.84	0.77	0.05	2.59	100.28
LPR6/12-74	altered pyroxenite	218.00	50.40	0.53	11.11	12.28	0.20	11.28	8.53	1.58	0.85	0.08	2.58	99.42
LPR6/12-77	pyroxenite	219.50	49.75	0.62	11.78	11.46	0.19	8.30	12.51	3.00	0.50	0.08	2.12	100.31
LPR6/12-82	hornfels	229.00	58.00	0.77	18.67	8.69	0.10	4.14	1.14	1.14	2.81	0.08	3.79	99.33
LPR6/12-83	hornfels	239.57	59.25	0.80	18.80	8.36	0.09	2.96	1.01	1.20	3.02	0.09	3.69	99.27

Appendix 4C - LPR6/12 XRF Whole Rock Analyses continued

Sample Number	Rock Type	Depth (m) from top of borehole	Rb	Sr	Y	Zr	Nb	Co	Ni	Cu	Zn	TiO2	V	Cr	Ba
LPR6/12 32.00	leuco-norite	32.00	16	373	8	21	5	23	119	21	41	0.18	63	398	125
LPR6/12-1	calc-silicate	33.40	13	134	42	34	6	95	2489	5	40	0.3	109	665	32
LPR6/12-2	calc-silicate	42.14	4	13	23	8	4	292	1575	2	54	0.17	108	466	15
LPR6/12 75.00	altered pyroxenite	75.00	21	75	8	23	5	74	686	98	92	0.24	97	4150	256
LPR6/12-3	pyroxenite	86.87	11	94	8	12	4	102	918	31	86	0.26	129	3087	113
LPR6/12 105.50	pyroxenite	105.50	56	61	15	33	6	56	568	53	89	0.27	117	3195	161
LPR6/12 119.50	altered pyroxenite	119.50	21	125	11	47	6	64	580	79	83	0.29	124	2757	254
LPR6/12-4	mela-norite	138.08	15	100	10	25	5	90	628	69	77	0.26	122	3101	144
LPR6/12 149.00	mela-norite	149.00	13	194	11	28	6	54	423	77	74	0.27	122	4660	145
LPR6/12 156.00	pyroxenite	156.00	21	215	10	28	6	49	323	38	78	0.32	116	1180	186
LPR6/12 171.50	leuco-norite	171.50	19	396	11	35	5	15	56	29	47	0.25	60	125	164
LPR6/12 175.50	leuco-norite	175.50	25	395	11	33	6	16	52	22	41	0.24	54	133	180
LPR6/12-5	norite pyroxenite	178.64	13	117	11	24	5	87	430	77	88	0.31	126	1753	130
LPR6/12-6	altered pyroxenite	184.00	26	76	15	31	6	109	855	136	102	0.42	146	1852	185
LPR6/12-8	altered pyroxenite	185.00	63	32	16	27	5	102	746	81	78	0.3	122	1547	151
LPR6/12-9	pegmatoidal pyroxenite	185.50	74	41	12	28	5	143	2264	593	83	0.34	124	2708	205
LPR6/12-12	pyroxenite	187.00	18	72	13	26	4	108	997	217	96	0.26	146	3323	137
LPR6/12-16	altered pyroxenite	189.00	21	62	17	43	6	117	2219	1202	90	0.36	162	2182	85
LPR6/12-19	mag pyroxenite	190.50	16	63	15	34	5	203	4272	2367	103	0.37	148	2645	89
LPR6/12-22	pyroxenite	192.00	9	71	7	<8	4	149	1418	784	91	0.19	156	2905	62
LPR6/12-25	pyroxenite	193.50	12	102	7	<8	4	142	1611	839	89	0.17	162	2294	97
LPR6/12-26	pyroxenite	194.00	11	91	8	<8	3	142	1726	855	84	0.19	171	2063	77
LPR6/12-28	pyroxenite	195.00	9	98	8	<8	3	114	1279	593	77	0.2	162	2166	74
LPR6/12-29	mag pyroxenite	195.50	6	64	6	<8	3	154	1352	374	90	0.16	143	3462	52
LPR6/12-31	altered pyroxenite	196.50	27	118	47	96	9	25	224	580	77	0.48	98	84	99
LPR6/12-32	mag pyroxenite	197.00	20	68	7	<8	3	168	2048	1171	107	0.18	205	3319	93
LPR6/12-34	pyroxenite	198.00	8	72	7	<8	3	154	2151	934	97	0.18	157	2944	57
LPR6/12-36	altered pyroxenite	199.00	19	101	13	42	5	102	1230	570	89	0.27	161	1497	79
LPR6/12-37	altered pyroxenite	199.50	38	158	18	51	8	63	687	164	74	0.51	161	806	143
LPR6/12-38	taxitic pyroxenite	200.00	30	96	19	20	5	82	579	187	89	0.29	197	1133	103
LPR6/12-41	pyroxenite	201.50	14	99	9	12	4	119	1346	530	98	0.29	187	2094	104
LPR6/12-45	altered pyroxenite	203.50	35	74	12	16	5	112	1561	625	85	0.32	172	2142	111
LPR6/12-46	pyroxenite	204.00	21	74	11	16	5	205	3849	1799	111	0.29	153	2052	119
LPR6/12-49	pyroxenite	205.50	16	100	11	20	4	174	2946	1660	97	0.3	139	1771	109
LPR6/12-52	pyroxenite	207.00	24	98	12	31	5	197	3347	2497	117	0.41	188	1598	147
LPR6/12-53	taxitic pyroxenite	207.50	25	121	14	24	6	294	4715	3394	128	0.43	162	1116	163
LPR6/12-56	mag pyroxenite	209.00	15	70	11	20	5	165	1535	515	92	0.33	132	3926	133
LPR6/12-59	pyroxenite	210.50	19	105	11	23	5	120	1274	606	101	0.34	133	2136	131
LPR6/12-60	pyroxenite	211.00	26	110	14	35	6	101	734	450	110	0.44	165	1529	146
LPR6/12-63	altered pyroxenite	212.50	53	134	17	27	5	125	1744	1245	121	0.42	177	1071	216

Appendix 4C - LPR6/12 XRF Whole Rock Analyses continued

Sample Number	Rock Type	Depth (m) from top of borehole	Rb	Sr	Y	Zr	Nb	Co	Ni	Cu	Zn	TiO2	V	Cr	Ba
LPR6/12-66	pyroxenite	214.00	43	150	18	43	6	288	7763	3584	136	0.44	165	683	173
LPR6/12-74	altered pyroxenite	218.00	49	150	21	47	7	123	2166	1783	95	0.56	204	1280	268
LPR6/12-77	pyroxenite	219.50	31	127	22	53	9	179	3876	519	93	0.63	170	268	98
LPR6/12-82	hornfels	229.00	177	83	25	112	16	27	63	27	139	0.73	149	133	443
LPR6/12-83	hornfels	239.57	185	102	27	113	16	23	59	18	141	0.91	141	135	415

Appendix 4D - LPR8/15 XRF Whole Rock Analyses

Sample Number	Rock Type	top of borehole	%SiO2	%TiO2	%Al2O3	%Fe2O3	%MnO	%MgO	%CaO	%Na2O	%K2O	%P2O5	%LOI	%TOTAL
LPR8/15 11.00	norite	11.00	51.91	0.23	15.81	8.82	0.15	12.19	9.08	2.00	0.12	0.02	0.06	100.39
LPR8/15 15.00	norite	15.00	52.82	0.27	13.23	9.80	0.17	14.11	8.15	1.75	0.13	0.03	0.05	100.51
LPR8/15 23.00	norite	23.00	51.97	0.25	15.32	8.71	0.15	12.55	8.89	2.02	0.16	0.03	0.27	100.32
LPR8/15 27.00	norite	27.00	50.79	0.26	14.73	9.73	0.17	13.47	8.55	1.86	0.20	0.04	0.32	100.12
LPR8/15 40.50	gabbro	40.50	51.65	0.36	8.03	9.04	0.19	12.69	15.48	0.99	0.19	0.04	0.65	99.31
LPR8/15 55.00	norite	55.00	49.82	0.17	26.02	4.00	0.03	3.60	13.13	2.74	0.16	0.02	0.46	100.15
LPR8/15 69.00	norite	69.00	50.82	0.19	22.19	5.04	0.09	6.26	11.71	2.52	0.19	0.03	0.59	99.63
LPR8/15 82.50	norite	82.50	51.14	0.18	24.42	4.03	0.08	4.91	12.52	2.46	0.15	0.04	0.22	100.15
LPR8/15 93.00	norite	93.00	50.66	0.17	23.48	4.45	0.08	5.44	11.67	2.51	0.13	0.03	0.26	98.88
LPR8/15 100.50	pyroxenite	100.50	49.56	0.23	4.65	10.70	0.18	28.76	3.07	0.66	0.25	0.04	0.56	98.66
LPR8/15 137.00	norite	137.00	49.74	0.16	23.16	4.38	0.08	6.43	12.51	1.98	0.95	0.03	1.97	101.39
LPR8/15 141.00	norite	141.00	49.40	0.14	21.83	5.59	0.10	7.21	11.04	2.14	0.45	0.02	1.05	98.97
LPR8/15 174.00	pyroxenite	174.00	48.51	0.15	4.24	12.42	0.21	28.60	3.58	0.42	0.00	0.02	0.78	98.93
LPR8/15 192.00	norite	192.00	52.29	0.27	13.98	8.88	0.15	13.26	7.67	1.91	0.26	0.04	0.10	98.81
LPR8/15 208.50	norite	208.50	52.54	0.29	13.89	9.40	0.17	13.40	7.76	1.75	0.32	0.04	0.46	100.02
LPR8/15 217.50	norite	217.50	53.01	0.30	15.89	8.26	0.15	11.40	8.60	2.35	0.27	0.04	0.13	100.40
LPR8/15 250.00	pyroxenite	250.00	51.51	0.23	6.67	10.92	0.23	21.87	7.08	0.62	0.09	0.04	0.98	100.24
LPR8/15 263.00	pyroxenite	263.00	52.72	0.30	7.25	11.37	0.22	20.08	6.59	1.19	0.24	0.04	0.30	100.30
LPR8/15 287.50	pyroxenite	287.50	52.85	0.28	6.79	10.36	0.20	21.18	4.87	1.31	0.36	0.04	0.64	98.88
LPR8/15 329.00	pyroxenite	329.00	52.20	0.31	7.15	10.97	0.19	20.21	5.62	1.10	0.31	0.06	0.58	98.70
LPR8/15 345.60	calc-silicate	345.60	51.75	0.13	0.85	8.58	0.18	15.82	21.91	0.07	0.10	0.02	0.87	100.28
LPR8/15 364.50	pyroxenite	364.50	52.38	0.28	5.43	12.42	0.21	23.24	4.56	0.81	0.13	0.05	0.74	100.25
LPR8/15 376.00	gabbronorite	376.00	43.18	0.35	12.32	16.07	0.20	7.93	16.40	0.69	0.11	0.05	1.73	99.03
LPR8/15 387.00	pyroxenite	387.00	48.67	0.41	8.19	14.59	0.18	17.68	6.05	1.38	0.44	0.06	1.14	98.79
LPR8/15 393.00	calc-silicate	393.00	49.50	0.44	7.14	11.79	0.21	8.62	17.47	2.34	0.00	0.66	1.36	99.53
LPR8/15 403.00	hornfels	403.00	57.94	0.77	20.01	8.31	0.06	3.05	0.67	1.06	3.36	0.08	3.62	98.93
LPR8/15 422.00	marginal norite	422.00	52.70	0.32	9.60	10.99	0.19	19.59	5.35	0.55	0.44	0.07	0.38	100.18
LPR8/15 432.00	marginal norite	432.00	52.10	0.26	7.26	10.95	0.18	21.17	4.77	0.97	0.36	0.05	0.68	98.75
LPR8/15 457.00	hornfels	457.00	61.66	0.71	18.61	7.93	0.07	3.07	0.93	1.06	2.68	0.08	3.63	100.43
LPR8/15 468.50	meta-sediment	468.50	11.83	0.13	1.90	1.19	1.41	3.26	45.32	0.15	0.16	0.14	33.36	98.85

Appendix 4D - LPR8/15 XRF Whole Rock Analyses continued

Sample Number	Rock Type	top of borehole	Rb	Sr	Y	Zr	Nb	Co	Ni	Cu	Zn	TiO2	V	Cr	Ba
LPR8/15 11.00W	norite	11.00	6	266	8	14	5	44	254	25	65	0.22	92	936	118
LPR8/15 15.00W	norite	15.00	9	217	10	22	5	52	305	32	81	0.28	113	1164	116
LPR8/15 23.00W	norite	23.00	9	246	10	17	5	45	265	33	75	0.26	100	1036	129
LPR8/15 27.00W	norite	27.00	11	226	9	19	5	48	285	28	71	0.28	104	1033	152
LPR8/15 40.50W	gabbro	40.50	12	132	18	31	5	46	353	131	73	0.34	179	1446	142
LPR8/15 55.00W	norite	55.00	9	402	8	17	5	16	70	16	40	0.15	49	182	130
LPR8/15 69.00W	norite	69.00	8	357	8	19	5	23	128	20	51	0.17	62	502	148
LPR8/15 82.50W	norite	82.50	9	384	8	20	5	19	93	18	35	0.16	49	285	132
LPR8/15 93.00W	norite	93.00	7	371	8	20	5	21	103	16	39	0.16	52	340	125
LPR8/15 100.50W	pyroxenite	100.50	19	67	9	26	6	85	1171	36	78	0.24	94	5104	196
LPR8/15 137.00W	norite	137.00	41	355	7	18	5	21	141	19	41	0.17	55	519	201
LPR8/15 141.00W	norite	141.00	22	319	6	11	4	25	159	20	46	0.14	52	580	154
LPR8/15 174.00W	pyroxenite	174.00	4	64	7	<8	5	99	1195	70	92	0.16	85	4915	84
LPR8/15 192.00W	norite	192.00	13	230	11	29	6	49	288	24	74	0.31	113	1204	153
LPR8/15 208.50W	norite	208.50	16	224	10	31	6	51	294	19	76	0.35	116	1168	175
LPR8/15 217.50W	norite	217.50	14	266	11	32	6	44	226	27	62	0.32	107	861	174
LPR8/15 250.00W	pyroxenite	250.00	12	64	10	13	6	68	570	117	90	0.27	118	3045	167
LPR8/15 263.00W	pyroxenite	263.00	16	111	12	28	6	64	490	41	94	0.35	129	1535	207
LPR8/15 287.50W	pyroxenite	287.50	21	99	11	35	6	66	600	29	89	0.34	129	2846	205
LPR8/15 329.00W	pyroxenite	329.00	20	103	12	27	6	66	544	77	85	0.31	144	2453	235
LPR8/15 345.60W	calc-silicate	345.60	20	10	15	19	6	22	226	8	48	0.12	39	16	35
LPR8/15 364.50W	pyroxenite	364.50	12	65	10	19	5	95	1534	878	91	0.31	137	2478	127
LPR8/15 376.00W	gabbronorite	376.00	3	97	40	33	11	163	3666	<6	67	0.32	155	197	31
LPR8/15 387.00W	pyroxenite	387.00	23	114	16	52	8	168	4787	3696	102	0.44	148	1937	238
LPR8/15 393.00W	calc-silicate	393.00	4	43	30	33	8	132	2145	<6	56	0.49	112	71	25
LPR8/15 403.00	hornfels	403.00	224	77	28	111	17	25	61	17	118	0.84	176	164	440
LPR8/15 422.00W	norite	422.00	35	86	14	56	7	73	855	41	109	0.37	131	2329	367
LPR8/15 432.00W	norite	432.00	20	103	10	24	6	73	781	54	85	0.33	141	2921	240
LPR8/15 457.00W	hornfels	457.00	177	93	24	101	16	24	57	43	94	0.78	161	159	464
LPR8/15 468.50W	meta-sed	468.50	20	172	11	38	6	9	30	11	43	0.09	17	28	219

Appendix 4E - LPR12/9 XRF Whole Rock Analyses (University of the Witwatersrand)

Sample Number	Rock Type	Depth (m) from top of borehole	%SiO2	%TiO2	%Al2O3	%Fe2O3	%MnO	%MgO	%CaO	%Na2O	%K2O	%P2O5	%LOI	%TOTAL
LPR12-9 36.00	pyroxenite	36.00	53.67	0.24	4.40	10.57	0.21	22.41	5.51	0.79	0.28	0.06	0.41	98.55
LPR12-9 50.50	pyroxenite	50.50	52.95	0.25	4.67	9.41	0.20	20.73	8.66	0.95	0.29	0.04	0.53	98.68
LPR12-9 65.00	pegmatoidal pyroxenite	65.00	53.67	0.26	4.26	10.21	0.19	20.60	7.54	1.11	0.24	0.06	0.40	98.54
LPR12-9 91.00	harzburgite	91.00	53.47	0.17	4.95	10.43	0.20	23.74	4.01	0.85	0.42	0.06	0.23	98.53
LPR12-9 144.50	pyroxenite	144.50	54.21	0.21	6.38	11.24	0.20	21.03	4.92	1.07	0.31	0.06	0.39	100.02
LPR12-9 178.75	pyroxenite	178.75	52.62	0.30	5.61	12.65	0.20	20.71	4.80	0.98	0.38	0.07	0.49	98.81
LPR12-9 208.90	pyroxenite	208.90	51.10	0.32	7.41	11.01	0.19	19.55	5.50	1.37	0.32	0.07	0.60	97.44
LPR12-9 247.50	pyroxenite	247.50	48.64	0.28	6.72	14.12	0.21	22.70	4.95	1.01	0.39	0.05	0.37	99.44
LPR12-9 269.30	pyroxenite	269.30	50.55	0.29	6.89	13.32	0.19	19.91	5.12	1.03	0.36	0.06	0.74	98.46
LPR12-9 270.96	pyroxenite	270.96	50.12	0.28	7.49	13.12	0.18	20.35	5.25	0.99	0.40	0.07	0.91	99.16
LPR12-9 298.00	marginal norite	298.00	54.89	0.29	10.93	10.63	0.20	12.73	5.91	0.88	0.96	0.08	0.76	98.26
LPR12-9 314.00	hornfels	314.00	56.88	0.81	20.17	8.30	0.09	2.90	0.84	1.45	3.12	0.06	4.23	98.85

Appendix 4E - LPR12/9 XRF Whole Rock Analyses (University of the Witwatersrand) continued

Sample Number	Rock Type	Depth (m) from top of borehole	Rb (ppm)	Sr (ppm)	Y (ppm)	Zr (ppm)	Nb (ppm)	Co (ppm)	Ni (ppm)	Cu (ppm)	Zn (ppm)	TiO2 (%)	V (ppm)	Cr (ppm)	Ba (ppm)
LPR12-9 36.00	pyroxenite	36.00	16	78	9	44	6	63	786	375	97	0.26	142	2661	167
LPR12-9 50.50	pyroxenite	50.50	15	86	6	44	5	57	579	80	74	0.25	107	3639	118
LPR12-9 65.00	pegmatoidal pyr	65.00	13	77	7	49	5	65	603	195	81	0.26	143	3187	112
LPR12-9 91.00	harzburgite	91.00	18	106	13	42	7	67	764	21	87	0.20	167	1348	167
LPR12-9 144.50	pyroxenite	144.50	16	112	9	37	5	70	630	186	82	0.24	124	2626	148
LPR12-9 178.75	pyroxenite	178.75	20	86	25	49	12	86	1229	435	93	0.36	171	169	166
LPR12-9 208.90	pyroxenite	208.90	16	125	9	53	5	80	1192	526	86	0.36	143	2902	164
LPR12-9 247.50	pyroxenite	247.50	16	93	9	47	4	96	1005	109	101	0.32	148	2843	123
LPR12-9 269.30	pyroxenite	269.30	16	99	9	63	5	118	2689	1727	105	0.35	166	2474	137
LPR12-9 270.96	pyroxenite	270.96	20	110	9	57	5	117	2425	1424	94	0.35	178	2049	166
LPR12-9 298.00	marginal norite	298.00	58	167	7	82	5	53	390	58	90	0.33	177	2569	242
LPR12-9 314.00	hornfels	314.00	173	97	10	126	6	27	90	51	103	0.91	156	2571	538

Appendix 4F - LPR12/9 Whole Rock XRF Analyses (provided by Ridge Mining)

BH ID	From	To	Rock Type	Number	Cu_XRF ppm	Ni_XRF ppm	SiO2_XRF wt %	Fe203_XRF wt %	MgO_XRF wt %	CaO_XRF wt %	Cr2O3_XRF wt %	Cr_XRF ppm	S_XRF ppm	SKA1_2M_XRF ppm
LPR12-09	256.87	257.34	PY+S	S00665	993	2454	43.04	11.65	22.13	4.66	0.46	3141	2725	2888
LPR12-09	257.34	257.84	GN+S	S00666	3238	4515	44.78	11.49	13.82	6.25	0.17	1159	6928	6885
LPR12-09	257.84	258.3	PY	S00667	122	1439	43.80	12.00	21.92	5.69	0.39	2697	1840	2028
LPR12-09	258.3	258.6	PY+S	S00668	1909	3532	42.52	13.16	19.65	4.54	0.47	3235	5721	5898
LPR12-09	258.6	258.94	PY+S	S00669	2213	4066	45.47	11.09	13.21	6.18	0.22	1488	7179	7090
LPR12-09	258.94	259.3	PY+MT	S00670	2105	3410	43.03	11.85	15.35	5.58	0.32	2160	7375	7412
LPR12-09	259.3	259.7	PY+S	S00671	153	1106	45.41	10.92	21.06	6.07	0.40	2768	484	557
LPR12-09	259.7	260.05	PY+S	S00672	1391	2644	44.58	12.43	22.29	4.62	0.45	3084	4740	4903
LPR12-09	260.05	260.45	PY+S	S00673	342	1382	41.34	12.71	21.61	4.63	0.50	3416	1157	1296
LPR12-09	260.45	260.9	PY	S00674	2371	3688	42.53	12.13	17.55	5.00	0.37	2536	6607	6626
LPR12-09	260.9	261.29	PY+S	S00675	187	1271	40.17	12.51	21.41	4.79	0.53	3638	553	658
LPR12-09	261.29	261.7	PY	S00676	108	1433	43.91	13.73	14.84	8.52	0.25	1713	231	282
LPR12-09	261.7	262.05	PY+S	S00677	555	1485	47.27	11.34	23.84	4.86	0.47	3215	2965	3160
LPR12-09	262.05	262.53	PY+S	S00678	863	2982	45.67	11.62	22.53	5.46	0.46	3143	3559	3741
LPR12-09	262.53	262.92	PY+S	S00679	1738	3041	43.63	11.61	21.21	6.00	0.42	2879	4510	4658
LPR12-09	262.92	263.3	PY+S	S00680	1343	2900	43.51	12.22	22.58	4.45	0.48	3257	3206	3382
LPR12-09	263.3	263.69	PY+S	S00681	2384	3297	39.72	12.42	21.23	5.13	0.46	3138	6776	6530
LPR12-09	263.69	264	PY+S	S00682	1392	2465	41.88	12.42	21.40	5.33	0.47	3187	5767	5702
LPR12-09	264	264.34	PY	S00683	277	756	45.05	10.57	19.79	5.97	0.42	2848	1141	1203
LPR12-09	264.34	264.75	PY+S	S00684	1806	3121	45.29	11.55	20.91	5.64	0.42	2846	5824	5761
LPR12-09	264.75	265.1	PY+S	S00685	2196	3626	44.68	11.88	19.64	5.46	0.41	2830	8369	8148
LPR12-09	265.1	265.5	PY+S	S00686	2238	3356	43.56	11.83	18.16	5.52	0.41	2809	8579	8305
LPR12-09	265.5	265.9	PY+S	S00687	2531	3460	44.57	11.95	18.18	5.54	0.41	2778	8802	8614
LPR12-09	265.9	266.2	PY+S	S00688	2409	3650	43.96	11.98	17.17	5.65	0.41	2778	9859	9473
LPR12-09	266.2	266.5	PY+S	S00689	2870	3816	43.86	12.19	16.94	5.72	0.39	2664	11133	10644
LPR12-09	266.5	266.8	PY+S	S00690	2373	3812	40.52	13.59	21.11	4.86	0.44	2988	10860	10498
LPR12-09	266.8	267.1	PY+S	S00691	1697	2869	42.98	12.74	21.30	4.96	0.44	2988	7702	7645
LPR12-09	267.1	267.4	PY+S	S00692	3495	5515	40.92	14.38	18.00	5.18	0.38	2619	14752	14040
LPR12-09	267.4	267.7	PY+S	S00693	1253	2029	40.89	13.12	21.34	5.02	0.47	3249	3699	3905
LPR12-09	267.7	268	PY+S	S00694	2309	3653	40.60	12.51	19.21	5.64	0.42	2867	7615	7556
LPR12-09	268	268.3	PY+S	S00695	1337	2209	40.73	12.46	21.57	5.11	0.48	3274	3841	3873
LPR12-09	268.3	268.6	PY+S	S00696	2727	3725	42.66	12.80	19.59	5.27	0.37	2519	7812	7802
LPR12-09	268.6	268.9	PY+S	S00697	2634	3830	41.12	13.28	20.31	5.12	0.48	3285	8622	8439
LPR12-09	268.9	269.3	PY+S	S00698	2211	3070	41.00	12.86	19.42	5.14	0.44	2999	6803	6789
LPR12-09	269.3	269.7	PY+S	S00699	1522	2162	42.94	12.18	19.75	5.31	0.42	2884	3966	4126
LPR12-09	269.7	270	PY+S	S00700	1966	2533	42.90	12.27	19.12	5.11	0.42	2903	4690	4738

Appendix 4F - LPR12/9 Whole Rock XRF Analyses (provided by Ridge Mining) continued

BH ID	From	To	Rock Type	Number	Cu_XRF ppm	Ni_XRF ppm	SiO2_XRF wt %	Fe203_XRF wt %	MgO_XRF wt %	CaO_XRF wt %	Cr2O3_XRF wt %	Cr_XRF ppm	S_XRF ppm	SKA1_2M_XRF ppm
LPR12-09	270	270.4	PY+S	S00701	3642	3568	41.88	12.16	18.21	4.94	0.40	2727	8140	7996
LPR12-09	270.4	270.66	PY	S00702	1497	2671	40.83	12.73	21.13	4.84	0.47	3223	4862	4986
LPR12-09	270.66	270.96	PY+S	S00703	189	923	43.32	12.12	21.11	4.99	0.49	3362	524	602
LPR12-09	270.96	271.42	PY+S	S00704	1141	1987	42.80	12.67	20.35	4.99	0.44	3023	3728	3962
LPR12-09	271.42	271.85	PY+S	S00705	485	1404	43.22	11.67	19.96	5.15	0.49	3353	1727	1873
LPR12-09	271.85	272.24	PY	S00706	2472	3490	42.20	12.36	18.64	5.43	0.40	2706	7605	7687
LPR12-09	272.24	272.65	PY+S	S00707	2305	3524	41.63	12.80	18.72	4.98	0.42	2857	7708	7650
LPR12-09	272.65	273.02	PY+S	S00708	7667	11055	36.54	16.90	14.89	5.59	0.28	1889	17603	28487
LPR12-09	273.02	273.3	PY+S	S00709	7514	19688	33.68	18.48	16.67	4.43	0.29	2015	38229	34753
LPR12-09	273.3	273.6	PY+S	S00710	3617	7036	36.63	15.50	19.54	4.30	0.39	2683	18140	17337
LPR12-09	273.6	273.85	PY+S	S00711	2592	3339	43.18	12.19	16.36	6.15	0.32	2219	7653	7825
LPR12-09	273.85	274.08	PY+S	S00712	3851	5858	42.00	13.95	15.25	5.81	0.27	1815	15821	14997
LPR12-09	274.08	274.28	PY+S	S00713	8706	12105	38.10	15.98	14.07	5.38	0.26	1811	33369	30727
LPR12-09	274.28	274.64	PY	S00714	211	1252	42.76	12.86	21.72	3.86	0.49	3350	273	463
LPR12-09	274.64	275.02	(PEG)+S	S00715	2187	7675	42.47	12.68	15.63	6.81	0.23	1541	11952	11567
LPR12-09	275.02	275.25	GA+S	S00716	1967	11377	41.33	14.75	15.99	5.61	0.24	1626	19650	18431
LPR12-09	275.25	275.59		S00717	116	3971	47.19	10.70	11.89	10.87	0.14	959	186	244
LPR12-09	275.59	275.99	PY+S	S00718	1144	5523	43.71	13.03	15.09	7.98	0.21	1431	6284	6389
LPR12-09	275.99	276.4	PY+S	S00719	1366	1509	42.39	12.81	21.20	5.18	0.47	3192	3768	4009
LPR12-09	276.4	276.7	PY+S	S00720	7661	7534	39.96	15.70	18.43	5.12	0.37	2500	20151	18879
LPR12-09	276.7	277.05	PY+S	S00721	3439	6744	40.86	15.17	17.99	5.06	0.37	2556	17460	16594
LPR12-09	277.05	277.4	PY+S	S00722	1665	2911	42.64	12.18	19.30	5.91	0.37	2552	5126	5302
LPR12-09	277.4	277.7	PY+S	S00723	5420	5444	42.68	13.52	15.36	5.78	0.28	1926	14776	14382
LPR12-09	277.7	278.05	PY+S	S00724	2226	2632	43.56	11.42	14.40	6.20	0.26	1745	6566	6664
LPR12-09	278.05	278.42	PY+S	S00725	1733	2027	43.39	13.00	19.02	5.45	0.46	3181	4433	4673
LPR12-09	278.42	278.7	PY+S	S00726	1119	1649	46.05	12.17	18.79	5.79	0.36	2430	3197	3471
LPR12-09	278.7	279.05	PY+S	S00727	6134	6929	42.25	13.36	15.69	5.85	0.30	2073	14776	14316
LPR12-09	279.05	279.5	PY	S00728	161	977	43.90	12.20	19.89	5.35	0.46	3174	657	789
LPR12-09	279.5	279.95	PY	S00729	374	994	46.77	10.79	18.31	5.94	0.37	2535	836	976
LPR12-09	279.95	280.4	PY	S00730	1080	1029	48.52	10.64	17.48	6.14	0.28	1886	961	1074
LPR12-09	280.4	280.9	PY	S00731	420	843	48.98	10.41	17.11	6.36	0.26	1790	615	737
LPR12-09	280.9	281.4	PY+S	S00732	1925	2352	48.50	10.91	15.72	6.14	0.22	1509	3349	3576
LPR12-09	281.4	281.8	PY+S	S00733	779	1458	47.94	11.26	17.31	6.23	0.28	1912	1546	1728
LPR12-09	281.8	282.2	PY+S	S00734	745	1092	48.01	11.22	16.21	6.63	0.21	1452	1205	1363
LPR12-09	282.2	282.59	PY+S	S00735	608	1427	46.83	11.52	17.87	5.74	0.30	2073	1436	1596

Appendix 4F - LPR12/9 Whole Rock XRF Analyses (provided by Ridge Mining) continued

BH ID	From	To	Rock Type	Number	Cu_XRF ppm	Ni_XRF ppm	SiO2_XRF wt %	Fe203_XRF wt %	MgO_XRF wt %	CaO_XRF wt %	Cr2O3_XRF wt %	Cr_XRF ppm	S_XRF ppm	SKA1_2M_XRF ppm
LPR12-09	282.59	282.9	PY+S	S00736	1040	2747	47.19	12.08	16.30	5.80	0.27	1845	6596	6730
LPR12-09	282.9	283.4	PY	S00737	260	601	48.67	10.20	15.90	6.51	0.21	1413	513	621
LPR12-09	283.4	283.85	PY	S00738	234	568	48.68	10.52	13.18	6.76	0.18	1231	844	1001
LPR12-09	283.85	284.35	PY	S00739	187	683	48.11	11.35	15.90	5.69	0.30	2028	560	670
LPR12-09	284.35	284.65	PY+S	S00740	2660	4684	45.91	13.13	14.98	5.75	0.25	1689	11858	11662
LPR12-09	284.65	285.05	PY+S	S00741	865	1257	48.42	11.15	14.07	6.47	0.21	1464	3337	3593
LPR12-09	285.05	285.24	GA (PEG)	S00742	685	1245	49.44	10.18	12.99	8.34	0.22	1536	3918	4190
LPR12-09	285.24	285.54	S	S00743	656	1215	48.96	11.22	14.92	6.18	0.23	1573	2870	3136
LPR12-09	285.54	285.84	S	S00744	874	1280	49.95	10.47	12.23	6.81	0.15	1017	3268	3507
LPR12-09	285.84	286.34	GA(PEG)	S00745	131	424	49.92	10.28	12.98	6.70	0.20	1360	655	749
LPR12-09	286.34	286.78	GA(PEG)	S00746	126	501	49.92	10.76	17.01	5.91	0.27	1880	328	437
LPR12-09	286.78	287.22	GA(PEG)	S00747	142	556	49.35	10.55	17.91	5.61	0.29	2009	243	323
LPR12-09	287.22	287.72	GA(PEG)	S00748	193	293	49.45	8.72	10.05	8.12	0.09	642	311	394
LPR12-09	287.72	288.22	GA(PEG)	S00749	128	254	49.48	7.42	9.80	8.77	0.05	342	154	203
LPR12-09	288.22	288.62	PY	S00750	211	818	48.63	10.07	21.01	7.88	0.28	1900	232	299
LPR12-09	288.62	289.09	PY	S00751	353	1412	47.82	10.83	19.63	6.17	0.27	1831	1343	1499
LPR12-09	289.09	289.29	PY	S00752	909	1210	47.59	11.79	18.78	5.56	0.25	1717	1953	2142
LPR12-09	289.29	289.65	PY+S	S00753	9704	3861	44.68	12.36	12.54	5.66	0.12	826	12040	11584
LPR12-09	289.65	290.1	PY	S00754	340	531	44.09	9.83	12.73	8.27	0.09	640	773	1147
LPR12-09	290.1	290.43	PY	S00755	829	1483	47.08	10.17	13.78	6.49	0.09	649	1649	1825
LPR12-09	290.43	290.65	PY+S	S00756	4495	4930	44.55	12.77	9.03	5.95	0.05	342	15774	14981
LPR12-09	290.65	290.86	PY+S	S00757	45873	43848	27.26	22.18	5.64	3.41	0.05	342		72588
LPR12-09	290.86	291.06	PY+S	S00758	17606	30787	31.84	20.90	7.24	4.14	0.05	342		53775
LPR12-09	291.06	291.16	PY+S	S00759	1407	2827	42.64	9.36	8.33	8.85	0.05	342	5655	5705
LPR12-09	291.16	291.6	MS	S00760	221	366	38.64	12.39	7.22	1.52	0.05	342	840	979
LPR12-09	291.6	291.99	PY+S	S00761	7845	4332	41.35	14.06	5.90	4.34	0.05	342	11911	11480
LPR12-09	291.99	292.4	MS	S00762	283	510	41.00	13.12	6.24	2.17	0.05	342	680	821
LPR12-09	292.4	292.7	MS	S00763	55	170	43.75	11.24	5.33	1.63	0.05	342	80	135
LPR12-09	292.7	293		S00764	35	131	49.14	10.17	4.39	1.05	0.05	342	83	135

Appendix 4G - Fire Assay Analyses (provided by Ridge Mining)

BH ID	From	To	RockType	SampleNum	Pt g/t	Pd g/t	Pt/Pd g/t	Au g/t	Cu ppm	Ni ppm
LPR12-09	256.87	257.34	PY+S	S00665	0.20	0.66	0.30	0.06	943	2526
LPR12-09	257.34	257.84	GN+S	S00666	0.74	1.84	0.40	0.44	2360	4710
LPR12-09	257.84	258.3	PY	S00667	0.08	0.30	0.27	0.23	82	1425
LPR12-09	258.3	258.6	PY+S	S00668	0.29	1.02	0.28	0.08	1690	3680
LPR12-09	258.6	258.94	PY+S	S00669	0.44	1.62	0.27	0.12	1878	3946
LPR12-09	258.94	259.3	PY+MT	S00670	0.30	1.07	0.28	0.07	1420	3220
LPR12-09	259.3	259.7	PY+S	S00671	0.08	0.21	0.38	0.11	118	1110
LPR12-09	259.7	260.05	PY+S	S00672	0.28	0.87	0.32	0.11	1070	2610
LPR12-09	260.05	260.45	PY+S	S00673	0.06	0.13	0.46	0.01	274	1412
LPR12-09	260.45	260.9	PY	S00674	0.41	1.32	0.31	0.13	2030	3746
LPR12-09	260.9	261.29	PY+S	S00675	0.01	0.03	0.33	0.03	135	1326
LPR12-09	261.29	261.7	PY	S00676	0.08	0.60	0.13	0.26	39	1331
LPR12-09	261.7	262.05	PY+S	S00677	0.11	0.30	0.37	0.04	474	1392
LPR12-09	262.05	262.53	PY+S	S00678	0.34	0.96	0.35	0.13	660	2990
LPR12-09	262.53	262.92	PY+S	S00679	0.32	1.16	0.28	0.11	1410	3360
LPR12-09	262.92	263.3	PY+S	S00680	0.31	1.01	0.31	0.08	990	2750
LPR12-09	263.3	263.69	PY+S	S00681	0.32	1.12	0.29	0.10	1710	3350
LPR12-09	263.69	264	PY+S	S00682	0.21	0.73	0.29	0.03	1216	2629
LPR12-09	264	264.34	PY	S00683	0.03	0.07	0.43	0.01	245	769
LPR12-09	264.34	264.75	PY+S	S00684	0.39	1.25	0.31	0.07	1340	2950
LPR12-09	264.75	265.1	PY+S	S00685	0.30	0.70	0.43	0.06	1510	3180
LPR12-09	265.1	265.5	PY+S	S00686	0.35	0.78	0.45	0.07	1570	2880
LPR12-09	265.5	265.9	PY+S	S00687	0.30	1.05	0.29	0.10	1770	2940
LPR12-09	265.9	266.2	PY+S	S00688	0.35	1.04	0.34	0.08	980	2020
LPR12-09	266.2	266.5	PY+S	S00689	0.42	1.11	0.38	0.10	1900	3340
LPR12-09	266.5	266.8	PY+S	S00690	0.35	1.18	0.30	0.09	1937	3787
LPR12-09	266.8	267.1	PY+S	S00691	0.23	0.77	0.30	0.08	1475	2898
LPR12-09	267.1	267.4	PY+S	S00692	0.17	0.92	0.18	0.14	2532	5064
LPR12-09	267.4	267.7	PY+S	S00693	0.25	0.58	0.43	0.07	1058	2093
LPR12-09	267.7	268	PY+S	S00694	0.47	1.18	0.40	0.10	1740	3500
LPR12-09	268	268.3	PY+S	S00695	0.21	0.63	0.33	0.07	1115	2158
LPR12-09	268.3	268.6	PY+S	S00696	0.45	1.18	0.38	0.12	2190	3459
LPR12-09	268.6	268.9	PY+S	S00697	0.38	1.14	0.33	0.08	1981	3439
LPR12-09	268.9	269.3	PY+S	S00698	0.37	0.91	0.41	0.06	1640	2670
LPR12-09	269.3	269.7	PY+S	S00699	0.25	0.57	0.44	0.09	1289	2096
LPR12-09	269.7	270	PY+S	S00700	0.43	0.89	0.48	0.07	1500	2170
LPR12-09	270	270.4	PY+S	S00701	0.79	1.62	0.49	0.11	2970	3440
LPR12-09	270.4	270.66	PY	S00702	0.18	0.59	0.31	0.04	1299	2640
LPR12-09	270.66	270.96	PY+S	S00703	0.01	0.03	0.33	0.05	131	931
LPR12-09	270.96	271.42	PY+S	S00704	0.08	0.47	0.17	0.06	951	1998
LPR12-09	271.42	271.85	PY+S	S00705	0.06	0.26	0.23	0.03	431	1451
LPR12-09	271.85	272.24	PY	S00706	0.35	1.11	0.32	0.09	1820	3250
LPR12-09	272.24	272.65	PY+S	S00707	0.45	1.07	0.42	0.13	1700	3060
LPR12-09	272.65	273.02	PY+S	S00708	0.18	1.59	0.11	0.12	4708	9575
LPR12-09	273.02	273.3	PY+S	S00709	0.09	1.67	0.05	0.19	4920	18200
LPR12-09	273.3	273.6	PY+S	S00710	0.12	0.87	0.14	0.08	2550	6384
LPR12-09	273.6	273.85	PY+S	S00711	0.37	0.87	0.43	0.11	2201	3345
LPR12-09	273.85	274.08	PY+S	S00712	0.98	1.49	0.66	0.14	2706	5227
LPR12-09	274.08	274.28	PY+S	S00713	0.14	2.19	0.06	0.18	5400	10232
LPR12-09	274.28	274.64	PY	S00714	0.09	0.03	3.00	0.02	170	1238
LPR12-09	274.64	275.02	)+S	S00715	0.90	1.44	0.63	0.63	1570	6945
LPR12-09	275.02	275.25	GA+S	S00716	0.12	0.81	0.15	0.05	1298	10086
LPR12-09	275.25	275.59		S00717	1.47	1.58	0.93	0.80	60	6140

Appendix 4G - Fire Assay Analyses (provided by Ridge Mining) continued

BH ID	From	To	RockType	SampleNum	Pt g/t	Pd g/t	Pt/Pd g/t	Au g/t	Cu ppm	Ni ppm
LPR12-09	275.59	275.99	PY+S	S00718	0.78	2.71	0.29	0.76	890	6640
LPR12-09	275.99	276.4	PY+S	S00719	0.09	0.50	0.18	0.06	1213	1667
LPR12-09	276.4	276.7	PY+S	S00720	1.00	2.27	0.44	0.21	5850	8240
LPR12-09	276.7	277.05	PY+S	S00721	0.11	1.02	0.11	0.05	2525	6758
LPR12-09	277.05	277.4	PY+S	S00722	0.46	1.29	0.36	0.20	1410	3600
LPR12-09	277.4	277.7	PY+S	S00723	0.34	1.07	0.32	0.21	4200	5640
LPR12-09	277.7	278.05	PY+S	S00724	0.38	0.83	0.46	0.09	1770	3070
LPR12-09	278.05	278.42	PY+S	S00725	0.24	0.63	0.38	0.11	1454	2074
LPR12-09	278.42	278.7	PY+S	S00726	0.03	0.08	0.38	0.02	1012	1718
LPR12-09	278.7	279.05	PY+S	S00727	0.63	2.72	0.23	0.22	4410	6250
LPR12-09	279.05	279.5	PY	S00728	0.22	0.48	0.46	0.05	123	985
LPR12-09	279.5	279.95	PY	S00729	0.01	0.08	0.13	0.03	341	988
LPR12-09	279.95	280.4	PY	S00730	0.04	0.19	0.21	0.06	950	998
LPR12-09	280.4	280.9	PY	S00731	0.05	0.11	0.45	0.04	360	830
LPR12-09	280.9	281.4	PY+S	S00732	0.18	0.71	0.25	0.13	1692	2302
LPR12-09	281.4	281.8	PY+S	S00733	0.01	0.44	0.02	0.03	673	1405
LPR12-09	281.8	282.2	PY+S	S00734	0.18	0.21	0.86	0.05	658	1081
LPR12-09	282.2	282.59	PY+S	S00735	0.09	0.33	0.27	0.04	545	1484
LPR12-09	282.59	282.9	PY+S	S00736	0.12	0.25	0.48	0.04	861	2643
LPR12-09	282.9	283.4	PY	S00737	0.03	0.01	3.00	0.02	214	582
LPR12-09	283.4	283.85	PY	S00738	0.03	0.01	3.00	0.01	187	560
LPR12-09	283.85	284.35	PY	S00739	0.02	0.01	2.00	0.02	142	674
LPR12-09	284.35	284.65	PY+S	S00740	0.38	1.53	0.25	0.10	1970	4360
LPR12-09	284.65	285.05	PY+S	S00741	0.15	0.28	0.54	0.03	704	1154
LPR12-09	285.05	285.24	GA(PEG)	S00742	0.05	0.21	0.24	0.03	563	1222
LPR12-09	285.24	285.54	GA(PEG)+S	S00743	0.11	0.20	0.55	0.03	560	1196
LPR12-09	285.54	285.84	GA(PEG)+S	S00744	0.14	0.27	0.52	0.05	745	1205
LPR12-09	285.84	286.34	GA(PEG)	S00745	0.05	0.01	5.00	0.01	97	386
LPR12-09	286.34	286.78	GA(PEG)	S00746	0.07	0.01	7.00	0.02	82	493
LPR12-09	286.78	287.22	GA(PEG)	S00747	0.07	0.01	7.00	0.02	113	568
LPR12-09	287.22	287.72	GA(PEG)	S00748	0.04	0.01	4.00	0.02	152	287
LPR12-09	287.72	288.22	GA(PEG)	S00749	0.01	0.01	1.00	0.01	103	248
LPR12-09	288.22	288.62	PY	S00750	0.29	0.30	0.97	0.04	177	852
LPR12-09	288.62	289.09	PY	S00751	2.11	1.25	1.69	0.09	315	1448
LPR12-09	289.09	289.29	PY	S00752	0.14	0.14	1.00	0.04	809	1222
LPR12-09	289.29	289.65	PY+S	S00753	0.31	0.28	1.11	0.05	7677	3727
LPR12-09	289.65	290.1	PY	S00754	0.04	0.01	4.00	0.02	283	534
LPR12-09	290.1	290.43	PY	S00755	0.21	0.38	0.55	0.08	759	1551
LPR12-09	290.43	290.65	PY+S	S00756	0.31	0.54	0.57	0.06	3356	4712
LPR12-09	290.65	290.86	PY+S	S00757	1.13	0.52	2.17	0.30	16985	
LPR12-09	290.86	291.06	PY+S	S00758	0.34	0.58	0.59	0.41	7692	
LPR12-09	291.06	291.16	PY+S	S00759	0.47	0.55	0.85	0.05	1110	2980
LPR12-09	291.16	291.6	MS	S00760	0.02	0.01	2.00	0.03		
LPR12-09	291.6	291.99	PY+S	S00761	1.33	2.05	0.65	0.29	6120	4290
LPR12-09	291.99	292.4	MS	S00762	0.03	0.05	0.60	0.02	279	578
LPR12-09	292.4	292.7	MS	S00763	0.01	0.01	1.00	0.01	34	174
LPR12-09	292.7	293		S00764	0.01	0.01	1.00	0.01	44	124

Appendix 5 – Operating Conditions for Electron Microprobe Analyses

Cameca 355 electron microprobe

A Cameca 355 electron microprobe with an oxford Link/Lens automated analysis system was used for determining the mineral compositions of plagioclase and orthopyroxene grains.

The operation conditions of the microprobe were as follows:

Accelerating voltage:	15 kV.
Absorbed current:	1 to 1.5 Na
Calibration element:	cobalt
Each analysis time:	60 seconds

Standards

The standards were collected from MAC

Certified mineral standards block-Block No: 2590 AND

Cameca Standard Block: 47E 80

Dectection Limits:

EDS:	0.01 %
WDS:	0.001 %
EDS:	±1.5 % of total
WDS:	± 0.1 % of total of a particular element

Jeol JXA840A electron probe micro analyser

Quantitative EDS analyses were collected on a Jeol JXA840A electron probe microanalyser equipped with a Noran Norvar EDS detector and Voyager EDS software. EDS data were collected over 200 s (dead time corrected) with an accelerating voltage of 15 kV and a 1 nA probe current using pure element standards for the PGMs (including Pt, Pd, Bi, Te, Sb and As; as supplied by Micro-Analysis Consultants Ltd). Analyses were run under the supervision of Dr Dave Hutchinson at the SPECTRAU Laboratories at the University of Johannesburg.

Appendix 5A - LSD34 Microprobe Analyses - Orthopyroxene Compositions

Sample Number	Rock Type	Depth (m) from top of borehole	%FeO	%MnO	%TiO2	%CaO	%Na2O	%SiO2	%Al2O3	%MgO	%Cr2O3	%K2O	Total
LSD34 139.00	gabbronorite	139.00	24.03	0.42	0.16	2.22	nd	53.58	0.68	21.95	0.03	nd	103.07
LSD34 139.00	gabbronorite	139.00	23.41	0.30	0.16	1.91	nd	53.57	0.76	21.29	0.14	0.00	101.54
LSD34 139.00	gabbronorite	139.00	27.20	0.30	-0.03	1.04	nd	53.36	0.34	19.64	0.22	nd	102.07
LSD34 139.00	gabbronorite	139.00	31.07	0.53	0.22	1.14	nd	52.38	0.21	17.83	0.04	nd	103.42
LSD34 139.00	gabbronorite	139.00	30.03	0.67	0.30	1.11	nd	52.38	0.42	17.63	0.02	nd	102.56
LSD34 139.00	gabbronorite	139.00	30.70	0.41	0.35	1.66	nd	52.92	0.43	17.61	0.06	nd	104.14
Average			27.74	0.44	0.19	1.51	nd	53.03	0.47	19.33	0.09	nd	102.80
LSD34 199.50	gabbronorite	199.50	15.65	0.43	0.36	2.29	nd	54.36	0.12	25.91	0.40	0.02	99.54
LSD34 199.50	gabbronorite	199.50	17.21	0.34	0.06	1.33	nd	54.69	0.04	26.14	0.04	0.04	99.89
LSD34 199.50	gabbronorite	199.50	17.98	0.52	0.14	1.45	nd	53.90	0.13	25.30	0.16	nd	99.58
LSD34 199.50	gabbronorite	199.50	18.28	0.39	0.39	1.22	nd	53.91	-0.22	25.30	0.12	0.10	99.49
LSD34 199.50	gabbronorite	199.50	18.28	0.39	0.27	1.50	nd	54.43	-0.24	25.33	0.15	0.02	100.13
Average			17.48	0.41	0.24	1.56	nd	54.26	-0.03	25.60	0.17	0.05	99.74
LSD 447.00	norite	447.00	16.35	0.42	0.24	1.43	nd	54.03	0.73	26.21	0.02	0.01	99.44
LSD 447.00	norite	447.00	13.70	0.16	0.14	5.31	nd	53.84	0.60	24.53	0.22	0.03	98.53
LSD 447.00	norite	447.00	16.33	0.38	0.16	1.05	nd	54.14	0.65	26.41	-0.03	nd	99.09
LSD 447.00	norite	447.00	15.57	0.17	0.20	2.08	nd	54.14	0.53	25.99	0.15	nd	98.83
LSD 447.00	norite	447.00	15.79	0.25	0.23	1.32	nd	54.30	0.68	26.58	-0.08	nd	99.07
LSD 447.00	norite	447.00	15.86	0.35	0.15	0.99	nd	54.40	0.49	26.47	0.19	0.01	98.91
Average			15.60	0.29	0.19	2.03	nd	54.14	0.61	26.03	0.08	0.02	98.99
LSD34 483.50	norite	483.50	19.71	0.42	0.45	1.52	nd	52.87	-0.20	23.47	0.18	0.07	98.49
LSD34 483.50	norite	483.50	20.11	0.27	0.54	1.38	nd	53.36	-0.02	23.28	0.37	0.00	99.29
LSD34 483.50	norite	483.50	18.65	0.37	0.43	1.17	nd	53.75	0.04	24.27	0.34	0.04	99.06
LSD34 483.50	norite	483.50	19.62	0.43	0.47	1.64	nd	52.81	-0.09	23.70	0.11	0.02	98.71
LSD34 483.50	norite	483.50	20.26	0.22	0.57	1.34	nd	53.25	-0.15	23.32	0.29	0.00	99.10
LSD34 483.50	norite	483.50	18.73	0.29	0.42	1.52	nd	53.53	-0.26	24.21	0.11	nd	98.55
LSD34 483.50	norite	483.50	18.39	0.35	0.46	2.78	nd	53.48	-0.10	23.95	0.22	nd	99.53
LSD34 483.50	norite	483.50	19.06	0.27	0.34	1.06	nd	53.52	-0.25	24.14	0.18	0.11	98.43
LSD34 483.50	norite	483.50	19.24	0.22	0.25	1.17	nd	53.21	0.00	24.34	0.27	0.05	98.75
Average			19.31	0.32	0.44	1.51	nd	53.31	-0.11	23.85	0.23	0.04	98.89
LSD34 526.00	pyroxenite	526.00	13.06	0.26	-0.02	0.93	nd	55.41	0.47	29.09	0.56	nd	99.76
LSD34 526.00	pyroxenite	526.00	11.37	0.27	0.16	0.77	nd	55.78	0.37	30.32	0.43	0.00	99.47
LSD34 526.00	pyroxenite	526.00	10.21	0.20	0.27	3.78	nd	55.88	0.62	28.16	0.57	nd	99.69
LSD34 526.00	pyroxenite	526.00	11.49	0.34	0.22	0.98	nd	55.71	0.59	30.24	0.69	0.00	100.26
LSD34 526.00	pyroxenite	526.00	11.51	0.32	0.20	3.09	nd	55.18	0.37	28.25	0.42	nd	99.34
Average			11.53	0.28	0.17	1.91	nd	55.59	0.48	29.21	0.53	0.00	99.70

Appendix 5A - LSD34 Microprobe Analyses - Orthopyroxene Compositions continued

Sample Number	Rock Type	Depth (m) from top of borehole	%FeO	%MnO	%TiO2	%CaO	%Na2O	%SiO2	%Al2O3	%MgO	%Cr2O3	%K2O	Total
LSD34 581.00	feldspathic pyroxenite	581.00	16.86	0.44	0.07	2.11	-0.40	53.55	0.85	24.57	0.46	0.05	98.56
LSD34 581.00	feldspathic pyroxenite	581.00	18.29	0.39	0.18	1.11	-0.49	53.43	0.89	24.72	0.48	nd	99.00
LSD34 581.00	feldspathic pyroxenite	581.00	16.87	0.37	0.23	1.00	-0.46	53.91	0.38	25.94	0.28	nd	98.52
LSD34 581.00	feldspathic pyroxenite	581.00	15.68	0.41	0.21	1.68	-0.36	53.56	0.44	25.65	0.70	0.02	97.99
LSD34 581.00	feldspathic pyroxenite	581.00	16.19	0.44	0.17	1.96	-0.56	54.09	0.59	25.38	0.43	nd	98.69
Average			16.78	0.41	0.17	1.57	-0.45	53.71	0.63	25.25	0.47	0.04	98.57
LSD34 618.50	norite	618.50	20.23	0.38	0.17	0.78	-0.24	53.54	1.13	23.72	0.26	0.03	100.00
LSD34 618.50	norite	618.50	20.61	0.07	0.18	0.81	-0.23	54.10	0.23	24.05	0.26	nd	100.08
LSD34 618.50	norite	618.50	20.71	0.52	0.29	1.59	-0.20	53.55	0.63	23.34	0.12	0.03	100.58
LSD34 618.50	norite	618.50	20.38	0.49	0.13	0.90	-0.10	54.01	0.41	23.72	0.19	nd	100.13
LSD34 618.50	norite	618.50	20.38	0.28	0.41	3.46	-0.28	53.77	0.27	22.00	0.28	nd	100.57
Average			20.46	0.35	0.24	1.51	-0.21	53.79	0.53	23.37	0.22	0.03	100.29
LSD34-6	pyroxenite	645.00	13.95	0.28	0.21	0.90	-0.25	55.05	0.52	28.34	0.37	0.05	99.42
LSD34-6	pyroxenite	645.00	14.43	0.24	0.15	1.07	-0.27	55.11	0.61	28.29	0.32	nd	99.95
LSD34-6	pyroxenite	645.00	12.95	0.08	0.20	0.85	-0.40	54.73	1.21	28.98	0.63	0.01	99.24
LSD34-6	pyroxenite	645.00	12.85	0.47	0.20	0.73	-0.38	54.98	0.29	28.94	0.16	0.07	98.31
LSD34-6	pyroxenite	645.00	13.47	0.29	0.17	0.66	-0.32	54.83	0.90	29.40	0.42	0.06	99.88
LSD34-6	pyroxenite	645.00	13.37	0.34	0.28	0.79	-0.26	55.24	0.93	28.52	0.32	0.05	99.58
Average			13.41	0.28	0.20	0.82	-0.33	54.98	0.79	28.83	0.37	0.05	99.40

Appendix 5B - LSD34 Microprobe Analyses - Plagioclase Compositions

Sample Number	Rock Type	of borehole	%MnO	%Na2O	%K2O	%SiO2	%Al2O3	%MgO	%FeO	%CaO	Total
LSD34 139.00	gabbronorite	139.00	nd	3.85	0.18	52.22	31.17	nd	0.26	13.97	101.65
LSD34 139.00	gabbronorite	139.00	0.10	3.88	0.19	52.19	31.03	nd	0.28	13.60	101.27
LSD34 139.00	gabbronorite	139.00	nd	3.60	0.19	51.92	31.32	nd	0.27	14.16	101.46
LSD34 139.00	gabbronorite	139.00	nd	3.96	0.17	51.84	30.92	nd	0.35	13.88	101.12
LSD34 139.00	gabbronorite	139.00	0.19	4.71	0.27	54.19	29.61	nd	0.47	12.24	101.68
Average			0.15	4.00	0.20	52.47	30.81	nd	0.33	13.57	101.52
LSD34 199.50	gabbronorite	199.50	nd	3.92	0.33	51.45	29.73	nd	0.26	13.05	98.74
LSD34 199.50	gabbronorite	199.50	0.00	2.61	0.19	48.49	32.18	nd	0.25	16.09	99.81
LSD34 199.50	gabbronorite	199.50	0.09	2.34	0.25	47.94	32.02	nd	0.25	16.15	99.04
LSD34 199.50	gabbronorite	199.50	0.08	3.72	0.24	51.58	29.92	nd	0.16	13.18	98.88
LSD34 199.50	gabbronorite	199.50	0.22	3.58	0.33	51.68	29.98	nd	0.35	13.92	100.06
LSD34 199.50	gabbronorite	199.50	0.09	2.82	0.40	49.10	31.95	nd	0.13	15.57	100.06
Average			0.05	3.17	0.29	50.04	30.96	nd	0.23	14.66	99.40
LSD34 447.00	norite	447.00	0.50	1.60	0.12	46.79	33.51	nd	0.66	17.24	100.42
LSD34 447.00	norite	447.00	0.20	1.74	0.09	46.83	32.95	nd	0.62	17.36	99.79
LSD34 447.00	norite	447.00	nd	1.88	0.01	46.26	33.52	nd	0.69	17.58	99.94
LSD34 447.00	norite	447.00	0.05	1.89	0.06	46.68	33.20	nd	0.63	17.17	99.68
LSD34 447.00	norite	447.00	nd	1.44	0.11	46.37	33.29	nd	0.64	16.96	98.81
Average			0.14	1.71	0.08	46.59	33.29	nd	0.65	17.26	99.72
LSD34 483.50	norite	483.50	nd	3.38	0.19	49.76	30.65	nd	0.27	14.53	98.78
LSD34 483.50	norite	483.50	nd	3.18	0.20	49.73	30.90	nd	0.07	14.76	98.84
LSD34 483.50	norite	483.50	nd	3.15	0.22	49.42	31.09	nd	0.19	14.53	98.60
LSD34 483.50	norite	483.50	nd	3.87	0.25	50.93	30.14	nd	0.07	14.02	99.28
LSD34 483.50	norite	483.50	0.09	3.04	0.12	49.43	30.95	nd	0.49	14.75	98.87
LSD34 483.50	norite	483.50	nd	3.68	0.21	50.36	30.12	nd	0.21	13.98	98.56
LSD34 483.50	norite	483.50	nd	3.84	0.17	51.66	30.39	nd	0.27	13.65	99.98
LSD34 483.50	norite	483.50	nd	4.00	0.19	52.43	30.32	nd	0.19	13.36	100.49
LSD34 483.50	norite	483.50	nd	3.65	0.36	51.52	30.18	nd	0.06	13.49	99.26
LSD34 483.50	norite	483.50	nd	3.73	0.25	51.44	30.67	nd	0.37	13.72	100.18
LSD34 483.50	norite	483.50	nd	3.56	0.28	51.24	30.69	nd	0.19	14.28	100.24
Average			nd	3.55	0.22	50.72	30.55	nd	0.22	14.10	99.36
LSD34 526.00	pyroxenite	526.00	nd	5.14	0.11	59.12	26.21	nd	0.20	8.31	99.09
LSD34 526.00	pyroxenite	526.00	nd	5.21	0.02	56.44	27.97	nd	0.02	10.13	99.79
LSD34 526.00	pyroxenite	526.00	0.04	4.91	0.13	53.92	29.18	nd	0.13	11.81	100.12
LSD34 526.00	pyroxenite	526.00	0.02	6.17	0.17	57.22	27.31	nd	0.16	9.25	100.30
LSD34 526.00	pyroxenite	526.00	nd	4.87	0.12	53.75	29.17	nd	0.03	11.79	99.73

Appendix 5B - LSD34 Microprobe Analyses - Plagioclase Compositions continued

Sample Number	Rock Type	of borehole	%MnO	%Na2O	%K2O	%SiO2	%Al2O3	%MgO	%FeO	%CaO	Total
Average			nd	5.26	0.11	56.09	27.97	nd	0.11	10.26	99.79
LSD34 581.00	feldspathic pyroxenite	581.00	nd	1.70	0.12	25.89	16.00	nd	0.54	7.55	51.80
LSD34 581.00	feldspathic pyroxenite	581.00	nd	2.84	0.15	49.14	31.88	nd	0.11	15.45	99.57
LSD34 581.00	feldspathic pyroxenite	581.00	nd	2.35	0.11	48.30	32.47	nd	0.35	16.19	99.77
LSD34 581.00	feldspathic pyroxenite	581.00	nd	3.42	0.24	49.95	30.75	nd	0.14	14.38	98.88
LSD34 581.00	feldspathic pyroxenite	581.00	0.04	4.49	0.25	52.63	29.58	nd	0.37	12.25	99.61
Average			0.03	3.28	0.19	50.01	31.17	nd	0.24	14.57	99.47
LSD34 618.50	norite	618.50	0.04	3.28	0.16	49.67	31.16	nd	0.28	14.62	99.21
LSD34 618.50	norite	618.50	0.04	4.30	0.18	52.75	29.87	nd	0.23	12.47	99.84
LSD34 618.50	norite	618.50	nd	3.28	0.13	50.01	31.48	nd	0.18	14.57	99.65
LSD34 618.50	norite	618.50	nd	2.57	0.09	48.77	32.51	nd	0.18	15.86	99.98
LSD34 618.50	norite	618.50	nd	2.83	0.07	49.84	32.63	nd	0.34	15.65	101.36
Average			nd	3.25	0.13	50.21	31.53	nd	0.24	14.63	99.99
LSD34-6	pyroxenite	645.00	nd	4.76	0.29	53.30	29.14	nd	0.23	11.57	99.29
LSD34-6	pyroxenite	645.00	nd	4.82	0.13	53.76	28.84	nd	0.20	11.54	99.29
LSD34-6	pyroxenite	645.00	0.06	4.70	0.20	55.18	28.09	nd	0.19	10.44	98.86
LSD34-6	pyroxenite	645.00	nd	5.73	0.33	59.37	26.22	nd	0.07	7.95	99.67
Average			nd	5.00	0.24	55.40	28.07	nd	0.17	10.38	99.26

Appendix 5C - LPR8/15 Microprobe Analyses - Orthopyroxene Compositions

Sample Number	Rock Type	top of borehole	%FeO	%MnO	%TiO2	%CaO	%Na2O	%SiO2	%Al2O3	%MgO	%Cr2O3	%K2O	Total
LPR8/15 11.00	norite	11.00	16.59	0.23	0.27	1.87	-0.43	54.51	0.73	25.29	0.36	0.03	99.88
LPR8/15 11.00	norite	11.00	15.97	0.40	0.26	2.19	-0.42	54.61	0.71	25.48	0.24	0.04	99.91
LPR8/15 11.00	norite	11.00	15.67	0.41	0.16	3.35	-0.32	54.84	0.68	25.51	0.31	-0.04	100.92
LPR8/15 11.00	norite	11.00	17.26	0.19	0.37	1.63	-0.16	55.00	0.74	25.56	0.21	0.04	101.00
LPR8/15 11.00	norite	11.00	16.62	0.32	0.36	1.55	-0.27	54.17	0.47	25.73	0.48	0.03	99.73
LPR8/15 11.00	norite	11.00	16.84	0.34	0.31	1.52	-0.31	54.29	0.53	25.99	0.12	0.05	100.00
Average			16.49	0.32	0.29	2.02	-0.32	54.57	0.64	25.59	0.29	0.03	100.24
LPR8/15 15.00	norite	15.00	16.27	0.25	0.27	2.02	-0.22	54.48	0.74	25.72	0.44	0.00	100.18
LPR8/15 15.00	norite	15.00	16.89	0.27	0.18	1.60	-0.30	53.72	0.47	25.64	0.36	0.00	99.14
LPR8/15 15.00	norite	15.00	16.26	0.52	0.42	1.90	-0.25	53.76	0.70	25.47	0.11	-0.02	99.15
LPR8/15 15.00	norite	15.00	15.93	0.22	0.29	2.21	-0.50	54.20	0.71	25.44	0.36	-0.04	99.36
LPR8/15 15.00	norite	15.00	16.15	0.24	0.37	2.04	-0.15	53.87	0.62	25.39	0.28	0.07	99.04
Average			16.30	0.30	0.31	1.95	-0.28	54.01	0.65	25.53	0.31	0.00	99.37
LPR8/15 55.00	norite	55.00	20.50	0.39	0.25	2.17	-0.01	53.77	0.54	23.52	-0.02	-0.02	101.13
LPR8/15 55.00	norite	55.00	18.04	0.38	0.16	3.06	-0.43	54.16	0.89	23.65	0.26	0.07	100.68
LPR8/15 55.00	norite	55.00	19.88	0.44	0.22	1.64	-0.27	54.24	0.60	24.08	0.19	-0.02	101.27
LPR8/15 55.00	norite	55.00	21.56	0.33	0.16	1.65	-0.34	53.97	0.49	23.24	0.02	0.07	101.48
LPR8/15 55.00	norite	55.00	19.92	0.28	0.05	1.97	-0.12	54.04	0.51	23.45	0.22	-0.01	100.44
Average			19.98	0.36	0.17	2.10	-0.23	54.04	0.61	23.59	0.13	0.02	101.00
LPR8/15 69.00	norite	69.00	16.49	0.32	0.35	3.29	-0.27	53.63	0.77	24.44	0.39	0.02	99.72
LPR8/15 69.00	norite	69.00	18.40	0.16	0.07	2.21	-0.27	53.74	0.30	24.14	0.39	0.01	99.40
LPR8/15 69.00	norite	69.00	18.72	0.35	0.11	3.06	0.00	53.79	0.67	23.50	0.47	-0.04	100.67
LPR8/15 69.00	norite	69.00	18.42	0.02	0.10	2.76	0.07	53.86	0.77	24.58	0.09	0.00	100.64
LPR8/15 69.00	norite	69.00	18.21	0.35	0.16	2.29	-0.37	55.08	0.58	24.49	0.34	-0.03	101.50
LPR8/15 69.00	norite	69.00	20.04	0.46	0.42	1.92	-0.15	54.04	0.51	23.44	0.21	0.03	101.05
Average			18.38	0.28	0.20	2.59	-0.17	54.02	0.60	24.10	0.32	0.00	100.50

Appendix 5D - LPR8/15 Microprobe Analyses - Plagioclase Compositions

Sample Number	Rock Type	of borehole	%MnO	%Na2O	%K2O	%SiO2	%Al2O3	%MgO	%FeO	%CaO	Total
LPR8/15 11.00	norite	11.00	nd	3.30	0.14	50.04	31.42	nd	0.18	14.81	99.89
LPR8/15 11.00	norite	11.00	nd	3.76	0.74	51.90	30.37	nd	0.31	12.93	100.01
LPR8/15 11.00	norite	11.00	nd	2.92	0.31	48.84	30.91	nd	0.94	14.08	98.00
LPR8/15 11.00	norite	11.00	nd	3.54	0.13	51.04	32.09	nd	0.32	14.80	101.92
LPR8/15 11.00	norite	11.00	nd	3.27	0.15	51.01	31.77	nd	0.06	14.70	100.96
Average			nd	3.36	0.29	50.57	31.31	nd	0.36	14.26	100.16
LPR8/15 15.00	norite	15.00	0.02	3.24	0.11	49.96	31.38	nd	0.15	14.49	99.35
LPR8/15 15.00	norite	15.00	0.10	4.26	0.23	52.14	29.97	nd	0.14	12.91	99.75
LPR8/15 15.00	norite	15.00	nd	3.53	0.12	50.40	31.12	nd	0.09	13.95	99.21
LPR8/15 15.00	norite	15.00	0.08	3.89	0.66	52.30	30.12	nd	0.21	12.18	99.44
LPR8/15 15.00	norite	15.00	0.07	3.23	0.09	49.70	31.78	nd	0.10	14.48	99.45
LPR8/15 15.00	norite	15.00	0.01	3.86	0.10	50.74	30.21	nd	0.68	13.06	98.66
Average			0.06	3.67	0.22	50.87	30.76	nd	0.23	13.51	99.32
LPR8/15 55.00	norite	55.00	0.08	3.27	0.07	51.58	28.13	nd	1.67	15.22	100.02
LPR8/15 55.00	norite	55.00	nd	3.05	0.10	50.53	31.14	nd	0.48	14.90	100.20
LPR8/15 55.00	norite	55.00	nd	3.31	0.10	50.14	31.92	nd	0.17	14.78	100.42
LPR8/15 55.00	norite	55.00	0.09	3.35	0.13	50.82	31.84	nd	-0.01	14.76	100.98
LPR8/15 55.00	norite	55.00	0.01	3.40	0.11	50.83	32.34	nd	0.14	14.86	101.69
Average			0.06	3.28	0.10	50.78	31.07	nd	0.49	14.90	100.69
LPR8/15 69.00	norite	69.00	0.05	4.21	0.18	51.40	30.50	nd	0.13	13.06	99.53
LPR8/15 69.00	norite	69.00	nd	3.20	0.10	49.14	31.43	nd	0.19	14.98	99.04
LPR8/15 69.00	norite	69.00	nd	3.54	0.12	49.83	31.19	nd	0.08	14.36	99.12
LPR8/15 69.00	norite	69.00	0.01	3.29	0.09	50.15	31.36	nd	0.24	14.73	99.87
LPR8/15 69.00	norite	69.00	nd	3.53	0.12	50.73	31.27	nd	-0.03	14.12	99.74
LPR8/15 69.00	norite	69.00	0.23	3.66	0.13	51.01	31.11	nd	0.10	13.70	99.94
LPR8/15 69.00	norite	69.00	0.04	3.56	0.12	51.22	31.10	nd	0.02	13.68	99.74
Average			0.08	3.57	0.12	50.50	31.14	nd	0.10	14.09	99.60

Appendix 5E - LSD34 & LPR8/15 Microprobe Analyses - Clinopyroxene Compositions

Sample Number	Rock Type	top of borehole	%FeO	%MnO	%TiO2	%CaO	%Na2O	%SiO2	%Al2O3	%MgO	%Cr2O3	%K2O	Total
LSD34 139.00	gabbronorite	139.40	11.40	0.39	0.34	22.07	0.27	53.33	1.17	13.52	0.10	0.04	102.63
LSD34 139.00	gabbronorite	139.40	12.85	0.21	0.50	22.20	0.08	51.87	0.94	12.44	0.11	nd	101.20
LSD34 199.50	gabbronorite	199.50	13.28	0.23	0.44	11.22	nd	54.43	1.34	16.04	nd	0.20	97.18
LSD34 199.50	gabbronorite	199.50	12.82	0.15	0.65	11.90	nd	53.70	1.49	15.47	0.00	0.20	96.38
LSD34 199.50	gabbronorite	199.50	13.17	0.24	0.35	12.13	0.11	53.81	1.28	15.87	0.17	0.12	97.24
LSD34 199.50	gabbronorite	199.50	9.28	0.35	0.24	16.83	nd	52.83	0.89	18.03	0.42	0.10	98.97
LSD34 483.50	norite	483.50	7.98	0.20	0.61	22.18	nd	51.96	0.77	14.70	0.46	0.03	98.88
LSD34 483.50	norite	483.50	7.61	0.21	1.09	21.48	nd	51.54	0.80	14.76	0.67	0.05	98.19
LSD34 581.00	feldspathic pyroxenite	581.00	9.96	0.24	0.46	12.03	nd	51.06	3.53	15.97	0.71	0.32	94.28
LSD34 618.50	norite	618.50	7.53	0.22	0.22	22.51	0.08	52.33	1.13	15.30	0.42	nd	99.73
LPR8/15 55.00	norite	55.00	8.19	0.26	0.57	22.69	0.05	51.88	1.51	14.39	0.26	nd	99.81
LPR8/15 69.00	norite	69.00	6.97	0.27	0.39	22.35	0.17	52.34	1.31	14.73	0.67	nd	99.23
LPR8/15 69.00	norite	69.00	7.49	0.19	0.58	21.41	0.21	53.12	2.16	15.25	0.45	nd	100.86

Appendix 5F - Orthopyroxene Compositions from Literature (references are given in tables)

Sample Number	Rock Type	Depth (m) from top of borehole	%FeO	%MnO	%TiO2	%CaO	%Na2O	%SiO2	%Al2O3	%MgO	%Cr2O3	%K2O	Total
Harris & Chaumba (2001), Mineral compositions orthopyroxenes of the Platreef at Sandsloot, Northern Limb, BC.													
PP8	pyroxenite		14.04	0.22	0.14	2.51	0.01	54.35	1.46	26.38	0.44	0.01	99.56
PP3	norite		12.15	0.26	0.15	1.22	0.01	55.13	1.19	29.38	0.42	0.01	99.92
PP4	norite		12.97	0.23	0.12	1.45	0.01	54.95	1.48	28.70	0.42	0.01	100.34

Sample Number	Rock Type	Depth (m) from top of borehole	%Fe2O3	%FeO	%MnO	%TiO2	%CaO	%Na2O	%SiO2	%Al2O3	%MgO	%Cr2O3	Total
Cawthorn et al (1990). Mineral compositions of orthopyroxenes from the Main Zone, BC with distance in (m) from the Pyroxenite Marke													
75			0.64	26.85	0.75	0.24	1.39	0.01	50.95	0.72	18.54	0.04	100.13
275			0.76	20.55	0.58	0.25	1.52	0.03	52.76	0.79	23.44	0.04	100.72
425			0.96	17.01	0.49	0.22	1.66	0.02	54.03	0.93	25.88	0.06	101.26
482			1.26	20.22	0.36	0.26	1.15	0.01	52.93	0.79	23.27	0.16	100.41
484			0.71	20.59	0.39	0.32	0.98	0.00	52.57	0.86	22.98	0.08	99.48
492			2.26	19.74	0.36	0.36	1.26	0.04	52.29	0.87	23.01	0.11	100.30
501			0.79	19.74	0.57	0.22	1.17	0.02	53.14	0.85	24.05	0.14	100.69
567			0.55	22.74	0.56	0.34	1.61	0.03	52.15	0.82	21.52	0.12	100.44
601			0.52	18.46	0.57	0.24	0.95	0.01	53.46	0.66	25.19	0.06	100.12
672			0.43	23.41	0.65	0.27	1.34	0.02	51.91	0.60	21.37	0.03	100.03
881			0.38	20.85	0.57	0.41	0.95	0.01	53.16	0.54	23.64	0.03	100.54
980			0.43	20.18	0.60	0.25	1.02	0.02	52.44	0.58	24.18	0.01	99.71
1095			0.77	18.93	0.51	0.29	1.43	0.01	52.70	0.86	24.18	0.03	99.71

Sample Number	Rock Type	Depth (m) from top of borehole	%FeO	%MnO	%TiO2	%CaO	%Na2O	%SiO2	%Al2O3	%MgO	%K2O	Total
von Gruenuwaldt & Weber-Diefenbach (1977). Orthopyroxene compositions from the Main Zone BC. (a = hypersthene, b = inverted pigeonite from the same sample												
PB397a			17.30	0.11	0.20	1.70	0.17	53.20	1.09	25.45	0.07	99.29
PB189a			19.90	0.08	0.18	1.28	0.08	53.00	1.20	24.20	0.07	99.99
G575a			20.70	0.10	0.31	1.40	0.12	52.80	1.00	23.70	0.07	100.20
G577a			21.30	0.11	0.25	1.16	0.03	52.20	0.82	23.20	-	99.07
G581a			21.50	0.19	0.20	1.40	0.06	53.20	1.20	22.40	-	100.15
G501a			21.90	0.13	0.39	1.60	0.05	52.00	2.15	22.40	-	100.62
G586a			23.00	0.15	0.24	1.40	0.02	52.30	0.90	21.90	-	99.91
G587a			23.00	0.40	0.13	2.00	0.02	53.30	1.40	21.10	-	101.35
G588a			23.70	0.40	0.10	1.80	0.05	52.60	1.00	20.40	0.08	100.13
PB397b			20.90	0.10	0.17	0.69	0.05	53.60	1.00	24.00	0.05	100.56
PB189b			22.20	0.14	0.19	0.62	0.05	53.30	1.30	22.30	0.08	100.18
G575b			22.50	0.16	0.30	0.90	0.10	52.90	1.00	22.20	0.07	100.13
G577b			23.70	0.45	0.29	1.10	0.02	52.10	1.10	21.20	-	99.96
G581b			22.20	0.10	0.20	0.60	0.06	53.40	1.20	21.60	-	99.36
G501b			22.60	0.12	0.37	0.40	0.04	52.70	2.20	21.50	-	99.93
G586b			27.60	0.44	0.19	0.90	0.02	52.00	0.65	18.20	-	100.00
G587b			23.80	0.37	0.24	1.20	0.02	53.00	1.10	20.90	-	100.63
G588b			24.70	0.35	0.18	1.80	0.08	52.50	0.75	19.60	-	99.96

Appendix 5F - Orthopyroxene Compositions from Literature (references are given in tables) continued

Sample Number	Rock Type	Depth (m) from top of borehole	%FeO	%MnO	%TiO2	%CaO	%Na2O	%SiO2	%Al2O3	%MgO	%Cr2O3	%NiO	Total
Eales et al (1993). Mineral compositions of orthopyroxenes from the Lower and Critical Zones (A, B, C) and from the Merensky Cyclic Unit (D, E, F													
A			9.32	0.21	0.07	1.27	0.03	56.19	1.11	31.12	0.48	0.07	99.86
B			10.77	0.23	0.10	1.28	0.02	55.73	1.22	29.81	0.47	0.08	99.72
C			11.67	0.24	0.13	1.23	0.01	55.28	1.24	29.53	0.46	0.08	99.88
D			12.61	0.26	0.16	1.22	0.02	55.00	1.29	28.95	0.43	0.09	100.03
E			13.54	0.28	0.20	1.32	0.02	54.83	1.03	28.27	0.38	0.08	99.96
F			18.33	0.36	0.26	1.05	0.01	53.79	0.84	24.93	0.19	0.08	99.84

Appendix 6A - LSD34 XRF Major and Trace Element data - Plagioclase Separates

Sample Number	Depth (m) from top of borehole	Rock Type	%SiO2	%TiO2	%Al2O3	%Fe2O3	%MnO	%MgO	%CaO	%Na2O	%K2O	%P2O5	%LOI	%TOTAL
LSD 34 139.00 PLAG	139.00	gabbro	53.37	0.07	29.00	0.81	0.01	0.30	12.12	3.35	0.47	0.05	0.65	100.20
LSD 34 159.00 PLAG	159.00	gabbro	52.22	0.07	28.96	0.78	0.01	0.32	12.23	3.35	0.52	0.03	0.54	99.03
LSD 34 191.00 PLAG	191.00	anorthosite	52.46	0.07	29.17	0.81	0.01	0.26	12.62	2.94	0.65	0.07	0.59	99.65
LSD 34 199.50 PLAG	199.50	gabbro	53.81	0.08	28.36	0.54	0.02	0.58	12.29	2.55	0.80	0.07	0.76	99.86
LSD 34 233.50 PLAG	233.50	gabbro	50.81	0.12	29.36	0.97	0.02	1.20	13.13	2.22	0.38	0.04	1.01	99.26
LSD 34/1 PLAG	630.20	f-pyroxenite	54.44	0.08	28.63	0.66	0.02	0.63	11.22	3.07	0.80	0.05	0.67	100.27
LSD 34/14 PLAG	671.15	norite	49.97	0.08	29.65	0.93	0.04	0.51	12.15	2.14	2.01	0.04	2.13	99.65
LSD 34/17 PLAG	692.72	norite	54.12	0.17	27.12	0.87	0.03	0.76	11.73	2.87	0.35	0.05	0.47	98.54

Sample Number	Depth (m) from top of borehole	Rock Type	Rb ppm	Sr ppm	Y ppm	Zr ppm	Nb ppm	Co ppm	Ni ppm	Cu ppm	Zn ppm	TiO2 %	V ppm	Cr ppm	Ba ppm
LSD 34 139.00 PLAG	139.00	gabbro	13	387	5	15	4	<6	8	16	22	0.05	<12	20	207
LSD 34 159.00 PLAG	159.00	gabbro	13	395	5	13	4	<6	11	16	19	0.05	<12	<12	208
LSD 34 191.00 PLAG	191.00	anorthosite	20	365	7	19	4	<6	9	17	23	0.05	<12	<12	222
LSD 34 199.50 PLAG	199.50	gabbro	26	369	5	43	4	6	18	25	24	0.06	<12	12	252
LSD 34 233.50 PLAG	233.50	gabbro	20	387	5	19	5	9	40	22	21	0.08	<12	63	137
LSD 34/1 PLAG	630.20	f-pyroxenite	29	461	5	24	4	6	55	92	17	0.05	<12	30	333
LSD 34/14 PLAG	671.15	norite	137	388	4	89	5	10	22	66	25	0.05	16	<12	349
LSD 34/17 PLAG	692.72	norite	13	396	4	209	10	<6	31	17	23	0.15	<12	40	209

Sample Number	Depth (m) from top of borehole	Rock Type	Pb ppm	Ga ppm	La ppm	Ce ppm	Sc ppm	Th ppm	As ppm	U ppm
LSD 34 139.00 PLAG	139.00	gabbro	<9	21	<12	34	11	<12	<12	<9
LSD 34 159.00 PLAG	159.00	gabbro	9	21	<12	33	<10	<12	<12	<9
LSD 34 191.00 PLAG	191.00	anorthosite	<9	21	12	39	10	<12	<12	<9
LSD 34 199.50 PLAG	199.50	gabbro	10	21	<12	30	<10	<12	<12	<9
LSD 34 233.50 PLAG	233.50	gabbro	10	19	<12	34	11	<12	<12	<9
LSD 34/1 PLAG	630.20	f-pyroxenite	10	20	15	33	<10	<12	<12	<9
LSD 34/14 PLAG	671.15	norite	25	23	14	37	<10	<12	<12	<9
LSD 34/17 PLAG	692.72	norite	21	20	<12	39	<10	<12	<12	<9

Appendix 6B - LPR6/12 XRF Major and Trace Element data - Plagioclase Separates

Sample Number	Depth (m) from top of borehole	Rock Type	%SiO2	%TiO2	%Al2O3	%Fe2O3	%MnO	%MgO	%CaO	%Na2O	%K2O	%P2O5	%LOI	%TOTAL
LPR6/12-5 PLAG	178.64	pyroxenite	54.16	0.08	29.20	0.54	0.01	0.59	12.14	3.20	0.13	0.04	0.37	100.46
LPR6/12-25 PLAG	193.50	pyroxenite	49.53	0.06	31.51	0.74	0.02	0.75	13.99	2.64	0.03	0.04	0.57	99.88
LPR6/12 28 PLAG	195.00	pyroxenite	29.61	0.00	15.37	1.37	0.01	0.00	48.41	2.93	0.16	0.04	0.81	98.71
LPR6/12-29 PLAG	195.50	pyroxenite	50.50	0.09	31.04	0.70	0.03	0.63	13.87	2.85	0.00	0.00	0.84	100.55
LPR6/12-49 PLAG	205.50	pyroxenite	51.99	0.07	30.37	0.67	0.02	0.65	12.60	1.63	0.11	0.05	0.50	98.66
LPR6/12-56 PLAG	209.00	pyroxenite	51.55	0.08	30.66	0.67	0.03	0.78	12.51	3.47	0.00	0.03	0.64	100.42
LPR6/12 60 PLAG	211.00	pyroxenite	54.32	0.08	28.54	1.10	0.03	0.77	11.24	3.10	0.48	0.08	0.71	100.45

Sample Number	Depth (m) from top of borehole	Rock Type	Rb ppm	Sr ppm	Y ppm	Zr ppm	Nb ppm	Co ppm	Ni ppm	Cu ppm	Zn ppm	TiO2 ppm	V ppm	Cr ppm	Ba ppm
LPR6/12-5 PLAG	178.64	pyroxenite	5	450	4	19	5	<6	50	92	23	0.07	12	44	177
LPR6/12-25 PLAG	193.50	pyroxenite	6	394	3	<8	4	49	1440	49	12	0.04	<12	39	76
LPR6/12 28 PLAG	195.00	pyroxenite	14	408	4	<8	4	43	1198	172	17	0.04	12	32	146
LPR6/12-29 PLAG	195.50	pyroxenite	4	404	4	<8	4	42	1614	81	14	0.04	<12	54	98
LPR6/12-49 PLAG	205.50	pyroxenite	8	467	5	68	5	25	1088	49	14	0.05	<12	27	155
LPR6/12-56 PLAG	209.00	pyroxenite	4	472	4	17	4	4	41	33	11	0.06	8	40	170
LPR6/12 60 PLAG	211.00	pyroxenite	24	392	5	95	5	10	201	197	19	0.05	<12	17	198

Sample Number	Depth (m) from top of borehole	Rock Type	Pb ppm	Ga ppm	La ppm	Ce ppm	Sc ppm	Th ppm	As ppm	U ppm
LPR6/12-5 PLAG	178.64	pyroxenite	13	20	<12	28	10	<12	<12	<9
LPR6/12-25 PLAG	193.50	pyroxenite	20	19	<12	23	12	<12	<12	<9
LPR6/12 28 PLAG	195.00	pyroxenite	17	19	<12	19	11	<12	<12	<9
LPR6/12-29 PLAG	195.50	pyroxenite	15	19	<12	16	12	<12	<12	<9
LPR6/12-49 PLAG	205.50	pyroxenite	22	21	17	26	11	<12	749	<9
LPR6/12-56 PLAG	209.00	pyroxenite	23	20	14	34	10	<12	<12	<9
LPR6/12 60 PLAG	211.00	pyroxenite	20	24	12	38	10	<12	<12	<9

Appendix 6C - LSD22 XRF Major and Trace Element data - Plagioclase Separates

Sample Number	Depth (m) from top of borehole	Rock Type	%SiO2	%TiO2	%Al2O3	%Fe2O3	%MnO	%MgO	%CaO	%Na2O	%K2O	%P2O5	%LOI	%TOTAL
LSD 22/2 PLAG	182.50	gabbro	52.55	0.07	29.23	0.90	0.02	0.35	12.78	2.70	0.61	0.05	0.77	100.03
LSD 22/3 PLAG	313.20	pyroxenite	51.00	0.07	30.83	0.73	0.01	0.35	13.99	2.60	0.36	0.03	0.35	100.32
LSD 22/4 PLAG	544.00	norite	51.96	0.07	30.02	0.86	0.01	0.61	13.19	2.80	0.43	0.03	0.53	100.51
LSD 22/5 PLAG	666.00	norite	28.61	0.08	9.19	0.28	0.08	0.25	35.08	1.11	0.22	0.50	23.80	99.20

Sample Number	Depth (m) from top of borehole	Rock Type	Rb ppm	Sr ppm	Y ppm	Zr ppm	Nb ppm	Co ppm	Ni ppm	Cu ppm	Zn ppm	TiO2 ppm	V ppm	Cr ppm	Ba ppm
LSD 22/2 PLAG	182.50	gabbro	21	364	6	26	5	<6	12	19	26	0.05	13	17	185
LSD 22/3 PLAG	313.20	pyroxenite	12	392	4	13	4	6	12	18	19	0.05	<12	14	156
LSD 22/4 PLAG	544.00	norite	13	466	6	13	5	<6	21	24	16	0.05	17	35	189
LSD 22/5 PLAG	666.00	norite	9	182	16	44	6	6	7	8	17	0.06	<12	12	143

Sample Number	Depth (m) from top of borehole	Rock Type	Pb ppm	Ga ppm	La ppm	Ce ppm	Sc ppm	Th ppm	As ppm	U ppm
LSD 22/2 PLAG	182.50	gabbro	15	21	<12	34	10	<12	<12	<9
LSD 22/3 PLAG	313.20	pyroxenite	<9	21	<12	25	11	<12	<12	<9
LSD 22/4 PLAG	544.00	norite	9	21	15	25	10	<12	<12	<9
LSD 22/5 PLAG	666.00	norite	27	<10	<12	44	33	<12	<12	<9